Mário Tyago Murakami

Estratégias de Inibição, Mecanismos Moleculares e Interações Intermoleculares em Complexos Macromoleculares

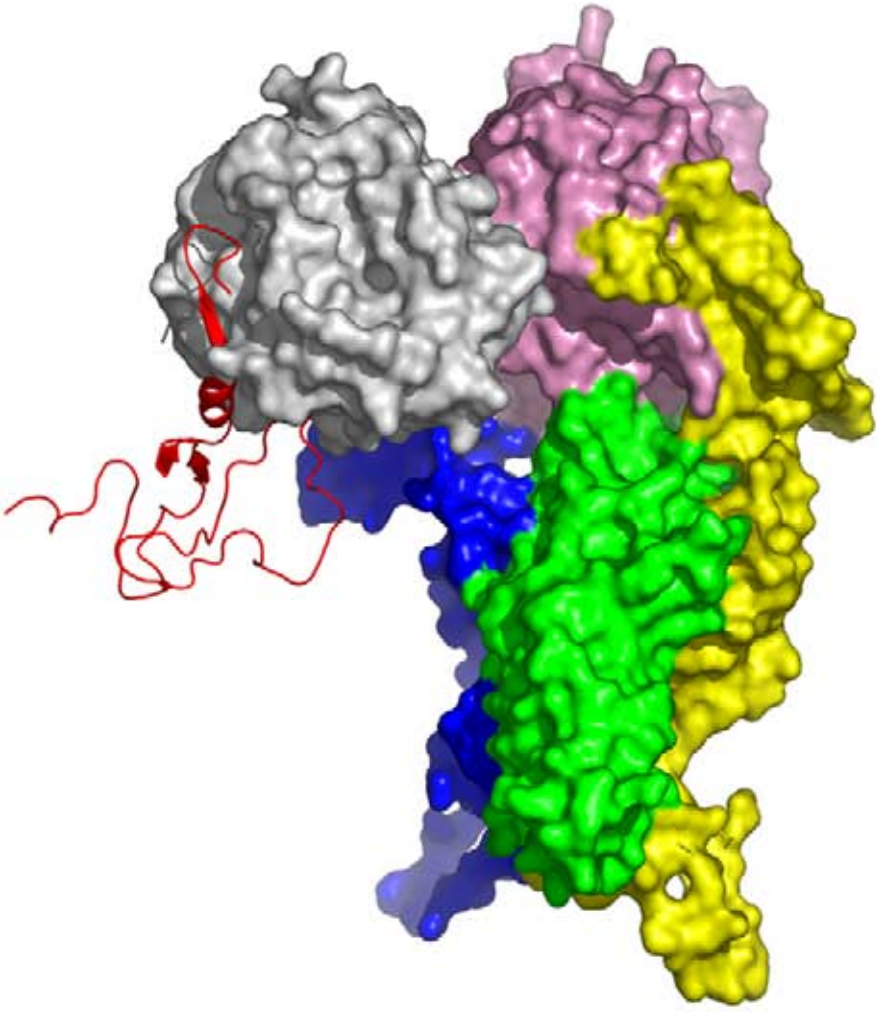

São José do Rio preto
2006

MÁRIO TYAGO MURAKAMI

Estratégias de Inibição, Mecanismos Moleculares e Interações Intermoleculares em Complexos Macromoleculares

Tese Apresentada ao Programa de Biofísica Molecular, Departamento de Física, Instituto de Biociências, Letras e Ciências Exatas, Universidade Estadual Paulista Júlio Mesquita Filho, para Obtenção do Título de Doutor em Biofísica Molecular, Área de Concentração em Cristalografia de Macromoléculas.

Orientador: *Prof. Dr. Raghuvir Krishnaswamy Arni*

Fomento: FAPESP – SMOLBNet – CEPID – CAPES

São José do Rio Preto – SP
Dezembro de 2006

Murakami, Mário Tyago.
Estratégia de inibição, mecanismos moleculares e interações intermoleculares em complexos macromoleculares / Mário Tyago Murakami. – São José do Rio Preto : [s.n.], 2006
152 f. : il. ; 30 cm.

Orientador: Raghuvir Krishnaswamy Arni
Co-orientador (se houver): Roy Edward Larson
Tese (doutorado) – Universidade Estadual Paulista, Instituto de Biociências, Letras e Ciências Exatas

1. Cristalografia de Raios X. 2. Proteínas. 3. Mecanismos de ação 4. Coagulação sangüínea. 5. Membranas biológicas. I. Arni, Raghuvir Krishnaswamy. II. Larson, Roy Edward. III. Universidade Estadual Paulista, Instituto de Biociências, Letras e Ciências Exatas. IV. Doutor.

CDU – 577.112

MÁRIO TYAGO MURAKAMI

Estratégias de Inibição, Mecanismos Moleculares e Interações Intermoleculares em Complexos Macromoleculares

Tese Apresentada ao Programa de Biofísica Molecular, Departamento de Física, Instituto de Biociências, Letras e Ciências Exatas, Universidade Estadual Paulista Júlio Mesquita Filho, para Obtenção do Título de Doutor em Biofísica Molecular, Área de Concentração em Cristalografia de Macromoléculas.

TESE PARA OBTENÇÃO DO TÍTULO DE DOUTOR

COMISSÃO JULGADORA:

Prof. Dr. Raghuvir Krishnaswamy Arni (Orientador)
Departamento de Física - IBILCE/UNESP

Prof. Dr. Antônio Carlos Martins Camargo
CAT/CEPID – Instituto Butantan

Prof. Dr. Nilson Ivo Tonin Zanchin
Laboratório Nacional de Luz Síncrotron

Prof. Dr. Beatriz Gómez Guimarães
Laboratório Nacional de Luz Síncrotron

Prof. Dr. Roberto da Silva
Departamento de Química – IBILCE/UNESP

São José do Rio Preto, dezembro de 2006

DADOS CURRICULARES

MÁRIO TYAGO MURAKAMI

O autor desse trabalho, Mário Tyago Murakami, nasceu em Taquarituba (SP), no ano de 1981 e realizou seus estudos pré-universitários em diversas escolas durante sua adolescência, onde teve participação destacada na Olimpíada Regional de Matemática realizada na UNESP - Campus Bauru e na Olimpíada de Matemática das Escolas Adventistas. No ano de 1999, iniciou seu curso universitário de Engenharia de Alimentos na UNESP - Campus São José do Rio Preto e no mesmo ano começou seu estágio científico na área de bioquímica e cristalografia de macromoléculas com bolsa FAPESP sob orientação do Prof. Dr. Raghuvir Krishnaswamy Arni onde publicou cinco artigos científicos *Qualis A*, incluindo um artigo de revisão sobre fosfolipases A_2. Durante a graduação, realizou diversos cursos de aprimoramento em expressão gênica, purificação e sequenciamento químico de proteínas. Participou, também, do concorrido Curso de Verão do Laboratório Nacional de Luz Síncrotron (Campinas-SP) no ano de 2002 e em 2004 iniciou seu curso de Doutorado Direto com bolsa FAPESP na área de Biofísica Molecular com concentração em Cristalografia de Macromoléculas, o qual resultou 17 manuscritos científicos e o 1º lugar no X Prêmio Jovem Talento em Ciências da Vida ocorrido na XXXV Reunião Anual da Sociedade Brasileira de Bioquímica e Biologia Molecular, Águas de Lindóia (2006). Um dos trabalhos apresentados na tese também foi escolhido como *Six Top Choices* no congresso anual de 2005 da *American Crystallographic Association* com *scholarship award*. No doutorado, também, realizou um doutorado sanduíche no *European Molecular Biology Laboratory / Deutsches Elektronen-Synchrotron* e na Universidade de Hamburgo - Alemanha, onde pode trabalhar intensamente com técnicas de automação no crescimento de cristais de proteínas e radiação síncrotron. Atualmente, está aprofundando em técnicas de "docking" de complexos macromoleculares e dinâmica molecular.

Dedico esse trabalho,

A todos os cientistas que sonham descobrir a origem da vida, a cura de doenças, por fim, descobrir fenômenos na sua essência a nível molecular e prático, mas que, apesar de muitos desses "problemas" aparentarem não ter solução aos nossos olhos, têm, por sua vez, sobre árduo e intenso trabalho, sua contribuição para sociedade.

AGRADECIMENTOS

A minha gratidão a todos que me apoiaram e incentivaram o meu crescimento pessoal e profissional.

Agradeço, especialmente, ao Prof. Dr. Raghuvir Krishnaswamy Arni pela confiança e severidade que me proporcionaram um excelente crescimento e amadurecimento científico.

Agradeço, especialmente, aos meus familiares, minha mãe que sempre esteve ao meu lado nos momentos mais difíceis da minha vida e ao Primo que foi, sem dúvidas, o grande responsável por tudo que alcancei até hoje. Minha eterna gratidão.

Agradeço à Letícia e sua família que, também, foram muito importantes nessa fase final do meu doutoramento.

Aos queridos amigos de Laboratório, em especial Magno, companheiro para todos os momentos, Karine, Flávia e Daniella.

A todos docentes do departamento que sempre foram muito amistosos e prestativos, em especial Jorge Chahine, responsável pelo meu ingresso no Departamento de Física e o João Ruggiero, sempre muito simpático e amigável.

Agradeço, também, aos colegas do Departamento, em especial ao Paulinho e Barbosa, uma dupla da pesada que sempre foram muito prestativos.

A todos colaboradores que fizeram parte desse trabalho, em especial Denise Tambourgi pelas amostras de esfingomielinase D e valiosa discussão, Paulo Melo pelas grandes dicas sobre suramina, Richard Ward pela histórica colaboração, Christian Betzel pela orientação no exterior e Adélia Cintra pelas infinitas amostras fornecidas.

À Fundação de Amparo à Pesquisa do Estado de São Paulo (FAPESP) pelo auxílio financeiro na execução desse trabalho e a CAPES pelo fomento no doutorado sanduíche na Universidade de Hamburgo / EMBL em Hamburgo na Alemanha.

ABREVIATURAS

C1-INH – inibidor C1 de esterase
CVX - convulxina
EMBL-DESY – *European Molecular Biology Laboratory / Deutsches Elektronen-Synchrotron*
LNLS – Laboratório Nacional de Luz Síncrotron
FIIa – fator II ativado
FVa – fator V ativado
FVIIa – fator VII ativado
FIX – fator IX zimogênio
FX – fator X zimogênio
FXa – fator X ativado
FXIa – fator XI ativado
FXIIa – fator XII ativado
FXIII – fator XIII
FXIIIa – fator XIII ativado
HMWK – cininogênio de alto peso molecular
KDR – *kinase domain-containing receptor*
NAPc2 – proteína anticoagulante da saliva do verme hematófago *Ancylostoma caninium* c2
NAP5 - proteína anticoagulante da saliva do verme hematófago *Ancylostoma caninium* 5
NAPs – Proteínas anticoagulantes de nematóides
PAI – inibidor de ativador do plasminogênio
PC – proteína C
PL – fosfolídios
PLA_2 – fosfolipase A_2
Selectide – nova classe de inibidor de fator Xa
TF – fator tissular
TFPI – inibidor da via do fator tissular
t-PA – ativador do plasminogênio tipo-tissular
TSV-PA – ativador de plasminogênio do veneno de *Trimeresurus stejnegeri*
u-PA – ativador do plasmingênio tipo-uroquinase

LISTA DE FIGURAS

RESUMO

O presente trabalho aborda alguns aspectos de processos biológicos essenciais à vida, como o sistema hemostático, integridade de membranas biológicas e a termoestabilidade de proteínas. Ferramentas cristalográficas combinadas com estudos *in silico* e caracterizações bioquímicas e espectroscópicas permitiram acessar informações a nível molecular dos mecanismos e vias de ativação ou inibição desses processos biológicos. Baseado em estudos com toxinas isoladas de vermes, serpentes, carrapatos, sanguessugas, aranhas e outros animais peçonhentos foi caracterizada uma nova molécula anti-dermonecrótica no tratamento de acidentes ofídicos, que não apresenta efeitos tóxicos secundários e revelou um papel chave do sítio ativo nominal no enigmático mecanismo de ação das Lys49 fosfolipases A_2. Estudos com as proteínas anticoagulantes do verme hematófago *Ancylostoma caninum* NAPc2 e NAP5 demonstraram um novo sítio do fator Xa, que é importante para o reconhecimento de substratos macromoleculares e inibição, que serve como uma nova plataforma para o desenho de drogas. Outra toxina hemostaticamente ativa estudada foi protac®, que tem habilidade de ativar a proteína C por uma via alternativa, independente do cofator fisiológico trombomodulina, onde o perfil eletrostático (básico) em torno do sítio ativo e o posicionamento estratégico dos três grupos de carboidratos na região interfacial são essenciais no reconhecimento, interação e ativação da proteína C. Além disso, foi determinada a primeira estrutura tridimensional a resolução de 1.75 Å usando o método "quick cryo-soaking" de uma enzima pertencente à família das esfingomielinases D, somente encontradas no veneno de aranhas do gênero *Loxosceles* e algumas bactérias patogênicas do gênero *Corynebacterium*. Baseados nesses resultados e com estudos comparativos com fosfolipase D e DNase I, foi proposto o mecanismo de ação da enzima, o qual foi posteriormente confirmado por estudos de mutação sítio-dirigida.

Palavras-chave: Difração de raios X, processos biológicos, mecanismos de ação e inibição.

ABSTRACT

This work presents some features of essential biological processes such as the haemostatic system, integrity of biological membranes and thermostability of proteins. Crystallographic, spectroscopic and *in silico* tools have been used to obtain information at the molecular level of macromolecular complexes, action mechanisms and inhibition pathways. Worms, snakes, ticks, leeches and spiders produce a variety of proteins, which interfere in the regulation of these systems. Different toxins isolated from these organisms were characterized providing necessary information for the development of a new anti-myonecrotic molecule and reveal a new factor Xa exosite that is important for macromolecular substrates recognition and inhibition. The first crystal structure of a member of the sphingomyelinases D family was determined by the 'quick cryo-soaking' technique and the catalytic mechanism was proposed, which involves a magnesium-binding site and two catalytic histidines. An alternative activation of the protein C pathway that does not require thrombomodulin was structurally characterized and revealed the dual role of the elestrotatic surface charge around the active site and the three strategically positioned carbohydrate moieties in the approach, recognition and activation of protein C.

Keywords: X-ray diffraction, biological processes, action mechanisms and inhibition.

SUMÁRIO

1) ***Overview***

A genômica no início dos anos 90 recebeu grandes incentivos sendo a promessa de cura de diversas moléstias congênitas e adquiridas. Porém, após a corrida do mapeamento do genoma humano, as perguntas a serem respondidas continuaram sem solução e serviram como berço para a proteômica, isto é, o estudo das moléculas que expressam as informações contidas no material genético, as proteínas. As proteínas na natureza estão destinadas, através de uma pressão seletiva, a exercer funções específicas numa enorme gama de bioprocessos e suas propriedades funcionais dependem de suas estruturas tridimensionais. Com a técnica do DNA recombinante, o número de seqüências protéicas aumentou exponencialmente e permitiu um grande avanço nos estudos estruturais de proteínas. Atualmente, mais de 40.000 estruturas protéicas foram determinadas principalmente por métodos cristalográficos, que teve um incrível avanço tecnológico e metodológico, principalmente nos últimos dez anos, que impulsionou a biologia estrutural. Hoje estamos em mais uma nova fase na ciência, onde não basta estudar estas biomoléculas de forma isolada, mas sim inserida no seu sistema biológico (*systems biology*) o que requer uma grande interatividade entre pesquisadores e a palavra chave é a multi-disciplinaridade.

Nesta tese, três sistemas biológicos foram abordados, o hemostático, a integridade de membranas biológicas e a termoestabilidade de proteínas, por métodos cristalográficos, *in silico*, bioquímicos e fisiológicos utilizando infra-estrutura e colaboração intelectual de diversos grupos de pesquisa da USP/RB, USP/SC, Centro de Toxinologia Aplicada – CEPID, SMOLBNet, Instituto Butantan e LNLS.

2) Sistemas Abordados

a. Hemostasia

A hemostasia é o conjunto de mecanismos desencadeados pelo organismo para manter o sangue fluído no interior dos vasos, impedindo a formação de trombos em vasos intactos e desencadeando uma série de reações que resultam no fechamento de lesões na parede vascular impedindo, assim, uma hemorragia prolongada (Colman et al. 1994). O mecanismo envolvido para essa manutenção depende de inúmeros fatores, tais como plaquetas, plasma e vasos sangüíneos. A integridade dos vasos sangüíneos garante a liberação de componentes inibidores da coagulação e agregação plaquetária.

Quando ocorre injúria vascular, a hemostasia primária é realizada por uma combinação de vasoconstricção, adesão e agregação plaquetária. Na ação primária, as plaquetas aderem-se á superfície lesada liberando componentes essenciais para o desenvolvimento da hemostasia. Além disso, suas membranas são importantes para adsorção e concentração dos fatores plasmáticos, acelerando a coagulação, com a formação de fibrina, que reforça o tampão plaquetário. A hemostasia secundária é marcada pela formação de fibrina, que resulta na coagulação sangüínea iniciada por dois mecanismos diferentes, o processo de ativação por contato e a ação do fator tissular (TF). Esses dois processos, também chamados de vias intrínseca e extrínseca da coagulação respectivamente, ativam uma outra via conhecida por via comum ou via do FX (Colman et al. 1994).

No plasma sangüíneo, existem os fatores de coagulação na forma de zimogênios que são ativados durante o desenvolvimento do sistema de coagulação. Esses fatores, quando ativados, convertem o precursor na sua forma ativa. Essas seqüências de transformações zimogênio-à-enzima são representadas pela cascata da coagulação (figura 1) (Neurath, 1984).

O evento iniciador para a coagulação sangüínea é a exposição do TF provocado por algum trauma vascular. O TF, na "via extrínseca", em combinação com FVIIa e fosfolipídios (PL) ativam os fatores IX e X. A "via intrínseca" inclui a ativação do fator XI pelo complexo cininogênio de alto peso molecular (HMWK)/FXIIa. O FXIa também ativa o FIX, que por sua vez, em combinação com FVIIIa, PL e íons cálcio (complexo tenase) converte FX em FXa. Porém, *in vivo*, essa divisão não ocorre, pois o complexo TF/FVIIa é um potente ativador de FIX e FX , fazendo com que a coagulação se desenvolva rapidamente (Colman et al., 1994; Mann, 1999).

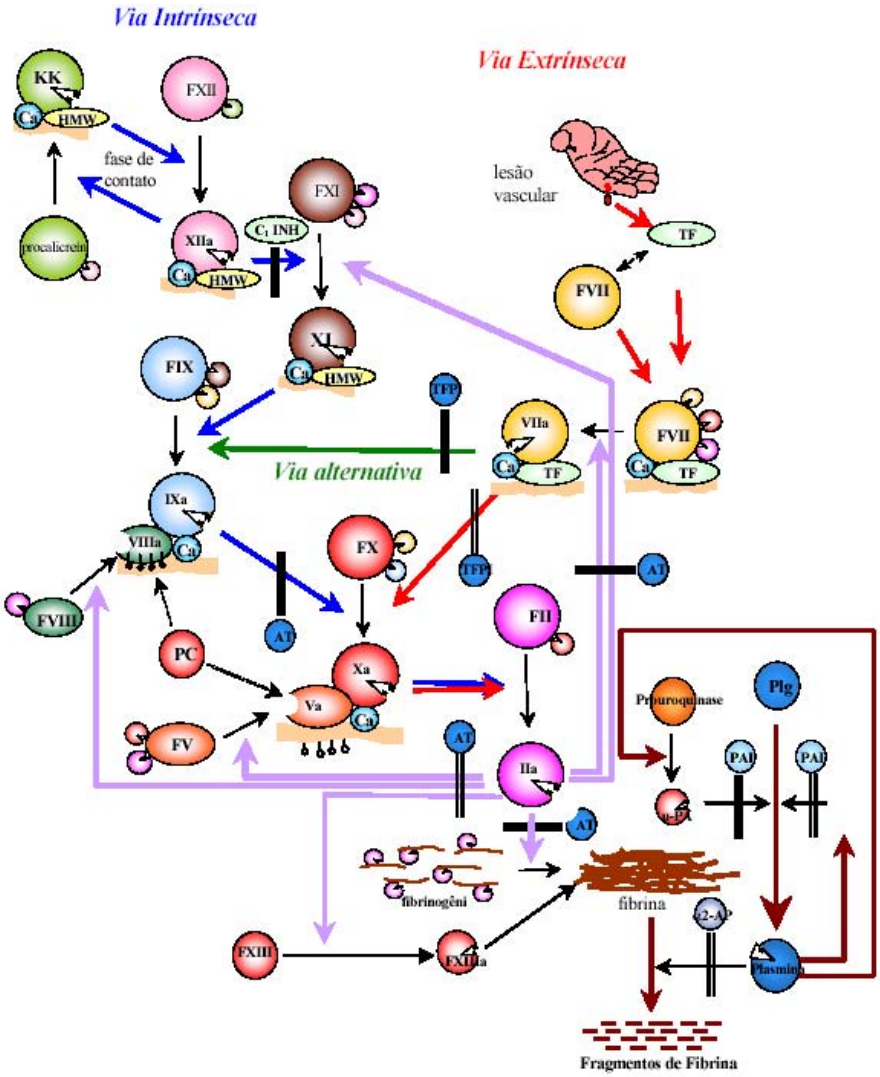

Figura 1: Esquema da cascata de coagulação sangüínea. Desencadeamento pela via extrínseca (vermelho), via intrínseca (azul), via alternativa (verde). Atividade proteolítica da trombina (roxo); proteólise (preto); sistema fibrinolítico (marrom) e inibição pela proteína C (preto tracejado).

Na via comum, FXa mais o FVa, PL e íons cálcio formam o complexo protrombinase, que converte a protrombina em trombina (FIIa). Esse FIIa formado, hidrolisa o fibrinogênio liberando os fibrinopeptídeo A e B e mudando suas cargas, permitindo a ligação entre as moléculas e formando a fibrina solúvel. O FXIII, ativado pelo FIIa, estabiliza o coágulo de fibrina através da reação de transaminação, formando ligações cruzadas de dímeros de fibrina que é insolúvel e mais resistente a degradação pelo sistema fibrinolítico (Bithell TC, 1998).

Para que sejam recanalizados os vasos sangüíneos lesados, o sistema fibrinolítico é o principal meio fisiológico de descartar a fibrina formada. A fibrinólise resulta da conversão do plasminogênio plasmático, em plasmina. Essa conversão é feita pela liberação do ativador tissular de plasminogênio (t-PA) presente no endotélio. Estímulos vasoativos fisiológicos e patológicos (exercícios, choque elétrico, estresse, adrenalina, histamina, pirógenos bacterianos, isquemia, hipóxia, trombina, FXa e substâncias liberadas de plaquetas) levam a liberação de ativadores endoteliais que provocam a liberação dos ativadores de plasminogênio. A plasmina formada pode seguir quatro vias possíveis de reação: (a) ser inibida pela α_2-AP inibindo a fibrinólise, (b) ativar pro-uroquinase a uroquinase (u-PA) e (c) ativar t-PA reforçando o sistema fibrinolítico e (d) degradar o coágulo de fibrina restabelecendo a fluídez do sangue. A u-PA liberada pelo endotélio, células renais e vários tumores, e a estreptoquinase (SK) presente no extrato de estreptococos β-hemolíticos, também são ativadores de plasminogênio. Atividades do t-PA e do u-PA, são inibidas pelo inibidor de ativador de plasminogênio (PAI) (Halkier, 1991). A plasmina cliva ligações de arginina e lisina dos hormônios, componentes do complemento, cininas, vários fatores de coagulação e fibrinogênio. A ação proteolítica da plasmina sobre a fibrina ou fibrinogênio leva à formação de fragmentos protéicos solúveis. Quando a fibrina insolúvel é lisada pela plasmina produz um produto de degradação específico de fibrina, chamado de dímero-D (Halkier, 1991), terminando, assim, o processo de coagulação e seu sistema de auto-regulação.

Várias proteínas agem como inibidores naturais retardando a coagulação como inibidor C1 do sistema de complemento, que também neutraliza os FXIa, FXIIa, plasmina e calicreína e o inibidor da via do fator tissular (TFPI) que bloqueia o complexo TF/FVIIa. Diversas proteínas exógenas produzidas por carrapatos, vermes, sanguessugas, serpentes, lagartos e insetos também são potentes inibidores da coagulação sangüínea e vem sendo extensivamente estudados para aplicações clinicas em doenças cardiovasculares (Colman et al., 1994; Halkier, 1991). Nesse capítulo, serão abordados diferentes aspectos estruturais dos mecanismos de inibição ou ativação de vias do sistema hemostático.

i. NAPs

Os vermes hematófagos *Ancylostoma caninum* produzem uma variedade de pequenas proteínas anticoagulantes. Duas das quais despertam interesse devido seus aspectos funcionais. Uma delas é NAPc2 que apresenta um potente efeito inibitório (Ki = 8,4 pM) sobre o complexo FVIIa/TF. NAPc2 possui um mecanismo em duas etapas onde primariamente forma um complexo binário com FX/FXa usando um exosite distante e remoto do sítio ativo e, então, atingindo seu alvo principal que é o complexo FVIIa/TF, bloqueando sítio ativo do FVIIa (Stanssens, 1996) (esquema ilustrativo da inibição na Figura 2). O complexo FVIIa/TF é a essencial na ativação da via extrínseca da coagulação sangüínea além de acelerar a via intrínseca. Outra NAP5 se liga diretamente no sítio ativo do FXa com um constante de inibição 43 pM, o mais potente inibidor natural de FXa conhecido até então. Ambas compartilham os mesmos elementos estruturais e apresentam alta homologia seqüencial, apesar dos diferentes mecanismos de inibição da formação de trombina.

As estruturas cristalográficas de NAPc2 e NAP5 complexada com FXa sem o domínio rico em resíduos modificados γ-carboxi-glumático foram determinadas a resolução de 2.2 Å e 3.1 Å, respectivamente, o que revelou um novo exosítio no FXa importante para reconhecimento macromolecular e formação de trombina. Esse novo exosítio do FXa é fisiologicamente relevante para o reconhecimento de substratos macromoleculares e inibição do FXa, fornecendo um motivo estrutural inédito para o desenvolvimento de uma nova classe de inibidores para o tratamento de doenças trombóticas.

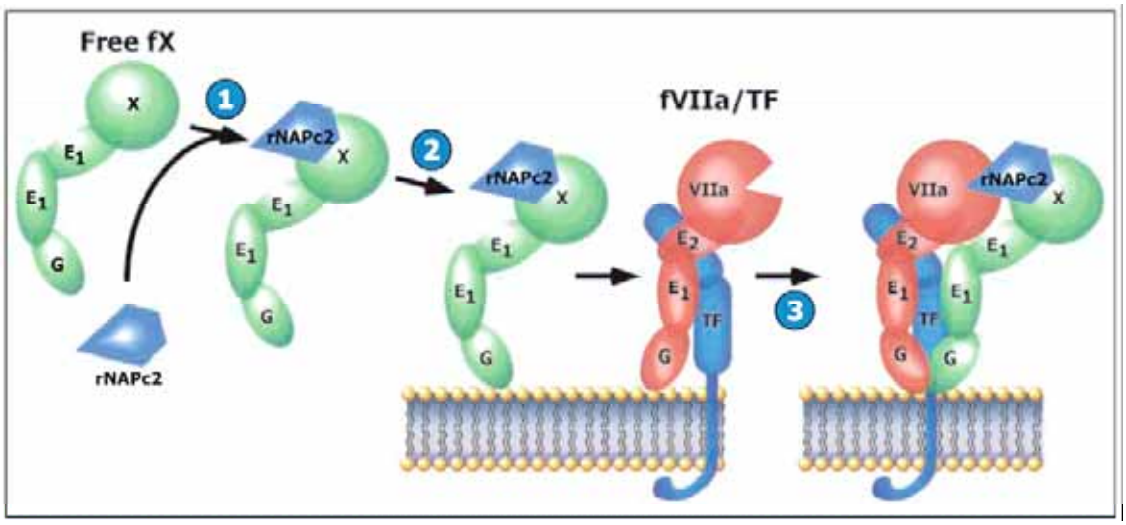

Figura 2: Esquema da inibição da via extrínseca da coagulação sangüínea pela NAPc2. Neste modelo FXa (verde) é inibido por NAPc2 (azul) e posteriormente forma um complexo quaternário com TF e FVIIa.

doi:10.1016/j.jmb.2006.11.040 J. Mol. Biol. (2006) xx, xxx–xxx

JMB

Available online at www.sciencedirect.com
ScienceDirect

ELSEVIER

Intermolecular Interactions and Characterization of the Novel Factor Xa Exosite Involved in Macromolecular Recognition and Inhibition: Crystal Structure of Human Gla-domainless Factor Xa complexed with the Anticoagulant Protein NAPc2 from the Hematophagous Nematode *Ancylostoma caninum*

M. T. Murakami[1], J. Rios-Steiner[2], S. E. Weaver[2], A. Tulinsky[2] J. H. Geiger[2]* and R. K. Arni[1,3]*

[1]*Department of Physics IBILCE/UNESP, São José do Rio Preto, SP, Brazil*

[2]*Department of Chemistry Michigan State University East Lansing, MI, USA*

[3]*Center for Applied Toxinology CAT-CEPID, São Paulo SP, Brazil*

*Corresponding authors

NAPc2, an anticoagulant protein from the hematophagous nematode *Ancylostoma caninum* evaluated in phase-II/IIa clinical trials, inhibits the extrinsic blood coagulation pathway by a two step mechanism, initially interacting with the hitherto uncharacterized factor Xa exosite involved in macromolecular recognition and subsequently inhibiting factor VIIa (K_i=8.4 pM) of the factor VIIa/tissue factor complex. NAPc2 is highly flexible, becoming partially ordered and undergoing significant structural changes in the C terminus upon binding to the factor Xa exosite. In the crystal structure of the ternary factor Xa/NAPc2/selectide complex, the binding interface consists of an intermolecular antiparallel β-sheet formed by the segment of the polypeptide chain consisting of residues 74–80 of the NAPc2 with the residues 86–93 of factor Xa that is additional maintained by contacts between the short helical segment (residues 67–73) and a turn (residues 26–29) of NAPc2 with the short C-terminal helix of factor Xa (residues 233–243). This exosite is physiologically highly relevant for the recognition and inhibition of factor X/Xa by macromolecular substrates and provides a structural motif for the development of a new class of inhibitors for the treatment of deep vein thrombosis and angioplasty.

Keywords: factor Xa exosite; nematode anticoagulant protein; selectide inhibitor; factor VIIa/tissue factor complex; inhibition

Introduction

Vascular injuries prompt the activation of an intricate and balanced cascade of reactions that involve a number of serine proteases and macromolecular cofactors ultimately culminating in the formation of a stable, cross-linked clot to stem blood loss. Factor Xa (fXa) plays a pivotal and central role in the coagulation cascade by uniting the intrinsic and extrinsic pathways and also by participating in the formation of the prothrombinase complex (prothrombin/fXa/factor Va/cellular surface/Ca^{+2}) that converts prothrombin to thrombin by limited proteolysis.[1] Thrombin subsequently reacts with fibrinogen to produce the fibrin network. The factor

Present address: J. Rios-Steiner, Department of Chemistry, University of Puerto Rico, Mayaguez, Puerto Rico.

Abbreviations used: fXa, activated factor X; Gla, γ-carboxyglutamic acid; EGF, epidermal growth factor; NAPs, nematode anticoagulant proteins; fVIIa, activated factor VII; TAP, tick anticoagulant protein; TF, tissue factor; des-fXa, fXa less its γ-carboxyglumatic domain; r.m.s.d., root mean square deviations.

E-mail addresses of the corresponding authors: geiger@cem.msu.edu; arni@ibilce.unesp.br

0022-2836/$ - see front matter © 2006 Published by Elsevier Ltd.

X (fX) light chain consists of an N-terminal Gla domain (post-translationally modified γ-carboxyglutamate residues)[2] and two epidermal-growth-factor-like (EGF) domains.[3,4] The heavy chain, which harbors the serine protease catalytic domain, shares extensive structural and sequential homology with other vitamin K-dependent serine proteases.[5]

Thrombosis, abnormal blood coagulation, occurs in a variety of cardiac disorders including angina, pulmonary embolism, atrial fibrillation, post myocardial infarction, and stroke. Nematode anticoagulant proteins (NAPs) from the hematophagous nematode *Ancylostoma caninum* inhibit blood coagulation and have been targeted as potential therapeutic agents for the control and regulation of thrombosis.[6,7] The NAPs, specifically NAP5, NAP6 and NAPc2, are small (75–84 amino acid residues) disulfide linked proteins that preferentially inhibit fXa and factor VIIa (fVIIa). NAP5 inhibits the amidolytic activity of fXa with a $K_i = 43$ pM; the only other natural inhibitor of fXa comparable to NAP5 is tick anticoagulant peptide (TAP) ($K_i = 59$ pM).[8] NAP6, a highly homologous member of the family, inhibits the catalytic activity of fXa with a K_i ~1.0 nM. TAP, NAP5 and NAP6, inhibit thrombin formation by direct association at the catalytic site of fXa. NAPc2 only partially inhibits the amidolytic activity of fXa and prevents the formation of α-thrombin by binding to a site distinct and remote from the active site, thus representing the basis for the development of a promising new class of fXa exosite inhibitors. The resultant binary complex inactivates the tissue factor (TF)-fVIIa complex with a $K_i = 8.4$ pM.[7] Isothermal titration calorimetry and fluorescence experiments indicate that the COOH terminus of the heavy chain of human fXa contributes to the high affinity interaction with NAPc2 however; the structural details of this interaction have not been characterized.[9] NMR results of NAPc2 indicate that the core is principally stabilized by five-disulfide bridges and two β sheets, each composed of two short antiparallel strands and that the molecule is highly flexible, exhibiting large amplitude structural variations at both the N and C termini and in the reactive-site binding loop.

Current clinical strategies for the control of blood coagulation are primarily based on molecules derived from coumarins that inhibit the post-translational γ-carboxylation of glutamate residues on vitamin K-dependent coagulations factors and heparin analogues that enhance inhibition of thrombin and fXa by antithrombin III. These anticoagulants drugs are non-selective and display therapeutic limitations in their ability to maintain the balance of the haemostatic system, thus providing the impetus for the search and development of new exosite anticoagulants with high macromolecular selectivity and low harmful side effects. NAPc2 represents a new class of the TF/fVIIa pathway inhibitors that is significantly more potent and specific than low molecular weight heparins and it is undergoing clinical trials to evaluate their utility as anticoagulants. NAPc2 is in Phase II clinical trials for the treatment and prevention of deep vein thrombosis following orthopedic surgery and in Phase IIa trials in angioplasty patients.

The crystal structure of human Gla-domainless fXa (des-fXa) complexed with recombinant NAPc2 determined at 2.2 Å resolution demonstrates that NAPc2 binds in a shallow surface depression at the COOH terminus of fXa that is parallel to the β-strand (β5) of the barrel, extending to the 60s-loop. This novel exosite on fXa could serve as a platform for the design of new drugs for the treatment of haemostatic disorders.

Results and Discussion

Overall structure of the ternary complex

Crystallographic refinement of the ternary complex fXa-NAPc2-selectide at 2.2 Å resolution converged to a crystallographic residual of 22.1% ($R_{free} = 26.7\%$). The asymmetric unit contains one des-fXa molecule (catalytic and EGF2 domains), one NAPc2 molecule, a selectide inhibitor (TyrD-Ile-Arg-Leu-PrN), one Na^+, three acetate and six PO_4^{2-} ions. Analysis of the stereochemistry of the final model indicates that the main-chain dihedral angles for all residues are located in the permitted regions of the Ramachandran diagram and that the root mean square deviations (r.m.s.d.) from ideal values are distributed within the expected ranges for well-refined structures (Table 1). Except for a few side-chains, which are present on the surface, the C-terminal EGF2 domain and the catalytic domain of des-fXa are well defined in the final ($2F_o–F_c$) electron density map. The entire N-terminal EGF1 domain, and its leading pentapeptide, which is flexibly disordered in other des-fXa structures[10–12] was not located in the electron density maps. As observed in other inhibited fXa structures,[11–13] there are no apparent cleavages in the autolysis loop region of the ternary complex (His145–Thr153) as reported for the native structure.[10] Optimal superpositioning of the C^α positions of the catalytic and EGF2 domains of the ternary complex on those of the native fXa (PDB code 1HCG) results in a r.m.s.d. of 0.46 Å for 256 of a total of 292 C^α atoms; a shift is observed in the 72–80 loop and additional deviations are principally located in the autolysis loop region.

The sodium-binding site first characterized in fXa[14] was subsequently identified in thrombin[15] and activated protein C.[16] In the structures of fXa and thrombin, the Na^+ is sandwiched between the 184–189 and 221–225 loops.[17] Similarly, the Na+ in the ternary complex structure is penta-coordinated by the carbonyl oxygen atoms of Tyr184 (3.05 Å), Lys186 (3.22 Å), Arg222 (2.94 Å), Lys224 (3.09 Å) and a water molecule, 43W (2.89 Å). Interestingly, each of the opposite faces of the 184–189 and 221–225 loops are coordinated by a PO_4^{2-} (Figure 1(a)). In the 184–189 loop, the PO_4^{2-} is coordinated by main-

t1.2 **Table 1.** Data collection and refinement statistics

t1.3	*Crystal preparation*	
t1.4	Cryoprotectant solution	20% glycerol
t1.5	Soaking time	20 s
t1.6		
t1.7	*Data collection*	
t1.8	Wavelength (Å)	1.00
t1.9	Temperature (K)	100
t1.10	Detector	MARCCD
t1.11	Synchrotron radiation source	Advanced Photon Source-IMCA-CAT beamline
t1.12	Space group	$P2_12_12_1$
t1.13	Unit cell parameters (Å)	$a=48.95$, $b=86.41$, $c=145.89$
t1.14	Resolution (Å)	40.0–2.2
t1.15	N° molecules in the asymmetric unit	1 fXa+ 1 NAPc2+ 1 selectide
t1.16	Solvent content (%)	66.9
t1.17	V_M ($Å^3Da^{-1}$)	3.7
t1.18	N° reflections	498,336
t1.19	N° unique reflections	32,280 (2.27)
t1.20	$I/\sigma<I>$	21.5 (7.5)
t1.21	Multiplicity	7.5 (7.0)
t1.22	Completeness (%)	100.0 (99.7)
t1.23	R_{merge}[a] (%)	6.8 (22.2)
t1.24		
t1.25	*Structure refinement statistics*	
t1.26	R_{factor} (%)	21.9
t1.27	R_{free} (%)	26.9
t1.28	r.m.s.d. bond distances (Å)	0.024
t1.29	r.m.s.d. bond angles (°)	2.14
t1.30	Average *B*-factors ($Å^2$)	45.4
t1.31		
t1.32	*Ramachandran plot Analysis*	
t1.33	Residues in most favored regions (%)	81.4
t1.34	Residues in allowed regions (%)	14.7
t1.35	Residues in generously allowed regions (%)	3.9
t1.36	Residues in disallowed regions (%)	0
t1.37	Number of non-glycine residues	285
t1.38		
t1.39	*Final model*	
t1.40	Number of amino acid residues	326
t1.41	Number of modeled water molecules	260
t1.42	Number of phosphate ions	6
t1.43	Number of acetate ions	3
t1.44	Number of sodium ions	1

Statistical values for the highest resolution shells are given in t1.45 parentheses.

[a] $R_{merge}=\Sigma|I(h)_I-\{I(h)\}|/\Sigma\{I(h)\}$, where I_h is the observed intensity of the *i*th measurement of reflection *h* and $\{I(h)\}$ is the t1.46 mean intensity of reflection *h* calculated after scaling.

chain amide N–H groups of residues Asp185A (phosphate O1 atom, 2.69 Å), Thr185B (phosphate O3 atom, 2.53 Å), Lys186 (phosphate O2 atom, 2.94 Å) and a water molecule 57W (phosphate O4 atom, 3.22 Å) (Figure 1(a)). In the 221–225 loop, the PO_4^{2-} occludes the entrance to the sodium-binding site by interacting with Glu187NE2 (phosphate O3 atom, 3.12 Å), Lys223 (phosphate O3 atom, 2.47 Å) and solvent molecules 146W and 415W (phosphate O4 atom, 2.89 and 2.63 Å, respectively). As in fVIIa,[18] factor IXa[19] and trypsin,[20] fXa also possesses a calcium-binding site in the catalytic domain formed by the 70–80 loop, however, no electron density that could be attributed to the presence of the Ca^{2+} was observed in this region.

Interactions between fXa and the selectide inhibitor

The selectide inhibitor represents a new class of fXa inhibitors and is formed by a penta-peptide containing a N-terminal D-tyrosine, followed by isoleucine, arginine, leucine and terminates with a modified proline possessing a carboxamide group instead of a carboxyl group. The selectide inhibitor binds in the active-site cleft occupying the S1, S2 and acyl binding sites. Despite the high specificity of fXa for arginine residues in the S1 specificity pocket, TyrD1 occupies this sub-site and the hydroxyl group of TyrD1 interacts *via* a water molecule with the carbonyl oxygen of Ile227 and the side-chain carboxylate oxygen of Asp189OD1 (Figure 1(b)). Additionally, TyrD1N is hydrogen bonded to the

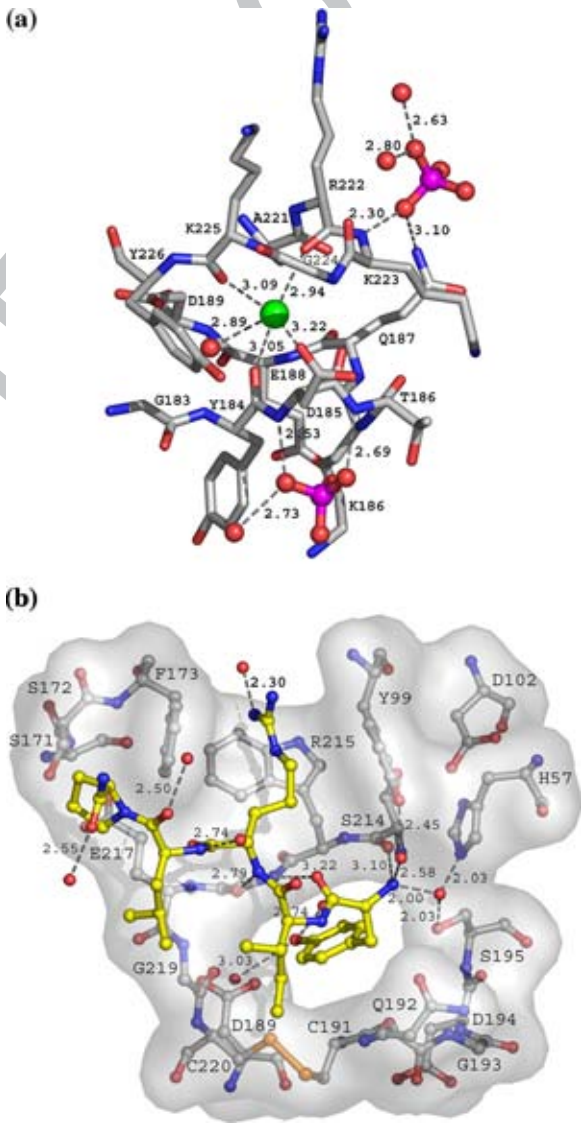

Figure 1. Interactions formed in: (a) the sodium-binding site (carbon in gray; sodium in green; phosphate in pink and red); and (b) the active-site pocket of fXa (carbon in gray) by the selectide inhibitor (carbon in yellow).

carbonyl oxygen of Ser214 and interacts with His57NE2 and Ser195OH *via* a water molecule (Figure 1(b)). Arg3NH2 of the selectide inhibitor also participates in a water-mediated interaction with the carbonyl oxygen of Ile174. The plane of the positively charged guanidinium group of Arg3 stacks parallel to the π-electron face of Phe174 of fXa (contacts <3.5 Å) leading to a cation-π electron-mediated interaction or ion-quadrupole attraction,[21–24] which appears to be unique to fXa (Figure 1(b)).[11,12,25,26] The phenyl group of Phe174 is slightly displaced by the encroaching guanidinium group of Arg3 of selectide compared to native fXa. Two other aromatic residues in the vicinity (Tyr99, Trp215) have also been implicated to play a role in the cation recognition interaction by fXa.[11,24,26] Additional contacts that occur between fXa and the selectide inhibitor are presented in Table 2.

Binding and conformational changes of NAPc2

NMR results indicate that NAPc2 is extremely flexible and it has been suggested that it is likely to become structured upon binding to fXa.[27] The β-strands and the two turns of α-helix are fairly well-defined in all 18 different NMR structures of NAPc2. Our crystallographic results indicate that NAPc2 only becomes partially structured after binding to fXa. Based on the electron density maps, we were able to construct the 6–13 and 21–30 regions and the C-terminal extension (50–83 residues) of NAPc2 (Figure 2(a) and (b)). The rest of the molecule is highly disordered and the electron density maps are characterized by diffuse electron density. The first residue observed is Cys6 that forms a disulfide bridge with Cys50. The next disordered region encompasses Cys14 to Glu20. Cys15 forms a disulfide bridge with Cys46; Cys46 is also part of a large, disordered region of NAPc2, which encompasses residues Glu31 to Asp49. The C-terminal region is mostly ordered and a dramatic conformational change occurs at the C terminus of NAPc2 when bound to fXa compared to the relative orientation of the C terminus observed in the NMR structure of NAPc2 (Figure 2(a)). The binding interface consists of an intermolecular antiparallel β-sheet formed between the segments comprised of residues 86–93 of fXa (residue numbering based on chymotrypsinogen)[28] and the C terminus (residues 74–80) of NAPc2 (Figure 3(c)) and additionally involves interactions between the 61–65 segment of fXa and the C-terminal extension (residues 81–83) of NAPc2. Other important contacts forming hydrogen bonds involve the 26–29 turn and the 67–73 helix from NAPc2 with the short C-terminal helix of fXa (a complete list of contacts is presented in Table 2). The interactions formed between NAPc2 and fXa are principally restricted to the well-ordered regions

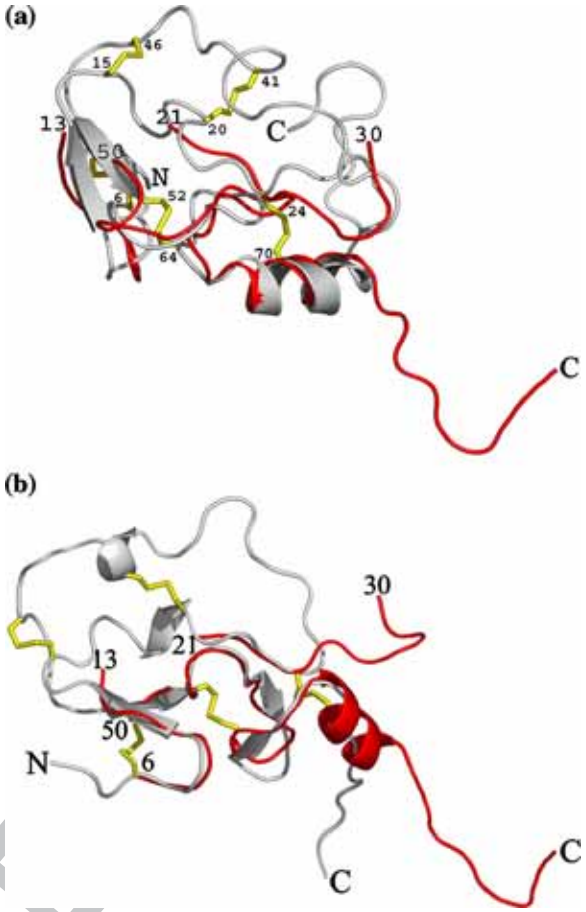

Figure 2. Overlays of the NAPc2 crystallographic structure (red) on (a) the NMR-derived average structure (gray); and (b) crystallographic structure of NAP5 (gray; J.R.S. and A.T., unpublished results).

t2.1 **Table 2.** Hydrogen bond interactions formed between
t2.2 NAPc2 and fXa, and selectide and fXa

t2.3	NAPc2	fXa	Distance (Å)
t2.4	Asp27OD1	Arg125NH2	2.38
t2.5	Asp27OD2	Trp237N	3.02
t2.6	Asp27OD2	Leu235N	3.28
t2.7	Asp27OD2	Lys236N	2.94
t2.8	Asp27OD2	Arg125NH2	2.96
t2.9	Gly28O	Asn178ND2	2.86
t2.10	Glu68OE2	Lys243NZ	2.79
t2.11	Asp69OD2	Arg240NH1	3.07
t2.12	Asp73O	Asn9ND2	2.99
t2.13	Asn74OD1	Arg93NE	3.35
t2.14	Asn74O	Asn92N	2.86
t2.15	Asn74O	Trp237NE1	3.18
t2.16	Asp76N	Lys90O	3.31
t2.17	Asp76O	Lys90N	2.90
t2.18	Ile78N	Val88O	3.25
t2.19	Ile78O	Val88N	2.66
t2.20	Gly81O	Lys62O	2.65
t2.21	Thr82N	Lys62O	2.52
t2.22	Arg83N	Ala61O	2.97
t2.23	Arg83N	Tyr60O	2.54
t2.24			
t2.25	Selectide	fXa	Distance (Å)
t2.26	TyrD1N	Ser214O	3.10
t2.27	TyrD1N	His57NE2	3.16
t2.28	TyrD1O	Gly216N	3.24
t2.29	Arg3N	Gly216O	2.79
t2.30	Arg3NH1	Glu97O	2.85

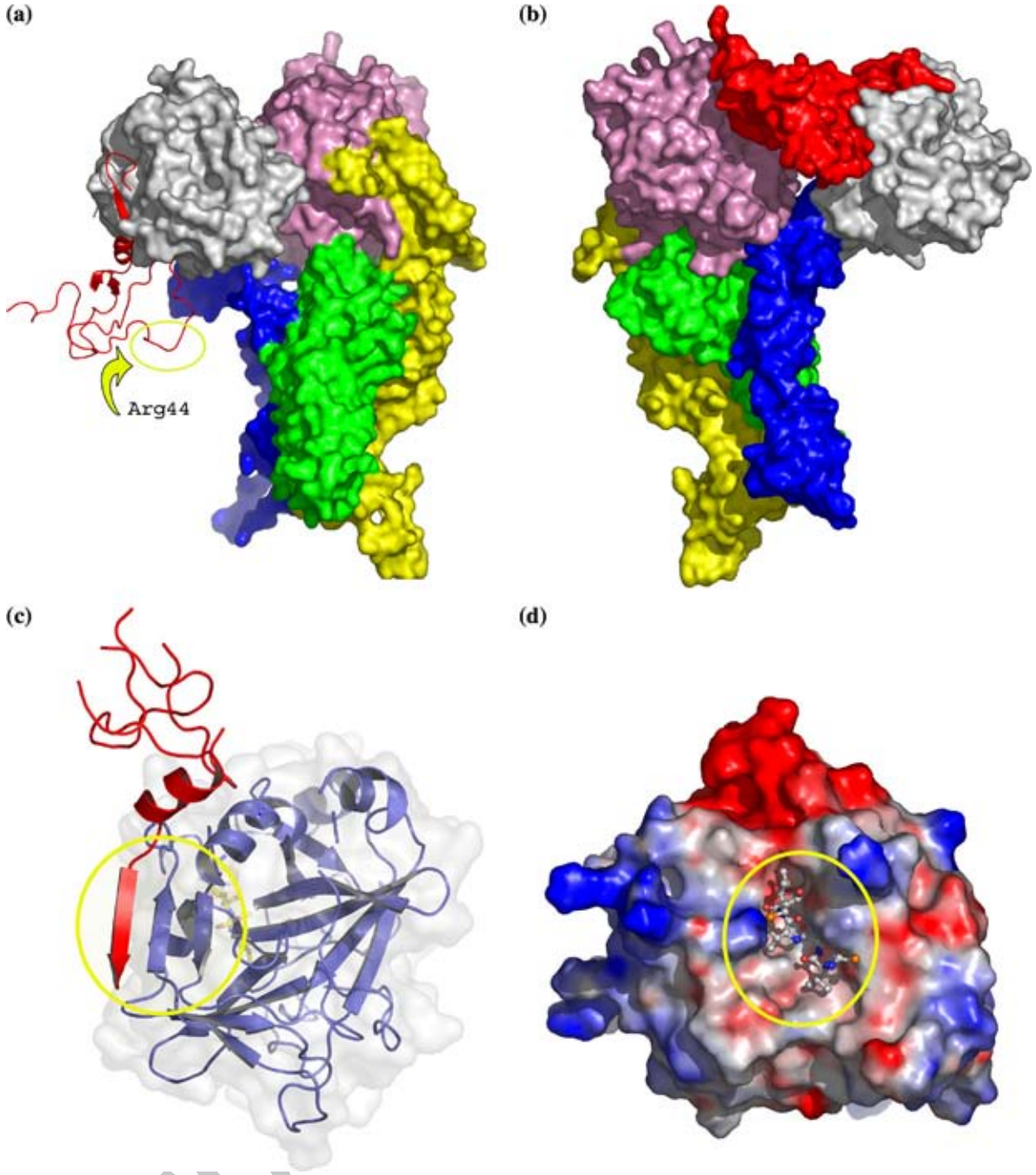

Figure 3. (a) Surface representation of the model of the complex TF (green), fVIIa (catalytic domain in pink and EGF1, EGF2 and Gla domains in yellow), fX (catalytic domain in gray and EGF1, EGF2 and Gla domains in blue). NAPc2 is in red (ribbon representation), yellow circle and arrow indicate the position of the insertion-loop containing the P1 (Arg44) residue. (b) Same as (a) but with the fXa re-positioned to permit the simultaneous binding of NAPc2 to the fXa exosite and the fVIIa active site. (c) Ribbon representation of the fXa-NAPc2 complex. The yellow circle indicates the antiparallel β-strand interactions between NAPc2 (red) and fXa (dark blue). (d) Surface charge of fVIIa with the modeled peptide fragment of the NAPc2 insertion-loop containing Arg44 in the active site cavity.

observed in the NMR structures and the C-terminal region of NAPc2.

Despite the high sequential (>54%) and structural homology between NAPc2 and NAP5 the mechanism of inhibition of fXa is different for NAP5 (active site inhibition, Figure 4(c)) and NAPc2 (Figure 4(a) and (c)).[7] Analogous to the reactive-site NAP5 P1 residue Arg40, NAPc2 contains an arginine at position 44 that likely interacts with the active site of fVIIa.

Interestingly, in the crystal structure of the binary complex of fXa/NAP5, a similar interaction is observed with relation to a symmetry-related fXa molecule, wherein the C terminus of NAP5 inter-

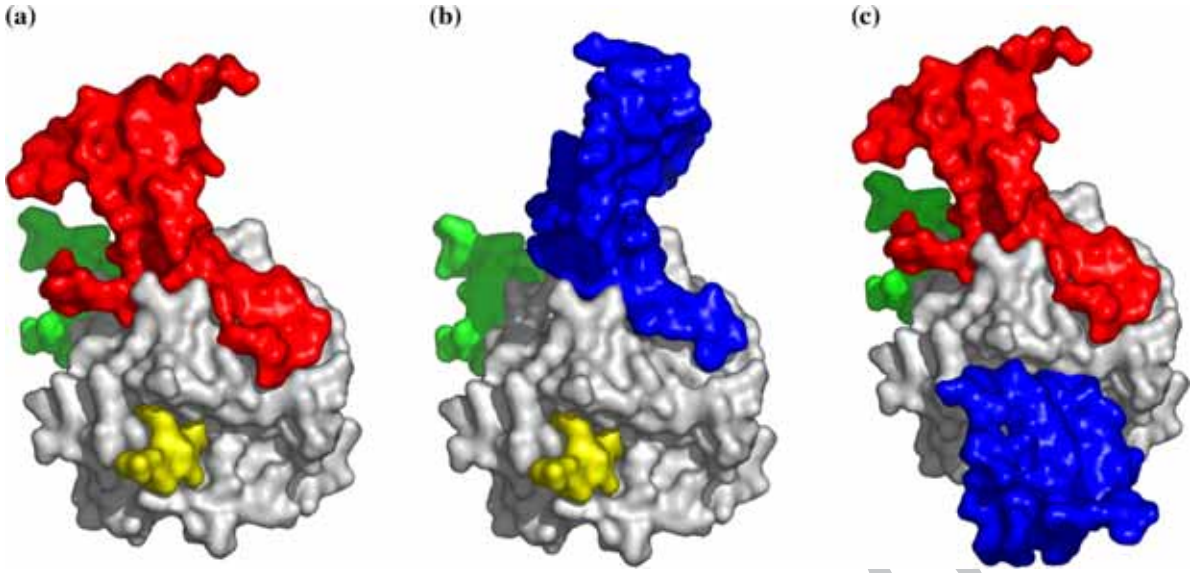

Figure 4. Active and exosite interactions: fXa (gray), EGF2 (green), selectide (yellow), NAPc2 (red) and NAP5 (blue). (a) The model of the fXa-NAPc2-selectide complex indicating the relative position of the exosite in relation to the active site. (b) The similar interaction of NAP5 with a symmetry-related fXa molecule at the exosite (J.R.S. and A.T., unpublished results). (c) Exosite binding of NAPc2 and active site binding of NAP5.

acts with this exosite (Figure 4(b)) (unpublished results).

Insights into the inhibition of the TF/fVIIa/fXa complex

The ternary complexes TF/fVII/fXa, TF/fVIIa/fX, and TF/fVIIa/fXa are of interest as targets for the inhibition of both the coagulation and cell-signaling pathways that are pivotal in cardiovascular disease and inflammation. In order to elucidate the mode of inhibition of TF/fVIIa by NAPc2 bound to fXa, the missing regions of NAPc2 were completed using the diffuse electron density and the NMR models as guides, since the important insertion-loop (31–49 loop) that contains the scissile bond Arg44–Val45 is disordered in the fXa-NAPc2-selectide complex. The interaction of NAPc2 with the catalytic site of fVIIa results in the insertion of the 31–49 loop that contains the cleavage site formed by Arg44. This loop region of the inhibitor was predicted to form the reactive sequence based on the sequence of analogous domains in similar small protein inhibitors of serine proteases[7] and compared with the structure of the NAP5-fXa complex (J.R.S. and A.T., unpublished results).

The proposed theoretical model of the TF/fVIIa/fXa complex built based on the available structures of the TF/fVIIa complex and fXa by protein–protein docking calculations and site-directed mutagenesis indicates that the fXa model adopts an extended conformation, similar to that of fVIIa in the TF/fVIIa complex, forming extensive interactions with TF and the protease domain of fVIIa. All four domains of fXa are involved in the interaction and the residues Glu51 and Asn57 in the EGF1 domain, Asp92 and Asp95 in the EGF2 domain and Asp185, Lys186, and Lys134 in the serine protease domain of fXa participate in the interaction with TF/fVIIa (PDB entry: 1NL8).[29]

Superpositioning the atomic coordinates of the NAPc2/fXa complex on the coordinates of the theoretical model of the TF/fVIIa/fXa complex indicates that the position of the NAPc2 insertion-loop containing the P1 (Arg44) residue is located more than 20 Å from the active-site pocket of fVIIa, thus being unable to simultaneously inhibit fVIIa and fX/Xa (Figure 3(a)). In order to obtain a more compatible model, the serine protease domain of fXa was re-positioned to permit the simultaneous interaction of NAPc2 with both the exosite of fXa and the active site of fVIIa (Figure 3(b)) without altering the interactions formed between the EGF and Gla domains of fXa with TF. In the absence of the crystal structure of the ternary complex fXa/fVIIa/TF that would precisely delineate the interface involved, the insertion-loop containing the P1 (Arg44) residue was modeled at the active site of fVIIa based on the crystal structure of the binary complex fXa-NAP5 (J.R.S. and A.T., unpublished results; Figure 3(d)). In this model, the side-chain of Arg44 occupies the S1 specificity site of fVIIa adopting an extended conformation and forming a N–O salt-bridge through its guanidium group and carboxylate oxygen atoms of Asp189. Val43, the P2 residue, is in close proximity to His57 and Lys60. Additionally, Leu42 is positioned optimally at the P3 position of the substrate forming hydrophobic contacts with Trp215 of fVIIa. Another valine residue (Val45) occupies the P1′ position followed by Cys46 at the P2′ position.

Bovine fXa *versus* human fXa

A weaker interaction (K_d = 260–500 nM) has been reported for the binding of NAPc2 with bovine fXa,

but the high affinity was restored to a recombinant chimeric bovine fX derivative containing 25 residues from the COOH terminus of the serine proteinase domain of human fX, suggesting that this region is responsible for species selectivity.[9] The lower affinity interaction between NAPc2 and bovine fXa is correlated with a more rapid elimination half-life of ~87 min in this species *versus* days in humans. Significant differences between the C terminus of bovine and human fXa are observed in the C-terminal region (244 to 251), which is structurally highly flexible in human fXa. This motif is ordered in only one structure of human fXa[10] (PDB entry: 1HCG) that is similar to bovine fXa. Upon NAPc2 binding to human fXa, the C-terminal region of fXa adopts a different conformation, by moving outwards as observed in the crystal structure (1HCG). Superpositioning the structures of bovine and human fXa (PDB entry: 1HGC) with the structure of human fXa bound to NAPc2 indicates the presence of several short contacts between the C-terminal regions (244–251) of bovine fXa and human fXa and the C-terminal extension of NAPc2. Sequence alignments of both bovine and human fXa indicate a high degree of sequence homology in the region 237 to 244, the exception being Ile241 in the bovine enzyme that is changed to Ser241 in the human enzyme. Ser241 does not participate in the binding of NAPc2 to human fXa, but the substitution of serine by isoleucine would prevent the approach and binding of NAPc2, resulting in steric clashes with Leu72, Met75 and Phe77. Another significant difference is observed in the 245–251 region of the C terminus; human fXa possesses predominantly positively charged residues (Gly-Leu-Pro-Lys-Ala-Lys), whereas this region in bovine fXa is mainly hydrophobic (Ala-Gly-Ala-Ala-Gly-Ser). Since this region does not participate in the binding of NAPc2 and is flexible, it likely does not play an important role in the binding of NAPc2 in either human or bovine fXa.

Functional implications and concluding remarks

The fVIIa/TF complex is an attractive target for the development of new anticoagulant drugs due to its strategic position in the blood coagulation cascade. Since NAPc2 binds to catalytically active, inhibited and a mutant of zymogen fX with similar affinities it represents a new class of fX/Xa and fVIIa/TF complex inhibitors with potential applications in the prevention and treatment of venous and arterial thrombosis and in the control of disseminated intravascular coagulopathies.

The crystal structure of the ternary fXa-NAPc2-selectide complex in conjunction with the biochemical results currently available; provide further insights in understanding its unique mechanism for fVIIa/TF inhibition. NMR and crystallographic results indicate that NAPc2 is extremely flexible even after binding to fXa, however, the C-terminal region becomes structured after binding to fXa and a large conformational change occurs resulting in the formation of an antiparallel β-sheet formed by residues 87–93 in the C-terminal region of fXa and residues 74–80 of NAPc2.

Despite the high specificity of fXa for arginine residues in the S1 specificity pocket, TyrD1 and not Arg3 occupies this position in the selectide inhibitor. TyrD1 does not directly interact with Asp189 but occludes the entrance of the S1 specificity pocket maintained by water-mediated interactions between the hydroxyl group of TyrD1 with the carbonyl oxygen of Ile227 and the carboxylate group of Asp189OD1.

These structural results and the delineation of the till now elusive exosite shed light on the direct inhibition of fXa and suggest modes for the indirect inhibition of VIIa.

Materials and Methods

Preparation and crystallization of the ternary complex

Human des-fXa[30] was purchased from Haematologic Technologies, Inc. Recombinant NAPc2[31] and the selectide inhibitor (TyrD-Ile-Arg-Leu-Prn; SEL2060) were provided by Corvas International, Inc and Selectide Corp., respectively. A molar ratio of 1.2:1.2:1 of NAPc2 and selectide to des-fXa was equilibrated overnight at 4 °C, dialyzed to remove excess ligands and concentrated to 10 mg/ml in 50 mM Tris-HCl, 20 mM NaCl buffer (pH 7.5). Single crystals of the ternary complex were obtained by the hanging-drop vapour-diffusion crystallization method where 1 μl of the complex was mixed with an equal volume of the reservoir solution containing 0.05 M potassium dihydrogen phosphate, 0.1 M sodium acetate (pH 5.6) and 16% (w/v) polyethylene glycol 8000.

Data collection, processing, structure determination and refinement

X-ray diffraction data were collected from cryo-protected crystals at 100 K at the Advanced Photon Source (IMCA-CAT beamline, Argonne National Laboratory) where the wavelength was set to 1.0 Å, a MAR-CCD detector was used to record the diffraction intensities and the data were reduced and scaled using the DENZO/SCALEPACK suite of programs.[32] The crystals belong to the orthorhombic space group $P2_12_12_1$ with cell dimensions $a=48.94$, $b=86.41$ and $c=145.89$ Å. The orientation and position of the catalytic and EGF2 domains of des-fXa were determined with the program AMoRe[33] using the coordinates of the same modules of native des-fXa[10] (PDB code 1HCG) stripped of solvent molecules. Examination of the $(2F_o–F_c)$ and $(F_o–F_c)$ difference electron density maps revealed density corresponding to segments of the NAPc2 molecule bound to the C terminus and β-strand (B5) of fXa and the selectide inhibitor bound at the active-site cleft. However, no electron density was present to account for the EGF1 domain as reported previously for both the native[10] and inhibited des-fXa structures.[12,13] The NAPc2 structure was determined by manual iterative interpretation of the electron density maps. The residues 1–5, 15–20 and 34–49 are highly disordered and were not included in the model during the refinement. In the final stages, the complete structure of NAPc2 was modeled based on the NMR structures using regions characterized

by diffuse density as a guide. Positional and restrained isotropic *B*-factor refinements were performed using REFMAC5,[34] all model building was carried out utilizing TURBO-FRODO[35] and PROCHECK[36] was utilized to evaluate the stereochemistry of the final structural model. Statistics of the intensity data processing and refinement are presented in Table 1.

Protein Data Bank accession code

The atomic coordinates and structure factors of human Gla-domainless factor Xa complexed with the anticoagulant protein NAPc2 from the hematophagous nematode *Ancylostoma caninum* and selectide inhibitor have been deposited with the RCSB Protein Data Bank, entry code 2H9E, Research Collaboration for Structural Bioinformatics, Rutgers University, New Brunswick, NJ†.

Acknowledgements

We are grateful to Dr G. Vlasuk for the NAPc2 samples used in this study and for reading the manuscript critically. This work was supported by grants from FAPESP (04/13082-3; 04/11258-0), CAPES/PROBRAL/DAAD (186/04), SMOLBNet (01/07537-2), CNPq (473097/2004-4; 501500/2005-7) and CAT/CEPID to R.K.A.; Michigan Economic Development Corp. to A.T. and J.H.G. and NIH grant HL43229 to A.T. M.T.M. is the recipient of a FAPESP (04/13054-3) fellowship.

References

1. Mann, K. G., Nesheim, M. E., Church, W. R., Haley, P. & Krishnaswamy, S. (1990). Surface-dependent reactions of the vitamin K-dependent enzyme complexes. *Blood*, **76**, 1–16.
2. Suttie, J. W. (1985). Vitamin K-dependent carboxylase. *Annu. Rev. Biochem.* **54**, 459–477.
3. McMullen, B. A., Fujikawa, K., Kisiel, W., Sasagawa, T., Howald, W. N., Kwa, E. Y. & Weinstein, B. (1983). Complete amino acid sequence of the light chain of human blood coagulation factor X: evidence for identification of residue 63 as beta-hydroxyaspartic acid. *Biochemistry*, **22**, 2875–2884.
4. Fernlund, P. & Stenflo, J. (1983). Beta-hydroxyaspartic acid in vitamin K-dependent proteins. *J. Biol. Chem.* **258**, 12509–12512.
5. Davie, E. W., Fujikawa, K. & Kisiel, W. (1991). The coagulation cascade: initiation, maintenance, and regulation. *Biochemistry*, **30**, 10363–10370.
6. Cappello, M., Vlasuk, G. P., Bergum, P. W., Huang, S. & Hotex, P. (1995). Ancylostoma caninum anticoagulant peptide: a hookworm-derived inhibitor of human coagulation factor Xa. *Proc. Natl Acad. Sci. USA*, **92**, 6152–6156.
7. Stanssens, P., Bergum, P. W., Gansemans, Y., Jespers, L., Laroche, Y., Huang, S. *et al.* (1996). Anticoagulant repertoire of the hookworm Ancylostoma caninum. *Proc. Natl Acad. Sci. USA*, **93**, 2149–2154.
8. Waxman, L., Smith, D. E., Arcuri, K. E. & Vlasuk, G. P. (1990). Tick anticoagulant peptide (TAP) is a novel inhibitor of blood coagulation factor Xa. *Science*, **248**, 586–593.
9. Buddai, S. K., Toulokhonova, L., Bergum, P. W., Vlasuk, P. & Krishnaswamy, S. (2002). Nematode anticoagulant protein c2 reveals a site on factor Xa that is important for macromolecular substrate binding to human prothrombinase. *J. Biol. Chem.* **277**, 26689–26698.
10. Padmanabhan, K., Pdmanabhan, K. P., Tulinsky, A., Park, C. H., Bode, W., Huber, R. *et al.* (1993). Structure of human des(1–45) factor Xa at 2.2 A resolution. *J. Mol. Biol.* **232**, 947–966.
11. Brandstetter, H., Kuhne, A., Bode, W., Huber, R., von der Saal, W., Wirthensohn, K. & Engh, R. A. (1996). X-ray structure of active site-inhibited clotting factor Xa. Implications for drug design and substrate recognition. *J. Biol. Chem.* **271**, 29988–29992.
12. Wei, A., Alexander, R. S., Duke, J., Ross, H., Rosenfeld, S. A. & Chang, C. H. (1998). Unexpected binding mode of tick anticoagulant peptide complexed to bovine factor Xa. *J. Mol. Biol.* **283**, 147–154.
13. Kamata, K., Kawamoto, H., Honma, T., Iwama, T. & Kim, S.-H. (1998). Structural basis for chemical inhibition of human blood coagulation factor Xa. *Proc. Natl Acad. Sci. USA*, **95**, 6630–6635.
14. Orthner, C. L. & Kosow, D. P. (1978). The effect of metal ions on the amidolytic acitivity of human factor Xa (activated Stuart-Prower factor). *Arch. Biochem. Biophys.* **185**, 400–406.
15. Orthner, C. L. & Kosow, D. P. (1980). Evidence that human alpha-thrombin is a monovalent cation-activated enzyme. *Arch. Biochem. Biophys.* **202**, 63–75.
16. Steiner, S. A., Amphlett, G. N. & Castellino, F. J. (1980). Stimulation of the amidase and esterase activity of activated bovine plasma protein C by monovalent cations. *Biochem. Biophys. Res. Commun.* **94**, 340–347.
17. Zhang, E. & Tulinsky, A. (1997). The molecular environment of the Na^+ binding site of thrombin. *Biophys. Chem.* **63**, 185–200.
18. Strickland, D. K. & Castellino, F. J. (1980). The binding of calcium to bovine factor VII. *Arch. Biochem. Biophys.* **190**, 687–692.
19. Bajaj, S. P., Sabharwal, A. K., Gorka, J. & Birktoft, J. J. (1992). Antibody-probed conformational transitions in the protease domain of human factor IX upon calcium binding and zymogen activation: putative high-affinity Ca(2+)-binding site in the protease domain. *Proc. Natl Acad. Sci. USA*, **89**, 152–156.
20. Bode, W. & Schwager, P. (1975). The refined crystal structure of bovine beta-trypsin at 1.8 A resolution. II. Crystallographic refinement, calcium binding site, benzamidine binding site and active site at pH 7.0. *J. Mol. Biol.* **98**, 693–717.
21. Dougherty, D. A. & Stauffer, D. A. (1990). Acetylcholine binding by a synthetic receptor: implications for biological recognition. *Science*, **250**, 1558–1560.
22. Stauffer, D. A., Barrans, R. E. & Dougherty, D. A. (1990). Concerning the thermodynamics of molecular recognition in aqueous and organic media. Evidence for significant heat capacity effects. *J. Org. Chem.* **55**, 2762–2767.
23. Schwabacher, A. W., Zhang, S. & Davy, W. (1993). Directionality of the cation-π effect: a charge-mediated size selectivity in binding. *J. Am. Chem. Soc.* **115**, 6995–6996.
24. Lim, Z. & Johnson, M. E. (1995). Proposed cation-π mediated binding by factor Xa: a novel enzymatic

† http://www.rcsb.org/

mechanism for molecular recognition. *FEBS Letters*, **370**, 1–5.
25. St. Charles, R., Padmananbhan, K., Arni, R. K., Padmanabhan, K. P. & Tulinsky, A. (2000). Structure of tick anticoagulant peptide at 1.6 Å resolution complexed with bovine pancreatic trypsin inhibitor. *Protein Sci.* **9**, 256–272.
26. Mochalkin, I. & Tulinsky, A. (1999). Structures of thrombin retro-inhibited with SEL2711 and SEL2770 as they relate to factor Xa binding. *Acta Crystallog. sect. D*, **55**, 785–793.
27. Duggan, B. M., Dyson, H. J. & Wright, P. E. (1999). Inherent flexibility in a potent inhibitor of blood coagulation, recombinant nematode anticoagulant protein c2. *Eur. J. Biochem.* **265**, 539–548.
28. Harley, B. S. & Shotton, D. M. (1971). In *The Enzymes* (Boyer, P. D., ed), 1st edit., pp. 323–373. Academic Press, New York.
29. Norledge, B. V., Petrovan, R. J., Ruf, W. & Olson, A. J. (2003). The tissue factor/factor VIIa/factor Xa complex: a model built by docking and site-directed mutagenesis. *Proteins: Struct. Funct. Genet.* **53**, 640–648.
30. Morita, T. & Jackson, C. M. (1986). Preparation and properties of derivatives of bovine factor X and factor Xa from which the gamma-carboxyglutamic acid containing domain has been removed. *J. Biol. Chem.* **261**, 4015–4023.
31. Laroche, Y., Storme, V., De Meutter, I., Messens, J. & Lauwereys, M. (1994). High-level secretion and very efficient isotopic labeling of tick anticoagulant peptide (TAP) expressed in the methylotrophic yeast, *Pichia pastoris*. *BioTechnology*, **12**, 1119–1124.
32. Otwinoski, Z. & Minor, W. (1997). Processing of X-ray diffraction data collection in oscillation mode. *Methods Enzymol.* **276**, 307–326.
33. Navaza, J. (1993). AMoRe: an automated package for molecular replacement. *Acta Crystallog. sect. D*, **49**, 588–591.
34. Murshudov, G. N., Vagin, A. A. & Dodson, E. J. (1997). Refinement of macromolecular structures by the maximum-likelihood method. *Acta Crystallog. sect. D*, **53**, 240–255.
35. Roussel, A. & Cambillau, C. (1989). Turbo-Frodo. In *Silicon Graphics Geometry Partner Directory* (Silicon Graphics, ed), pp. 77. Mountain View, CA.
36. Laskowski, R. A., MacArthur, M. W., Moss, D. S. & Thorton, J. M. (1993). PROCHECK: a program to check the stereochemical quality of protein structures. *J. Appl. Crystallog.* **26**, 283–291.

Edited by R. Huber

(Received 7 August 2006; received in revised form 4 November 2006)

ii. Serino Proteases de Venenos de Serpentes

Serino proteases de venenos de serpentes pertencem à subfamília das tripsinas/quimotripsinas, que apresentam alta identidade seqüencial e estrutural (50-70%), apesar de serem altamente específicas e seletivas para substratos macromoleculares, tais como os fatores da coagulação sangüínea. Essas enzimas interferem no controle e regulação do sistema hemostático em diferentes níveis desde a cascata de coagulação sanguínea até o sistema anticoagulante e fibrinolítico (Tu, 1991), sendo caracterizadas como ativadoras do sistema fibrinolítico, procoagulantes, anticoagulantes e agregadoras de plaquetas (Marsh e Willian, 2005). A proteína ativadora de plasminogênio isolada do veneno de *Trimeresurus stejne*geri (TSV-PA) converte plasminogênio em plasmina pela clivagem da ligação peptidica Arg561-Val562 com alta especificidade e resistência de inibição (Zhang, et al., 1997). Batroxobin, uma trombina-símile isolado do veneno de *Bothrops atrox*, usada para o tratamento de doenças trombóticas, converte fibrinogênio em fibrina pela clivagem do fibrinopeptídeo α na região N-terminal da cadeia A do fibrinogênio. Esse processo resulta na formação de um coágulo fraco que é rapidamente removido do sistema circulatório pelo mecanismo fibrinolítico resultando num efeito defibrinogenante. A ativadora de proteína C (PC) isolada do veneno de *Agkistrodon contortrix contortrix*, comercialmente referida como protac®, especificamente converte o zimogênio de PC em PC ativada pela clivagem da ligação peptídica Arg169-Leu170, independente de trombomodulina (Kisiel et al., 1987) (Figura 3). Protac® é clinicamente usado em ensaios de quantificação de proteína S e testes de funcionalidade de PC *in vivo* (Gempler-Messina et al., 2001). Nesse trabalho, resolvemos à estrutura de protac® no estado nativo e inibido e foi observado o fator duplo de cargas positivas em torno do sítio ativo e do posicionamento estratégico de três grupos de carboidratos na região interfacial no reconhecimento e ativação da PC.

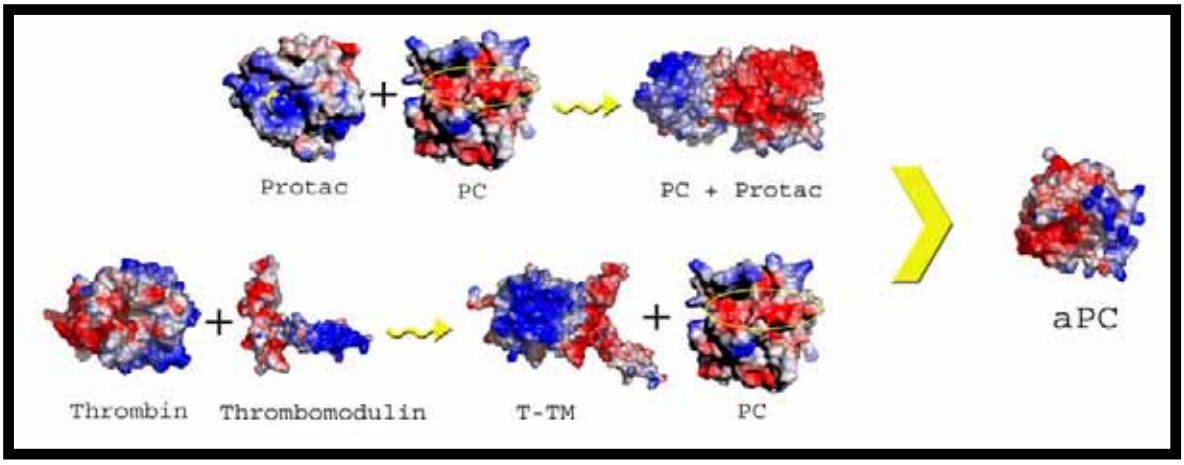

Figura 3: Via anticoagulante da proteína C. Acima: via alternativa iniciada por protac®. Abaixo: via fisiológica iniciada pelo complexo FIIa/Trombomodulina.

ELSEVIER

Toxicon 40 (2002) 1307–1312

TOXICON

www.elsevier.com/locate/toxicon

Purification, characterization and crystallization of Jararacussin-I, a fibrinogen-clotting enzyme isolated from the venom of *Bothrops jararacussu*

Raquel K. Bortoleto[a], Mário T. Murakami[a], Leandra Watanabe[a], Andreimar M. Soares[b], Raghuvir K. Arni[a,*]

[a]*Department of Physics, IBILCE/UNESP, Cristovão Colombo, 2265, Caixa Postal 136, São José do Rio Preto, SP, 15054-000, Brazil*
[b]*Department of Biotechnology, UNAERP, Ribeirão Preto, SP, Brazil*

Received 19 February 2002; accepted 30 April 2002

Abstract

A fibrinogen-clotting enzyme, Jararacussin-I, was purified from the venom of *Bothrops jararacussu* by a combination of ion exchange chromatography using Resource 15S resin and affinity chromatography using Benzamidine Sepharose 6B resin. Jararacussin-I displays a molecular mass of 28 kDa as estimated by sodium dodecyl sulphate–PAGE and possesses an isoelectric point of 5.0. The coagulant specific activity of the enzyme was determined to be 45.8 NIH U/mg using bovine fibrinogen as the substrate and the esterase specific activity was determined to be 258.7 U/mg. The protease inhibitors, benzamidine and DTT inhibited the esterase specific activity by 72.4 and 69.7%, respectively. The optimal temperature and pH for the degradation of both chains of fibrinogen and esterase specific activity were determined to be 37 °C and 7.4–8.0, respectively. The enzyme was inactivated at both 4 and 75 °C. Single crystals of Jararacussin-I were obtained and complete three-dimensional X-ray diffraction data was collected at the Brazilian National Synchrotron Source (LNLS) to a resolution of 2.4 Å. © 2002 Published by Elsevier Science Ltd.

Keywords: *Bothrops jararacussu* snake venom; Thrombin-like enzyme; Fibrinogen-clotting enzyme; Purification; Characterization and crystallization

1. Introduction

Snake venoms are rich sources of serine and metalloproteases and many of these proteases have been purified and characterized (Markland, 1991, 1998; Pirkle, 1998; Matsui et al., 2000). The complete amino acid sequences of approximately 40 of these proteases have been determined by protein sequencing or deduced from their cDNA. Some of these proteases are particularly interesting since they interfere with the control and regulation of the haemostatic systems of their prey and activate or inactivate various enzymes which participate in the blood coagulation cascade.

Recently, the three-dimensional structures of five venom proteases, four of which are metalloproteases (Matsui et al., 2000) and one serine protease (Parry et al., 1998) have been determined at high resolution by X-ray crystallography providing us with a structural basis for understanding the steric requirements for the activities of these enzymes.

A number of serine proteases have been identified in snake venoms, for example, *Calloselasma rodhostoma* Ancrod (Burkhart et al., 1992), *Bothrops atrox moojeni* Batroxobin (Itoh et al., 1987), *Bothrops jararaca* Bothrombin (Nishida et al., 1994), *Crotalus atrox* Calobin (Halton, 1973), *Crotalus adamanteus* Crotalase (Henschen-Edman et al., 1999), *Trimeresurus flavoviridis* Flavoxobin (Shieh

Abbreviations: TLEs, thrombin-like enzymes; SERPINs, serine protease inhibitors; SDS, sodium dodecyl sulphate; PMSF, phenylmethylsulfonyl fluoride; DFP, diisopropyl fluorophosphate; DTT, ditiothreitol; EDTA, ethylene diaminetetraacetic acid; EGTA, ethylene-glycol-bis(β-amino ethyl ether)tetra acetic acid; TAME, N_{α}-P-tosyl-L-arginine-methyl ester.

* Corresponding author. Tel.: + 55-17-221-2707; fax: + 55-17-221-2247.

E-mail address: arni@df.ibilce.unesp.br (R.K. Arni).

0041-0101/02/$ - see front matter © 2002 Published by Elsevier Science Ltd.
PII: S0041-0101(02)00140-X

et al., 1988) and have been shown to share high sequence identity with each other and to a lesser degree with mammalian serine proteases such as trypsin and thrombin.

These venom proteases are often referred to as thrombin-like enzymes due to their ability to cleave fibrinogen, releasing fibrinopeptide A, fibrinopeptide B or both. Some of these venom serine proteases also participate in diverse biological processes such as activation of plasminogen, protein C, factors V and X, fibrinolysis, blood coagulation and platelet aggregation. They serve as important tools and are used clinically for clotting assays, diagnosis, determination of protein C, protein S, plasma fibrinogen, study of platelet function, as defibrinogenating agents, to investigate desfibrinogenemias, test the contractile system of platelets and for defibrinogenation of plasma.

Alignments of the amino acid sequence of these serine proteases indicate that the residues forming the catalytic triad His^{57}, Asp^{102} and Ser^{195} are conserved in analagous positions as in the mammalian serine proteases (Matsui et al., 2000, 1998; Burkhart et al., 1992). Venom serine protease are inhibited by many of the commonly used serine protease inhibitors such diisopropyl fluorophosphate (DFP) and phenylmethylsulfonyl fluoride (PMSF). The venom thrombin-like serine proteases preferentially release either fibrinopeptide A or B from fibrinogen to produce abnormal fibrin clots composed of short polymers, thus interfering with the blood coagulation system of their prey (Markland, 1998; Pirkle, 1998; Ouyang et al., 1992; Tu, 1996).

This communication describes the isolation, biochemical and structural characterization of Jararacussin-I, a clotting factor of the thrombin-like enzymes (TLE) type from *Bothrops jararacussu* snake venom. Elucidation of the three-dimensional structure by X-ray diffraction techniques is currently in progress and will provide information which will be useful to understand the structure-function relationship of this enzyme.

2. Materials and methods

2.1. Materials

Desiccated *B. jararacussu* venom was obtained from a local serpentarium. Benzamidine Sepharose 6B (Amersham Pharmacia Biotech), Resource 15S (Amersham Pharmacia Biotech) and bovine fibrinogen were purchased from Sigma Chemical Co. Molecular mass standards (Amersham Pharmacia Biotech) were bovine serum albumin (66 kDa); ovoalbumin (44 kDa), carbonic anhydrase (30 kDa), soybean trypsin inhibitor (20.1 kDa) and α-lactalbumin (14.4 kDa).

2.2. Purification

Crude desiccated venom (400 mg) was dissolved in 3 ml of 0.02 M pH 7.8 phosphate buffer and centrifuged at 20,000 g to remove insoluble materials. A Pharmacia FPLC system was used for the chromatographic experiments. The clear supernatant was filtered and applied to a column packed with Resource 15S resin which had been pre-equilibrated with a 0.02 M phosphate buffer (pH 7.8). The column was washed at a flow rate of 3 ml/min with the aforementioned phosphate buffer and the unbound protein fractions were collected. The bound fractions were eluted using a linear NaCl gradient which ranged from 0 to 1.0 M in the above buffer (total elution volume was 250 ml) at a flow rate of 3 ml/min. Bovine fibrinogen was used as a substrate to test the fractions for their clotting activity. Only the fraction that did not bind to the column demonstrated clotting activity. This fraction was subsequently applied to a Benzamidine Sepharose 6B affinity column which had been pre-equilibrated with a 0.02 M phosphate buffer (pH 7.8). Unspecifically bound protein was eluted by washing with the above buffer which additionally contained 0.5 M NaCl. Once the baseline had stabilized, the tightly bound Jararacussin-I was eluted by rapidly changing the pH to 3.2 using a 0.02 M glycine–HCl buffer. The protein was immediately dialyzed against the 0.02 M phosphate buffer (pH 7.8), concentrated and stored at −80 °C.

2.3. Biochemical characterization

The molecular mass estimation was carried out by SDS–PAGE both with and without the inclusion of a reducing agent (Laemmli, 1970). Isoelectric focusing was carried out according to method of Vesterberg (1972). Buffalyte, pH range 3.5–9.5 (Pierce, IL) was used to generate the pH gradient. Neutral carbohydrate analysis was performed as previously described (Dubois et al., 1956). Protein concentration was determined by the method of Bradford (1976) using lysozyme as the standard.

2.4. Enzyme assay

Esterase activity was determined using 0.01 M N_{α}-P-tosyl-L-arginine-methyl ester (TAME) as the substrate in a solution containing 0.15 M KCl at pH 8.0 and 37 °C as described by Ehrempreis and Scheraga (1957). For the potentiometric titration, a 0.0448N KOH solution was dispensed from a Gilmont microburet. One unit of esterase activity was defined as the amount of enzyme capable of releasing 0.1 μmol of acid per 10 min at 37 °C. Clotting activity, was carried out using purified bovine fibrinogen (Sigma Chem. Co.) and was determined according to the method of Ware and Seegers (1949). One unit of coagulant activity was considered to be equivalent to one NIH thrombin unit.

2.5. Fibrinogenolytic activity

The method of Rodrigues et al. (2000) was used with

Table 1
Effects of variation of temperature, pH and the addition of inhibitors on the esterase activity of Jararacussin-I (*B. jararacussu*)

Temperature (°C)	Esterase activity (U/mg)	pH	Esterase activity (U/mg)	Inhibitors	Esterase activity (U/mg)
Control	258.72 ± 7.88	Control	258.72 ± 7.88	Control	258.72 ± 7.88
4	65.87 ± 2.13	3.5	167.34 ± 9.23	PMSF	179.55 ± 5.89
28	255.67 ± 6.45	5.5	189.45 ± 5.76	Benzamidine	78.42 ± 2.35
37	259.91 ± 6.21	7.4	241.89 ± 4.68	Aprotinin	255.98 ± 6.77
45	198.34 ± 9.84	8.0	260.34 ± 7.12	β-mercaptoethanol	114.57 ± 3.98
75	38.25 ± 4.67	9.5	202.85 ± 8.16	DTT	71.22 ± 2.61
				EDTA	261.22 ± 6.85
				EGTA	259.13 ± 5.76
				Heparin	258.93 ± 7.09

some modifications. Samples of 50 μl of bovine fibrinogen (1 mg/ml PBS) were incubated with different amounts of enzyme (0.1–4.0 μg) at 37 °C for 24 h, pH 8.0. The reaction was terminated with 25 μl of 0.05 M, pH 8.8, Tris–HCl buffer containing 10% (v/v) 2-mercaptoethanol, 2% (v/v) SDS, and 0.05% (w/v) bromophenol blue. The samples were then analyzed by SDS–PAGE gels (13.5%, w/v). Analogously, 1.0 μg of enzyme was incubated with 50 μg of fibrinogen for different periods of time (60 min to 48 h).

2.6. Heat, pH stability and enzyme inhibitors

Enzyme (2 μg) in 0.1 M Tris–HCl buffer, pH 8.0 was incubated for 60 min at different temperatures (4, 28, 37, 45 and 75 °C) and pHs (3.5, 5.0, 7.4, 8.0 and 9.5). Inhibition of esterase and fibrinogenolytic activities were assayed after preincubation of 2 μg of enzyme in 0.1 M Tris–HCl buffer, pH 8.0 for 30 min at 37 °C containing one of the following inhibitors: 10 mM PMSF, 10 mM Aprotinin, 10 mM β-mercaptoethanol, 10 mM ditiothreitol (DTT), 10 mM ethylene diaminetetraacetic acid (EDTA), 10 mM ethyleneglycol-bis(β-amino ethyl ether)tetra acetic acid (EGTA) and 100 IU/ml Heparin, as previously described.

2.7. Crystallization

The serine protease sample was concentrated to 16 mg ml^{-1} in micro concentrators, (Amicon, Centripep) and stored in a 0.02 M pH 7.8 phosphate buffer at −80 °C. Crystallization was performed by the hanging-drop vapor-diffusion method using 24-well tissue-culture plates (Jancarik and Kim, 1991). Typically, 1 μl drops of protein solution were mixed with an equal volume of the screening solution and equilibrated over a reservoir containing 1 ml of the latter solution. Once initial crystallization conditions had been determined, they were optimized and large single crystals (~0.2 mm in each dimension) were obtained when a 2 μl protein droplet was mixed with an equal volume of reservoir solution consisting of 0.1 M sodium cacodylate (pH 6.5), 0.2 M calcium acetate and 12% polyethylene glycol 8000.

The crystals were flash frozen after being transferred to a solution containing 20% glycerol. X-ray diffraction data was collected at the Brazilian National Synchrotron Source (LNLS, Campinas-Brazil) (Polikarpov et al., 1998). The wavelength of the radiation source was set to 1.54 Å and a total of 90 images with an oscillation range of 1° were collected using a MAR 345 imaging plate detector (Mar Research). The raw intensities were scaled and reduced using the HKL suite of programs (Otwinowski and Minor, 1997).

3. Results

The protein fractions of *B. jararacussu* venom which were eluted from the Resource 15S column (results not shown) were concentrated and the fractions which possessed clotting activity were further purified on a Benzamidine Sepharose column. Fig. 1(A) presents the elution profile of Jararacussin-I which was carried out by rapidly changing the pH to 3.2. On SDS–PAGE gels under reduced conditions, the purified Jararacussin-I migrated as a single protein band corresponding to a molecular mass of ~28 kDa (Fig. 1(B)).

In isoelectric focusing gels the enzyme migrated as a diffuse protein band corresponding to a pI ~ 5.0. Neutral sugar determination revealed that the enzyme was glycosylated with 5.4 μg carbohydrate/100 μg enzyme (5.4% carbohydrate content) (results not shown).

Jararacussin-I presented a coagulant specific activity of 45.8 NIH U/mg using bovine fibrinogen as the substrate, whereas the esterase specific activity was 258.7 U/mg (Table 1).

The purified enzyme degraded the Aα and Bβ chains of fibrinogen, in a dose-time-dependent manner (Fig. 2). The optimal temperature and pH for the degradation of both chains of fibrinogen (results not shown) and esterase specific activity were determined to be 37 °C and 7.4–8.0, respectively (Table 1). The enzyme was inactivated at both 4 and 75 °C.

Table 1 presents the effects of protease inhibitors on the esterase activity of Jararacussin-I. The serine protease inhibitors PMSF and benzamidine inhibited the esterase activity of the enzyme by 29.2 and 76.7%, respectively. The

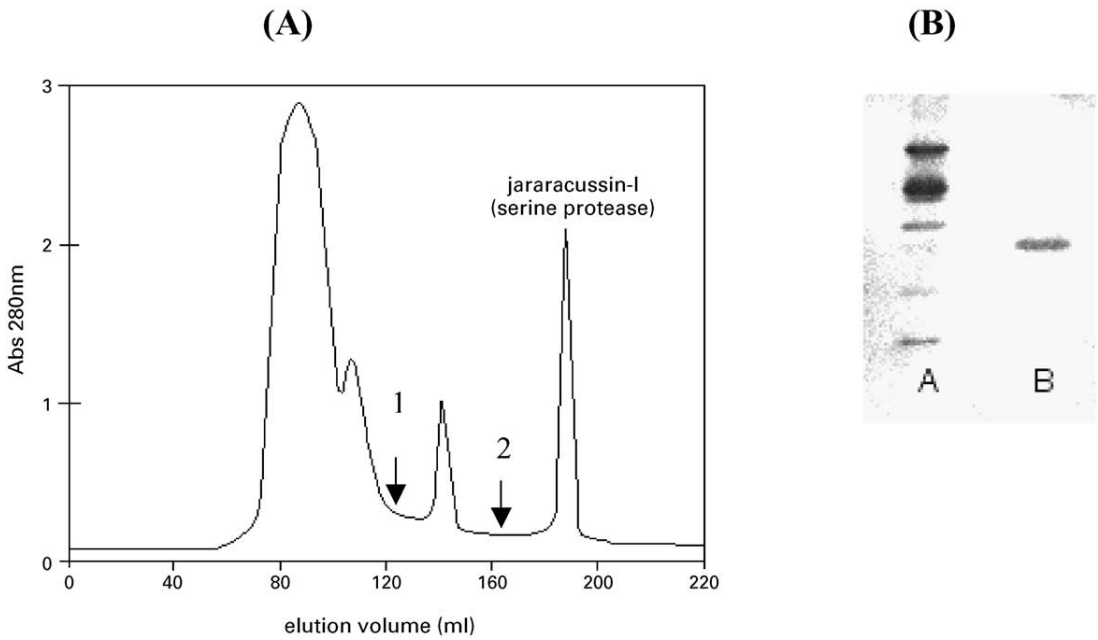

Fig. 1. (A) Chromatographic profile of Jararacussin-I on a Benzamidine Sepharose 6B affinity column. Unbound protein fractions were eluted by washing with 0.02 M, pH 7.8 phosphate buffer. Initial elution was performed by including 0.5 M NaCl in the same buffer (arrow 1). Jararacussin-I was eluted by using a 0.02 M, pH 3.2 glycine–HCl buffer (arrow 2). (B) SDS–PAGE: Lane A—molecular mass standards were bovine serum albumin (66 kDa); ovoalbumin (44 kDa), carbonic anhydrase (30 kDa), soybean trypsin inhibitor (20 kDa) and lactalbumin (14.4 kDa): Lane B—Jararacussin-I.

esterase activity of the enzyme was also inhibited by β-mercaptoethanol (45.1%) and DTT (66.5%). As expected, the enzymatic activity was not affected by EDTA, EGTA, aprotinin and heparin.

Large single crystals which were suitable for X-ray diffraction analysis were obtained from a solution containing 0.1 M sodium cacodylate (pH 6.5), 0.2 M calcium acetate and 12% PEG 8000 (Fig. 3). Processing of the 579,596 observations to 2.28 Å, resulted in an R_{merge} of 5.9% for 65,695 independent reflections. Examination of the systematic absences indicated that the crystals belong to the space group $P2_12_12_1$ with unit cell parameters of $a = 94.63$ Å, $b = 116.04$ Å and $c = 155.78$ Å. Calculation of the Matthews coefficient resulted in a V_M of 2.54 Da^{-1} assuming the existence of six molecules of Jararacussin-I (molecular mass = 28 kDa) in the asymmetric unit, this represents a solvent content of 51%.

4. Discussion

Reports describing TLEs from snake venoms indicate that some of them display thrombin-like coagulant activity, whereas others possess a wide range of activities (Markland, 1991, 1998; Pirkle, 1998; Matsui et al., 2000) and sequence alignments demonstrate that these enzymes are highly homologous.

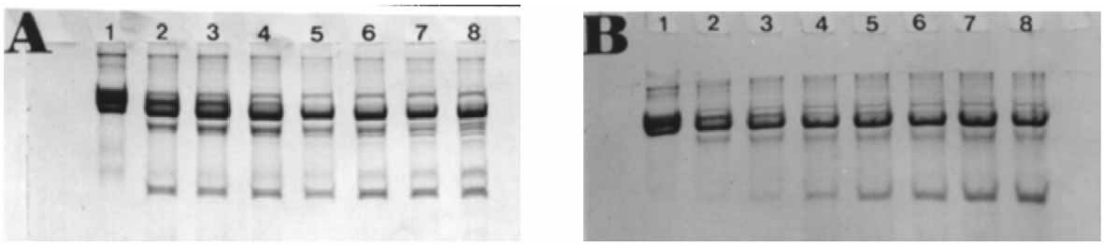

Fig. 2. SDS–PAGE at 13.5% (w/v) of bovine fibrinogen after incubation with Jararacussin-I. Samples of 50 μl fibrinogen (1 mg/ml) were incubated with the enzyme in different conditions as follows: (A) varying enzyme concentration (incubation time, 24 h). Lanes: (1) Fibrinogen control, (2) 0.1 μg, (3) 0.25 μg, (4) 0.5 μg, (5) 1.0 μg, (6) 2.0 μg, (7) 3.0 μg and (8) 4 μg; and (B) varying incubation time (enzyme concentration, 1 μg, pH 8.0). Lanes: (1) fibrinogen control, (2) 1 h, (3) 4 h, (4) 6 h, (5) 12 h, (6) 24 h, (7) 30 h and (8) 48 h.

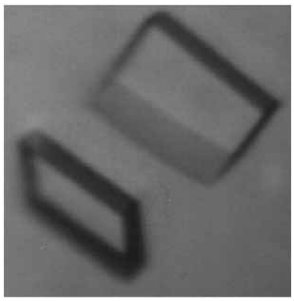

Fig. 3. Photomicrograph of single crystals of Jararacussin-I (*B. jararacussu*). Approximate maximum dimension 0.2 mm.

Jararacussin-I, a serine protease with fibrinogen converting and clotting activities was isolated and purified from the snake venom of *B. jararacussu* by a combination of ion-exchange and affinity chromatography. The enzyme was pure as indicated by PAGE and additionally by the fact that the protein readily formed single crystals. The heterogeneity of purified Jararacussin-I as observed by isoelectric focusing can probably be attributed to different levels glycosylation. Some physiological and biochemical properties of the proteases were similar to those of TLEs purified from the venoms of other snake species such as *Trimeresurus flavaviridis* (Shieh et al., 1985), *Lachesis muta* (Aragon-Ortiz and Gubensek, 1993; Aguiar et al., 1996), *B. jararacussu* (Zaganelli et al., 1996; Andriao-Escarso et al., 1997) and *Agkistrodon acutus* (Huang et al., 1983).

Like the TLEs from the venoms of *Bitis gabonica* (Gaffney et al., 1973) and *Cerastes vipera* (Farid and Tu, 1989), Jararacussin-I was able to cleave fibrinogen releasing both FPA and FPB in vitro, and its proteolytic activity was inhibited by PMSF, benzamidine, 2-mercaptoethanol and DTT, but not by heparin, EDTA or EGTA. The inability of heparin to inhibit the esterase activity of Jararacussin-I is interesting and indicates that significant structural differences exist between this enzyme and thrombin.

The crystal structures of many mammalian and bacterial serine proteases both in the native state and with bound inhibitors, substrates and substrate analogs have been determined. However, the only crystal structure of a venom serine protease currently available is that of the snake venom plasminogen activator TSV-PA (Parry et al., 1998).

Results of our structural study of Jararacussin-I isolated from the venom *B. jararacussu* should provide us with an insight into the mechanism by which this enzyme converts fibrinogen into fibrin and its ability to produce abnormal fibrin clots. This ability of these enzymes to form fibrin clots made up of short polymers has potential therapeutic application for the treatment of patients with occlusive arterial or venous thrombotic diseases without stimulating the endogenous fibrinolysis system (Markland, 1998; Ouyang et al., 1992; Farid and Tu, 1989).

Detailed high resolution structural information of these unique snake venom proteases should also provide useful information for the rational design of drugs that could be applied in the medical and pharmacological fields of homeostasis and thrombosis.

Acknowledgements

This research was supported by grants from FAPESP and CNPq (Brazil) to RKA; BRK, MMT, and WL are recipients of FAPESP fellowships.

References

Andriao-Escarso, S.H., Sampaio, S.V., Cunha, O.A.B., Marangoni, S., Oliveira, B., Giglio, J.R., 1997. Isolation and characterization of a new clotting factor from *Bothrops jararacussu* (jararacuçu) venom. Toxicon 35, 1043–1052.

Aguiar, A.S., Alves, C.R., Melgarejo, A., Giovanni-de-Simone, S., 1996. Purification and partial characterization of a thrombin-like/gyroxin enzyme from bushmaster (*Lachesis muta rhombeata*) venom. Toxicon 34, 555–565.

Aragon-Ortiz, F., Gubensek, F., 1993. A thrombin-like enzyme from bushmaster (*Lachesis muta stenophyrs*) venom. Toxicon 31, 1435–1443.

Bradford, M.M., 1976. A rapid and sensitive method for the quantitation of microgram quantities of protein utilizing the principle of protein dye binding. Anal. Biochem. 72, 248–254.

Burkhart, W., Smith, G.F., Su, J.L., Parikh, I., Levine, H., 1992. Amino acid sequence determination of ancrod, the thrombin-like α-fibrinogenase from the venom of Agkistrodon rhodostoma. FEBS Lett. 297, 297–301.

Dubois, M., Gilles, K.A., Hamilton, J.K., Rebers, P.A., Smith, F., 1956. Colorimetric method for determination of sugars and related substances. Anal. Chem. 28, 350–356.

Ehrempreis, S., Scheraga, H.A., 1957. Observations on analysis for thrombin and the inactivation of fibrin monomer. J. Biol. Chem. 227, 1043–1061.

Farid, T.M., Tu, A.T., 1989. Characterization of cerastobin, a thrombin-like enzyme from the venom of *Cerastes vipera* (Sahara sandviper). Biochemistry 28, 371–377.

Gaffney, P.J., Marsh, N.A., Whaler, B.C., 1973. A coagulant enzyme from gaboon vipera venom: some aspects of its mode of action. Biochem. Soc. Trans. 1, 1208–1209.

Halton, M.W.C., 1973. Studies on the coagulant enzyme from *Agkistrodon rhodostoma* venom. Isolation and some properties of the enzyme. Biochem. J. 131, 799–807.

Henschen-Edman, A.H., Theodor, I., Edwards, B.F.P., Pirkle, H., 1999. Crotalase, a fibrinogen-clotting snake venom enzyme: primary structure and evidence for a fibrinogen recognition exocite different from thrombin. Thromb. Haemostasis 81, 81–86.

Huang, Q.Q., Teng, M.K., Niu, L.W., 1983. Purification and characterization of two fibrionogen-clotting enzymes from five-pace snake (*Agkistrodon acutus*) venom. Toxicon 37, 999–1013.

Itoh, N., Tanaka, N., Mihashi, S., Yamashina, I., 1987. Molecular cloning and sequence analysis of cDNA for batroxobin, a

thrombin-like snake venom enzyme. J. Biol. Chem. 262, 3132–3135.

Jancarik, J., Kim, S.-H., 1991. Sparse matrix sampling: a screening method for crystallization of proteins. J. Appl. Crystallogr. 24, 409–411.

Laemmli, U.K., 1970. Cleavage of structural proteins during the assembly of head of bacteriophage T4. Nature 227, 680–685.

Markland, F.S. Jr., 1991. Inventory of α and β fibrinogenases from snake venom. Thromb. Haemostasis 65, 438–443.

Markland, F.S., 1998. Snake venoms and the hemostatic system. Toxicon 36, 1749–1800.

Matsui, T., Sakurai, Y., Fujimura, Y., Hayashi, I., Oh-Ishi, S., Suzuki, M., Hamako, J., Yamamoto, Y., Yamazaki, J., Kinoshita, M., Titani, K., 1998. Purification and amino acid sequence of halystase from snake venom of *Agkistrodon halys blomhoffii*, a serine protease that cleaves specifically fibrinogen and kininogen. Eur. J. Biochem. 252, 569–575.

Matsui, T., Fujimura, Y., Titani, K., 2000. Snake venom proteases affecting hemostasis and thrombosis. Biochim. Biophys. Acta 1477, 146–156.

Nishida, S., Fujimura, Y., Miura, S., Ozeki, Y., Usami, Y., Suzuki, M., Titani, K., Yoshida, E., Sugimoto, M., Yoshioka, A., Fukui, H., 1994. Purification and characterization of bothrombin, a fibrinogen-clotting serine protease from the venom of *Bothrops jararaca*. Biochemistry 33, 1843–1849.

Otwinowski, Z., Minor, W., 1997. Processing of X-ray diffraction data collected in oscillation mode. Meth. Enzymol. 276, 307–326.

Ouyang, C., Teng, T.F., Huang, T., 1992. Characterization of snake venom components acting on blood coagulation and platelet function. Toxicon 30, 945–966.

Parry, M.A., Jacob, U., Huber, R., Wisner, A., Bon, C., Bode, W., 1998. The crystal structure of the novel snake venom plasminogen activator TSV-PA: a prototype structure for snake venom serine proteinases. Structure 6, 1195–1206.

Pirkle, H., 1998. Thrombin-like enzymes from snake venoms: an updated inventory. Thromb. Haemostasis 79, 675–683.

Polikarpov, I., Perles, L.A., de Oliveira, R.T., Oliva, G., Castellano, E.E., Garratt, R.C., Craievich, A., 1998. Set-up and experimental parameters of the protein crystallography beam line at the Brazilian National Synchrotron Laboratory. J. Synchrotron Rad. 5, 72–76.

Rodrigues, V.M., Soares, A.M., Guerra-Sá, R., Rodrigues, V., Fontes, M.R.M., Giglio, J.R., 2000. Structural and functional characterization of neuwiedase, a nonhemorrhagic fibrin(ogen)-olytic metalloprotease from *Bothrops neuwiedi* snake venom. Arch. Biochem. Biophys. 381, 213–224.

Shieh, T.C., Tanaka, S., Kihara, H., Ohno, M., Makisumi, S., 1985. Purification and characterization of a coagulant enzyme from *Trimeresurus flavoriridis* venom. J. Biochem. 98, 713–721.

Shieh, T.C., Kawabata, S.I., Kihara, M.O., Iwanaga, S., 1988. Amino acid sequence of a coagulant enzyme, flavoxobin, from *Trimeresurus flavoviridis* venom. J. Biochem. 103, 596–605.

Tu, A.T., 1996. Overview of snake venom chemistry. Adv. Exp. Med. Biol. 391, 37–62.

Vesterberg, O., 1972. Isoelectric foccussing of proteins in polyacrylamide gels. Biochim. Biophys. Acta 257, 11–13.

Ware, A.G., Seegers, W.H., 1949. Two stage procedure for the quantitative determination of prothrombin concentration. Am. J. Clin. Pathol. 19, 471–482.

Zaganelli, G.L., Zaganelli, M.G., Magalhaes, A., Diniz, C.R., de Lima, M.E., 1996. Purification and characterization of a fibrinogen-clotting enzyme from the venom of jararacuçu (*Bothrops jararacussu*). Toxicon 34, 807–819.

Available online at www.sciencedirect.com
SCIENCE DIRECT
Biochimica et Biophysica Acta 1752 (2005) 202 – 204
BIOCHIMICA ET BIOPHYSICA ACTA BBA
http://www.elsevier.com/locate/bba

Short crystallization paper

Crystallization and preliminary X-ray crystallographic studies of Protac®, a commercial protein C activator isolated from *Agkistrodon contortrix contortrix* venom

Mário T. Murakami, Raghuvir K. Arni*

Department of Physics, IBILCE/UNESP, Cristovão Colombo 2265, 15054-000, São José do Rio Preto, São Paulo, Brazil

Received 8 June 2005; received in revised form 30 July 2005; accepted 6 August 2005
Available online 19 August 2005

Abstract

The protein C pathway plays an important role in the control and regulation of the blood coagulation cascade and prevents the propagation of the clotting process on the endothelium surface. In physiological systems, protein C activation is catalyzed by thrombin, which requires thrombomodulin as a cofactor. The protein C activator from *Agkistrodon contortrix contortrix* acts directly on the zymogen of protein C converting it into the active form, independently of thrombomodulin. Suitable crystals of the protein C activator from *Agkistrodon contortrix contortrix* were obtained from a solution containing 2 M ammonium sulfate as the precipitant and these crystals diffracted to 1.95 Å resolution at a synchrotron beamline. The crystalline array belongs to the monoclinic space group C2 with unit cell dimensions $a=80.4$, $b=63.3$ and $c=48.2$ Å, $\alpha=\gamma=90.0°$ and $\beta=90.8°$.

Keywords: Protein C activator; Serine proteinase; *Agkistrodon contortrix contortrix* venom; X-ray diffraction analysis

The protein C (PC) pathway comprises the major physiological anticoagulant mechanism that regulates and controls blood coagulation. Protein C, a vitamin K-dependent glycoprotein, circulates in the plasma as an inactive zymogen and is activated on the surface of endothelial cells by the thrombin–thrombomodulin complex [1], a process that can be further enhanced when protein C binds to its membrane receptor, the endothelial-cell protein C receptor [2]. The activated protein C (APC) subsequently binds protein S and inhibits the propagation of blood coagulation by degrading FVIIIa and FVa on the surface of negatively charged phospholipid membranes and by stimulating fibrinolytic activity [3,4]. Deficiencies or defects in the PC anticoagulant pathway are associated with the increased risk of venous thromboembolism (VTE) [5]. The PC pathway also plays an important role in inflammatory processes and APC has been implicated in anti-apoptotic and neuroprotective activities [6].

Several PC activators have been purified from snake venoms, mainly from *Agkistrodon* ssp. [7–12]. The snake venom PC activators, unlike the activators present in the physiological system, act directly on the zymogen of PC releasing APC independently of additional co-factors such as thrombomodulin. The PC activators can be divided in two groups: low molecular weight (<40 kDa) PC activators from new world species of the genus *Agkistrodon* with optimal activity at basic pH, and high molecular weight (>40 kDA) PC activators from old world species of the genus *Agkistrodon* with optimal activity at acid pH [11]. Several types of assays have been established with snake venoms PC activators, such as immunological assays for total protein S (PS), immunological assays for free PS and PS functional assays [13–18]. The most widely used PC activator is Protac®, a commercial preparation of PC activator isolated from *Agkistrodon contortrix contortrix* venom [19–21]. The pharmacological activities and amino acid sequence have been determined, however, the structural determinants for

* Corresponding author. Tel.: +55 17 3221 2460; fax: +55 17 3221 2247.
E-mail address: arni@ibilce.unesp.br (R.K. Arni).

1570-9639/$ - see front matter © 2005 Elsevier B.V. All rights reserved.
doi:10.1016/j.bbapap.2005.08.003

specificity is unknown, since the three-dimensional structure has not yet been determined.

Dynamic light scattering (DLS) experiments were performed using a broad range of pH for Protac® that indicates a monodispersive state in the pH range between 6.0 and 8.0. The hydrodynamic radius at pH 7.0 extrapoled from the diffusion coefficient using the Stokes–Einstein equation was determined to be 3.2±0.01 nm with a corresponding molecular weight of 28.3 kDa, estimated using a calibration curve based on the diffusion coefficients of globular proteins. However, the protein is composed of 231 amino acids with a calculated molecular weight of 25,095 Da. This discrepancy can be attributed to the high carbohydrate content (approximately 20%). Similar effects are observed in the electrophoresis experiments, which indicates an estimated molecular weight of 37 kDa [20]. Crystallization experiments were carried out with Protac® purified from crude venom without treatment for the removal of carbohydrate groups.

Crystallization trials were performed by the hanging-drop vapor diffusion method at 20 °C. Micro crystals were initially obtained from a solution containing 2.4 M ammonium sulfate and 0.1 M sodium cacodylate buffer at pH 6.5. Screening in the monodispersive range of pH observed in the DLS experiments lead to the formation of single crystals after 7 days by mixing 1 μL of the protein (10 mg/ml) and 1 μL of the solution containing 2.0 M ammonium sulfate and 0.1 M HEPES buffer at pH 7.3 (Fig. 1).

X-ray diffraction data were collected at the CPr beam line at the Laboratório Nacional de Luz Síncrotron (LNLS, Brazil). A single crystal with a maximum dimension of 0.3 mm was flash-frozen in the crystallization solution to which was added 15% glycerol (v/v). The data were integrated with the program DENZO and scaled with SCALEPACK at 1.95 Å resolution [22]. The crystal belongs to the monoclinic space group C 2 with unit cell parameters of $a=80.4$, $b=63.3$ and $c=48.2$ Å, $\alpha=\gamma=90.0$ and $\beta=99.8°$. The calculation of the Matthew's coefficient based on the molecular weight of 25,095 kDa results in a V_M of 2.2 Å^{3}Da^{-1} and a solvent content of 43.8%, which corresponds to the presence of one molecule in the asymmetric unit [23]. The statistics of the data processing are summarized in Table 1.

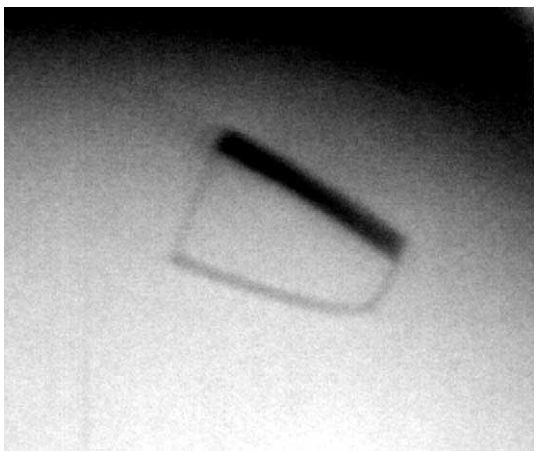

Fig. 1. Microphotograph of a Protac® crystal. Maximum dimensions: 0.3 × 0.2 × 0.1mm.

Table 1
Data collection and structure determination statistics

Data collection	
Temperature (K)	100
Synchrotron source	Laboratório Nacional de Luz Síncrotron Campinas, Brazil
Wavelength used (Å)	1.438
Detector	MARCCD
Space group	C 2
Unit cell parameters (Å, °)	$a=80.4$, $b=63.3$ and $c=48.2$; $\alpha=\gamma=90.0$ and $\beta=99.8$
Resolution range (Å)	40.0–1.95
No. of observed reflections	107,105
Data completeness (%)	97.8 (95.7)
No. of unique reflections	17,060
I/sigma(I)	26.8 (11.4)
$*R_{merge}$ (%)	5.6 (13.5)
V_m (Å^{3}Da^{-1})	2.2
Solvent content (%)	43.8
Molecules per asymmetric unit	1
Molecular replacement	
Correlation coeffecients (%)	
Rotation	31.2
Translation	49.4
Rigid body refinement	63.7
Rigid body refinement R-factor (%)	43.7

Values in parentheses are for the high-resolution bin (1.97–1.95 Å).
$*R_{merge}=\sum|I(h)_I-\{I(h)\}|/\sum\{I(h)\}$, where I_h is the observed intensity of the i-th measurement of reflection h and $\{I(h)\}$ is the mean intensity of reflection h calculated after scaling.

Molecular replacement (MR) was carried out with the program AMoRe [24] using the atomic coordinates of *Trimeresurus stejnejeri* venom plasminogen activator (TSV-PA, PDB code: 1BQY) [25] as a search model. Rigid-body refinement of the best MR solution in the resolution range of 40.0 to 3.0 Å resulted in a correlation coefficient of 63.7% and an R-factor of 43.7%. Isotropic and restrained refinement with REFMAC5 [26] and manual model building using TURBO FRODO [27] is currently in progress. Similar to the TSV-PA and others trypsin-like serine proteinases, the structure of ACC-C consists of two domains, each containing a six-stranded β-barrel, various surface turns, loops and two short α-helices. The two β-barrel domains are inter-connected by three *trans* segments, and the catalytic site is situated in a cleft located at the junction between these two domains with the catalytic triad conserved. This work represents the first crystallization report of a protein C activator from snake venom and the determination of the three-dimensional structure of the Protac® should be useful for structure-based drug design of inhibitors which should be useful for the treatment of venous thromboembolism and other disorders in the PC pathway.

Acknowledgements

We are grateful to Pentapharm Ltd. for providing samples of Protac. This research was supported by grants from Fundação de Amparo à Pesquisa do Estado de São Paulo (FAPESP), Structural Molecular Biology Network (SMOLBNet), Conselho Nacional de Desenvolvimento Científico e Tecnológico (CNPq), Coordenação de Aperfeiçoamento de Pessoal de Nível Superior (CAPES/DAAD) and Centros de Pesquisa, Inovação e Difusão (CEPID). MTM is the recipient of a FAPESP doctoral fellowship.

References

[1] C.T. Esmon, K. Fukudome, Cellular regulation of the protein C pathway, Semin. Cell Biol. 6 (1995) 259–268.
[2] F.B. Taylor, G.T. Peer, M.S. Lockhart, G. Ferrell, C.T. Esmon, Endothelial cell protein C receptor plays an important role in protein C activation in vivo, Blood 97 (2001) 1685–1688.
[3] F.J. Walker, P.W. Sexton, C.T. Esmon, The inhibition of blood coagulation by activated Protein C through the selective inactivation of activated Factor V, Biochim. Biophys. Acta 571 (1979) 333–342.
[4] C.A. Fulcher, J.E. Gardiner, J.H. Griffin, T.S. Zimmerman, Proteolytic inactivation of human factor VIII procoagulant protein by activated human protein C and its analogy with factor V, Blood 63 (1984) 486–489.
[5] H.P. Schwarz, M. Fischer, P. Hopmeier, M.A. Batard, J.H. Griffin, Plasma protein S deficiency in familial thrombotic disease, Blood 64 (1984) 1297–1300.
[6] J.H. Griffin, B. Zlokovic, J.A. Fernandez, Activated protein C: potential therapy for severe sepsis, thrombosis, and stroke, Semin. Hematol. 39 (2002) 197–205.
[7] K. Stocker, H. Fischer, J. Meier, M. Brogli, L. Svendsen, Protein C activators in snake venoms, Behring-Inst.-Mitt. 79 (1986) 7–47.
[8] J. Meier, Proteinases activating protein C, in: G.S. Bailey (Ed.), The Enzymology of Snake Venoms, Fort Collins, Alaken, 1998, pp. 253–285.
[9] H.M. Bakker, G. Tans, L.Y. Yukelson, T.W. Janssen-Claessen, R.M. Bertina, H.C. Hemker, J. Rosing, Protein C activation by an activator purified from the venom of *Agkistrodon halys halys*, Blood Coagul. Fibrinolysis 4 (1993) 605–614.
[10] A.E. Kogan, G.V. Bashkov, I.D. Bobruskin, E.P. Romanova, V.A. Makarov, S.M. Strukova, Protein C activator from the venom of *Agkistrodon blomhoffi ussuriensis* retards thrombus formation in the arterio-venous shunt in rats, Thromb. Res. 70 (1993) 385–393.
[11] A.E. Kogan, A.N. Makarov, I.D. Bobruskin, S.M. Strukova, Comparative study of protein C activators from the Agkistrodon snake venoms, Thromb. Res. 62 (1991) 775–780.
[12] L. Sun, J. Guang, S. Huang, Q. Yu, Identification of protein C activator from nine species of Chinese snake venoms, Zhongguo Bingli Shengli Zazhi 17 (2001) 241–244.
[13] R.M. Bertina, A. Van Wijngaarden, J. Reinalda-Poot, S.R. Poort, V.J.J. Bom, Determination of plasma protein S—the protein cofactor of activated protein C, Thromb. Haemost. 53 (1985) 268–272.
[14] B.J. Woodhams, The simultaneous measurement of total and free protein S by ELISA, Thromb. Res. 50 (1988) 213–220.
[15] J.R. Edson, J.M. Vogt, D.A. Huesman, Laboratory diagnosis of inherited protein S deficiency, Am. J. Clin. Pathol. 94 (1990) 176–186.
[16] K. Suzuki, J. Nishioka, Plasma protein S activity measured using Protac®, a snake venom derived activator of protein C, Thromb. Res. 49 (1988) 241–251.
[17] M. Wolf, C. Boyer-Neumann, J.L. Martinoli, C. Leroy-Matheron, J. Amiral, D. Meyer, M.J. Larrieu, A new functional assay for human protein S activity using activated factor V as substrate, Thromb. Haemost. 62 (1989) 1144–1145.
[18] I. Kobayashi, N. Amemiya, T. Endo, K. Okuyama, K. Tamura, S. Kume, Functional activity of protein S determined with use of protein C activated by venom activator, Clin. Chem. 35 (1989) 1644–1648.
[19] J.L. Martinoli, K. Stocker, Fast functional protein C assay using Protac®, a novel protein C activator, Thromb. Res. 43 (1986) 253–264.
[20] K. Stocker, H. Fischer, J. Meier, M. Brogli, L. Svendsen, Characterization of the protein C activator Protac® from the venom of the southern copperhead (*Agkistrodon contortrix*) snake, Toxicon 25 (1987) 239–252.
[21] K. Stocker, H. Fischer, J. Meier, Practical application of the protein C activator Protac® from *Agkistrodon contortrix* venom, Folia Haematol. 115 (1988) 260–264.
[22] Z. Otwinowski, W. Minor, Processing of X-ray diffraction data collected in oscillation mode, Methods Enzymol. 276 (1997) 307–326.
[23] B.W. Matthews, Solvent content of protein crystals, J. Mol. Biol. 33 (1968) 491–497.
[24] J. Navaza, AmoRe: an automated package for molecular replacement, Acta Crystallogr. A50 (1994) 157–163.
[25] M.A Parry, U. Jacob, R. Huber, A. Wisner, C. Bon, W. Bode, The crystal structure of the novel snake venom plasminogen activator TSV-PA: a prototype structure for snake venom serine proteinases, Structure 6 (1998) 195–206.
[26] G.N. Murshudov, A.A. Vagin, E.J. Dodson, Refinement of macromolecular structure by the maximum-likelihood method, Acta Crystallogr. D53 (1997) 240–255.
[27] T.A. Jones, Diffraction methods for biological macromolecules. Interactive computer graphics: FRODO, Methods Enzymol. 115 (1985) 157–171.

THE JOURNAL OF BIOLOGICAL CHEMISTRY VOL. 280, NO. 47, pp. 39309–39315, November 25, 2005

Thrombomodulin-independent Activation of Protein C and Specificity of Hemostatically Active Snake Venom Serine Proteinases

*CRYSTAL STRUCTURES OF NATIVE AND INHIBITED AGKISTRODON CONTORTRIX CONTORTRIX PROTEIN C ACTIVATOR**

Received for publication, August 3, 2005, and in revised form, August 31, 2005 Published, JBC Papers in Press, September 14, 2005, DOI 10.1074/jbc.M508502200

Mário T. Murakami[1] **and Raghuvir K. Arni**[2]

From the Biochemistry and Structural Biology Group, Department of Physics, IBILCE/UNESP, São José do Rio Preto, SP 15054-000, Brazil

Protein C activation initiated by the thrombin-thrombomodulin complex forms the major physiological anticoagulant pathway. *Agkistrodon contortrix contortrix* protein C activator, a glycosylated single-chain serine proteinase, activates protein C without relying on thrombomodulin. The crystal structures of native and inhibited *Agkistrodon contortrix contortrix* protein C activator determined at 1.65 and 1.54 Å resolutions, respectively, indicate the pivotal roles played by the positively charged belt and the strategic positioning of the three carbohydrate moieties surrounding the catalytic site in protein C recognition, binding, and activation. Structural changes in the benzamidine-inhibited enzyme suggest a probable function in allosteric regulation for the anion-binding site located in the C-terminal extension, which is fully conserved in snake venom serine proteinases, that preferentially binds Cl^{1-} instead of SO_4^{2-}.

Hemostasis, a complex system responsible for maintaining the fluidity of blood under physiological conditions, is primed to react rapidly to vascular injury, stemming blood loss by locally sealing the injured vessel wall (1). The highly regulated hemostatic system functions in equilibrium between two extremes: coagulation and fibrinolysis (2). On one hand by initiating the coagulation cascade, which comprises a network of highly, correlated and controlled reactions and is triggered either by the extrinsic (tissue factor) or the intrinsic pathways (Factor XIa), activating thrombin to generate cross-linked fibrin polymers (1). On the other hand, in the fibrinolytic system, the protein C pathway comprises the major physiological anticoagulant mechanism and is activated on the surface of endothelial cells by the thrombin-thrombomodulin complex (3). Activated protein C subsequently binds protein S and inhibits coagulation by degrading FVIIIa and FVa on the surface of negatively charged membranes by stimulating fibrinolytic activity (4, 5). Deficiencies or defects in the protein C (PC)[3] anticoagulant pathway are associated with the increased risk of venous thromboembolism (6). The PC pathway also plays an important role in inflammatory processes and activated PC has been implicated in anti-apoptotic and neuroprotective activities (7).

Snake venom serine proteinases belong to the trypsin subfamily of enzymes, share significant sequence identity (50–70%), and display high specificity toward macromolecular substrates. These enzymes interfere in the control and regulation of the hemostatic system at different key points ranging from the coagulation cascade to the fibrinolytic feedback system (8) and are characterized as activators of the fibrinolytic system (plasminogen activators), procoagulant (thrombin-like enzymes), anticoagulant (PC activators), and platelet-aggregating enzymes (9). *Trimeresurus stejnegeri* venom plasminogen activator converts plasminogen to plasmin by cleavage of the peptide bond Arg^{561}–Val^{562} with high substrate specificity and is resistant to inhibition (10, 11). Batroxobin, a thrombin-like enzyme from *Bothrops atrox* venom used for the treatment of thrombotic diseases (12), converts fibrinogen to fibrin by cleaving fibrinopeptide A (Aα 1–16) at the N-terminal portion of the Aα-chain forming a non-cross-linked "soft clot" that is rapidly removed from the circulatory system by the fibrinolytic mechanism resulting in a defibrinogenerating effect. The PC activator from *Agkistrodon contortrix contortrix* venom, commercially referred to as Protac®, specifically converts PC to activated PC by hydrolyzing the Arg^{169}–Leu^{170} bond, functioning independently of plasmatic factors in comparison to the physiological activation of PC by thrombin which is dependent on the participation of thrombomodulin (13). The PC activator, from *A. contortrix contortrix* venom, induced zymogen activation is clinically used in assays of functional PC determination, total protein S content, and other protein S functional assays (14) in plasma, since catalytically active PC can easily be detected by coagulation tests or by utilizing chromogenic substrates.

We present the first crystal structures of the PC activator from the venom of the copperhead snake *A. contortrix contortrix* (ACC-C), a single-chain glycosylated serine proteinase that is a fast-acting PC activator, both in the native and inhibited states at 1.65 and 1.54 Å resolutions, respectively. These results provide information at the molecular level concerning the alternative PC activation pathway that is independent of thrombomodulin, the central physiological barrier against thrombosis and could serve as a basis for the structure-based design of clinically useful molecules and in the treatment of thromboembolism.

* This work was supported by grants from the Fundação de Amparo à Pesquisa do Estado de São Paulo (FAPESP) (Grant 04/11258-0), Conselho Nacional de Desenvolvimento Cientifico e Tecnológico (CNPq) (473097/2004-4), Coordenação de Aperfeiçoamento de Pessoal de Nível Superior/Deutscher Akademischer Austauschdienst (Grant 186/04), Structural Molecular Biology Network (SMOLBNet), and Centros de Pesquisa, Inovação e Difusão (CEPID). The costs of publication of this article were defrayed in part by the payment of page charges. This article must therefore be hereby marked "*advertisement*" in accordance with 18 U.S.C. Section 1734 solely to indicate this fact.

The atomic coordinates and structure factors (codes 2AIP and 2AIQ) have been deposited in the Protein Data Bank, Research Collaboratory for Structural Bioinformatics, Rutgers University, New Brunswick, NJ (http://www.rcsb.org/).

[1] Recipient of a doctoral fellowship from FAPESP.

[2] To whom correspondence should be addressed. Tel.: 55-17-2212460; Fax: 55-17-2212247; E-mail: arni@ibilce.unesp.br.

[3] The abbreviations used are: PC, protein C; TSV-PA, *Trimeresurus stejnegeri* venom plasminogen activator; ACC-C, protein C activator from *Agkistrodon contortrix contortrix* venom; cmk, chloromethyl ketone; TME45, thrombomodulin epidermal growth factor-like domains 4 and 5; NAP5, nematode anticoagulant protein 5 from *Ancylostoma caninium*; dansyl, 5-dimethylaminonaphthalene-1-sulfonyl; r.m.s., root mean square.

TABLE ONE

Data collection and refinement statistics

Statistical values for the highest resolution shells are indicated in parentheses. LNLS, Laboratório Nacional de Luz Síncrotron.

	Native state	Inhibited state
Crystal preparation		
Cryoprotectant solution	Mother liquor + 20% glycerol	Mother liquor + 20% glycerol + 50 mM benzamidine
Soaking time	30 s	45 s
Data collection		
Wavelength (Å)	1.438	1.438
Temperature (K)	100	100
Detector	MARCCD	MARCCD
Synchrotron radiation source	CPr beamline/LNLS-Brazil	CPr beamline/LNLS-Brazil
Space group	C 2	C 2
Unit cell parameters (Å, °)	$a = 79.87$, $b = 63.30$, and $c = 48.24$; $\beta = 99.80$	$a = 80.52$, $b = 63.46$, and $c = 48.22$; $\beta = 99.85$
Number of molecules in the asymmetric unit	1	1
Solvent content (%)	42.4	41.7
V_M (Å^3/Da)	2.15	2.12
Number of reflections	487,208	409,068
Number of unique reflections	28,664 (2835)	35,447 (5817)
$\langle I/\sigma(I)\rangle$	20.0 (2.9)	18.3 (3.5)
Multiplicity	7.8 (7.5)	6.4 (5.8)
Completeness (%)	99.8 (99.6)	99.9 (99.8)
R_{merge}[a] (%)	9.0 (64.5)	8.4 (49.2)
Refinement statistics		
R_{factor} (%)	16.7	16.7
R_{free} (%)	19.6	19.1
r.m.s. deviation bond distances (Å)	0.011	0.010
r.m.s. deviation bond angles (°)	1.492	1.453
Average *B*-factors (Å^2)	21.2	17.3
Ramachandran plot analysis		
Most favored regions (%)	83.9	82.8
Allowed regions (%)	15.1	16.1
Generously allowed regions (%)	1.0	1.0

[a] $R_{merge} = \Sigma|I(h)_I - \{I(h)\}|/\Sigma\{I(h)\}$, where I_h is the observed intensity of the *ih* measurement of reflection *h*, and $\{I(h)\}$ is the mean intensity of reflection *h* calculated after scaling.

MATERIALS AND METHODS

ACC-C, provided by Pentapharm (Basel, Switzerland), was dissolved to a concentration of 10 mg/ml in a 20 mM Hepes (pH 7.5) buffer that also contained 10 mM sodium chloride and 1 mM dithiothreitol. Crystals were obtained at 18 °C by equilibration of the protein solution (1 μl) against a reservoir solution containing 2.0 M ammonium sulfate and 100 mM sodium acetate (pH 4.6) utilizing the hanging-drop vapor diffusion method. The benzamidine-inhibited ACC-C complex was obtained by soaking crystals for 45 s in a cryo-protectant solution (20% (v/v) glycerol) that additionally contained 50 mM benzamidine. Dose-dependent x-ray diffraction data were collected from cryo-protected crystals at 100 K at a synchrotron radiation source (CPr Beamline-Laboratório Nacional de Luz Síncrotron, Campinas, Brazil) where the wavelength was fixed at 1.438 Å, diffraction intensities were measured utilizing a Mar CCD165 detector (Mar Inc.), and the diffraction intensities were reduced and scaled using the DENZO/SCALEPACK suite of programs (15). Both the native and benzamidine-inhibited crystals are isomorphous, belong to the monoclinic space group C2, and contain one protein molecule in the asymmetric unit. The crystal structure of ACC-C was solved by molecular replacement (AMoRe) (16) initially using the atomic coordinates of *T. stejnegeri* venom plasminogen activator (Protein Data Bank entry: 1BQY) (11) as a search model. Positional and restrained isotropic *B*-factor refinements were performed using REFMAC5 (17), all model building was carried out utilizing TURBO-FRODO (18), and PROCHECK (19) was utilized to evaluate the stereochemistry of the final models. The data collection, processing, and refinement statistics are presented in TABLE ONE.

RESULTS

The crystal structures of both native and benzamidine-inhibited ACC-C have been refined at 1.65 and 1.54 Å resolutions to crystallographic residuals of 16.7% (R_{free} = 19.6%) and 16.7% (R_{free} = 19.1%), respectively. An analysis of the stereochemistry of the final models indicates that the main-chain dihedral angles for all residues are located in the permitted regions of the Ramachandran diagram and that the root mean square (r.m.s.) deviations from ideal values are distributed within the expected ranges for well refined structures (TABLE ONE).

In analogy to the structures of trypsin-like serine proteinases, the structure of ACC-C consists of two domains (S and S′) each containing a six-stranded β-barrel and two short α-helices (residues: 165–173 and 235–244, sequence numbering is based on chymotrypsinogen) (20) (Fig. 1, *A* and *B*). The catalytic triad (His^{57}, Asp^{102}, and Ser^{195}) is located at the junction of both barrels and is surrounded by the conserved 70-, 148-, and 218-loops, and the non-conserved 37-, 60-, 99-, and 174-loops (Fig. 1, *A* and *B*).

ACC-C contains 16% carbohydrate, including glucosamine, neura-

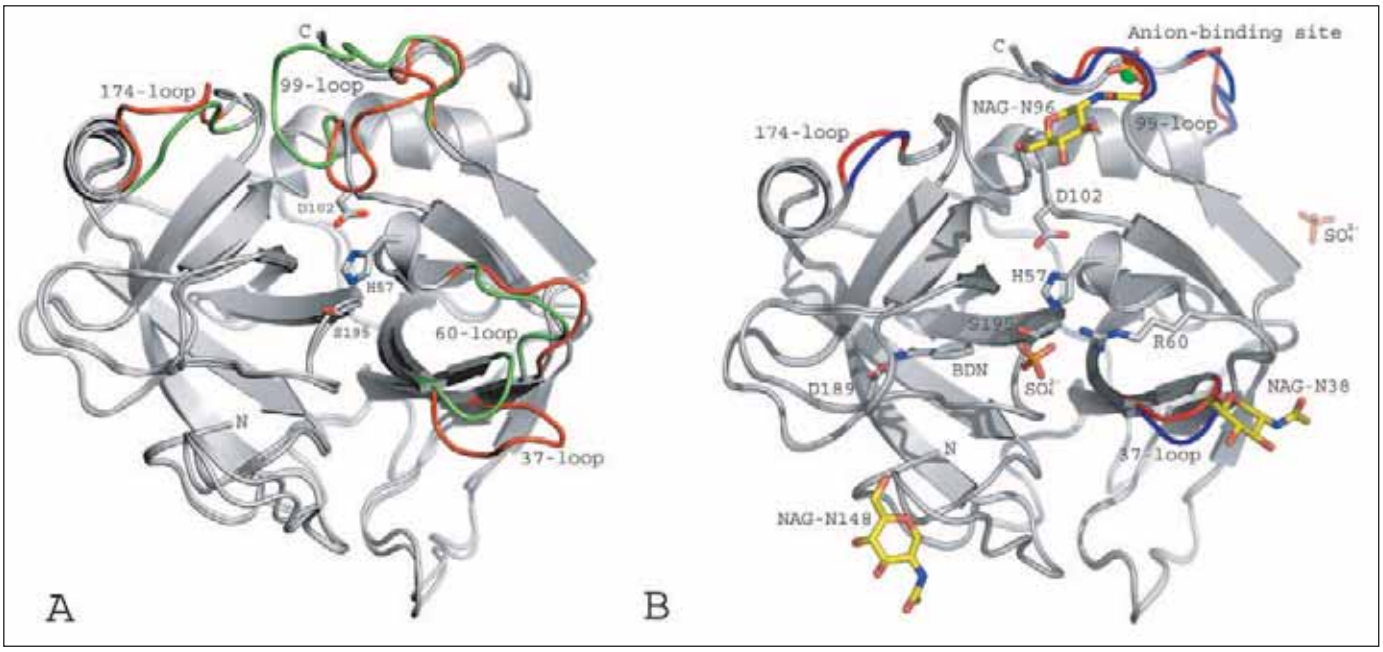

FIGURE 1. Ribbon representations of the superimposed crystal structures of ACC-C and TSV-PA (*A*), highliting the loops that are different in ACC-C (*red*) and TSV-PA (*blue*), the amino acids that form the catalytic triad are atom color-coded (*white*, carbon; *red*, oxygen; and *blue*, nitrogen). *B*, the superimposed structures of ACC-C in the native and benzamidine-inhibited states. The carbohydrate moieties are color-coded (yellow, carbon; red, oxygen; and blue, nitrogen) and the catalytic triad, sulfate ion, and benzamidine molecule are color-coded as described for *A*. The structural changes between native and inhibited ACC-C are colored in *blue* and *red*, respectively.

minic acid, and neutral hexose (13, 21), the consensus signal sequence for the attachment of carbohydrate moieties to asparagines (Asn-*X*-Thr/Ser, where *X* represents any amino acid) was identified at positions 38, 96A, and 148. In both the structures, clear electron density was observed for the *N*-acetyl-D-glucosamine monosaccharide, which is *N*-linked to Asn^{96a} and Asn^{148}; however, the moiety linked to Asn^{38} was inserted based on the presence of diffuse electron density (Fig. 1*B*). The three carbohydrate moieties are strategically positioned at the tips of the 37-, 99-, and 148-loops, which form the entrance to the active-site pocket (Fig. 1*B*) and modulate the selectivity toward macromolecular substrates (discussed below). Two snake venom serine proteinase isoforms, AaV-SP-I and AaV-SP-II, from *Agkistrodon acutus*, also posses an *N*-linked carbohydrate group (Asn^{35}) that is considered to interfere with the binding of macromolecular inhibitors (22). In contrast, *T. stejnegeri* venom plasminogen activator (TSV-PA) has a unique glycosylation site at Asn^{178} located on the opposite face (23) and apparently does not play a role in the binding macromolecular substrates at the interfacial site.

The electron density (2 σ level) for the benzamidine molecule bound to the carboxylate oxygen atoms of Asp^{189} is clearly defined (Fig. 2*A*) and indicates a mode of interaction similar to that observed in the structures of benzamidine-inhibited trypsin-like enzymes (24). A sulfate ion is coordinated by His^{57}, Arg^{60}, Gly^{193}, Ser^{195}, and two water molecules both in the native state and benzamidine-inhibited states (Fig. 2*B*), which suggests that the catalytic triad is unaffected by benzamidine binding and could account for the residual amidolytic activity observed in benzamidine-inhibited ACC-C toward small substrates (25).

The binding of benzamidine at the S1 subsite results in significant, structural modifications in the C-terminal extension (244–245e), 99-loop (Cys^{91}, Leu^{92}, and Asn^{93}), 174-loop, and in the 37-loop (r.m.s. deviations up 2.97 Å) (Figs. 1*B* and 3). The anion-binding pocket formed between the highly conserved C-terminal extension and the 99-loop, stabilized by a disulfide bridge (Cys^{91}–Cys^{245e}) and a salt bridge (between Pro^{245g} and Lys^{101}), binds either SO_4^{2-} or Cl^{1-} ions depending on the presence or absence of a benzamidine molecule at the active site (Figs. 1*B* and 3). In native ACC-C, $Arg^{82\#}$ (# indicates amino acids from a symmetry equivalent molecule) also participates in the coordination of the sulfate ion by forming a hydrophilic pocket (between $Arg^{82\#}$, $Arg^{83\#}$, and $Phe^{84\#}$, Fig. 3) and binds a water molecule. In benzamidine-inhibited ACC-C, $Arg^{82\#}$ also coordinates the Cl^{1-} ion but adopts a different conformation thereby modifying the $Arg^{82\#}$, $Arg^{83\#}$, $Phe^{84\#}$ loop. The phenyl ring of $Phe^{84\#}$ functioning as a lid moves inwards creating a local hydrophobic environment that prevents the binding of the fore mentioned water molecule. These structural changes suggest the possible existence of an allosteric mechanism functioning between the active-site pocket and the C-terminal extension that preferentially binds Cl^{1-} instead of SO_4^{2-} in response to substrate or inhibitor binding at the S1 subsite.

Superpositioning of the structure of ACC-C with TSV-PA results in 179 topologically equivalent Cα positions with r.m.s. deviations of 0.54 Å, indicating a high degree of structural similarity in agreement with the observed sequence identity of 75% (Fig. 1*A*). The S domain is highly conserved and the notable structural differences are in the surface loops surrounding the active-site pocket, mainly, the 37-, 60-, and 99-loops which form the S′ domain (Fig. 4). The 37-loop located at southeast corner of the S′ domain, is stabilized by a disulfide bridge (Cys^{42}–Cys^{58}), presents a single deletion at position 37 and a *N*-linked Asn at position 38, which results in the formation of a truncated loop when compared with TSV-PA (r.m.s. deviation up 5.5 Å). The 60-loop is positively charged in ACC-C due to Arg^{60} and Arg^{64}, whereas in TSV-PA it is negatively charged (Fig. 4). The positioning of Arg^{60} and Asp^{189} creates a polar environment between the S and S′ domains (Fig. 5). Thus, zwitterzonic inhibitors, such as 4-(4-amidinephenyl)butanoic acid, that contain a guanidine head group and a carboxylic tail could bind simultaneously to Asp^{189} and Arg^{60} blocking the S1 subsite and restricting access to the catalytic triad.

Dansyl-Glu-Gly-Arg-chloromethyl ketone (dansyl-EGR-cmk) and D-Phe-Pro-Arg-cmk rapidly inhibit both the amidolytic and anticoagulant activities of ACC-C (13). The structure of ACC-C was superimposed on the structure of the human single-chain tissue plasminogen

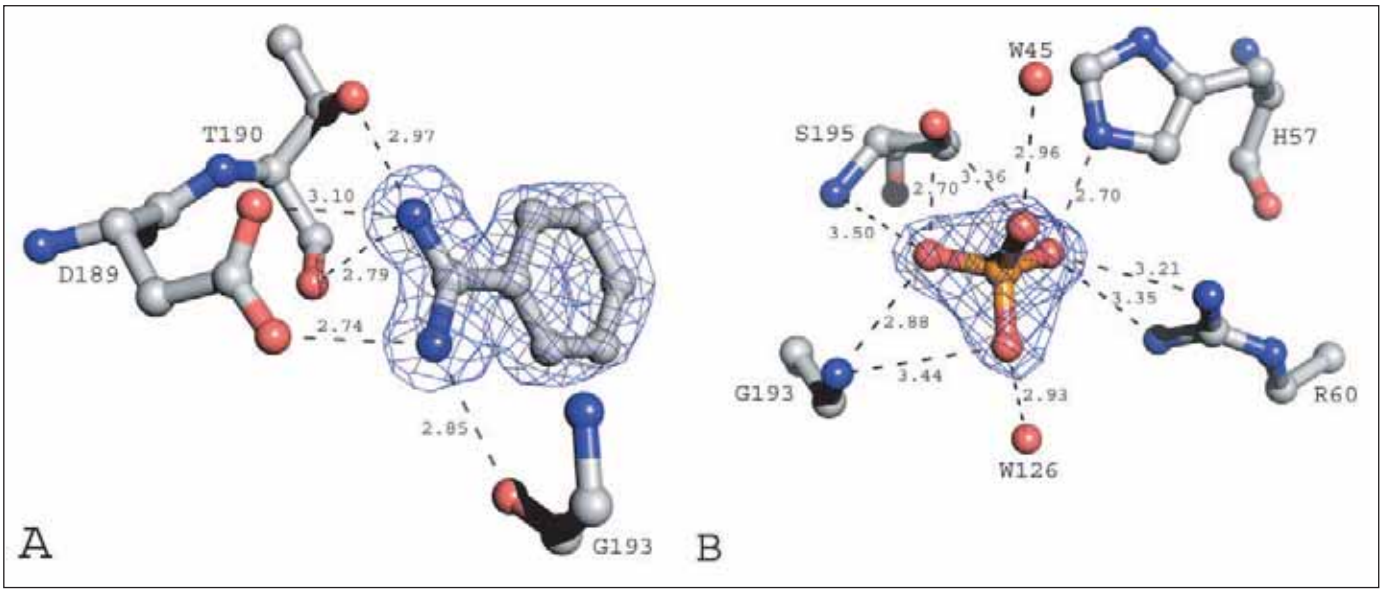

FIGURE 2. **Electron densities and interactions observed for the benzamidine molecule (*A*) and the sulfate ion at the S1 subsite and the catalytic site (*B*), respectively.** The electron densities (*blue cages*) are contoured at the 1 σ level in the $2F_o - F_c$ map; *interrupted lines* and *numbers* indicate hydrogen bonds and distances, respectively.

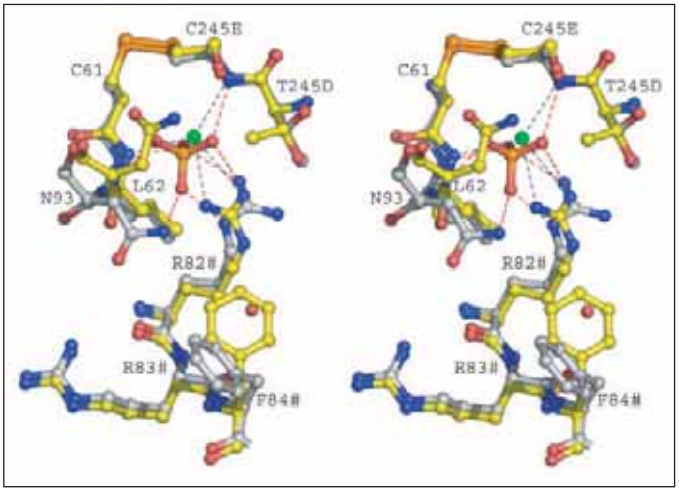

FIGURE 3. **Stereo view of the anion-binding site for the superimposed native (*white*, carbon) and inhibited (*yellow*, carbon) states.** The sulfate ion is color-coded (red, oxygen and *orange*, sulfur), and the chloride ion is represented by a *green sphere*. The hydrogen bonds (*broken lines*) formed between the sulfate ion and the amino acids residues in native-ACC are colored *red*, and the hydrogen bonds between the chloride ion and the amino acid residues in inhibited ACC-C are in *black*. Atoms belonging to a symmetry equivalent molecule are indicated by a # following the number.

complexed with dansyl-EGR-cmk (Protein Data Bank entry: 1BDA) (26), and the relative position of dansyl-Glu-Gly-Arg-cmk was subjected to energy minimization. This indicates that the interaction between Arg^4 from dansyl-Glu-Gly-Arg-cmk and Asp^{189} at the S1 subsite is maintained by hydrogen bonds formed between the carbonyl oxygen of Gly^3, $Lys^{192}N^{\epsilon}$, and the carboxylate group of Glu^2 and $Asn^{218}N^{\delta 2}$. The dansyl naphthalene ring forms hydrophobic interactions with the side chains of Trp^{99}, Leu^{172}, and Val^{215}. These interactions could account for the efficient inactivation of ACC-C by Arg-chloromethyl ketone derivatives.

Binding of natural macromolecular inhibitors (bovine pancreatic trypsin inhibitor and soybean trypsin inhibitor) would be prevented by the steric clash caused by the indole ring of Trp^{99} in ACC-C and by the phenyl ring of Phe^{193} in TSV-PA (Fig. 5). Interactions of these inhibitors would also be restricted by the carbohydrate moieties present on the interfacial surface of ACC-C (Fig. 1*B*) and AaV-SP-I/II from *Agkistrodon acutus* venom (22).

Another significant feature of ACC-C, apart from the three carbohydrate moieties distributed strategically around the active-site pocket, is the significant positive charge present on the interfacial surface (Fig. 6*A*) due to the presence of several arginine residues exposed to the bulk solvent that could bind polyanionic compounds. The amidolytic activity of ACC-C is almost completely (98%) inhibited by heparin (13) probably as a result of binding at this site. This site is negatively charged in TSV-PA (Fig. 6*B*) and may account for the role of electrostatic interactions in the selectivity of snake venom serine proteinases.

Under physiological conditions, the primary binding site of the 37- and 70-loops of PC zymogen in the thrombin-thrombomodulin complex is formed by a number of polar and charged side chains, which form an extended solvent-exposed region on thrombomodulin epidermal growth factor-like domains 4 and 5 (TME45) (27). The negatively charged activation peptide (sequence QVDPRLIDGK) of PC was modeled based on the crystal structure of Gla-domainless activated PC (Protein Data Bank entry: 1AUT) (28) and the interactions formed by nematode anticoagulant protein 5 from *Ancylostoma caninium* (NAP5) with factor Xa. In this model, electrostatic interactions formed between the positively charged surface of ACC-C created by the eight arginine residues (at positions 56, 60, 65, 82, 83, 107, 110, and 113) and the acidic residues of the activation peptide and the interaction of Arg^{60} (discussed above) that forms the P3′ subsite with Asp^{172} (P3′) are crucial (Fig. 6, *C* and *D*).

Additionally, the three carbohydrate moieties that form prongs on the interfacial surface of ACC-C are probably important in the recognition and orientation of PC zymogen during activation. In physiological PC activation, the carbohydrate moieties are not considered to be important and are not required either for thrombin binding or for cofactor activity as indicated by the activity of thrombomodulin expressed in *Escherichia coli* (29, 30).

DISCUSSION

The vitamin K-dependent enzyme PC (31) is physiologically activated by cleavage of the Arg^{169}–Leu^{170} bond by the thrombin/thrombomodu-

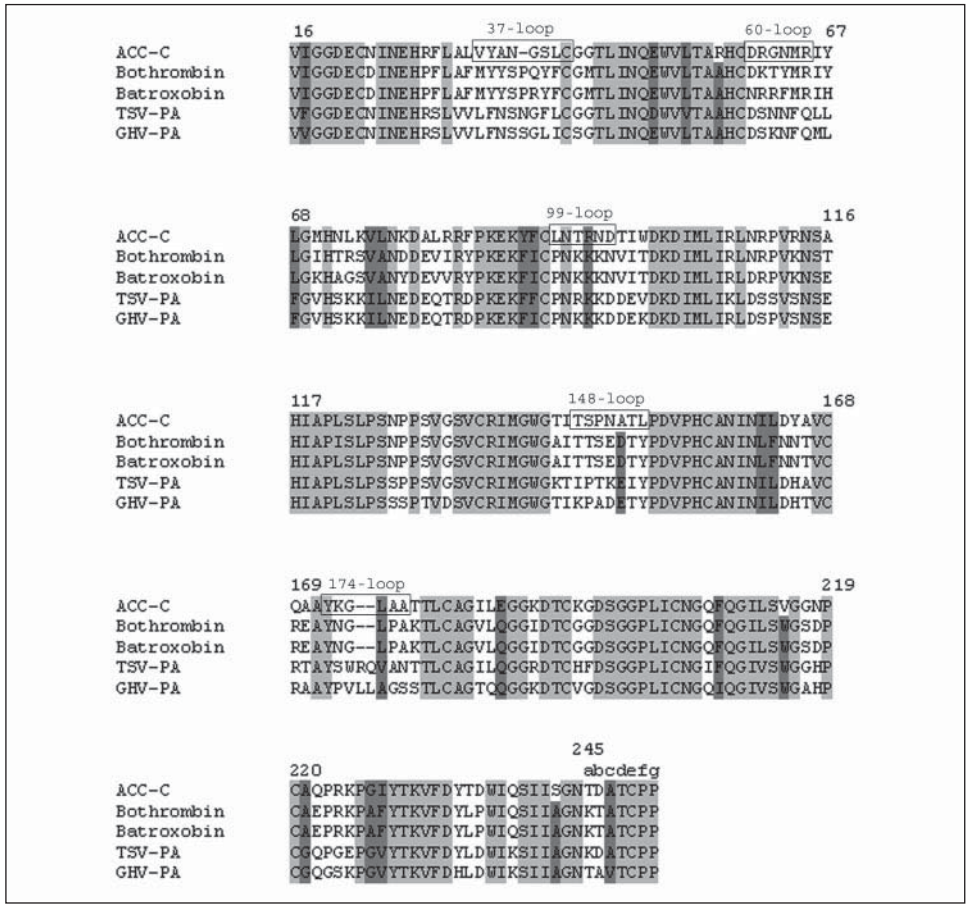

FIGURE 4. **Multiple sequence alignment of ACC-C (*A. contortrix contortrix* protein C activator, GenBank™ accession code P33588), bothrombin (thrombin-like enzyme from *Bothrops jararaca*, GenBank™ accession code P81661), batroxobin (thrombin-like enzyme from *B. atrox*, GenBank™ accession code CAA31240), TSV-PA (*T. stejnegeri* venom plasminogen activator, GenBank™ accession code Q91516), and GHV-PA (*Gloydius halys* venom plasminogen activator, GenBank™ accession code AAD01624).** The numbering scheme refers to chymotrypsinogen. Residues colored in *light gray* are identities and in *dark gray* are highly conserved, and the loops discussed in the text are *boxed*.

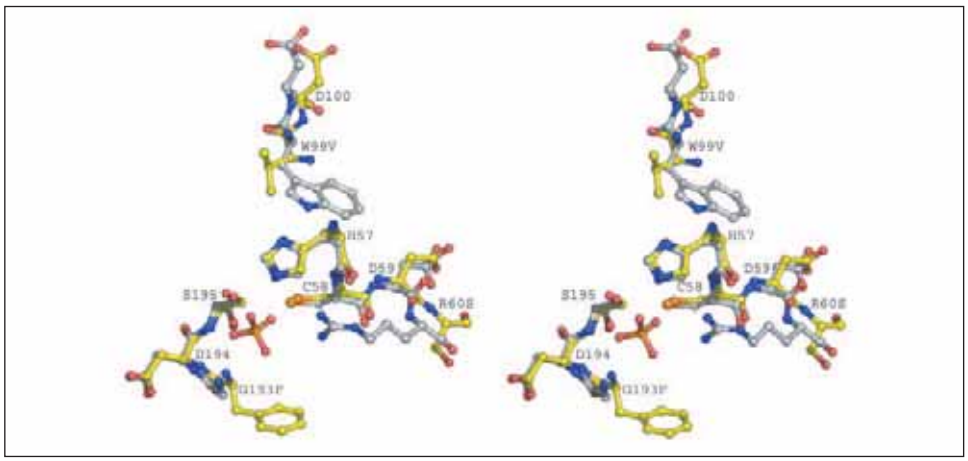

FIGURE 5. **Stereo view of the active-site pocket for the superimposed structures of ACC-C (*white*, carbon) and TSV-PA (*yellow*, carbon).**

lin complex and functions as an anticoagulant enzyme by deactivating factors Va and VIIIa (32). Functional assays of PC activation are complicated either by incomplete activation by thrombin or by the interference of thrombin in chromogenic assays. The ACC-C commercialized by Pentapharm as Protac® does not rely on other plasmatic factors and is clinically used for PC assays by the direct chromogenic method, by the indirect chromogenic method based on activated partial thromboplastin time, or by a functional clotting assay (13, 14). Since the activation product of ACC-C is not influenced by the inhibitory effect of PC inhibitors, time-consuming adsorption steps to separate PC are not required (14).

Analysis of the crystal structures of native and inhibited ACC-C indicates that binding of benzamidine does not involve the residues of the catalytic triad, which could account for the residual amidolytic activity observed when benzamidine and benzamidine derivatives are used as inhibitors (25). However, benzamidine binding induces significant structural changes: (i) the 37-loop adopts a different conformation, (ii) the anion-binding site located at the extended C terminus formed by Cys^{91}, Leu^{92}, Asn^{93}, Cys^{245e}, Thr^{245d}, and $Arg^{82\#}$ (from a symmetry equivalent molecule) preferentially binds Cl^{1-} instead of SO_4^{2-}, and (iii) when the N^{ϵ} and $N^{\eta 2}$ atoms of $Arg^{82\#}$ coordinate the SO_4^{2-} ion, the phenyl ring of $Phe^{84\#}$ shields the hydrophobic micro-environment formed between $Arg^{82\#}$ and $Phe^{84\#}$. However, when the $N^{\eta 1}$ and $N^{\eta 2}$ atoms of $Arg^{82\#}$ coordinate the Cl^{1-} ion, the phenyl ring of $Phe^{84\#}$ flips out and the resulting altered geometry at this site creates a hydrophilic microenvironment, which permits the binding of a water molecule.

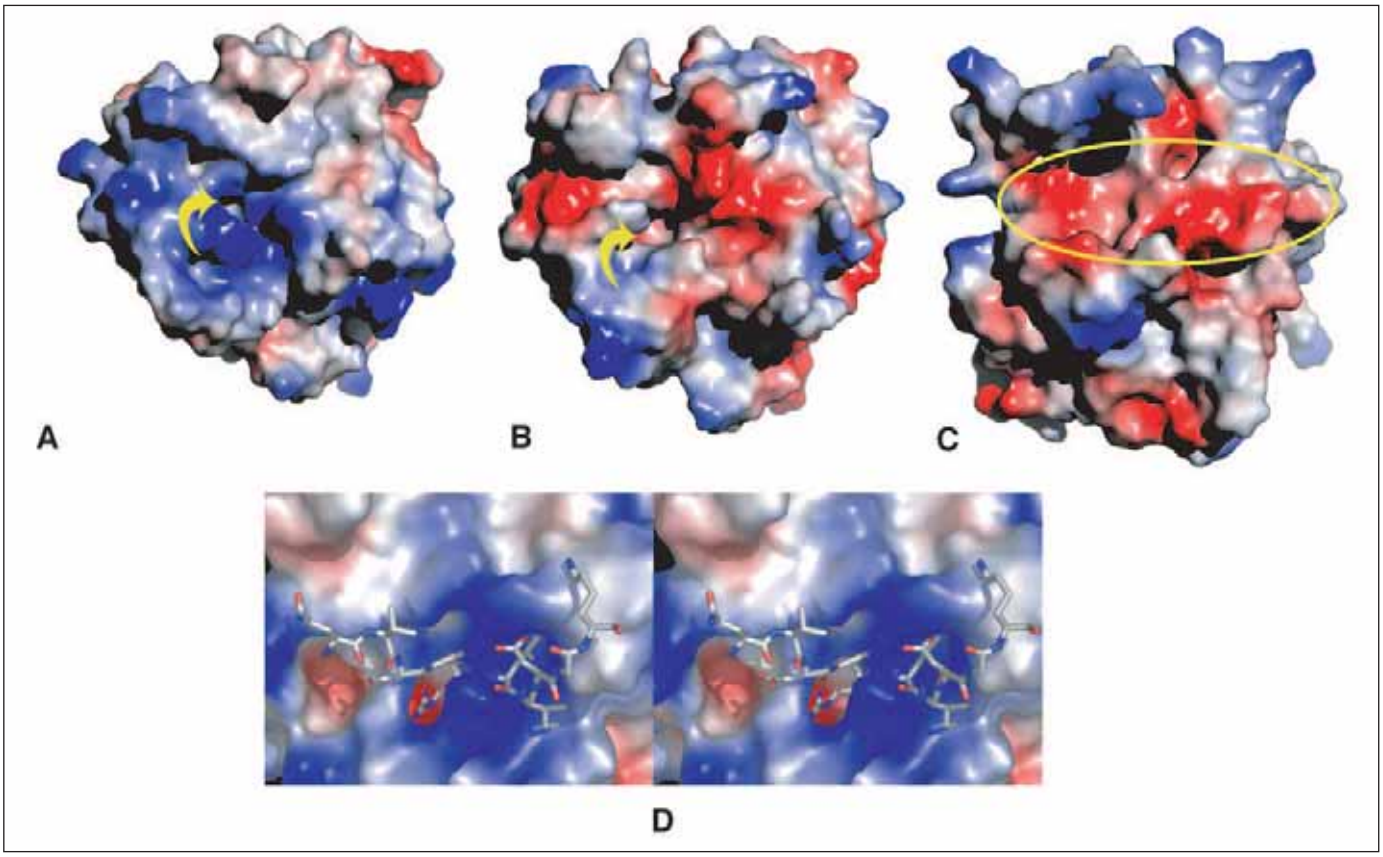

FIGURE 6. Surface charge distribution of the channel leading to the catalytic site in ACC-C (*A*) and TSV-PA (*B*) in the same relative orientation. The S1 subsites are indicated by *yellow arrows*. *C*, surface charge of protein C zymogen; the *yellow ring* indicates the position of the modeled activation peptide. *D*, stereo view of the proposed interactions of the modeled activation peptide of protein C (*stick model*) in the active site cleft (charged surface).

These structural changes indicate the possible existence of an allosteric mechanism.

The polar character of the ends of the active site observed in the crystal structure of ACC-C indicates that zwitterzonic inhibitors such as 4-(4-amidinephenyl)butanoic acid would bind optimally with the guanidine and carboxylic sections interacting with Asp^{189} and Arg^{60}, respectively, thus contributing to substrate specificity. The potent inhibitory effects on both amidolytic and anticoagulant activities induced by D-Phe-Pro-Arg-cmk and derivatives such as dansyl-Glu-Gly-Arg-cmk and dansyl-Gly-Gly-Arg-cmk are mainly due to the hydrogen bonds formed to Lys^{192} and Asn^{218} and hydrophobic interactions with Trp^{99}, Leu^{172}, and Val^{215}, which simultaneously occupy the S1 subsite and modulate access to the catalytic site.

The two significant differences between ACC-C and TSV-PA are: (i) the positively charged surface surrounding the catalytic site and (ii) the three carbohydrate moieties that protrude on the surface of ACC-C, which probably play a pivotal role in macromolecular substrate recognition or specificity. Both ACC-C and TSV-PA share a long circulating half-life and demonstrate high resistance to protein-type macromolecular inhibitors, making them interesting targets for drug design. Macromolecular substrates such as bovine pancreatic trypsin and soybean trypsin inhibitors are unable to bind to TSV-PA due the positioning of the phenyl ring of Phe^{193} and in AaV-SP-I/II due to the presence of extended *N*-linked carbohydrate groups in the 37-loop. In ACC-C, both these strategies are utilized simultaneously, whereas position 193 is occupied by a glycine, the indole of Trp^{99} and the *N*-linked oligosaccharides are positioned to prevent interaction with these macromolecular inhibitors.

Under physiological conditions, thrombin depends on thrombomodulin to switch between functioning as a coagulant or anticoagulant enzyme and the TME45 domains form the primary binding site of the PC zymogen, permitting the hydrolysis of the scissile bond between Arg^{169} and Leu^{170}. In the thrombomodulin-independent activation of PC by ACC-C the positive charge present on the interfacial surface and carbohydrate moieties are important features that could play crucial roles in PC recognition/binding/activation.

Acknowledgment—We are grateful to Dr. T. Schreier (Pentapharm, Basel) for providing the samples of ACC-C (Protac®).

REFERENCES

1. Colman, R. W., Marder, V. J., Salzman, E. W., and Hirsh, J. (1994) in *Hemostasis and Thrombosis: Basic Principles and Clinical Practice* (Colman, R. W., ed) 3rd Ed., pp. 3–18, J. B. Lippincott Company, Philadelphia
2. Davie, E. W., Fujikawa, K., and Kisiel, W. (1991) *Biochemistry* **30,** 10363–10370
3. Esmon, C. T., and Fukudome, K. (1995) *Semin. Cell Biol.* **6,** 259–268
4. Walker, F. J., Sexton, P. W., and Esmon, C. T. (1979) *Biochim. Biophys. Acta* **571,** 333–342
5. Fulcher, C. A., Gardiner, J. E., Griffin, J. H., and Zimmerman, T. S. (1984) *Blood* **63,** 486–489
6. Schwarz, H. P., Fischer, M., Hopmeier, P., Batard, M. A., and Griffin, J. H. (1984) *Blood* **64,** 1297–1300
7. Griffin, J. H., Zlokovic, B., and Fernandez, J. A. (2002) *Semin. Hematol.* **39,** 197–205
8. Tu, A. T. (1991) in *Handbook of Natural Toxins* (Tu, A. T., ed) 1st Ed., pp. 827–830, Marcel Dekker, New York
9. Marsh, N., and Williams, V. (2005) *Toxicon* **45,** 1171–1181
10. Zhang, Y., Wisner, A., Maroun, R. C., Choumet, V., Xiong, Y., and Bon, C. (1997) *J. Biol. Chem.* **272,** 20531–20537
11. Parry, M. A., Jacob, U., Huber, R., Wisner, A., Bon, C., and Bode, W. (1998) *Structure*

(*Camb.*) **6,** 1195–1206
12. Stocker, K. (1978) in *Handbook of Experimental Pharmacology* (Markwardt, F., ed) 1st Ed., pp. 451–484, Springer-Verlag, Berlin
13. Kisiel., W., Kondo, S., Smith, K. J., McMullen, B. A., and Smith, L. F. (1987) *J. Biol. Chem.* **262,** 12607–12613
14. Gempeler-Messina, P. M., Volz, K., Bühler, B., and Muller, C. (2001) *Haemostasis* **31,** 266–272
15. Otwinowski, Z., and Minor, W. (1997) *Methods Enzymol.* **276,** 307–326
16. Navaza, J. (1994) *Acta Crystallogr. Sect. A* **50,** 157–163
17. Murshudov, G. N., Vagin, A. A., and Dodson, E. J. (1997) *Acta Crystallogr. Sect. D Biol. Crystallogr.* **53,** 240–255
18. Jones, T. A. (1985) *Methods Enzymol.* **115,** 157–171
19. Laskowski, R. A., MacArthur, M. W., Moss, D. S., and Thornton, J. M. (1993) *J. Appl. Crystallogr.* **26,** 283–291
20. Harley, B. S., and Shotton, D. M. (1971) in *The Enzymes* (Boyer, P. D., ed) 1st Ed., pp. 323–373, Academic Press, New York
21. McMullen, B. A., Fujikawa., J., and Kisiel, W. (1988) *Biochemistry* **28,** 674–679
22. Zhu, Z., Liang, Z., Zhang, T., Zhu, Z., Xu, W., Teng, M., and Niu, L. (2005) *J. Biol. Chem.* **280,** 10524–10529
23. Zhang, Y., Wisner, A., Xiong, Y., and Bon, C. (1995) *J. Biol. Chem.* **270,** 10246–10255
24. Bode, W., and Schwager, P. (1975) *J. Mol. Biol.* **98,** 693–717
25. Sturzebecher, J., Neumann, U., and Meier, J. (1991) *Toxicon* **29,** 151–155
26. Renatus, M., Engh, R. A., Stubbs, M. T., Huber, R., Fischer, S., Kohnert, U., and Bode, W. (1997) *EMBO J.* **16,** 4797–4805
27. Fuentes-Prior. P., Iwanaga, Y., Huber, R., Pagila, R., Rumennik, G., Seto, M., Morser, J., Light, D. R., and Bode, W. (2000) *Nature* **404,** 518–525
28. Mather, T., Oganessyan, V., Hof, P., Huber, R., Foundling, S., Esmon, C., and Bode, W. (1996) *EMBO J.* **15,** 6822–6831
29. Nagashima, M., Lundh, E., Leonard, J. C., Morser, J., and Parkinson, J. F. (1993) *J. Biol. Chem.* **268,** 2888–2892
30. Adler, M., Seto, M. H., Nitecki, D. E., Lin, J. H., Light, D. R., and Morser, J. (1995) *J. Biol. Chem.* **270,** 23366–23372
31. Stenflo, J. (1976) *J. Biol. Chem.* **251,** 355–363
32. Esmon, C. T. (1989) *J. Biol. Chem.* **264,** 4743–4746

iii. Convulxina

Convulxina (CVX), uma lectina tipo C, isolada do veneno da serpente *Crotalus durissus terrificus*, causa distúrbios cardiovasculares e respiratórios e é uma potente ativadora de plaquetas via interação com glicoproteína VI (Vargaftig et al., 1980). A estrutura cristalina de CVX mostrou que sua estrutura quaternária é formada por 4 heterodímeros $(\alpha/\beta)_4$ ligados por pontes disulfeto formando uma estrutura cíclica, o que explica seu comportamento hidrodinâmico atípico. Outra peculiaridade da CVX é não ser capaz de ligar cálcio como nas proteínas de ligação de FIX e flavocetina A devidas mutações locais que interferem no perfil eletrostático do sítio de ligação de cálcio. A sobreposição da CVX sobre outras lectinas tipo C do veneno de serpentes estruturalmente homólogas, mostra que CVX unicamente não interage com fator von Willebrand, pois apresenta deleções no laço de interação com fator von Willebrand, que está localizado na região entre as cadeias α e β da estrutura heterodimérica. Outras lectinas tipo C de venenos de serpentes também ativam a agregação plaquetária, porém dependem da prévia complexação com fator von Willebrand e posterior interação com glicoproteina Ibα. Estes estudos comparativos e espalhamento de raios X a baixos ângulos estão atualmente sendo usados para compreender seu modo de funcionamento.

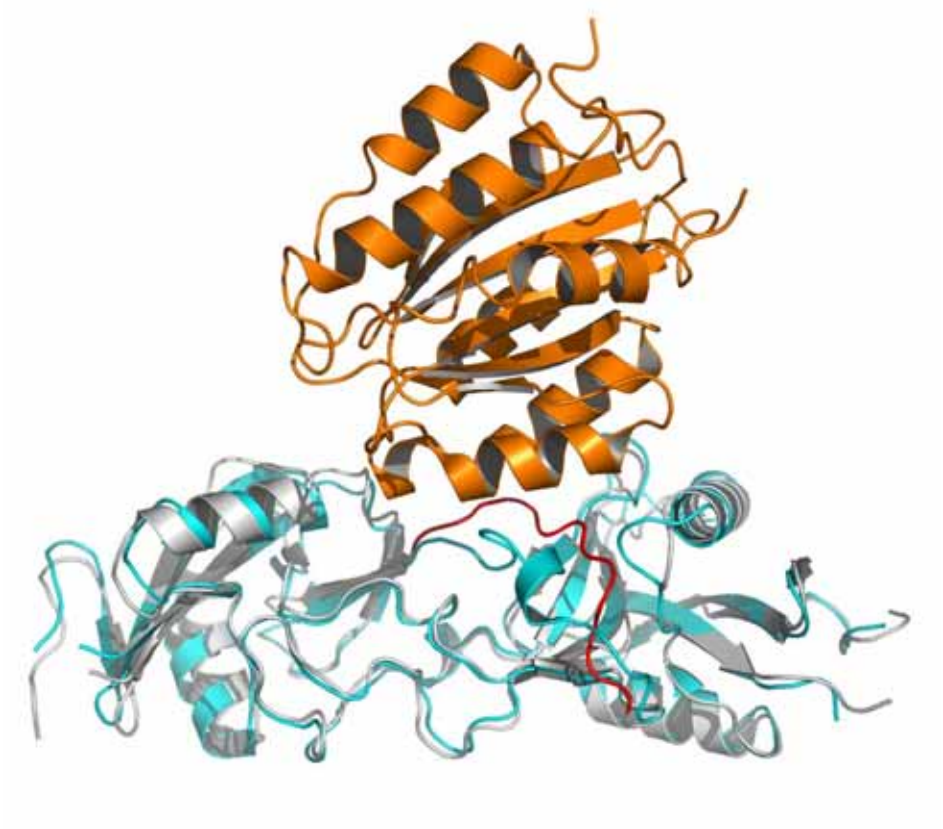

Figura 4: Sobreposição das estruturas de CVX (cinza) sobre a botrocetin (azul) complexada com fator von Willebrand (laranja). As diferenças estruturas no sítio de interação com fator von Willebrand está evidenciado em vermelho.

Acta Crystallographica Section D
Biological Crystallography
ISSN 0907-4449

Initial structural analysis of an $\alpha_4\beta_4$ C-type lectin from the venom of *Crotalus durissus terrificus*

M. T. Murakami,[a] L. Watanabe,[a] L. M. Gava,[a] S. P. Zela,[a] A. C. O. Cintra[b] and R. K. Arni[a]*

[a]Department of Physics, IBILCE/UNESP, R. Cristovão Colombo 2265, CEP 150054-000, São Jose do Rio Preto-SP, Brazil, and [b]Faculdade de Ciências Farmacêuticas de Ribeirão Preto, USP, CEP 14040-903, Ribeirão Preto-SP, Brazil

Correspondence e-mail: arni@df.ibilce.unesp.br

Received 2 July 2003
Accepted 22 July 2003

Convulxin, an $\alpha\beta$ C-type lectin, is a potent platelet activator isolated from the venom of the South American rattlesnake *Crotalus durissus terrificus*. It is a 26.5 kDa $\alpha\beta$ heterodimer consisting of two homologous disulfide-linked chains. The crystals belong to space group $I4$, with unit-cell parameters $a = b = 131.61$, $c = 121.85$ Å, and diffraction data were collected to 2.7 Å. The structure was solved by molecular replacement and the asymmetric unit contains two $\alpha\beta$ heterodimers, each of which forms a disulfide-linked cyclic $\alpha_4\beta_4$ tetramer in the unit cell. These $\alpha_4\beta_4$ tetramers are stacked to form a large solvent channel.

1. Introduction

Thrombus formation involves platelet adhesion receptors, glycoproteins Ib-IX-V and VI, which bind von Willebrand Factor (vWF) and collagen. Platelet adhesion is mediated by the receptor glycoprotein (GP), which plays a key role in haemostasis. Adhesion of activated platelets to sites of vascular injury is initiated by the interaction of vWF, which is exposed on the subendothelium, with the platelet GPIb. These interactions then initiate intracellular signals which lead to degranulation, significant elevation of cytosolic Ca^{2+} levels and activation of integrin and GPIIb-IIIa which binds vWF or fibrinogen and mediates platelet aggregation (Andrews *et al.*, 1996).

A number of snake-venom proteins which are haemostatically active and interfere with the interaction of vWF and platelet GPs have been characterized (Fujimara *et al.*, 1996). Some of these inhibit coagulation factors and platelet components. These proteins affect vWF–platelet GPIb-V-IX. Echicetin (Peng *et al.*, 1993), alboaggregin-B and agglucetin (Wang & Huang, 2001) bind GPIbα, while rhodocetin interacts with GPIa-IIa (Wang *et al.*, 1999) and convulxin (CVX) interacts with GPVI (Prado-Franceschi & Brazil, 1981). However, alboaggregin-A (Asazuma *et al.*, 2001) and alboluxin bind both GPVI and GPIbα (Andrews *et al.*, 1996).

CVX, a C-type lectin (Drickamer, 1993) is a potent platelet-aggregation inducer (Vargaftig *et al.*, 1980; Francischetti *et al.*, 1997; Polgár *et al.*, 1997; Jandrot-Perrus *et al.*, 1997) isolated from the venom of the Brazilian rattlesnake *Crotalus durissus terrificus*. This protein is a disulfide-linked heterodimer composed of two homologous subunits CVXα (13.9 kDa) and CVXβ (12.6 kDa) (Leduc & Bon, 1998). These subunits display significant homology to the carbohydrate-recognition domain (CRD) of the C-type lectin family, but lack the consensus sequences for both carbohydrate and Ca^{2+} binding (Leduc & Bon, 1998). Binding of CVX is not inhibited by α-thrombin, fibrinogen, ADP, RGDS peptides or adrenaline. The mechanism of CVX-mediated activation of platelets has been shown to be dependent on Ca^{2+} but independent of galactose or mannose, fibrinogen, ADP and cyclooxygenase (Vargaftig *et al.*, 1983). In human platelets, collagen binds to GPIa-IIa and GPVI and it has been proposed that CVX binds to the collagen receptor GPVI with high affinity (K_d = 30 p*M*; Prado-Franceschi & Brazil, 1981).

CVX has been suggested to exist as a trimer ($\alpha_3\beta_3$) in solution with a molecular weight of between 72 and 80 kDa (Niedergang *et al.*, 2000). We have crystallized CVX and solved the structure by molecular-replacement methods. In the crystal structure, the asymmetric unit contains two $\alpha\beta$ heterodimers, resulting in the presence of two cyclic $\alpha_4\beta_4$ tetramers in the unit cell. An interchain disulfide bridge between the C-terminus of the α-subunit of one heterodimer and the N-terminus of the β-subunit of a neighbouring heterodimer stabilize each $\alpha_4\beta_4$ tetramer, indicating that this protein exists as an $\alpha_4\beta_4$ tetramer in solution, like flavocetin (Fukuda *et al.*, 2000).

2. Methods

2.1. Protein purification

C. durissus terrificus crude venom was obtained in lyophilized form from a local serpentarium and 250 mg was dissolved in 5 ml of 20 m*M* Tris–HCl pH 8.0 buffer. This solution was centrifuged, filtered (0.4 μ*M*) and applied

to a benzamidine Sepharose (CL6B) column to remove gyroxin, a thrombin-like enzyme. The unbound fraction which contained CVX was collected and further purified on a Sephacryl S300 column. The sample was then concentrated to 10 mg ml^{-1} in Centricon microconcentrators (Amicon).

Silver-stained SDS–PAGE gels (9%) indicated the presence of a number of protein bands. Dynamic light-scattering (Dynapro 801) experiments conducted at 291 K indicated the presence of a single monodispersive population.

2.2. Crystallization

Crystallization trials were conducted using the vapour-diffusion technique, in which 1 µl of protein was mixed with an equal amount of the corresponding reservoir solution. Crystals were obtained when the protein was equilibrated against 100 m*M* sodium acetate buffer containing 200 m*M* $CaCl_2$ pH 4.6 and when 14% 2-methyl-2,4-pentanediol was used as a precipitant.

2.3. X-ray diffraction analysis

Monocromatic X-rays were produced by a Rigaku RU300 (Rigaku-Denki) rotating-anode generator operating at 50 kV and 80 mA equipped with Osmic mirrors and diffraction intensities were recorded using a MAR345 (MAR Research) imaging-plate detector. A single crystal with a maximum dimension of 0.1 mm (Fig. 1) was mounted in a cryoloop (20% glycerol), flash-frozen and diffraction data were collected at 100 K. Diffraction was observed to a maximum resolution of 2.2 Å; however, data beyond 2.7 Å were weak and were not included in the processing. Data were indexed with *DENZO* and scaled and reduced using *SCALEPACK* (Otwinowski & Minor, 1997) (Table 1).

3. Results

The SDS gels showed a ladder-like distribution, with a number of protein bands which can be attributed to different states of aggregation of the α- and β-subunits. The dynamic light-scattering experiment, however, indicated the existence of a monomodal distribution.

The crystals belong to the space goup *I*4, with unit-cell parameterers $a = b = 131.61$, $c = 121.85$ Å. Processing of the 244 151 measured reflections to 2.2 Å led to 25 792 unique reflections with an $R_{\rm merge}$ of 4.9% for data to 2.7 Å (20.7% in the last shell).

Assuming a molecular mass of 26.5 kDa per asymmetric unit, Matthews parameter ($V_{\rm M}$) values (Matthews, 1968) of 4.8 and 3.2 Å^3 Da^{-1} were obtained for the presence of two and three heterodimers per asymmetric unit, corresponding to solvent contents of 73.9 and 60.9%, respectively.

Molecular replacement was carried out using the program *AMoRe* (Navaza, 1994) using a model built based on the atomic coordinates of the C-type lectin flavocetin-A from the venom of *Trimeresurus flavoviridis* (Fukuda *et al.*, 2000; PDB code 1c3a). A solution was obtained for two molecules present in the asymmetric unit. Rigid-body refinement of this solution using data in the resolution range 30.0–3.0 Å resulted in a correlation coefficient of 41.5 and an *R* factor of 50.3%. Refinement with *CNS* (Brünger *et al.*, 1998) and model building using *TURBO-FRODO* resulted in an *R* factor of 27% ($R_{\rm free}$ = 33%) for data in the same resolution range.

Table 1
Data-collection and processing statistics.

Values in parentheses are for the last resolution shell.

Space group	*I*4
Unit-cell parameters (Å)	$a = b = 131.61$, $c = 121.85$
Maximum resolution (Å)	2.7
No. of unique reflections	25792
$R_{\rm merge}$† (%)	4.9 (20.7)
Completeness (%)	96.9 (99.3)
$V_{\rm M}$ (Å^3 Da^{-1})	4.8
No. of molecules per AU	2
$I/\sigma(I)$	15.5 (4.0)

† $R_{\rm merge} = \sum\sum I(h)_i - \langle I(h)\rangle / \sum\langle I(h)\rangle$, where I_h is the observed intensity of the *i*th measurement of reflection *h* and $\langle I(h)\rangle$ is the mean intensity of reflection *h* calculated after scaling.

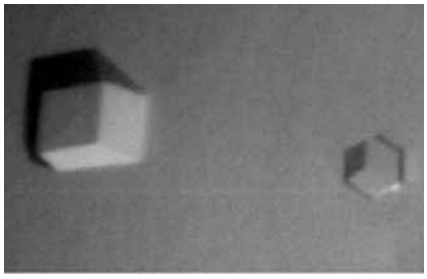

Figure 1
Photomicrograph of tetragonal crystals of CVX (maximum dimension 0.1 mm).

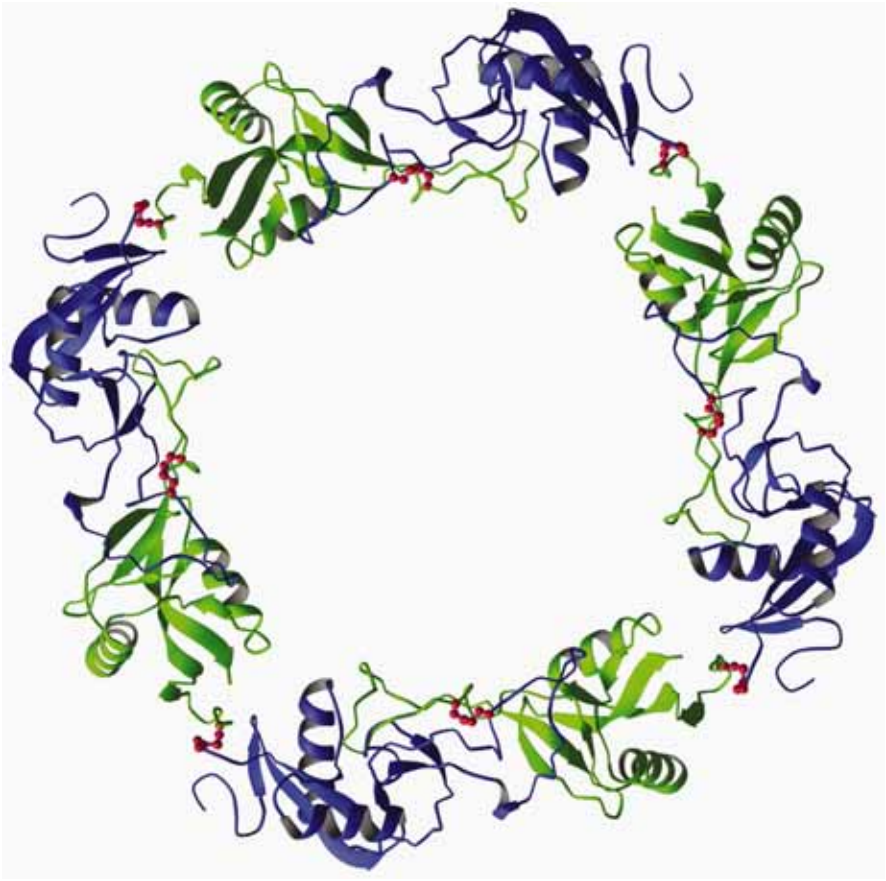

Figure 2
Ribbon representation of the tetrameric structure of CVX. The α- and β-subunits are shown in blue and green, respectively. The disulfide bonds (C^{α}, C^{β}, S^{γ}) stabilizing the $\alpha\beta$ heterodimers and the $\alpha_4\beta_4$ cyclic tetramer are shown in red. The figure was generated using *RIBBONS* (Carson, 1991).

The asymmetric unit contains two $\alpha\beta$ heterodimers. Each heterodimer is linked by a disulfide bridge formed between the α-subunit of one heterodimer and the β-subunit of a neighbouring heterodimer to form a cyclic $\alpha_4\beta_4$ tetramer (Fig. 2) analogous to the cyclic $\alpha_4\beta_4$ tetramer reported in the crystal stucture of flavocetin-A (Fukuda *et al.*, 2000). In contrast to the structure of flavocetin-A, which contains only one $\alpha_4\beta_4$ tetramer, the unit cell of CVX contains two $\alpha_4\beta_4$ tetramers. These cyclic tetramers are stacked on each other, forming a large solvent channel with a diameter of approximately 65 Å. These results indicate that CVX could also be present as an $\alpha_4\beta_4$ tetramer in solution and not as an $\alpha_3\beta_3$ protein (Leduc & Bon, 1998).

Higher resolution data will be collected at the Laboratorio Nacional de Luz Síncrotron (Campinas, Brazil) and structure refinement will be initiated.

This study was supported by grants from FAPESP/SMOLBNet and CNPq (Brazil). MTM and LW are recipients of FAPESP fellowships and LMG is the recipient of a CNPq fellowship. We are grateful to C. B. Oliva for expert assistence.

References

Andrews, R. K., Kroll, M. H., Ward, C. M., Rose, J. W., Scarborough, R. M., Smith, A. I., Lopez, J. A. & Berdnt, M. C. (1996). *Biochemistry*, **35**, 12629–12639.

Asazuma, N., Marshall, S. J., Berlanga, O., Snell, D., Poole, A. W., Berndt, M. C., Andrews, R. K. & Watson, S. P. (2001). *Blood*, **97**, 3989–3991.

Brünger, A. T., Adams, P. D., Clore, G. M., DeLano, W. L., Gros, P., Grosse-Kunstleve, R. W., Jiang, J.-S., Kuszewski, J., Nilges, M., Pannu, N. S., Read, R. J., Rice, L. M., Simonson, T. & Warren, G. L. (1998). *Acta Cryst.* D**54**, 905–921.

Carson, M. (1991). *J. Appl. Cryst.* **24**, 958–961.

Drickamer, K. (1993). *Prog. Nucleic Acid Res. Mol. Biol.* **45**, 207–232.

Francischetti, I. M. B., Saliou, B., Leduc, M., Carlini, C. R., Hatmi, M., Randon, J., Faili, A. & Bon, C. (1997). *Toxicon*, **35**, 1217–1228.

Fujimara, Y., Kawasaki, T. & Titani, K. (1996). *Thromb. Haemost.* **76**, 633–639.

Fukuda, K., Mizuno, H., Atoda, H. & Morita, A. (2000). *Biochemistry*, **39**, 1915–1923.

Jandrot-Perrus, M., Lagrue, A.-H., Okuma, M. & Bom, C. (1997). *J. Biol. Chem.* **272**, 27035–27041.

Leduc, M. & Bon, C. (1998). *Biochem. J.* **333**, 389–393.

Matthews, B. W. (1968). *J. Mol. Biol.* **33**, 491–497.

Navaza, J. (1994). *Acta Cryst.* A**50**, 157–163.

Niedergang, F., Alcover, A., Knight, C. G., Farndale, R. W., Barnes, M. J., Francischetti, I. M. B., Bom, C. & Leduc, M. (2000). *Biochem. Biophys. Res. Commun.* **273**, 246–250.

Otwinowski, Z. & Minor, W. (1997). *Methods Enzymol.* **276**, 307–326.

Peng, M., Lu, W., Beviglia, L., Niewiarowski, S. & Kirby, E. P. (1993). *Blood*, **81**, 2321–2328.

Polgár, J., Clemetson, J. M., Kehrel, B. E., Wiedemann, M., Magnenat, E. M., Wells, T. N. C. & Clementson, K. J. (1997). *J. Biol. Chem.* **272**, 13576–13583.

Prado-Franceschi, J. & Brazil, O. V. (1981). *Toxicon*, **19**, 875–887.

Vargaftig, B. B., Joseph, D., Wal, F., Marlas, G., Chignard, M. & Chevance, G. L. (1983). *Eur. J. Pharmacol.* **92**, 57–68.

Vargaftig, B. B., Prado-Franceschi, J., Chignard, M., Lefort, J. & Marlas, G. (1980). *Eur. J. Pharmacol.* **68**, 451–464.

Wang, R., Kini, R. M. & Chung, M. C. (1999). *Biochemistry*, **38**, 7584–7593.

Wang, W.-J. & Huang, T.-F. (2001). *Thromb. Haemost.* **86**, 1077–1082.

Available online at www.sciencedirect.com
SCIENCE DIRECT®
Biochemical and Biophysical Research Communications 310 (2003) 478–482
BBRC
www.elsevier.com/locate/ybbrc

Crystal structure of the platelet activator convulxin, a disulfide-linked $\alpha_4\beta_4$ cyclic tetramer from the venom of *Crotalus durissus terrificus*

M.T. Murakami,[a] S.P. Zela,[a] L.M. Gava,[a] S. Michelan-Duarte,[a] A.C.O. Cintra,[b] and R.K. Arni[a,*]

[a] *Department of Physics, IBILCE/UNESP, R. Cristovão Colombo 2265, CEP 15054-000, São Josédo Rio Preto-SP, Brazil*
[b] *Faculdade de Ciências Farmacêuticas de Ribeirão Preto, USP, CEP 14040-903, Ribeirão Preto-SP, Brazil*

Received 26 August 2003

Abstract

Convulxin (CVX), a C-type lectin, isolated from the venom of the South American rattlesnake *Crotalus durissus terrificus*, causes cardiovascular and respiratory disturbances and is a potent platelet activator which binds to platelet glycoprotein GPVI. The structure of CVX has been solved at 2.4 Å resolution to a crystallographic residual of 18.6% ($R_{free} = 26.4\%$). CVX is a disulfide linked heterodimer consisting of homologous α and β chains. The heterodimers are additionally linked by disulfide bridges to form cyclic $\alpha_4\beta_4$heterotetramers. These domains exhibit significant homology to the carbohydrate-binding domains of C-type lectins, to the factor IX-binding protein (IX-bp), and to flavocetin-A (Fl-A) but sequence and structural differences are observed in both the domains in the putative $Ca^{2+}$and carbohydrate binding regions.

Keywords: C-type lectin; Platelet activation factor; Snake venom; *Crotalus durissus terrificus*; Crystal structure; Cyclic $\alpha_4\beta_4$heterotetramer

Convulxin (CVX), a glycosylated C-type lectin isolated from the venom of the South American rattlesnake *Crotalus durissus terrificus* [1], does not display phospholipase, esterolytic or amidolytic activities and does not interfere with the plasmatic factors. CVX is a potent platelet activation factor (PAF) [1–5] which causes cardiovascular and respiratory disturbances. CVX stimulates thrombocytes resulting in aggregation and the release of ADP, and interacts with the platelet glycoprotein GPVI [6]. CVX activates mammalian platelets through a mechanism that involves binding and clustering of GPVI receptors [4]. This clustering of GPVI receptors results in the activation of Src kinases [7], phosphorylation of the Fc receptor, and activation of p72SYK which are considered to play a role in downstream activation of platelets [4]. CVX functions via a Ca^{2+} dependent mechanism which is independent of galactose or mannose, fibrinogen, and ADP [2]. Aspirin (100 μM) does not interfere with activity, indicating that thromboxane A_2 synthesis which is stimulated by CVX is independent of cyclooxygenase. Fibrinogen, α-thrombin, RGDS peptides [8], and adrenaline do not inhibit the high affinity ($K_d = 30$ pM) binding of CVX to the collagen receptor GPVI [9]. CVX activity can be reversed by the inclusion of EDTA or protacyclin and prostaglandins are strong inhibitors of CVX-induced aggregation. Doses of 0.001–0.1 μg/mL result in about 50% activation of washed platelets [10]. Small doses of CVX do not cause lysis of the platelet membrane, whereas intravenously administered larger doses (3 μg/kg) may be cytolytic as evidenced by the liberation of serotonin and biogenic amines [11].

CVX is a disulfide linked heterodimer composed of two homologous subunits CVXα (13.9 kDa) and CVXβ (12.6 kDa) [12] which also display significant homology to the carbohydrate recognition domain (CRD) of the C-type lectin family [13], but lack the

* Corresponding author. Fax: +55-17-221-22-47.
E-mail address: arni@df.ibilce.unesp.br (R.K. Arni).

0006-291X/$ - see front matter © 2003 Elsevier Inc. All rights reserved.
doi:10.1016/j.bbrc.2003.09.032

consensus sequence for both carbohydrate and Ca^{2+} binding [12].

We present here the crystal structure of CVX which is the first structure of a protein isolated from the venom of *C. d. terrificus* using high-resolution X-ray crystallographic techniques.

Materials and methods

CVX was purified and crystallized as described previously [14]. Briefly, crude lyophilized venom was obtained from a local serpentarium and 250 mg was dissolved in 5 ml of a 20 mM Tris–HCl (pH 8.0) buffer. This solution was then applied on a benzamidine–Sepharose (CL6B) affinity column to remove the thrombin-like enzyme giroxin. The unbound fraction which contained CVX was pooled and further purified on a Sephacryl S300 column. The sample was then concentrated to 10 mg ml^{-1} in Centricon micro-concentrators (Amicon).

Silver stained SDS gels (9%) indicated the presence of a ladder-like distribution attributed to various states of aggregation of the α and β chains. However, dynamic light scattering (Dynapro 801) conducted at 18 °C indicated the presence of a single mono-dispersive population with an estimated molecular mass of 100,000 kDa.

Crystals were obtained when a 10 mg ml^{-1} protein solution of CVX was equilibrated against a reservoir solution of 100 mM sodium acetate buffer containing 200 mM $CaCl_2$, pH 4.6, and 14% of 2-methyl-2,4-pentanediol [14].

X-ray diffraction data were collected using a Rigaku RU300 rotating anode generator operating at 50 kV and 80 mA equipped with osmic mirrors and a MAR345 (MAR Research) imaging plate detector. A single crystal with a maximum dimension of 0.1 mm was transferred to a cryoprotectant solution which contained 20% glycerol and flash-frozen and diffraction data were collected at 100 K. The crystals belong to the space group *I*4 with unit cell parameters $a = b = 131.55$ Å and $c = 112.91$ Å and diffraction was observed to a maximum resolution of 2.2 Å; however, data beyond 2.4 Å were weak and were not used. The data were indexed and reduced using the DENZO/SCALEPACK [15] suite of programs (Table 1).

Table 1
Data collection and refinement statistics

Data collection	
Space group	*I*4
Unit cell dimensions (Å)	$a = b = 131.55$; $c = 112.91$
Max. resolution (Å)	2.4
No. of unique reflections	36,900
R_{merge} (%) (last shell)	6.1 (40.4)
Completeness (%) (last shell)	97.6 (98.8)
$I/\sigma I$ (last shell)	12.1 (1.9)
Refinement	
Resolution range (Å)	30.0–2.4
R (%)	18.4
R_{free} (%)	25.7
No. of non-hydrogen atoms	4318
No. of solvent molecules	197
Mean *B*-value protein atoms (Å^2)	47.3
Mean *B*-value solvent atoms (Å^2)	45.9
r.m.s. deviations from ideal values	
Bond lengths (Å)	0.032
Bond angles (°)	2.639
Torsion angles (°)	8.429

The molecular masses of the α- and β-subunits of CVX are 13.9 and 12.6 kDa, respectively, resulting in a combined molecular mass of 26.5 kDa for the αβ-heterodimer. Matthews parameter values [16] of 4.8 and 3.2 were obtained for the presence of two or three heterodimers in the asymmetric unit which correspond to solvent contents of 73.2% and 59.8%, respectively.

The crystal structure was solved using the atomic coordinates of the C-type lectin Fl-A [17; PDB Code 1C3A] stripped of solvent molecules. Molecular replacement using the program AMoRe [18] provided a clear solution for the two αβ-heterodimers in the asymmetric unit using data in the resolution range 30.0–3.0 Å, confirming the existence of two heterodimers in the asymmetric unit with a corresponding solvent content of 73.2%. Rigid body refinement of this solution resulted in a correlation coefficient of 41.5% and an *R*-factor of 50.3%. Refinement was carried out imposing non-crystallographic symmetry restraints and following the simulated annealing (3000 K) and positional refinement procedures as incorporated in the program CNS [19]. The refinement was interspersed with successive rounds of model building using TURBO FRODO (Biographics, Marseille, France) and resulted in an *R*-factor of 27.3% ($R_{free} = 33.1\%$). TLS and restrained refinement was carried out with Refmac5 [20] as implemented in the CCP4 package [21] and the refinement converged to a *R*-factor of 18.4% ($R_{free} = 25.7\%$) for all data between 30.0 and 2.4 Å without utilizing either a σ or an intensity cutoff (Table 1).

The stereochemistry of the final model was examined using PROCHECK [22] (Table 1) and indicated that the model possessed excellent stereochemistry. As much as 99.1% of the residues are located in the favoured region in the Ramachandran plot [23]. The only exceptions are amino acids Asp12α and Asp12β in both molecules in the asymmetric unit which form a turn.

Results

Sequence alignments of the α- and β-subunits of CVX with the corresponding subunits of IX-bp and Fl-A from the venom of *Trimeresurus flavoviridis* indicate high sequence homology (Fig. 1). The disulfide bonding pattern is highly conserved except that counterparts of the C-terminal cysteine (Cys135) of the α-subunit and N-terminal cysteine (Cys3) of the β-subunit in CVX are present in Fl-A but are absent in IX-bp.

Quatenary structure

The α- and β-subunits of CVX are linked by a disulfide bridge formed between Cys81α and Cys77β (Fig. 2) and these αβ-heterodimers are structurally similar to the heterodimers reported in the crystal structures of the IX-bp [24] and Fl-A [17] from *T. flavoviridis*.

A number of studies have indicated that CVX exists as an $\alpha_3\beta_3$ protein based on its hydrodynamic behaviour. However, the presence of an additional disulfide bridge formed between neighbouring αβ-heterodimers (Cys135α and Cys3β) results in the generation of a cyclic $\alpha_4\beta_4$ tetramer in the structures of CVX (Fig. 3) and Fl-A [17]. The crystal structure of Fl-A contains a single disulfide linked cyclic α_4 β_4 tetramer in the asymmetric unit [17]. In CVX, two αβ-heterodimers are

```
                1       10        20        30        40        50        60        70
                |-------+---------+---------+---------+---------+---------+---------|
cvx_alpha       GLHCPSDWYYYDQHCYRIFNEEMNWEDAEWFCTKQAKGAHLVSIKSAKEADFVAWMVTQNIEESFSHVSI
FL-A_alpha      DFDCIPGWSAYDRYCYQAFSKPKNWEDAESFCEEGVKTSHLVSIESSGEGDFVAQLVAEKIKTSFQYVWI
IX-bp_alpha       DCPSGWSSYEGHCYKPFKLYKTWDDAERFCTEQAKGGHLVSIESAGEADFVAQLVTENIQNTKSYVWI

                71      80        90        100       110       120       130  135
                |-------+---------+---------+---------+---------+---------+----|
cvx_alpha       GLRVQNKEKQCSTKWSDGSSVSYDNLLDLYITKCSLLKKETGFRKWFVASCIGKIPFVCKFPPQC
FL-A_alpha      GLRIQNKEQQCRSEWSDASSVNYENLVKQFSKKCYALKKGTELRTWFNVYCGTENPEVCKYTPEC
IX-bp_alpha     GLRVQGKEKQCSSEWSDGSSVSYENWIEAESKTCLGLEKETGFRKWVNIYCGQQNPFVCEA

                1       10        20        30        40        50        60        70
                |-------+---------+---------+---------+---------+---------+---------|
cvx_beta        GFCCPSHWSSYDRYCYKVFKQEMTWADAEKFCTQQHTGSHLVSFHSTEEVDFVVKMTHQSLKSTFFWIGA
FL-A_beta       GFCCPLGWSSYDEHCYQVFQQKMNWEDAEKFCTQQHKGSHLVSFHSSEEVDFVTSKTFPILKYDFVWIGL
IX-bp_beta        DCPSDWSSYEGHCYKPFSEPKNWADAENFCTQQHAGGHLVSFQSSEEADFVVKLAFQTFGHSIFWMGL

                71      80        90        100       110       120  125
                |-------+---------+---------+---------+---------+----|
cvx_beta        NNIWNKCNWQWSDGTKPEYKEWHEEFECLISRTFDNQWLSAPCSDTYSFVCKFEA
FL-A_beta       SNVWNECTKEWSDGTKLDYKAWSGGSDCIVSKTTDNQWLSMDCSSKYYVVCKFQA
IX-bp_beta      SNVWNQCNWQWSNAAMLRYKAWAEESYCVYFKSTNNKWRSRACRMMAQFVCEFQA
```

Fig. 1. Sequence alignment of the α and β chains of CVX, Fl-A, and IX-bp. This figure was produced using MULTIALIGN [25].

Fig. 2. Ribbon representation of the CVX $\alpha_4\beta_4$ cyclic tetramer. The α and β chains are presented in blue and green, respectively. Inter-chain and intra-chain disulfide bonds (Cα, Cβ, and Sγ) are in pink. Figure generated using RIBBONS [26]. (For interpretation of the references to color in this figure legend, the reader is referred to the web version of this paper.)

present in the asymmetric unit each forming cyclic $\alpha_4\beta_4$ tetramers which are stacked on each other and reflect the *I*4 space group symmetry (Fig. 2). Thus, the anomalous behaviour of CVX in size exclusion chromatography and in native gels suggesting that it is an $\alpha_3\beta_3$ can be attributed to the presence of the large solvent channel with a mean diameter of approximately 70 Å (Fig. 2).

Putative Ca^{2+}-binding site

In the α-subunit of IX-bp, the calcium ion is coordinated by Ser43, Glu45, Glu49, and Glu130 (amino acid numbering based on homology with CVX). In CVXα, the sequence in this region is Ser43, Lys45, Glu49, and Lys130. In both Fl-A and CVX, the substitution of Glu130 by Lys results in the Nζ atom occupying the position of the calcium ion in IX-bp (Fig. 3A). In the β-subunit of IX-bp, the Ca^{2+} ion is coordinated by Ser43, His45, Glu49, and Glu122. In Fl-A and CVX, this site contains Ser43, His45, Glu49, and Lys122 (Fig. 3B). Thus, the α- and β-subunits of Fl-A and CVX do not bind Ca^{2+}.

CVX is a potent inducer of platelet aggregation that binds to and acts predominantly via p62/GPVI [4]. Binding to GP receptors by oligomeric proteins which consist of four copies of the αβ-heterodimer has been suggested to be more efficient than proteins made up of single copies of the αβ-heterodimer due to cooperative binding utilizing the multiple binding sites [17].

The crystal structure of CVX determined at 2.4 Å demonstrates that the α- and β-subunits are linked by a disulfide bond to form a heterotetramer which is linked by an additional disulfide bond to form a cyclical $\alpha_4\beta_4$heterotetramer as in the structure of Fl-A [17]. The subunits of CVX do not bind Ca^{2+} due to amino acid sequence and structural changes in the putative calcium binding loop. The unique structure and properties of CVX reported here should be useful to further our understanding of the mechanism of platelet aggregation and activation via the p62/GPVI component of the platelet collagen receptor.

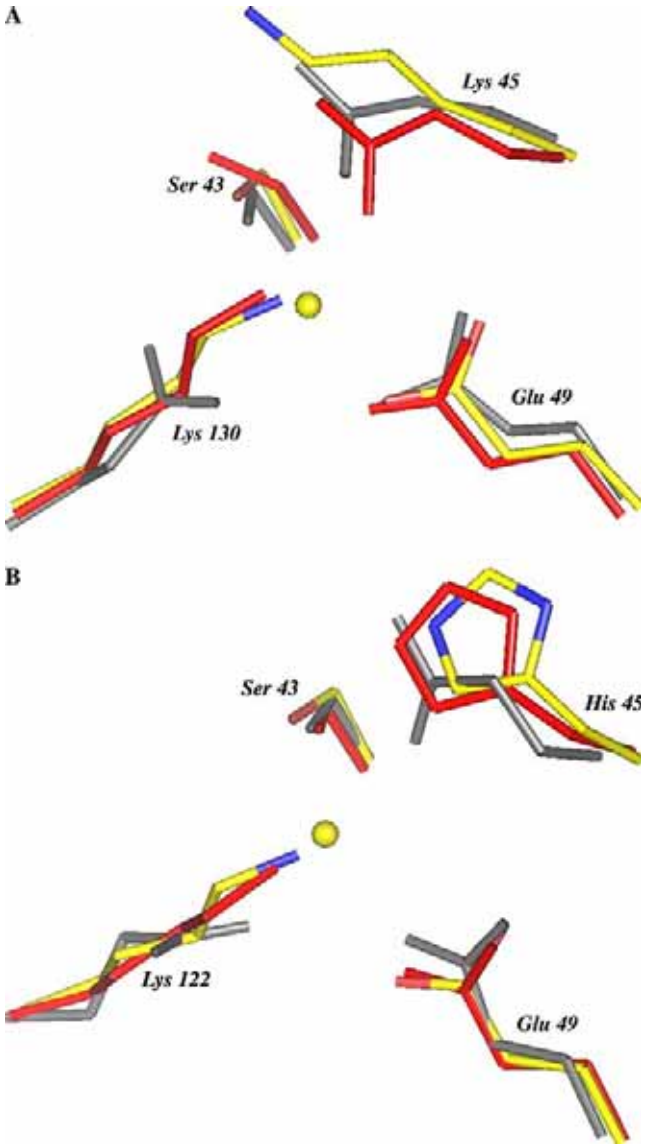

Fig. 3. Results of the superpositioning of the amino acids in IX-bp (grey), Fl-A (red) ,and CVX (atom colors) for the α (A) and β (B) chains. The amino acid labels and numbering are based on the sequence of CVX. The bound calcium from the structure of IX-bp is in yellow. Figure produced using PyMOL [27]. (For interpretation of the references to color in this figure legend, the reader is referred to the web version of this paper.)

Acknowledgments

M.T.M. is the recipient of a FAPESP fellowship. S.P.Z. and L.M.G. are supported by grants from CNPq. This work was supported by grants from FAPESP (SMOLBNet) and CNPq to R.K.A. Atomic coordinates have been deposited in the Brookhaven Protein Data Bank, Accession code: 1UMR.

References

[1] B.B. Vargaftig, J. Prado-Franceschi, M. Chignard, J. Lefort, G. Marlas, Activation of guinea-pig platelets induced by convulxin, a substance extracted from the venom of *Crotalus durissus cascavella*, Eur. J. Pharmacol. 68 (1980) 451–464.

[2] B.B. Vargaftig, Platelet activation by non-coagulant snake venom components, Toxicon 20 (1982) 279–287.

[3] I.M. Francischetti, B. Saliou, M. Leduc, C.R. Carlini, M. Hatmi, J. Randon, A. Faili, C. Bon, Convulxin, a potent platelet-aggregating protein from *Crotalus durissus terrificus* venom, specifically binds to platelets, Toxicon 35 (1997) 1217–1228.

[4] J. Polgar, J.M. Clemetson, B.E. Kehrel, M. Wiedemann, E.M. Magnenat, T.N. Wells, K.J. Clemetson, Platelet activation and signal transduction by convulxin, a C-type lectin from *Crotalus durissus terrificus* (tropical rattlesnake) venom via the p62/GPVI collagen receptor, J. Biol. Chem. 272 (1997) 13576–13583.

[5] M. Jandrot-Perrus, A.H. Lagrue, M. Okuma, C. Bon, Adhesion and activation of human platelets induced by convulxin involve glycoprotein VI and integrin alpha2beta1, J. Biol. Chem. 272 (1997) 27035–27041.

[6] F. Niedergang, A. Alcover, C.G. Knight, R.W. Farndale, M.J. Barnes, I.M. Francischetti, C. Bon, M. Leduc, Convulxin binding to platelet receptor GPVI: competition with collagen related peptides, Biochem. Biophys. Res. Commun. 273 (2000) 246–250.

[7] M. Cicmil, J.M. Thomas, T. Sage, F.A. Barry, M. Leduc, C. Bon, J.M. Gibbins, Collagen, convulxin, and thrombin stimulate aggregation-independent tyrosine phosphorylation of CD31 in platelets. Evidence for the involvement of Src family kinases, J. Biol. Chem. 275 (2000) 27339–27347.

[8] I.M. Francischetti, C.R. Carlini, J.A. Guimaraes, cAMP does not inhibit convulxin-induced tyrosyl-phosphorylation of human platelet proteins, including PLCgamma2, but completely blocks the integrin alphaIIb beta3-dependent dephosphorylation step: comparisons with RGDS peptide, cytochalasin D, and phenylarsine oxide, Arch. Biochem. Biophys. 354 (1998) 255–262.

[9] J. Prado-Franceschi, O.V. Brazil, Convulxin, a new toxin from the venom of the South American rattlesnake *Crotalus durissus terrificus*, Toxicon 19 (1981) 875–887.

[10] G. Marlas, Purification and preliminary structure of a potent platelet aggregating glycoprotein isolated from the venom of *Crotalus durissus cascavella*, Toxicon 20 (1982) 289–290.

[11] J. Prado-Franceschi, D.Q. Tavares, R. Hertel, A. Lobo de Araújo, Effects of convulxin, a toxin from rattlesnake venom, on platelets and leukocytes of anesthetized rabbits, Toxicon 19 (1981) 661–666.

[12] M. Leduc, C. Bon, Cloning of subunits of convulxin, a collagen-like platelet-aggregating protein from *Crotalus durissus terrificus* venom, Biochem. J. 15 (1998) 389–393.

[13] K. Drickamer, Evolution of Ca(2+)-dependent animal lectins, Prog. Nucleic Acids Res. Mol. Biol. 45 (1993) 207–232.

[14] M.T. Murakami, L. Watanabe, L.M. Gava, S.P. Zela, A.C.O. Cintra, R.K. Arni, Initial structural analysis of an $\alpha_4\beta_4$ c-type lectin from the venom of *Crotalus durissus terrificus*, Acta Cryst. D (in press).

[15] Z. Otwinowski, W. Minor, Processing of X-ray diffraction data collected in oscillation mode, in: C.W. Carter, R.M. Sweet (Eds.), Volume 276: Macromolecular Crystallography, Methods in Enzymology, Academic Press, New York, 1997, pp. 307–326.

[16] B.W. Matthews, Solvent content of protein crystals, J. Mol. Biol. 33 (1968) 491–497.

[17] K. Fukuda, H. Mizuno, H. Atoda, T. Morita, Crystal structure of flavocetin-A, a platelet glycoprotein Ib-binding protein, reveals a novel cyclic tetramer of C-type lectin-like heterodimers, Biochemistry 39 (2000) 1915–1923.

[18] J. Navaza, Implementation of molecular replacement in AMoRe, Acta Crystallogr. D Biol. Crystallogr. 57 (2001) 1367–1372.

[19] A.T. Brunger, P.D. Adams, G.M. Clore, W.L. DeLano, P. Gros, R.W. Grosse-Kunstleve, J.S. Jiang, J. Kuszewski, M. Nilges, N.S. Pannu, R.J. Read, L.M. Rice, T. Simonson, G.L. Warren,

Crystallography & NMR system: a new software suite for macromolecular structure determination, Acta Crystallogr. D Biol. Crystallogr. 54 (1998) 905–921.

[20] G.N. Murshudov, A.A. Vagin, E.J. Dodson, Refinement of macromolecular structure by the maximum-likelihood method, Acta Crystallogr. D 53 (1997) 240–255.

[21] Collaborative computational project, Number 4, The CCP4 suite: programs for protein crystallography, Acta Crystallogr. D 50 (1994) 760–763.

[22] R.A. Laskowski, D.S. Moss, J.M. Thornton, Main-chain bond lengths and bond angles in protein structures, J. Mol. Biol. 231 (1993) 1049–1067.

[23] C. Ramakrishnan, G.N. Ramachandran, Stereochemical criteria for polypeptide and protein chain conformations. II. Allowed conformations for a pair of peptide units, Biophys. J. 5 (1965) 909–933.

[24] H. Mizuno, Z. Fujimoto, M. Koizumi, H. Kano, H. Atoda, T. Morita, Crystal structure of coagulation factor IX-binding protein from habu snake venom at 2.6 A: implication of central loop swapping based on deletion in the linker region, J. Mol. Biol. 289 (1999) 103–112.

[25] F. Corpet, Multiple sequence alignment with hierarchical clustering, Nucleic Acids Res. 16 (1988) 10881–10890.

[26] M. Carson, Ribbons, in: R.M. Sweet, C.W. Carter (Eds.), Volume 277: Macromolecular Crystallography, Methods in Enzymology, Academic press, New York, 1997, pp. 493–505.

[27] W.L. DeLano, The PyMOL Molecular Graphics System, DeLano Scientific, San Carlos, CA, USA, 2002.

b. Disrupção de Membranas Biológicas

As membranas biológicas são conjuntos de proteínas, lipídios e glicídios, dispostos em uma bicamada, que circundam as células, suas organelas e seus produtos de secreção (Figura 5). Altamente reativas e com uma capacidade enorme de adquirir as mais diversas conformações espaciais, as membranas celulares constituem os limites das diversas organelas no interior celular e da própria célula, cabendo à membrana plasmática essa última função. A membrana plasmática pode ser considerada como a entidade reveladora dos estados metabólicos celulares, uma vez que é responsável pelas relações intercelulares ou aquelas realizadas entre a célula e o seu meio. Seu funcionamento e integridade dependem fundamentalmente da reposição de seus elementos constituintes, principalmente de proteínas e lipídios. Qualquer alteração, portanto, dos sistemas celulares de produção de lipídios ou de proteínas afeta a membrana celular pela mudança em sua composição bioquímica. Desse modo, as funções da membrana plasmática ficam comprometidas, fato extremamente crítico para a manutenção da vitalidade celular.

Nesse capítulo, diversas toxinas responsáveis pela hidrólise de diferentes componentes lipídicos de membranas biológicas foram caracterizadas estruturalmente, tais como esfingomielinases D e fosfolipases A_2 são apresentadas.

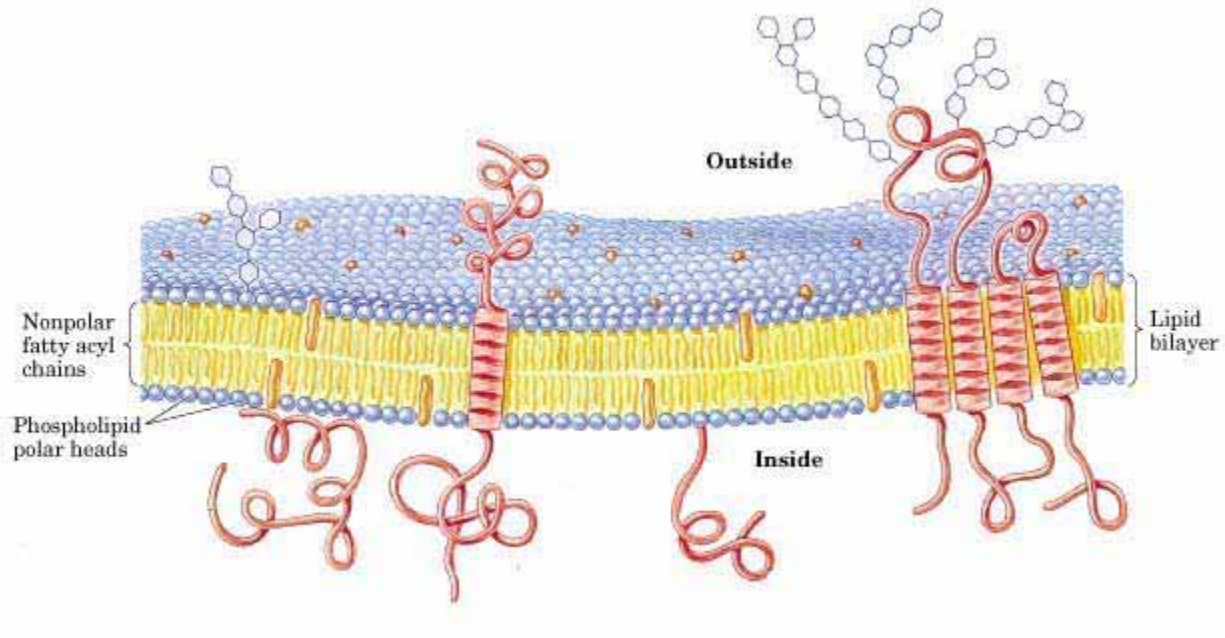

Figura 5: Modelo mosaico fluido de membranas biológicas.

i. Esfingomielinase D

Esfingomielinase D é o principal componente tóxico do veneno de aranhas do gênero *Loxosceles* responsáveis pela manifestação de dermonecrose, hemólise intravascular e falha renal aguda, sendo que alguns casos podem resultar em morte. Essas enzimas catalisam a hidrólise de esfingomielina (Figura 6), um componente de membranas biológicas semelhante aos fosfolipídios (Figura 6) resultando na formação de ceramida-1-fosfato e colina ou na hidrólise de lisofosfatidil colina gerando acido lisofosfatídico.

Nesse trabalho, a primeira estrutura cristalina de um membro da família das esfingomielinases D foi resolvida pelo método de "quick cryo-soaking" (Dauter et al., 2000), sendo as fases obtidas a partir de um único derivado de iodo e os dados coletados em um anodo rotatório. As esfingomielinases D têm uma estrutura $(\alpha/\beta)_8$ e um sítio ativo conjugado a um sítio de ligação de magnésio. Baseados nesses dados estruturais, o mecanismo de ação ácido-base foi proposto e, posteriormente, confirmado por Lee & Lynch (2005). Outro resultado interessante foi encontrar o mesmo sítio ativo na enzima glicerofosfodiester fosfodiesterase, considerada enzima chave no metabolismo do glicerol em mamíferos. Estudos comparativos, análises estruturais e mecanismo de ação estão detalhados nos trabalhos a seguir.

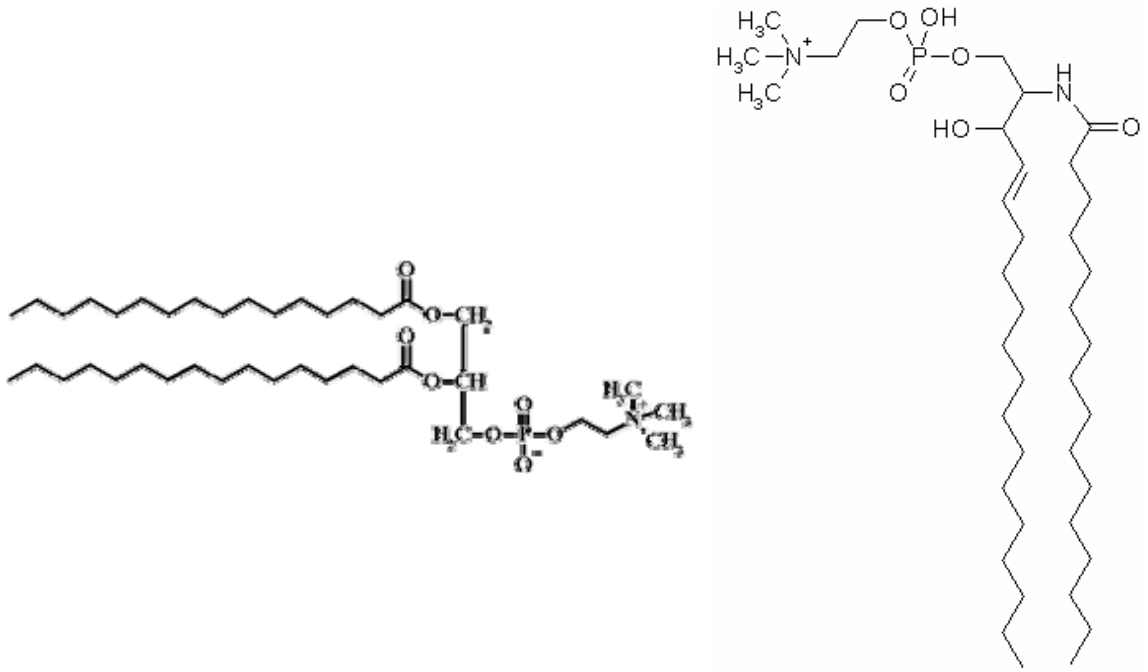

Figura 6: Representação esquemática de um fosfolipídio (esquerda) e um esfingolipídio (direita).

crystallization papers

Acta Crystallographica Section D
Biological Crystallography
ISSN 0907-4449

Crystallization and preliminary crystallographic analysis of SMase I, a sphingomyelinase from *Loxosceles laeta* spider venom

S. P. Zela,[a] M. F. Fernandes Pedrosa,[b] M. T. Murakami,[a] S. A. de Andrade,[b] R. K. Arni[a]* and D. V. Tambourgi[b]*

[a]Department of Physics, IBILCE/UNESP, CP 136, São José do Rio Preto, SP, CEP 15054-000, Brazil, and [b]Immunochemistry Laboratory, Butantan Institute, São Paulo, SP, CEP 05503-900, Brazil

Correspondence e-mail: arni@df.ibilce.unesp.br, dvtambourgi@butantan.gov.br

Received 12 February 2004
Accepted 22 March 2004

SMase I, a 32 kDa sphingomyelinase found in *Loxosceles laeta* venom, is responsible for the major pathological effects of spider envenomation. This toxin has been cloned and functionally expressed as a fusion protein containing a 6×His tag at its N-terminus to yield a 33 kDa protein [Fernandes-Pedrosa *et al.* (2002), *Biochem. Biophys. Res. Commun.* **298**, 638–645]. The recombinant protein possesses all the biological properties ascribed to the whole *L. laeta* venom, including dermonecrotic and complement-dependent haemolytic activities. Dynamic light-scattering experiments conducted at 291 K demonstrate that the sample possesses a monomodal distribution, with a hydrodynamic radius of 3.57 nm. *L. laeta* SMase I was crystallized by the hanging-drop vapour-diffusion technique using the sparse-matrix method. Single crystals were obtained using a buffer solution consisting of 0.08 *M* HEPES and 0.9 *M* trisodium citrate, which was titrated to pH 7.5 using 0.25 *M* sodium hydroxide. Complete three-dimensional diffraction data were collected to 1.8 Å at the Laboratório Nacional de Luz Síncrotron (LNLS, Campinas, Brazil). The crystals belong to the hexagonal system (space group $P6_1$ or $P6_5$), with unit-cell parameters $a = b = 140.6$, $c = 113.6$ Å. A search for heavy-atom derivatives has been initiated and elucidation of the crystal structure is currently in progress.

1. Introduction

Loxoscelism is the clinical condition produced by the venom of spiders belonging to the genus *Loxosceles*, which can be observed as two well defined clinical variants: cutaneous loxoscelism and systemic or viscerocutaneous loxoscelism. We have recently identified, purified and characterized the toxins from *L. intermedia* venom that are responsible for all the local and systemic effects induced by whole venom (Tambourgi *et al.*, 1995; Tambourgi, Magnoli *et al.*, 1998). Two highly homologous proteins with molecular weights of 35 kDa were purified to homogeneity and shown to possess sphingomyelinase activity. Both these proteins are able to induce dermonecrosis in laboratory animals and rendered human erythrocytes (E) susceptible to lysis by complement (C) *in vitro*. In a mouse model of *Loxosceles* envenomation, the toxins also induced intravascular haemolysis and provoked a cytokine response similar to that observed in endotoxic shock (Tambourgi, Petricevich *et al.*, 1998).

Our research has focused on the effects of *Loxosceles* sphingomyelinases on erythrocytes and nucleated cells and our results indicate that the toxins induce the activation of membrane-bound metalloproteinases (Tambourgi *et al.*, 2000; van den Berg *et al.*, 2002). In the case of erythrocytes, this leads to increased susceptibility to activation of C *via* the classical pathway, possibly by inducing loss of membrane asymmetry (Tambourgi *et al.*, 2002), and *via* the alternative pathway because of metalloproteinase-induced cleavage of glycophorins (Tambourgi *et al.*, 2000). However, on nucleated cells the result is a decrease in C susceptibility (van den Berg *et al.*, 2002). The exact mechanisms of these events and their role in the pathology of loxoscelism remain to be elucidated.

The only proteins that display significant sequence homology to *Loxosceles* sphingomyelinases are bacterial toxins from *Corynebacterium pseudotuberculosis* (accession No. AAA99867; Bernheimer *et al.*, 1985) and *Arcanobacterium haemolyticum* (accession No. Q59121; Cuevas & Songer, 1993). These toxins are also sphingomyelinases but are generally referred to as phospholipases D (PLD). No significant sequence or structural homology was found with other phospholipases.

Phospholipases are frequently found as toxic components in animal venoms and bacterial toxins. Phospholipases promote the hydrolysis of ester bonds in phospholipids and are classified as phospholipases A_1, A_2, C and D depending on the position in the ester bond that is hydrolysed (van den Bosch, 1980). In contrast to most phospholipases, the *Loxosceles* and bacterial phospholipases display

unusual substrate specificity. Of the four major phospholipids in mammalian cell membranes, only sphingomyelin (SM) is hydrolysed by bacterial PLD and spider toxins, resulting in the formation of choline and ceramide-1-phosphate (Bernheimer *et al.*, 1985). We have recently demonstrated that SMase D from spiders and bacteria has intrinsic lysophospholipase D activity toward lysophosphatidyl choline (LPC). LPC hydrolysis yields the lipid mediator lysophosphatidic acid (LPA), a known inducer of platelet aggregation, endothelial hyperpermeability and pro-inflammatory responses (van Meeteren *et al.*, 2004).

The difficulty in obtaining large quantities of venom and purified venom components is the principal limiting factor in studying the mechanisms involved in loxoscelism. Recombinant expression of the sphingomyelinase is thus necessary for further functional and structural characterization of the toxin. We have cloned and expressed one of the sphingomyelinases from *L. laeta* venom, named SMase I (GenBank accession No. AY093599), which possessed all the biological properties ascribed to the whole venom, *e.g.* dermonecrotic and complement-dependent haemolytic activities and the ability to hydrolyse SM and LPC (Fernandes-Pedrosa *et al.*, 2002; van Meeteren *et al.*, 2004).

2. Methods

2.1. Recombinant protein expression and purification

L. laeta SMase I recombinant protein was produced as described previously (Fernandes-Pedrosa *et al.*, 2002). Briefly, pAE-*L. laeta* H17 cDNA-transformed *E. coli* BL21 (DE3) cells were inoculated in 50 ml of 2YT/amp and grown overnight at 310 K, induced with IPTG. Recombinant protein was harvested from the pellet using a French pressure cell and was purified on an Ni^{2+} Chelating Sepharose Fast Flow column (Pharmacia, Sweden; 64 × 10 mm). Homogeneity was determined by SDS–PAGE run under reducing and non-reducing conditions using 12% acrylamide gels (Laemmli, 1970). A single band of 33 kDa was observed in the gels. Samples were dialysed against PBS and stored at 253 K.

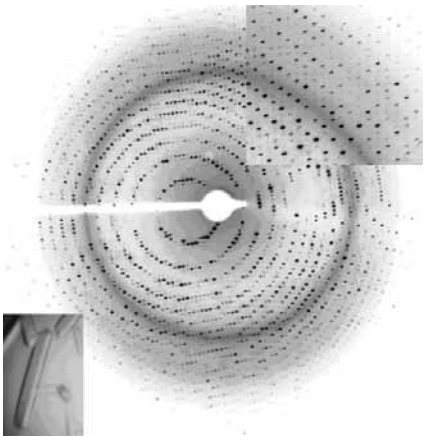

Figure 1
X-ray diffraction pattern of SMase I, a sphingomyelinase from *L. laeta* spider venom, obtained at the Laboratório Nacional de Luz Síncrotron using a MAR CCD detector. Top right inset, enlargement (×3) of part of the image; bottom left inset, photomicrograph of the crystals.

2.2. Dynamic light scattering

Dynamic light-scattering experiments were carried out using a DynaPro 810 (Protein Solutions) apparatus equipped with a temperature stabilizer. A protein solution of 1.0 mg ml^{-1} was prepared in 0.1 *M* imidazole pH 8.0. Standard curves of bovine serum albumin were used for calibration and the experiments were conducted at 291 K.

2.3. Crystallization

The sample was dialysed against 20 m*M* HEPES buffer pH 7.5 and concentrated to 10 mg ml^{-1}. Crystallization was performed by the hanging-drop vapour-diffusion method using 24-well tissue-culture plates. Initial trials were carried out by the sparse-matrix method with some modifications (Jancarik & Kim, 1991). Typically, 1 µl drops of protein solution were mixed with an equal volume of screening solution and equilibrated over 0.8 ml of the latter in the reservoir solution. Large single crystals were obtained when a 1 µl protein droplet was mixed with an equal volume of reservoir solution consisting of 0.08 *M* HEPES buffer including 0.9 *M* trisodium citrate and was titrated to pH 7.5 with 0.25 *M* sodium hydroxide.

2.4. Data collection

The crystal was transferred to a cryoprotectant solution containing 20% glycerol and flash-frozen. The diffraction data were collected at the Laboratório Nacional de Luz Síncrotron (Campinas, Brazil), with the wavelength fixed at 1.423 Å. Diffraction intensities were measured using a MAR CCD detector. The data were indexed and scaled using the *DENZO* and *SCALEPACK* programs from the *HKL* package (Otwinowski & Minor, 1997).

Table 1
Data-collection results.

Values in parentheses are for the last resolution shell (1.86–1.80 Å).

Space group	$P6_1$ or $P6_5$
Unit-cell parameters (Å)	$a = b = 140.6$, $c = 113.6$
Maximum resolution (Å)	1.8
No. unique reflections	115146
$R_{\rm merge}$ (%)	4.5%(40.4)
Completeness (%)	97.8 (95.5)
$V_{\rm M}$ (Å^3 Da^{-1})	2.5
Solvent content (%)	49
No. molecules per AU	4
$I/\sigma(I)$	34.2 (4.1)

3. Results

Structural homogeneity in solution was observed by dynamic light scattering, which presented a monomodal distribution. Single crystals with dimensions 0.2 × 0.2 × 0.4 mm (inset in Fig. 1) were obtained and diffraction data were collected to 1.8 Å (Fig. 1) under cryogenic conditions (100 K). The diffraction data were indexed in space group *P*6, with unit-cell parameters $a = b = 140.6$, $c = 113.6$ Å. An examination of the systematic absences indicated that the crystals belonged to either space group $P6_1$ or to its enantiomorph $P6_5$. Processing of the 1 475 030 measured reflections to 1.8 Å led to 115 146 unique reflections with an $R_{\rm merge}$ of 4.5% (40.4% in the last shell, 1.86–1.80 Å) and a completeness of 97.8% (95.5% in the last shell). Data-processing statistics are presented in Table 1. Calculation of the self-rotation function assuming a molecular weight of 33 kDa per molecule resulted in a Matthews coefficient (Matthews, 1968) of 2.5 Å^3 Da^{-1} (49% solvent content) for four molecules in the asymmetric unit.

A search of the Protein Data Bank indicated that the highest sequence identity (26%) was observed between human Dj-1 (PDB code 1pdv) and the C-terminal region of SMase I. As a result of this low sequence identity with structures currently deposited in the Protein Data Bank, the phase problem will be solved using either multiple anomalous dispersion (MAD) or multiple isomorphous replacement methods (MIR). Knowledge of the three-dimensional structure will be important for understanding the steric requirements and mechanism of sphingomyelinases.

This study was supported by FAPESP, SMOLBNet, The Wellcome Trust and CNPq. We are grateful to Dr J. Medrano and the staff at LNLS, Campinas (Brazil) for expert assistance.

References

Berg, C. W. van den, Gonçalves de Andrade, R. M., Magnoli, F. C., Marchbank, K. J. & Tambourgi, D. V. (2002). *Immunology*, **107**, 102–110.

Bernheimer, A. W., Campbell, B. J. & Forrester, L. J. (1985). *Science*, **228**, 590–591.

Bosch, H. van den (1980). *Biochim. Biophys. Acta*, **604**, 191–246.

Cuevas, W. A. & Songer, J. G. (1993). *Infect. Immun.* **61**, 4310–4316.

Fernandes-Pedrosa, M. F., Junqueira de Azevedo, I. L., Gonçalves-de-Andrade, R. M., van den Berg, C. W., Ramos, C. R., Ho, P. L. & Tambourgi, D. V. (2002). *Biochem. Biophys. Res. Commun.* **298**, 638–645.

Jancarik, J. & Kim, S. H. (1991). *J. Appl. Cryst.* **24**, 409–411.

Laemmli, U. K. (1970). *Nature (London)*, **277**, 680–687.

Matthews, B. W. (1968). *J. Mol. Biol.* **33**, 491–497.

Meeteren, L. A. van, Frederiks, F., Giepmans, B. N. G., Fernandes-Pedrosa, M. F., Billington, S. J., Jost, B. H., Tambourgi, D. V. & Moolenaar, W. H. (2004). *J. Biol. Chem.* **279**, 10833–10836.

Otwinowski, Z. & Minor, W. (1997). *Methods Enzymol.* **276**, 307–326.

Tambourgi, D. V., Magnoli, F. C., van den Berg, C. W., Morgan, B. P., de Araujo, P. S., Alves, E. W. & Dias da Silva, W. D. (1998). *Biochem. Biophys. Res. Commun.* **251**, 366–373.

Tambourgi, D. V., Magnoli, F. C., Von Eickstedt, V. R., Benedetti, Z. C., Petricevich, V. L. & Dias da Silva, W. D. (1995). *J. Immunol.* **155**, 4459–4466.

Tambourgi, D. V., Morgan, B. P., Gonçalves de Andrade, R. M., Magnoli, F. C. & van den Berg, C. W. (2000). *Blood*, **95**, 683–691.

Tambourgi, D. V., Petricevich, V. L., Magnoli, F. C., Assaf, S. L., Jancar, S. & Dias Da Silva, W. (1998). *Toxicon*, **36**, 391–403.

Tambourgi, D. V., Silva, M. S., Billington, S. J., Gonçalves de Andrade, R. M., Magnoli, F. C., Songer, J. G. & van den Berg, C. W. (2002). *Immunology*, **107**, 93–101.

THE JOURNAL OF BIOLOGICAL CHEMISTRY
Vol. 280, No. 14, Issue of April 8, pp. 13658–13664, 2005

Printed in U.S.A.

Structural Basis for Metal Ion Coordination and the Catalytic Mechanism of Sphingomyelinases D*

Received for publication, November 3, 2004, and in revised form, January 10, 2005
Published, JBC Papers in Press, January 14, 2005, DOI 10.1074/jbc.M412437200

Mário T. Murakami‡§, Matheus F. Fernandes-Pedrosa§¶, Denise V. Tambourgi¶‖ and Raghuvir K. Arni‡**

From the ‡Department of Physics, Instituto de Biociências, Letras e Ciências Exatas/Universidade Estadual Paulista, São José do Rio Preto, SP 15054-000, Brazil, and the ¶Immunochemistry Laboratory, Butantan Institute, São Paulo, SP 05503-900, Brazil

Sphingomyelinases D (SMases D) from *Loxosceles* spider venom are the principal toxins responsible for the manifestation of dermonecrosis, intravascular hemolysis, and acute renal failure, which can result in death. These enzymes catalyze the hydrolysis of sphingomyelin, resulting in the formation of ceramide 1-phosphate and choline or the hydrolysis of lysophosphatidyl choline, generating the lipid mediator lysophosphatidic acid. This report represents the first crystal structure of a member of the sphingomyelinase D family from *Loxosceles laeta* (SMase I), which has been determined at 1.75-Å resolution using the "quick cryo-soaking" technique and phases obtained from a single iodine derivative and data collected from a conventional rotating anode x-ray source. SMase I folds as an $(\alpha/\beta)_8$ barrel, the interfacial and catalytic sites encompass hydrophobic loops and a negatively charged surface. Substrate binding and/or the transition state are stabilized by a Mg^{2+} ion, which is coordinated by Glu^{32}, Asp^{34}, Asp^{91}, and solvent molecules. In the proposed acid base catalytic mechanism, His^{12} and His^{47} play key roles and are supported by a network of hydrogen bonds between Asp^{34}, Asp^{52}, Trp^{230}, Asp^{233}, and Asn^{252}.

Envenomation by arachnids of the genus *Loxosceles* (brown spider), endemic to temperate and tropical regions of the Americas, Africa, and Europe, leads to local dermonecrosis and also to serious systemic toxicity. Three principal *Loxosceles* species of medical importance are encountered in Brazil (*Loxosceles laeta*, *Loxosceles intermedia*, *Loxosceles gaucho*), and more than 2,000 cases of envenomation by *L. intermedia* alone are reported each year. In the United States, six *Loxosceles* species (including *Loxosceles reclusa*, brown recluse) are responsible for numerous incidents (1). *L. laeta*, possibly the most toxic and dangerous of all the species, is widely distributed and is encountered as far north as Canada (2, 3) and is endemic primarily in South and Central America.

* This research was supported by grants from FAPESP (SMOLBNet), CNPq and CAPES/DAAD (to R. K. A.). The costs of publication of this article were defrayed in part by the payment of page charges. This article must therefore be hereby marked "*advertisement*" in accordance with 18 U.S.C. Section 1734 solely to indicate this fact.

The atomic coordinates and structure factors (code 1XX1) have been deposited in the Protein Data Bank, Research Collaboratory for Structural Bioinformatics, Rutgers University, New Brunswick, NJ (http://www.rcsb.org/).

§ Recipients of FAPESP doctoral fellowships.

‖ Supported by FAPESP and The Welcome Trust.

** To whom correspondence should be addressed: Dept. of Physics, IBILCE/UNESP, Rua Cristovão Colombo 2265, São José do Rio Preto, SP 15054-000, Brazil. Tel.: 55-17-2212460; Fax: 55-17-2212247; E-mail: arni@df.ibilce.unesp.br.

The site of envenomation, which initially causes only minor discomfort, begins as an expanding area of erythema and edema. A centrally located necrotic ulcer often forms 8–24 h after envenomation (4, 5). Extensive tissue destruction follows, with the ulcer taking many months to heal, and in extreme cases requires debridement or skin grafting. The lesions are remarkable considering that *Loxosceles* spiders inject only a few tenths of a microliter of venom containing no more than 30 μg of protein.

Mild systemic effects induced by envenomation, such as fever, malaise, pruritus, and exanthema are common, whereas intravascular hemolysis and coagulation, sometimes accompanied by thrombocytopenia and renal failure, occur in ~16% of the victims (1, 6–11). Although systemic loxoscelism is less common than the cutaneous form, it is the main cause of death associated with *Loxosceles* envenomation. Most of the deaths occur in children and are related to the South American species *L. laeta* (1). Due to our limited understanding of the venom's mechanism of action, effective treatment is currently not available.

The recombinant sphingomyelinases (SMases)[1] D of *L. laeta* and *L. intermedia* retain all the local and systemic effects observed in the whole venom, inducing dermonecrosis in rabbits and rendering human erythrocytes susceptible to lysis by complement (12–15). In a mouse model of *Loxosceles* envenomation, they also induce intravascular hemolysis and provoke a cytokine response, which resembles that observed in endotoxic shock (16). SMases facilitate activation of the alternative pathway of complement on human erythrocytes by removal of glycophorins as a consequence of the activation of an endogenous metalloproteinase (17) and activation of the classical pathway of complement, possibly by disruption of the membrane asymmetry (18). SMases D are not encountered elsewhere in the animal kingdom; however, a similar enzyme is produced as an exotoxin by some pathogenic bacteria, notably *Corynebacterium pseudotuberculosis*, *Corynebacterium ulcerans*, and *Arcanobacterium* (formerly *Corynebacterium) hemolyticum* (19–21). *C. pseudotuberculosis* causes lymphadenitis in animals and is also pathogenic to humans, whereas *C. ulcerans* and *A. hemolyticum* are pathogens of pharyngitis and other human infections (22). The SMase D from *C. pseudotuberculosis*, also named sphingomyelin (SM)-specific phospholipase D (PLD), is an essential virulence determinant that contributes to the persistence and spread of the bacteria within the host (23).

The *Loxosceles* and bacterial SMases D possess similar molecular masses (31–35 kDa) but share only limited sequence homology (13, 24). In model systems, the *Loxosceles* and

[1] The abbreviations used are: SMase, sphingomyelinase; SM, sphingomyelin; PLD, phospholipase D.

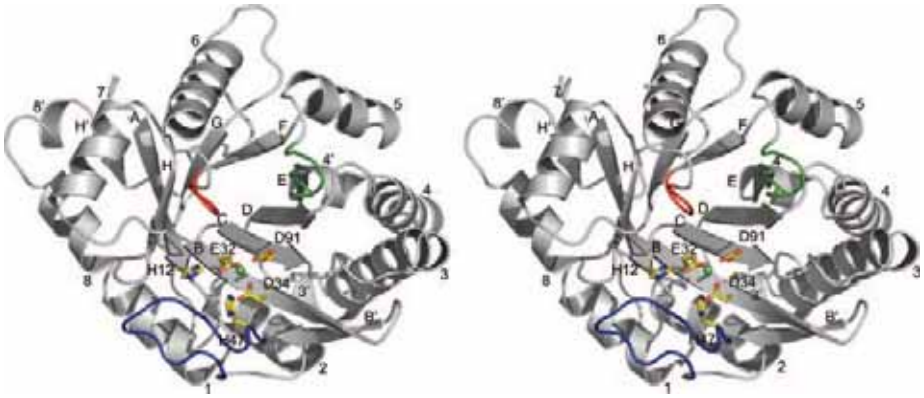

FIG. 1. **Stereo ribbon representation of the structure of *L. laeta* SMase I viewed along the axis of the (α/β)8 barrel.** The N and C termini are labeled, and the functionally important His^{12}, Glu^{32}, Asp^{34}, His^{47}, Asp^{91}, and the Mg^{2+} ion (*green sphere*) are included. The catalytic loop B (*blue*), the variable loop E (*green*), and the flexible loop F (*red*) are indicated. The β-strands and α-helices are labeled as in Fig. 3. Figs. 1, 2*A*, 4, and 6 were generated using Pymol (DeLano, www.pymol.org).

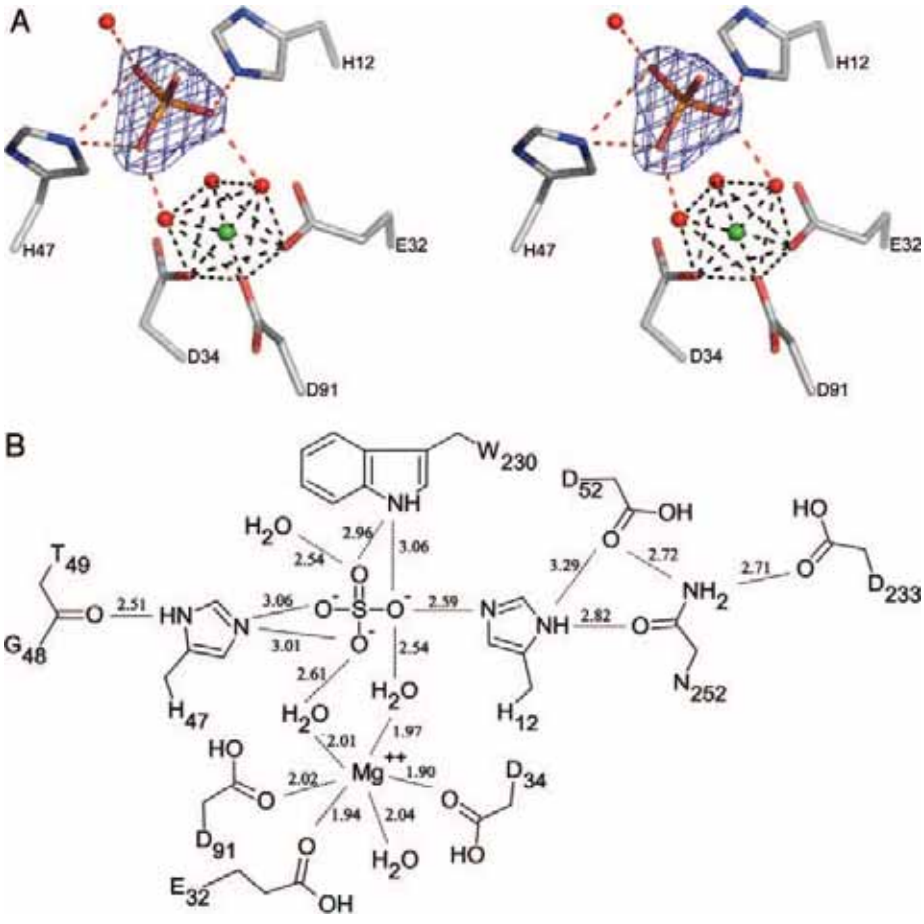

FIG. 2. *A*, stereo view of the amino acids and hydrogen bonding in the catalytic and metal ion binding (*green sphere*) sites; the electron density (*blue*) in the $2F_o - F_c$ map is contoured at 2.0σ. *B*, schematic representation of the principal hydrogen bonds to the sulfate and metal ion.

C. pseudotuberculosis enzymes provoke similar pathophysiological effects, including platelet aggregation, endothelial hyperpermeability, complement-dependent hemolysis, and neutrophil recruitment (13–15, 25–28).

Of the four major phospholipids present in the outer leaflet of the mammalian plasma membranes, only sphingomyelin is hydrolyzed by bacterial PLD and spider toxins, resulting in the formation of ceramide-1-phosphate (Cer-1-P or *N*-acyl-sphingosine-1-phosphate) (13, 25, 26).

In the presence of Mg^{2+}, spider and bacterial SMases D catalyze the release of choline from lysophosphatidylcholine but not from phosphatidylcholine (24). Plasma lysophosphatidylcholine is tightly bound to albumin, and removal of its choline headgroup yields lysophosphatidic acid, a potent lipid mediator with numerous biological activities in many different cell types (29, 30). The crystal structure of SMase I (sphingomyelin phosphodiesterase; E.C. 3.1.4.12), one of the sphingomyelinase D isoforms from *L. laeta* venom (determined at 1.75 Å), provides a structural basis for understanding the role of the metal ion binding and the acid-base catalytic mechanism.

EXPERIMENTAL PROCEDURES

Sphingomyelinase Expression—L. laeta SMase I (GenBank™ accession number AY093599) was expressed in *Escherichia coli* strain BL21 (DE3) as a fusion protein composed of the mature SMase with an N-terminal extension containing a His_6 tag (15). Recombinant SMase I was purified from the soluble fraction of cell lysates on a Ni(II)-chelating-Sepharose Fast Flow column (Amersham Biosciences). Recombinant protein was eluted (elution buffer: 100 mM Tris-HCl, pH 8.0, 300

TABLE I
Data collection and refinement statistics of SMase I

	Native-SMase I	Iodine-SMase I
Crystal preparation		
Cryprotectant solution	Mother liquor + 20% glycerol	Mother liquor + 20% glycerol + 0.5 M NaI
Soaking time	60 s	20 min
Data collection		
Wavelength (Å)	1.43	1.54
Space group	$P6_5$	$P6_5$
Unit cell parameters (Å)	$a = b = 139.82$, $c = 113.46$	$a = b = 142.59$, $c = 115.36$
Resolution (Å)	30.0–1.75 (1.79–1.75)	30.0–2.10 (2.15–2.10)
No. of molecules in arbitrary units	4	
Solvent content (%)	52	
V_m ($Å^3Da^{-1}$)	2.6	
No. of reflections	2,578,417	1,580,276
No. of unique reflections[a]	125,875	151,663
$I/\sigma(I)$	22.0 (3.4)[c]	11.3 (2.4)[c]
Multiplicity	20.5 (6.5)	10.4 (3.5)
Completeness (%)	99.5 (99.5)	99.0 (98.2)
R_{merge}[b] (%)	6.4 (43.9)	10.8 (48.3)
Structure refinement statistics		
R_{factor} (%)	18.6	
R_{free} (%)	22.5	
Root mean square deviation bond distances (Å)	0.013	
Root mean square deviation bond angles (°)	1.549	
Average *B*-factors ($Å^2$)	24.2	

[a] Multiplicities of the derivative data sets were calculated with the Friedel-related reflections treated separately. Multiplicity of the native data set was calculated with the Friedel pairs treated as equivalent.

[b] $R_{merge} = \Sigma|I(h)_I - \{I(h)\}|/\Sigma\{I(h)\}$, where I_h is the observed intensity of the *i*th measurement of reflection *h* and $\{I(h)\}$ is the mean intensity of reflection *h* calculated after scaling.

[c] Statistical values for the highest resolution shells are given in parentheses.

mM NaCl, 0.8 M imidazole) at >95% purity and dialyzed against phosphate-buffered saline, pH 7.2 (10 mM sodium phosphate, 150 mM NaCl). Dynamic light-scattering experiments carried out in the above buffer at 293 K (DynaPro 801-Protein Solutions) indicated that the protein was monomeric in solution.

Crystallization, Heavy Atom Derivative, and Data Collection—Initial crystals of *L. laeta* SMase I were obtained by the hanging drop vapor diffusion method in which 2-μl drops containing 1 μl of the protein solution (5 mg ml^{-1} in 25 mM Hepes, pH 7.5) were equilibrated against a reservoir solution containing 8 mM Hepes and 0.9 M trisodium citrate (pH 7.5) (31). Subsequently, crystals obtained from 2.7 M ammonium sulfate (pH 5.6) were easier to reproduce and were used for structure determination. Cryo-conditions included the addition of 20% (w/v) glycerol to the reservoir solution. The native crystals belong to the space group $P6_5$ with cell parameters of $a = b = 139.82$ Å and $c = 113.46$ Å, and the asymmetric unit contains four molecules with a solvent content of 52% ($V_M = 2.6$ $Å^3$ Da^{-1}). The iodine derivative for the "quick cryo-soaking" method was prepared by soaking a single crystal in the cryo-solution, which additionally contained 0.5 M iodine chloride, for 20 min. Diffraction intensities for the native crystal were measured by a MARCCD detector at the protein crystallography beam line at the Brazilian National Synchrotron Light Source (LNLS, Campinas, Brazil), and the derivative diffraction data were collected using x-rays generated by a Rigaku RU300 rotating anode source equipped with Osmic confocal mirrors. Diffraction intensities were measured using a MAR 345 imaging plate detector. Data were scaled and reduced using DENZO/SCALEPACK (32); the data collection and processing statistics are presented in Table I.

Structure Determination and Refinement—The quick cryo-soaking method (33, 34) was used for derivatization and phasing. The structure was determined at 1.95 Å using the single isomorphous replacement anomalous dispersion method, and the anomalous differences were used to locate 41 iodine sites with the SHELXD program (35) by integrated-direct and Patterson methods. These heavy atom positions were used without further refinement to estimate phases that were subsequently extended to 1.75-Å resolution applying the sphere of influence algorithm as incorporated in the SHELXE program (35), and the electron density was improved by solvent flattening with SOLOMON (36). The deduced amino acid sequence based on the *L. laeta* SMase I gene (GenBank™ accession number AAM21154) was utilized for automatic model building into the 1.75-Å resolution electron density map with the ARP/wARP program (37), which was able to trace 97% of the molecule. The refinement was initiated at a 2.0-Å resolution with an *R*-factor of 22.2% ($R_{free} = 26.4\%$). Initial cycles of refinement involved translation, libration, and screw rotation, a restrained and overall *B*-factor refinement that was carried out by REFMAC5 (38) with the inclusion of non-crystallographic restraints. After each cycle of refinement, the model was inspected and manually adjusted to correspond to the computed σA-weighted ($2F_o - F_c$)- and ($F_o - F_c$)-type electron density maps using the program TURBO FRODO (Biographics, Marseille, France). In the later cycles, the non-crystallographic restraints were relaxed, and individual isotropic B-factors were refined. Solvent water molecules were added manually at the position of positive peaks (>3σ) in the difference Fourier maps, taking into consideration hydrogen bonding potential. In the final cycles of refinement, additional density was observed in the difference electron density maps, which was attributed to the presence of Mg^{2+}, sulfate ions, and Hepes molecules.

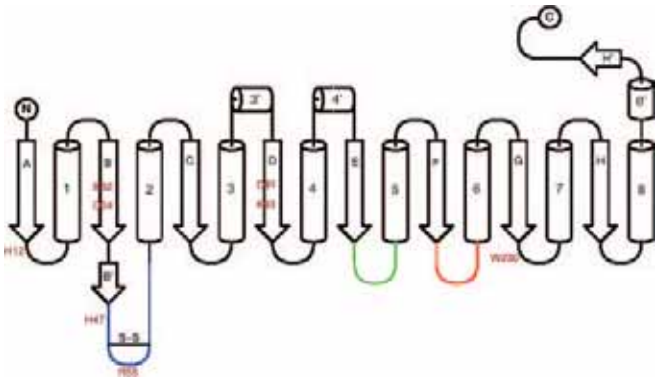

FIG. 3. **Topology schematic of *L. laeta* SMase I.** The β-strands (*arrows*) and α-helices (*cylinders*) forming the $(\alpha/\beta)_8$ barrel are labeled *A–H* and *1–8* respectively. The β-strands and α-helices not belonging to the core are primed. The positions of the catalytic loop B (*blue*), variable loop E (*green*), flexible loop F (*red*), and the disulfide bridge (*S–S*) are indicated. The approximate relative positions of the amino acids involved in catalysis and Mg^{2+} ion binding are indicated.

RESULTS

The refinement of the structure of SMase I from *L. laeta* converged to a crystallographic residual of 18.6% ($R_{free} = 22.5\%$ for 5% of the data) for all data between 30.0 and 1.75 Å (no σ or intensity cutoff; 99.5% data completeness). The residual electron density that was observed was attributed to the presence of a Mg^{2+} ion based on the temperature factor (*B*-factor = 7.5 $Å^2$) and coordination (Figs. 1 and 2*A*). Because the concentration of the phosphate in the dialysis

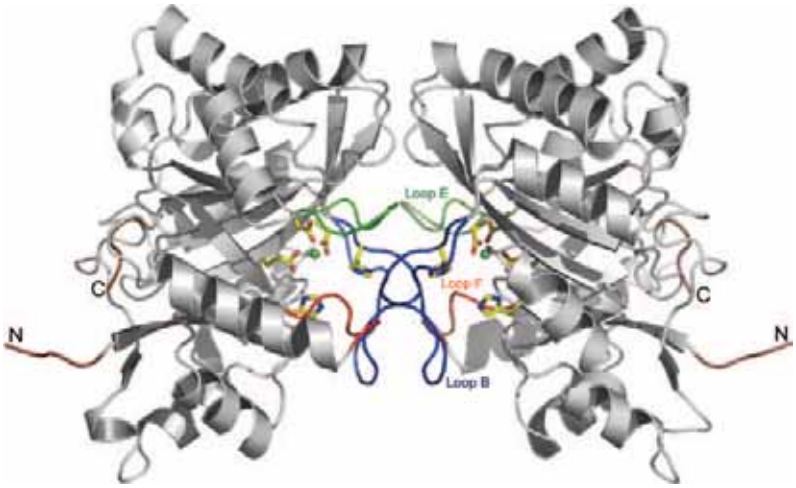

FIG. 4. **Ribbon representation of the dimer.** The amino acids His^{12}, Glu^{32}, Asp^{34}, His^{47}, and Asp^{91} are represented by *balls and sticks*, and the Mg^{2+} ion is represented as a *green sphere*. Residues in the catalytic (*loop B*), variable (*loop E*), and the flexible (*loop F*) loops are *blue*, *green*, and *red*, respectively. The N and C termini are labeled and are *brown*.

buffer (10 mM) was lower than the sulfate concentration (2.6 M) used in crystallization, the tetrahedrally shaped residual density observed in close proximity to the Mg^{2+} binding site was considered to represent an SO^{4-} ion (Fig. 2*A*). Although hydrolytic activity is Mg^{2+}-dependent and this site is surrounded by highly conserved amino acids, it is considered to represent the active site, and the SO^{4-} ion likely mimics the binding of the phosphate group of the substrate.

The refined model of SMase I contains 1140 amino acid residues, 4 Mg^{2+} ions, 23 sulfate ions, 3 Hepes, and 1018 solvent water molecules. An analysis of the stereochemistry (PROCHECK) (39) of the final model indicates that the main-chain dihedral angles for all residues are located in the permitted regions of the Ramachandran diagram and that the root mean square deviations from ideal values are distributed within the expected ranges for a well refined structure (Table I).

The fundamental structural unit of SMase I is formed by a distorted triose phosphate isomerase or $(\alpha/\beta)_8$ barrel (surface area = 11,254 Å^2) with the insertion of additional β-strands and α-helices (Figs. 1 and 3). The N and C termini flank one side of the barrel, and the N terminus leads directly to the first β-strand, whereas the C terminus contains a short helix (8′) and a β-strand (H′) and caps the torus of the barrel (Figs. 1 and 3). The asymmetric unit contains four molecules and can be considered to be made up of two dimers. The monomers forming the dimer are related by a 2-fold axis of rotation perpendicular to the barrel (Fig. 4) and results in 3402 Å^2 (or 33%) of the surface area of each monomer being buried. Dimerization is likely an artifact of the crystal packing interactions, because the dynamic light-scattering experiments indicate that the protein is monomeric in solution.

The opposite face of the barrel is surrounded by a ring of negatively charged amino acids and hydrophobic loops (Fig. 1). The active site pocket contains His^{12}, Glu^{32}, Asp^{34}, Asp^{91}, His^{47}, Asp^{52}, Trp^{230}, Asp^{233}, and Asn^{252}, which are fully conserved in the *Loxosceles* species SMases D isoforms (Fig. 5). Mutagenesis studies of Mg^{2+}-dependent neutral SMase (40) and the crystal structure of phospholipase D (41) indicate the involvement of two histidine residues that are in close proximity to the metal ion binding site in the acid-base catalytic mechanism. Based on the structural results, His^{12} and His^{47} of SMase D have been identified as the key residues for catalysis and are assisted by a hydrogen bond network that involves Asp^{52}, Asn^{252}, and Asp^{233}. The metal ion is coordinated by Glu^{32}, Asp^{34}, Asp^{91}, and solvent molecules.

His^{12} is located at the tip of the first β-strand (strand A, Figs. 1 and 3), and $N^{\epsilon 2}$ forms a hydrogen bond to O_2 of the bound sulfate ion. $His^{12}N^{\delta 1}$ is hydrogen bonded to $Asn^{252}O^{\delta 1}$ and $Asn^{252}N^{\delta 2}$ is further hydrogen bonded to $Asp^{52}O^{\delta 2}$, and $Asp^{233}O^{\delta 2}$ (Fig. 2).

The catalytic loop (loop B, residues 46–60) is stabilized at the tip by a disulfide bridge (Cys^{51}-Cys^{57}, Figs. 3 and 6), which is a conserved feature of all spider SMases D (Fig. 5), and His^{47} is located at the base of the loop. Multiple hydrogen bonds are formed between $Arg^{55}NH_1$ and the main-chain carbonyl oxygen of His^{12} and $Arg^{55}NH_2$ and $Met^{13}O$ (Fig. 6), and additionally $Arg^{55}NH_1$ also bonds $Asp^{252}O^{\delta 1}$. A structural sulfate ion binds via O_1 to $Arg^{55}N^{\epsilon}$ and the main chain amide nitrogen of Asp^{56}. O_4 of the sulfate ion binds two solvent molecules, both of which are hydrogen bonded to $Arg^{59}NH_1$. $Arg^{59}N^{\epsilon}$ binds a molecule of Hepes, the latter interacting with the indole of Trp^{60} located at the base of the catalytic loop (loop B) on the external surface of the barrel. This network of bonds ensures the orientation of the catalytic loop in relation to the active site. $His^{47}N^{\epsilon 2}$ is hydrogen bonded to O_1 and O_3 of the sulfate ion located in the catalytic site, and $His^{47}N^{\delta 1}$ interacts with the carbonyl oxygen atom of Gly^{48} (Fig. 2*B*).

The bound Mg^{2+} ion (Fig. 2) is octahedrally coordinated (mean Mg^{2+}–O distance of 1.98 Å), equatorially by carboxylate oxygens from the side chains of Glu^{32}, Asp^{34}, and two water molecules and apically by the side-chain carboxylate oxygen atoms of Asp^{91} and a water molecule, which is additionally hydrogen bonded to $Glu^{32}O^{\epsilon 1}$. The sulfate ion is coordinated by three solvent molecules, two of which also coordinate the Mg^{2+} ion, $His^{12}N^{\epsilon 2}$, $His^{47}N^{\epsilon 2}$, and $Trp^{230}N^{\epsilon 1}$. Trp^{230} is located in loop G (Fig. 1), which is structurally adjacent to the flexible loop (loop F) and is strictly conserved in bacterial and spider SMases D. The indole ring is partially disordered in three of the four molecules in the asymmetric unit, is aligned along the axis of the barrel, and could be involved in stabilizing the choline headgroup of the substrate.

DISCUSSION

The branching pathways of sphingolipid metabolism mediate either apoptotic or mitogenic responses, depending on the cell type and the nature of the stimulus (42). Events involving SM metabolites include proliferation, differentiation, and growth arrest, as well as the induction of apoptosis.

Loxosceles spiders and *Corynebacteria* SMases D catalyze the hydrolysis of sphingomyelin in a Mg^{2+}-dependent manner, with the concerted action of two histidines producing ceramide 1-phosphate and choline, and also display intrinsic lysophospholipase D activity toward lysophosphatidylcholine producing lysophosphatidic acid, a known inducer of platelet aggregation, endothelial hyperpermeability, and pro-inflammatory responses. However, sequence alignments indicate that SMases

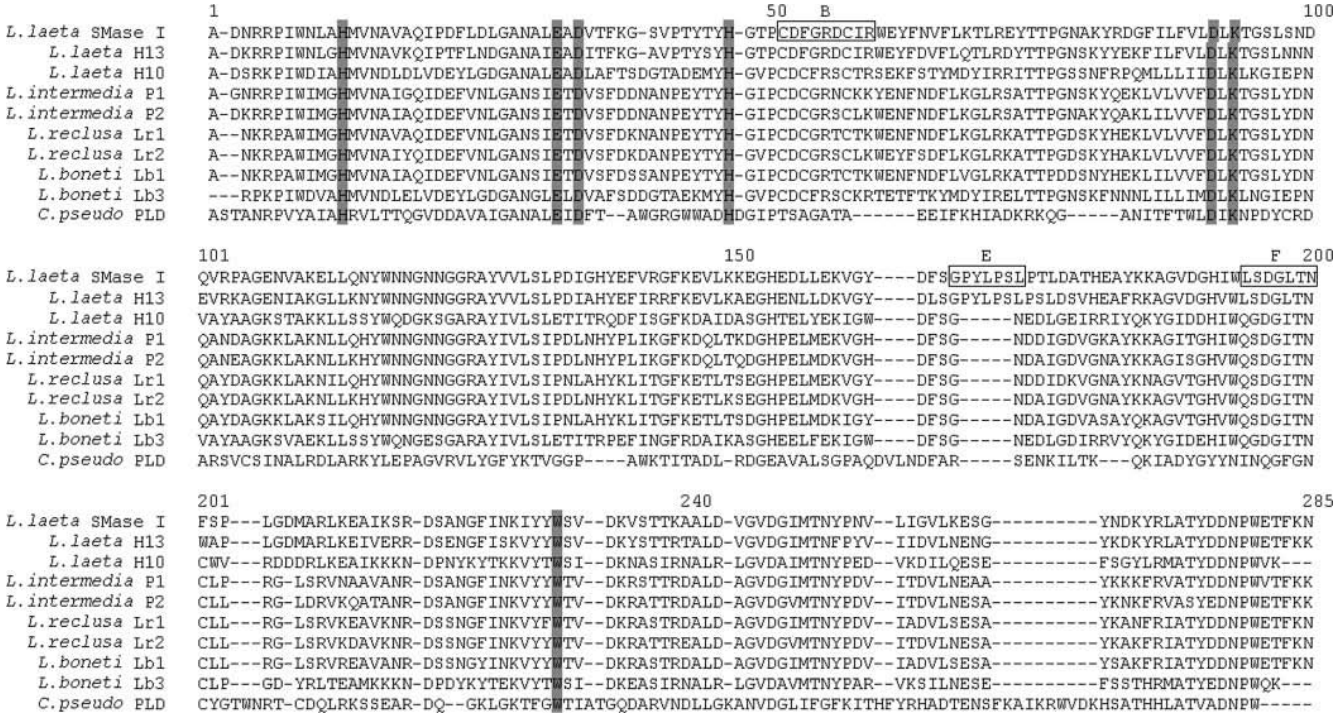

FIG. 5. **Structure-based multiple sequence alignments of the SMases D isoforms performed using three-dimensional Coffee 2004 (49).** *L. laeta*: SMase I, H10, and H13 (GenBank™ accession numbers AY093599, AY093600 and AY093601, respectively) (15); *L. intermedia*: P1 and P2 (accession numbers AY304471 and AY304472, respectively) (14); *L. reclusa*: Lr1 and Lr2 (accession numbers AY559846 and AY559847, respectively) (19); *Loxosceles boneti*: Lb1 and Lb3 (accession numbers AY559844 and AY559845, respectively) (50) and *C. pseudotuberculosis*: PLD (accession number L16586) (21). Residues involved in catalysis or metal ion coordination are *shaded gray*. Amino acids in loops *B*, *E*, and *F* are *boxed*. Sequence numbers indicated are for *L. laeta* SMase I.

D lack the conserved HKD sequence motif characteristic of the PLD superfamily (43), indicating different catalytic site architectures.

The Mg^{2+} binding site is strictly conserved in spider and *C. pseudotuberculosis* SMases D (Fig. 5), and enzymatic activity is absolutely dependent on Mg^{2+}. In the crystal structure, the Mg^{2+} ion is octahedrally coordinated by the carboxyl oxygens of Glu^{32}, Asp^{34}, Asp^{91}, and three solvent molecules. The Mg^{2+} ion positions the two equatorial solvent molecules, which in turn could orient the phosphate group of the substrate or could participate in the stabilization of the reaction intermediate. Trp^{230}, which is fully conserved in SMases D, could also play a role in orienting the phosphate moiety, permitting nucleophilic attack, and also in stabilizing the transition state. Lys^{93}, located in the catalytic pocket, is also highly conserved and may play a crucial role in balancing the charge during catalysis or in orienting the bound substrate.

Although mammalian desoxyribonuclease I and bacterial SMases C share <10% sequence identity, the two enzymes are considered to be evolutionarily related, and the structure of desoxyribonuclease I (44, 45) (Protein Data Bank code 3DNI) has been used as a template to model the structure of *Bacillus cereus* SMase C (46). Based on the results of modeling and site-directed mutagenesis, an acid-base mechanism has been suggested for bacterial and mammalian Mg^{2+}-dependent neutral sphingomyelinases (40, 46), where His^{296} activates a neighboring water molecule, which in turn attacks the scissile phosphodiester bond of SM. The electron then transfers to the general acid (His^{151}) through the penta-covalent intermediate, resulting in the release of ceramide from SM. The intermediate is then stabilized by Mg^{2+} liganded by Glu^{53}, Asp^{195}, and Asp^{295}, which suggests that the latter play dual roles by maintaining the appropriate pK_a and relative orientation of His^{151} and His^{296}. Mutation of either His^{136} or His^{272} in rat neutral

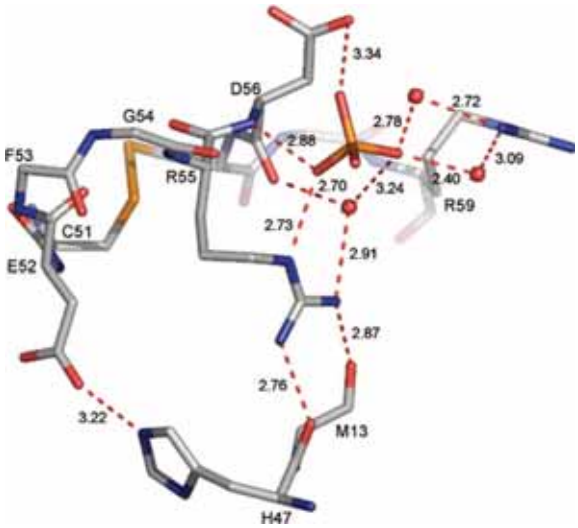

FIG. 6. **Network of hydrogen bonds (*dashed red lines*) participating in the stabilization of the catalytic loop (loop B).** The structural SO^{4-} ion, disulfide bridge (*yellow bond*), and solvent molecules (*red spheres*) are also included.

sphingomyelinase or Asp^{195} and His^{296} in *B. cereus* (40) sphingomyelinase entirely abolished hydrolytic activity. The His^{151}→Ala and His^{151}→Gln mutants of the *B. cereus* enzyme retained partial activity (40).

We are now able to infer the catalytic mechanism of SMase D, which is based on the direct nucleophilic attack of water in a fashion analogous to the mechanisms proposed for desoxyribonuclease I (44, 45, 47), PLD (41–48), and for *B. cereus* SMase C (46). In this model (Fig. 7), the concerted action of two histidines (His^{12} and His^{47}) is required for catalysis. His^{12}

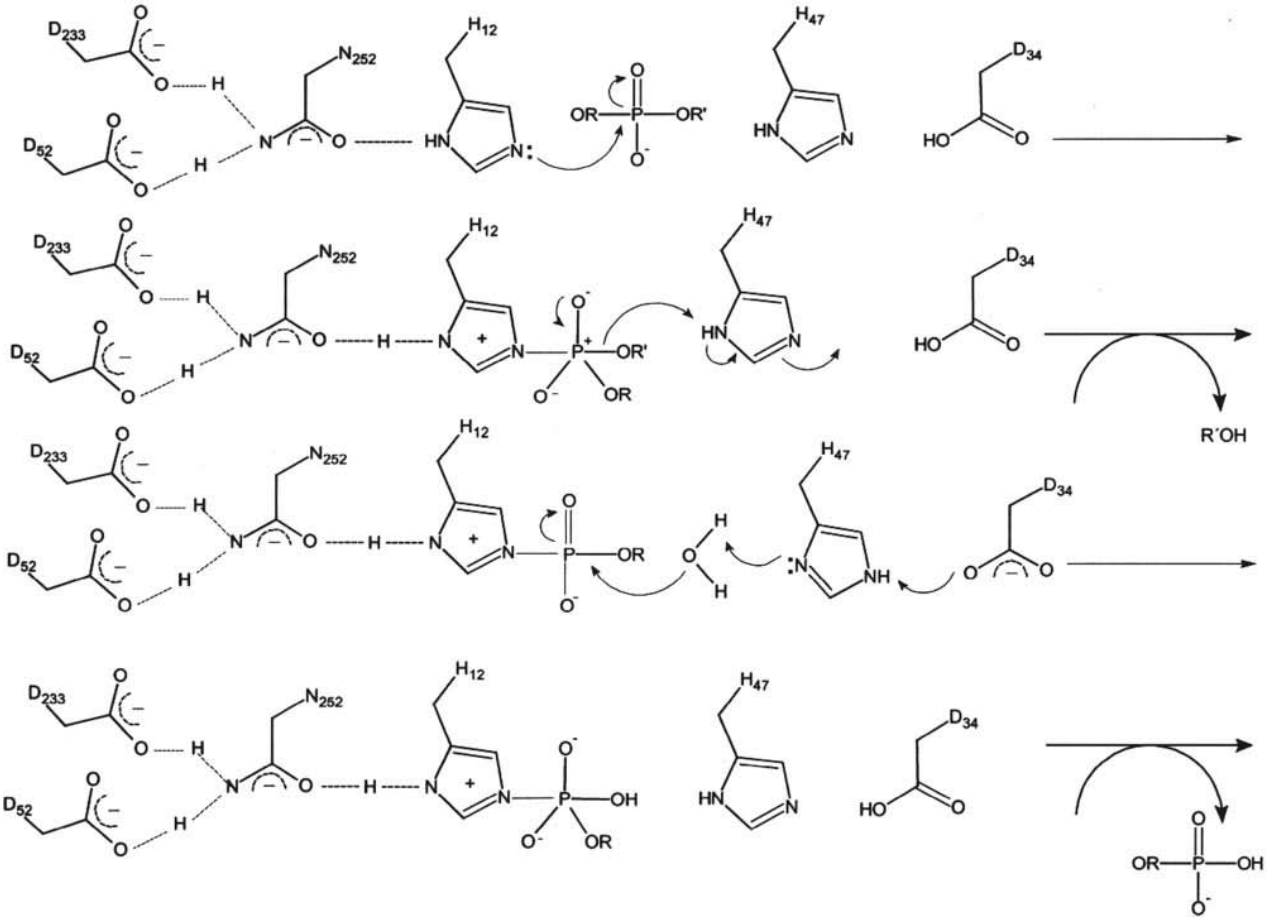

FIG. 7. **The proposed mechanism for the catalytic hydrolysis of the sphingomyelin substrate by SMase I, His^{12}, and His^{47} participate in the reaction as the acid and base.** *R* and *R′* represent ceramide 1-phosphate and choline, respectively. The figure was generated using ChemSketch (www.acdlabs.com).

functions as the nucleophile that initiates the attack on the scissile phosphodiester bond of the SM substrate. This is followed by the formation of a short-lived penta-coordinated covalent intermediate, which is subsequently destabilized by the donation of a hydrogen atom by His^{47} to produce choline. The resulting tetrahedral reaction intermediate is stabilized by a covalent bond formed to $His^{12}N^{\epsilon 2}$. Because His^{47} donates a proton to the group first to leave, it is now able to (partially) deprotonate a nearby water molecule that initiates a nucleophilic attack on the stable covalent histidine intermediate, thereby resulting in the formation of the second product, ceramide 1-phosphate, which also proceeds via the formation of a short-lived, penta-coordinated phosphorus intermediate, culminating in a second inversion of the configuration of the phosphorus atom and a return to the initial state.

In this proposed model, His^{12} functions as the nucleophile, which is assisted by a network of hydrogen bonds formed to the carboxylate oxygen of Asn^{252}, which in turn is hydrogen bonded through $N^{\delta 2}$ to $Asp^{52}O^{\delta 2}$ and $Asp^{233}O^{\delta 2}$. Additionally, $His^{12}N^{\delta 1}$ is also hydrogen bonded to $Asp^{52}O^{\delta 2}$. $His^{47}N^{\delta 1}$ is hydrogen bonded to the carbonyl oxygen atom of Gly^{48} (distance = 2.7 Å) and thus cannot serve as a proton donor in this orientation (Fig. 2*B*). To overcome this, a rotation of the imidazole ring around $\kappa 1$ and $\kappa 2$ would be required and would permit $His^{47}N^{\delta 1}$ to interact with the only possible proton donor in the vicinity, which is $Asp^{34}O^{\delta 2}$. Asp^{34} could exist in the protonated state because of its configuration around the metal ion binding site, transferring the proton to His^{47} during catalysis.

Loxosceles spider venom SMases D share high sequence homology, and the amino acids considered to be involved in catalysis are strictly conserved. Structure-based alignment (Fig. 5) and modeling indicate that the five deletions in all other *Loxosceles* sp. SMases D, except in SMase I from *L. laeta* venom, result in a shortened surface loop (variable loop or loop E). Additionally, the disulfide bond formed between Cys^{53} (located in the catalytic loop B) and Cys^{201} (located in the flexible loop F), present in other *Loxosceles* sp. SMases D, probably serve as a bridge and bring loops B and F closer together (Figs. 1, 3, and 5).

In conclusion, in bacterial and spider SMases D, interfacial catalysis is mediated by metal ion binding, and two histidine residues are involved in hydrolyzing sphingomyelin and lysophosphatidylcholine via acid base catalysis. Mg^{2+}-dependent SMases probably share a common catalytic mechanism regardless of the species. These results provide structural data important in further dissecting the mechanism of SMases D, in particular, and Mg^{2+}-dependent neutral SMases, in general.

Acknowledgments—We are grateful to Drs. I. Polikarpov, A. L. Rojas, and R. A. P. Nagem for helpful discussions.

REFERENCES

1. Futrell, J. M. (1992) *Am. J. Med. Sci.* **304,** 261–267
2. Nelson, J. (1988) *Can. Med. Assoc. J.* **138,** 888–889
3. Allen, P. B. (1988) *Can. Med. Assoc. J.* **138,** 792
4. Atkins, J. A., Wingo, C. W., Sodeman, W. A., and Flynn, J. E. (1958) *Am. J. Trop. Med. Hyg.* **7,** 165–184
5. Wasserman, G. S., and Anderson, D. O. (1983) *J. Toxicol. Clin. Toxicol.* **21,** 451–455
6. Barreto, O. C., Cardoso, J. L., and De Cillo, D. (1985) *Rev. Inst. Med. Trop. São Paulo* **27,** 264–267

7. Schenone, H., Saavedra, T., Rojas, A., and Villarroel, F. (1989) *Rev. Inst. Med. Trop. São Paulo* **31,** 403–415
8. Ginsburg, C. M., and Weinberg, A. G. (1988) *J. Pediatr.* **112,** 496–499
9. Sezerino, U. M., Zannin, M., Coelho, L. K., Gonçalves, J., Jr., Grando, M., Mattosinho, S. G., Cardoso, J. L., von Eickstedt, V. R., França, F. O., Barbaro, K. C., and Fan, H. W. (1998) *Trans. R. Soc. Trop. Med. Hyg.* **92,** 546–548
10. Gendron, B. P., (1990) *Am. J. Emerg. Med.* **8,** 51–54
11. Bey, T. A., Walter, F. G., Lober, W., Schmidt, J., Spark, R., and Schlievert, P. M. (1997) *Ann. Emerg. Med.* **30,** 701–703
12. Tambourgi, D. V., Magnoli, F. C., Von Eickstedt, V. R., Benedetti, Z. C., Petricevich, V. L., and da Silva, W. D. (1995) *J. Immunol.* **155,** 4459–4466
13. Tambourgi, D. V., Magnoli, F. C., van den Berg, C. W., Morgan, B. P., de Araujo, P. S., Alves, E. W., and da Silva. W. D. (1998) *Biochem. Biophys. Res. Commun.* **251,** 366–373C. W.
14. Tambourgi, D. V., Fernandes-Pedrosa, M. F., van den Berg, C. W., Gonçalves-de-Andrade, R. M., Ferracini, M., Paixão-Cavalcante, D., Morgan, B. P., and Rushmere, N. K. (2004) *Mol. Immunol.* **41,** 831–840M. F.
15. Fernandes-Pedrosa, M. F., Junqueira de Azevedo, I. L., Gonçalves-de-Andrade, R. M., van den Berg, C. W., Ramos, C. R., Ho, P. L., and Tambourgi, D. V. (2002) *Biochem. Biophys. Res. Commun.* **298,** 638–645
16. Tambourgi, D. V., Petricevich, V. L., Magnoli, F. C., Assaf, S. L., Jancar, S., and Da Silva, W. D. (1998) *Toxicon* **36,** 391–403
17. Tambourgi, D. V., Morgan, B. P., Gonçalves de Andrade, R. M., Magnoli, F. C., and van den Berg, C. W. (2000) *Blood* **95,** 683–691
18. Tambourgi, D. V., Silva, M. S., Billington, S. J., Gonçalves de Andrade, R. M., Magnoli, F. C., Songer, J. G., and van den Berg, C. W. (2002) *Immunology* **107,** 93–101
19. Soucek, A., Michalec, C., and Souckova, A. (1967) *Biochim. Biophys. Acta* **144,** 180–182
20. Truett, A. P., and King, L. E., Jr. (1993) *Adv. Lipid Res.* **26,** 275–291
21. McNamara, P. J., Cuevas, W. A., and Songer, J. G. (1995) *Gene* **156,** 113–118
22. Songer, J. G. (1997) *Trends Microbiol.* **5,** 156–161
23. McNamara, P. J., Bradley, G. A., and Songer, J. G. (1994) *Mol. Microbiol.* **12,** 921–930
24. van Meeteren, L. A., Frederiks, F., Giepmans, B. N., Fernandes-Pedrosa, M. F., Billington, S. J., Jost, B. H., Tambourgi, D. V., and Moolenaar, W. H. (2004) *J. Biol. Chem.* **279,** 10833–10836
25. Forrester, L. J., Barrett, J. T., and Campbell, B. J. (1978) *Arch. Biochem. Biophys.* **187,** 355–365
26. Kurpiewski, G., Forrester, L. J., Barrett, J. T., and Campbell, B. J. (1981) *Biochim. Biophys. Acta* **678,** 467–476
27. Carne, H. R., and Onon, E. O. (1978) *Nature* **271,** 246–248
28. Bernheimer, A. W., Campbell, B. J., and Forrester, L. J. (1985) *Science* **228,** 590–591
29. Moolenaar, W. H. (1999) *Exp. Cell Res.* **253,** 230–238
30. Chun, J., Goetzl, E. J., Hla, T., Igarashi, Y., Lynch, K. R., Moolenaar, W., Pyne, S., and Tigyi, G. (2002) *Pharmacol. Rev.* **54,** 265–269
31. Zela, S. P., Fernandes-Pedrosa, M. F., Murakami, M. T., De Andrade, S. A., Arni, R. K., and Tambourgi, D. V. (2004) *Acta Crystallogr. Sect. D Biol. Crystallogr.* **60,** 1112–1114
32. Otwinowski, Z., and Minor, W. (1997) *Methods Enzymol.* **276,** 307–326
33. Dauter, Z., Dauter, M., and Rajashankar, K. R. (2000) *Acta Crystallogr. Sect. D Biol. Crystallogr.* **56,** 232–237
34. Nagem, R. A., Dauter, Z., and Polikarpov, I. (2001) *Acta Crystallogr. Sect. D Biol. Crystallogr.* **57,** 996–1002
35. Schneider, T. R., and Sheldrick, G. M. (2002) *Acta Crystallogr. Sect. D Biol. Crystallogr.* **58,** 1772–1779
36. Abrahams, J. P., and Leslie, A. J. W. (1996) *Acta Crystallogr. Sect. D* **52,** 30–42
37. Perrakis, A., Morris, R. J. H., and Lamzin, V. (1999) *Nat. Struct. Biol.* **6,** 458–463
38. Murshudov, G. N., Vagin, A. A., and Dodson, E. J. (1997) *Acta Crystallogr. Sect. D* **53,** 240–255
39. Laskowski, R. A., MacArthur, M. W., Moss, D. S., and Thornton, J. M. (1993) *J. Appl. Crystallogr.* **26,** 283–291
40. Obama, T., Fujii, S., Ikezawa, H., Ikeda, K., Imagawa, M., and Tsukamoto, K. (2003) *Biol. Pharm. Bull.* **26,** 920–926
41. Stuckey, J. A., and Dixon, J. E. (1999) *Nat. Struct. Biol.* **6,** 278–284
42. Claus, R., Russwurm, S., Meisner, M., Kinscherf, R., and Deigner, H. P. (2000) *Curr. Drug Targets* **1,** 185–205
43. Exton, J. H. (2002) *FEBS Lett.* **531,** 58–61
44. Suck, D., and Oefner, C. (1986) *Nature* **321,** 620–625
45. Suck, D., Lahm, A., and Oefner, C. (1988) *Nature* **332,** 464–468
46. Matsuo, Y. O., Yamada, A., Tsukamoto, K., Tamura, H-O., Ikezawa, H., Nakamura, H., and Nishikawa, K. (1996) *Protein Sci.* **5,** 2459–2467
47. Jones, S. J., Worrall, A. F., and Connolly, B. A. (1996) *J. Mol. Biol.* **264,** 1154–1163
48. Leiros, I., McSweeney, S., and Hough, E. (2004) *J. Mol. Biol.* **339,** 805–820
49. O′Sullivan, O., Suhre, K., Abergel, C., Higgins, D. G., and Notredam, C. (2004) *J. Mol. Biol.*, **340,** 385–395
50. Ramos-Cerrillo, B., Olivera, A., Odell, G. V., Zamudio, F., Paniagua-Solis, J., Alagon, A., and Stock, R. P. (2004) *Toxicon* **44,** 507–514

Available online at www.sciencedirect.com
SCIENCE DIRECT
ELSEVIER
Biochemical and Biophysical Research Communications 342 (2006) 323–329
BBRC
www.elsevier.com/locate/ybbrc

Structural insights into the catalytic mechanism of sphingomyelinases D and evolutionary relationship to glycerophosphodiester phosphodiesterases

Mário T. Murakami [a], Matheus Freitas Fernandes-Pedrosa [b], Sonia A. de Andrade [b], Azat Gabdoulkhakov [c], Christian Betzel [d], Denise V. Tambourgi [b,e,*], Raghuvir K. Arni [a,e,*]

[a] *Department of Physics, IBILCE/UNESP, São José do Rio Preto-SP, Brazil*
[b] *Immunochemistry Laboratory, Butantan Institute, São Paulo-SP, Brazil*
[c] *Institute for Protein Research RAS, Moscow, Russia*
[d] *Division of Biochemistry and Molecular Biology, Hamburg University, Germany*
[e] *Center for Applied Toxinology, Butantan Institute, São Paulo-SP, Brazil*

Received 14 January 2006
Available online 3 February 2006

Abstract

Spider venom sphingomyelinases D catalyze the hydrolysis of sphingomyelin via an Mg^{2+} ion-dependent acid–base catalytic mechanism which involves two histidines. In the crystal structure of the sulfate free enzyme determined at 1.85 Å resolution, the metal ion is tetrahedrally coordinated instead of the trigonal–bipyramidal coordination observed in the sulfate bound form. The observed hyperpolarized state of His47 requires a revision of the previously suggested catalytic mechanism. Molecular modeling indicates that the fundamental structural features important for catalysis are fully conserved in both classes of SMases D and that the Class II SMases D contain an additional intra-chain disulphide bridge (Cys53–Cys201). Structural analysis suggests that the highly homologous enzyme from *Loxosceles bonetti* is unable to hydrolyze sphingomyelin due to the 95Gly → Asn and 134Pro → Glu mutations that modify the local charge and hydrophobicity of the interfacial face. Structural and sequence comparisons confirm the evolutionary relationship between sphingomyelinases D and the glicerophosphodiester phosphoesterases which utilize a similar catalytic mechanism.

Keywords: Sphingomyelinase D; Catalytic mechanism; Mg^{2+}-binding site; Hydrodynamic behavior; Crystal structure; Glycerophosphodiester phosphodiesterases

Sphingomyelinases D (SMases D) (sphingomyelin phosphodiesterase D; E.C. 3.1.4.41) catalyze the hydrolysis of sphingomyelin resulting in the formation of ceramide 1-phosphate (C1P) and choline or the hydrolysis of lysophosphatidyl choline, generating the lipid mediator lysophosphatidic acid (LPA) [1]. C1P is implicated in the stimulation of cell proliferation via a pathway that involves inhibition of acid sphingomyelinase and the simultaneous blocking of ceramide synthesis [2]. LPA is known to induce various biological and pathological responses such as platelet aggregation, endothelial hyperpermeability, and pro-inflammatory responses by signaling through three G-protein-coupled receptors [3,4]. SMases D, the main components of spider venoms of the genus *Loxosceles*, induce severe local dermonecrosis, acute renal failure, thrombocytopenia, platelet aggregation, and systemic intravascular haemolysis, which, in rare cases, lead to death [5].

Surprisingly, SMase D activity is not encountered elsewhere in the animal kingdom, but is present in strains of pathogenic *Corynebacterium*. The bacterial and spider venom SMases D possess similar molecular masses

* Corresponding authors. Fax: +55 17 2212240 (R.K. Arni).
E-mail addresses: dvtambourgi@yahoo.com (D.V. Tambourgi), arni@ibilce.unesp.br (R.K. Arni).

0006-291X/$ - see front matter © 2006 Elsevier Inc. All rights reserved.
doi:10.1016/j.bbrc.2006.01.123

(31–35 kDa) but display low sequence identity and are considered to have originated from a common ancestor, the glycerophosphodiester phosphodiesterases (GDPD; E.C. 3.1.4.46). GDPDs are ubiquitous enzymes, encountered in bacteria and eukaryotes, display a wide specificity and are involved in glycerol metabolism since they catalyze the reaction of glycerophosphodiester and water to alcohol and *sn*-glycerol-3-phosphate.

We have recently reported the results of the first crystal structure of a SMase D from *Loxosceles laeta* (SMase I) in the presence of a bound sulfate ion [6] and described the acid–base catalytic mechanism involving two histidine residues, His12 and His47, and the role of the Mg^{2+} ion. We now report the crystal structure of SMase I determined in the absence of the sulfate ion. In the light of which, the previously suggested mechanism has been revised and we extend this mechanism to encompass the structurally related GDPDs that also utilize a similar catalytic mechanism.

Materials and methods

Protein expression and purification. SMase I (GenBank™ Accession No. AY093599) was expressed in *Escherichia coli* strain BL21 as a fusion protein of SMase I with an N-terminal extension containing a His6 tag [7]. Recombinant SMase I was purified from the soluble fraction of cell lysates on a Ni(II)-chelating-Sepharose Fast Flow column (Amersham Biosciences). Recombinant protein was eluted with a buffer solution containing 100 mM Tris–HCl, pH 8.0, 300 mM NaCl, and 0.8 M imidazole and dialyzed against phosphate-buffered saline, pH 7.2 (10 mM sodium phosphate, 150 mM NaCl).

Dynamic light scattering. Dynamic light scattering (DLS) measurements were performed using a DynaPro-801 Instrument (Protein Solutions, Inc., Charlottesville, VA) equipped with a 25 mW, 780 nm solid-state lazer and a peltier cell. The protein samples were prepared at a concentration of 5 mg/mL in 5 mM Hepes buffer, containing 0.02 M NaCl, pH 7.0, at 20 °C and were loaded in a 20 μL quartz flow cell. The scattered photons were detected by an avalanche photodiode at a fixed scattering angle of 90° and 30 measurements were carried out in a time interval of 30 s. The hydrodynamic radii of gyration, molecular masses, and degree of sample polydispersity were calculated based on the autocorrelation function using the manufacturer's software wherein the radius of gyration (R_g) is extrapolated via the Stokes–Einstein equation. The apparent molecular mass was derived from a standard curve of molecular weights versus measured values of the translational diffusion coefficient obtained from a set of calibrated standard values.

Small angle X-ray scattering. Small angle X-ray scattering (SAXS) experiments were performed at the SAS1 beamline, Laboratório Nacional de Luz Síncrotron (LNLS, Campinas, Brazil). To minimize aggregation effects, the protein concentration used was 2 mg/mL and all experiments were conducted at 20 °C. The wavelength was set to 1.48 Å and the sample-to-detector distance was fixed at 1.07 m. The vertical linear-sensitive position detector was translated upwards in relation to the incident beam so that the scattered intensities for higher scattering angles could be measured and three frames with exposure times of 600 s were recorded. Background scattering was measured before and after each protein sample using the corresponding buffer solution (50 mM Hepes, pH 7.0, 150 mM sodium chloride) and this contribution was subsequently subtracted from the protein scattering patterns after normalization and correction. The R_g and intensity values were obtained by utilizing the Guinier approximations and the theoretical R_g values were calculated based on the atomic coordinates of the model using the program CRYSOL [8].

Crystallization and data collection. Crystals of sulfate ion free SMase I were obtained by the hanging-drop vapour-diffusion method. Equal volumes (1 μL) of protein and mother solution were mixed over wells containing 2.4 M trisodium citrate that was titrated to pH 9.0, using a 0.1 M sodium hydroxide solution. Crystals were soaked in the mother solution which additionally contained 25% glycerol as a cryoprotectant and were cooled to 100 K in a nitrogen-gas stream (Oxford Cryosystems). Diffraction intensities were recorded at the Consortium Beamline X13 at HASYLAB/DESY–Hamburg equipped with an imaging plate detector (MAR345). Integration, scaling and merging of the intensities were carried out using DENZO and SCALEPACK [9]. Analysis of the structure factors using SFCHECK [10] indicated a twinning fraction of 0.373. The twin-related reflections (h, $-h-k$, $-l$) were treated using DETWIN [11] and the detwinned data display residual twinning of 0.035 with an overall completeness of 83.5%.

Structure determination and refinement. The crystal structure of the sulfate free form of SMase I was solved by molecular replacement using the atomic coordinates of the sulfate bound form (PDB entry: 1XX1) [6] as a search model and the program AMoRe [12] as implemented in the CCP4 suite of programs. Initial cycles of restrained refinement were carried out by REFMAC5 [13] and non-crystallographic restraints were imposed. The model was inspected and manually adjusted based on the $2F_o-F_c$ and F_o-F_c electron density maps using the programs TURBO FRODO [14] and COOT [15]. In the later cycles, the non-crystallographic restraints were relaxed and individual isotropic $B_{factors}$ were refined. Solvent molecules, added automatically using ARP/wARP [16], were checked by visual inspection and retained by taking hydrogen bonding potential into consideration. The quality of the model was assessed using *PROCHECK* [17], data collection and refinement statistics are presented in Table 1. The structure factors and atomic coordinates have been deposited with the Protein Data Bank and have been assigned the code 2F9R.

Table 1
Data collection and refinement statistics

PDB code	2F9R
Data-collection statistics	
Space group	$P6_5$
Unit-cell parameters (Å)	$a = b = 140.5$, and $c = 113.6$
Resolution range (Å)	20.0 − 1.85 (1.89 − 1.85)
Unique reflections	101,876
Redundancy	6.1 (5.8)
Completeness (%)	93.9 (96.6)
$I/\sigma(I)$	25.5 (5.2)
R_{merge} (%)[a]	5.7 (27.9)
V_M (Å^3 Da^{-1})	2.34
Solvent content (%)	47.04
Refinement statistics	
R_{factor} (%)[b]	18.7
R_{free} value (%)[c]	23.4
No. of protein atoms	9380 (4 × 285 amino acid residues)
No. of solvent molecules	510
No. of Hepes molecules	3
Mean temperature factor (Å^2)[d]	24.2
r.m.s.d. bond lengths (Å)	0.011
r.m.s.d. bond angles (°)	1.340
Ramachandran plot	
Most favored region (%)	89.7
Additionally allowed regions (%)	10.3
Generously allowed regions (%)	0.0
Disallowed regions (%)	0.0

Values in parentheses are for the highest resolution shell.

[a] $R_{merge} = 100 \times \sum|I(h) - \langle I(h)\rangle|/\sum I(h)$, where $I(h)$ is observed intensity and $\langle I(h)\rangle$ is mean intensity of reflection h over all measurements of $I(h)$.

[b] $R_{factor} = 100 \times \sum|F_o - F_c|/\sum(F_o)$ the sums being taken over all reflections with $F/\sigma(F) > 2$ cutoff.

[c] $R_{free} = R_{factor}$ for 5% of the data, which were not included during crystallographic refinement.

[d] B values are average B values for all non-hydrogen atoms.

Molecular modeling. The atomic coordinates of SMase I (PDB Accession code: 1XX1) [6] served as the template for generating structural models of both the active and inactive SMases D from *L. bonetti* by restraint-based modeling as implemented in the MODELLER program [18]. The overall model was improved enforcing the proper stereochemistry using spatial restraints and CHARMM energy terms, followed by conjugate gradient simulation based on the variable target function method [18]. The loops were optimized using ModLoop [19] taking into consideration the satisfaction of spatial restraints, without relying on a database of known protein structures.

Results and discussion

Hydrodynamic behavior of SMases D

DLS experiments indicate that SMase I (Class I) posses a hydrodynamic radius of 3.43 ± 0.03 nm with a corresponding molecular weight of the monomer of approximately 34.2 kDa in solution. The SAXS experiments carried out with the P1 enzyme (Class II) at low protein concentrations in the presence of 150 mM sodium chloride indicate a R_g of 17.4 Å that is in good agreement with the theoretical R_g calculated from the atomic coordinates of the modeled structure using CRYSOL [8] of 17.7 Å. These results indicate that both the enzymes are monomeric in solution and that the dimeric form encountered in the crystal structure of SMase I could represent an artifact as a result of the high protein and salt concentrations used in the crystallization experiments.

Crystal structure of SMase I

The refinement converged to a crystallographic residual of 18.7% ($R_{free} = 23.4\%$), the asymmetric unit comprises of two dimers (285 residues in each monomer), 3 Hepes (4-(2-hydroxyethyl)-1-piperazineethanesulfonic acid) molecules, 4 Mg^{2+} ions, and 510 solvent water molecules. The quality of the model assessed by PROCHECK [17] indicates that all the stereochemical parameters lie within the expected range (Table 1). The Ramachandran diagram [20] indicates that 89.7% of the main-chain dihedral angles of all non-glycine and non-proline residues are located in the energetically most favored regions and only 10.3% lie in the permitted region. Superpositioning of the atomic coordinates of the sulfate free and sulfate bound forms indicates that the flexible loop regions (residues 198–210), which are disordered and are characterized by diffuse electron densities, adopt different conformations.

Overall structure of SMases D

SMase D folds to form a distorted $(\alpha/\beta)_8$ barrel with the insertion of additional β-strands, α-helices, and several connecting loops [6]. The catalytic loop (blue), variable loop (green), and flexible loop (red) along with other short hydrophobic loops form the interfacial face (*i*-face) of the enzyme where the active site is located in a shallow cleft (Fig. 1A). The catalytic loop (residues 46–60) which contains the catalytically important residue, His47, is fully

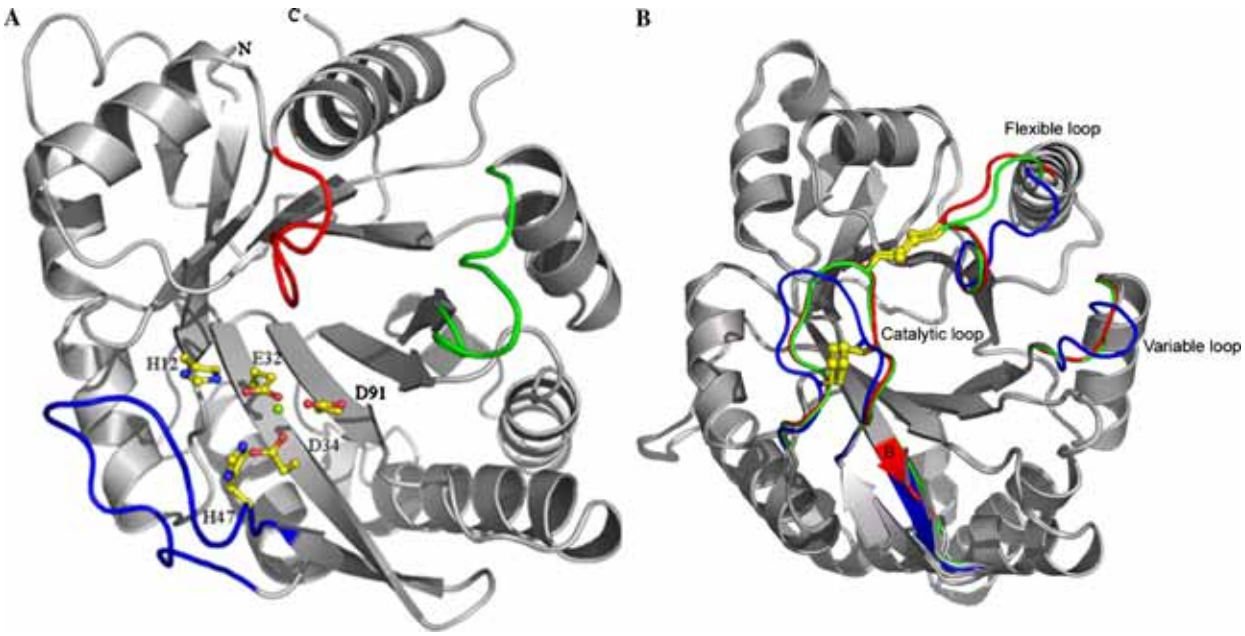

Fig. 1. (A) Ribbon representation of SMase I. The amino acids involved in metal-ion binding and catalysis are presented in atom colors (PDB code: 1XX1, chain A). The catalytic, flexible, and variable loops are colored blue, red, and green, respectively. (B) Differences in the catalytic, flexible, and variable loops in class I (blue), IIa (red), and IIb (green) SMases D. The disulphide bridges are presented by yellow ball and sticks. (For interpretation of the references to color in this figure legend, the reader is referred to the web version of this paper.)

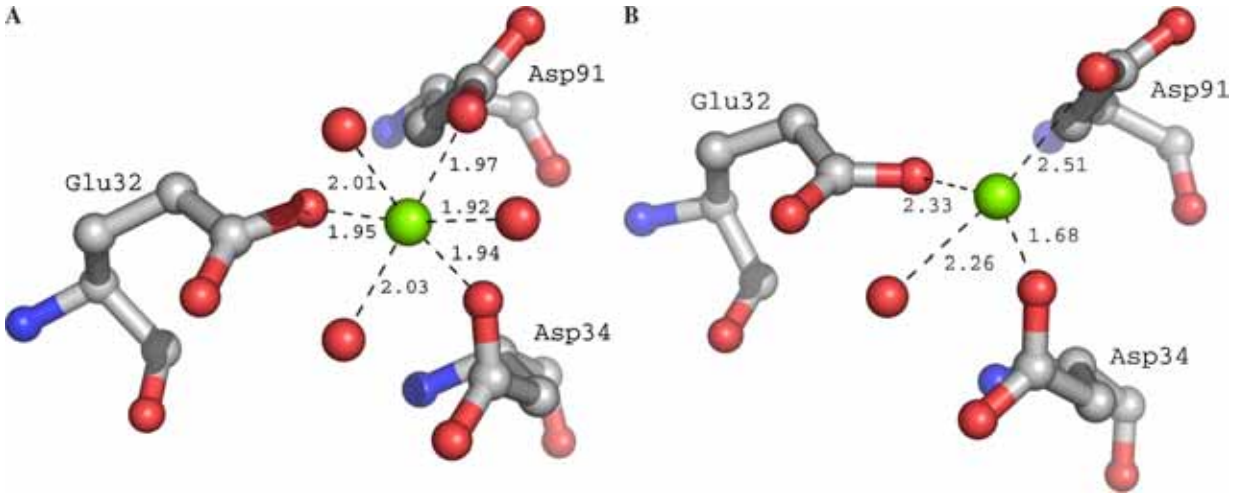

Fig. 2. Coordination sphere of the Mg^{2+} ion (A) in the presence of sulfate ion and (B) in the absence of sulfate ion.

conserved in all SMases D, forms a hairpin due to the presence of a disulphide bridge (Cys51–Cys57) and a network of hydrogen bonds ensures the correct relative orientation of the hairpin with respect to the core of the protein.

Mg^{2+}-binding site

The Mg^{2+}-binding site residues along with Trp230, Ly93, and the two catalytic histidine residues (His12 and His47) form the active-site pocket that is strictly conserved in both spider and bacterial SMases D [6]. In the structure of the sulfate bound SMase I determined at pH 5.5, the Mg^{2+} ion (B_{factor} of ~7.5 Å^2 and a mean Mg–O bond distance of ~2.01 Å) is hexacoordinated by a trigonal–bipyramid formed by the carboxyl oxygens of Glu32, Asp34, Asp91, and three water molecules (Fig. 2A). The latter bind the sulfate ion that is considered to represent the phosphate head group of the sphingomyelin substrate, suggesting a key role for the Mg^{2+} ion in the coordination and stabilization of the phosphonate of sphingomyelin during hydrolysis. In the crystal structure of the sulfate free SMase I determined at pH 9.0, the Mg^{2+} ion is coordinated tetrahedrally by the same three residues (Glu32, Asp34, and Asp91) and a single water molecule (Fig. 2B).

Catalytic mechanism of SMases D

The catalytic mechanism proposed for SMases D based on an acid–base reaction combined with metal ion stabilization [6] involves two histidines, His12 and His47, the former assisted by a hydrogen bond network formed between the carboxylate oxygens of Asp52, Asp233, and Asn252 and the latter by a short bond to Gly48O (distance = 2.7 Å, Figs. 3A and B). In the earlier model, we suggested that His12 functions as the nucleophile that initiates the attack on the scissile phosphodiester bond of the sphingomyelin substrate and His47, after undergoing a rotation of 180° around κ2, functions as the proton donor destabilization a short-lived penta-coordinated covalent intermediate to produce choline [6].

In the structure of SMase I determined in the absence of SO^{4-}, the position previously occupied by a tetrahedral ion is now occupied by a single water molecule which is simultaneously bound to His12 (His12NE2–O = 3.3 Å) and His 47 (His47NE2–O = 2.7 Å) (Fig. 3B). The shorter bond distance observed between His47NE2 and the water molecule indicates that His47 is present in a hyperpolarized state due to the short bond formed between His47ND1 and Gly48O. Thus, indicating that the roles of the two histidines are reversed, i.e., His47 behaves as the nucleophile which initiates the process of hydrolysis by attacking the scissile phosphodiester bond of the substrate, that is subsequently followed by the formation of a short-lived penta-coordinated intermediate. Donation of a hydrogen atom by His12 leads to the formation of choline and the resulting tetrahedral reaction intermediate is stabilized by a covalent bond formed to His47NE2. The previously deprotonated His12 is now able to abstract a proton from a solvent water molecule that initiates a nucleophilic attack on the reaction intermediate, thus resulting in the formation and release of ceramide 1-phosphate followed by a return to the initial state (Fig. 4). In this modified schematic, the energetically highly unfavorable rotation of His47 around κ2 would not be a prerequisite.

Structural classification of SMases D

All spider venom SMases D sequenced to date [8,21,22] display a significant level of sequence homology and thus likely possess the same $(\alpha/\beta)_8$ or TIM barrel fold (Figs. 1A and B). In this family of enzymes, the amino acids essential for metal-ion binding and catalysis are strictly conserved (Fig. 5), however, minor sequence differences result in decreased activity levels or, in the complete absence of hydrolytic activity upon sphingomyelin. Based on the sequence alignment, biochemical and structural

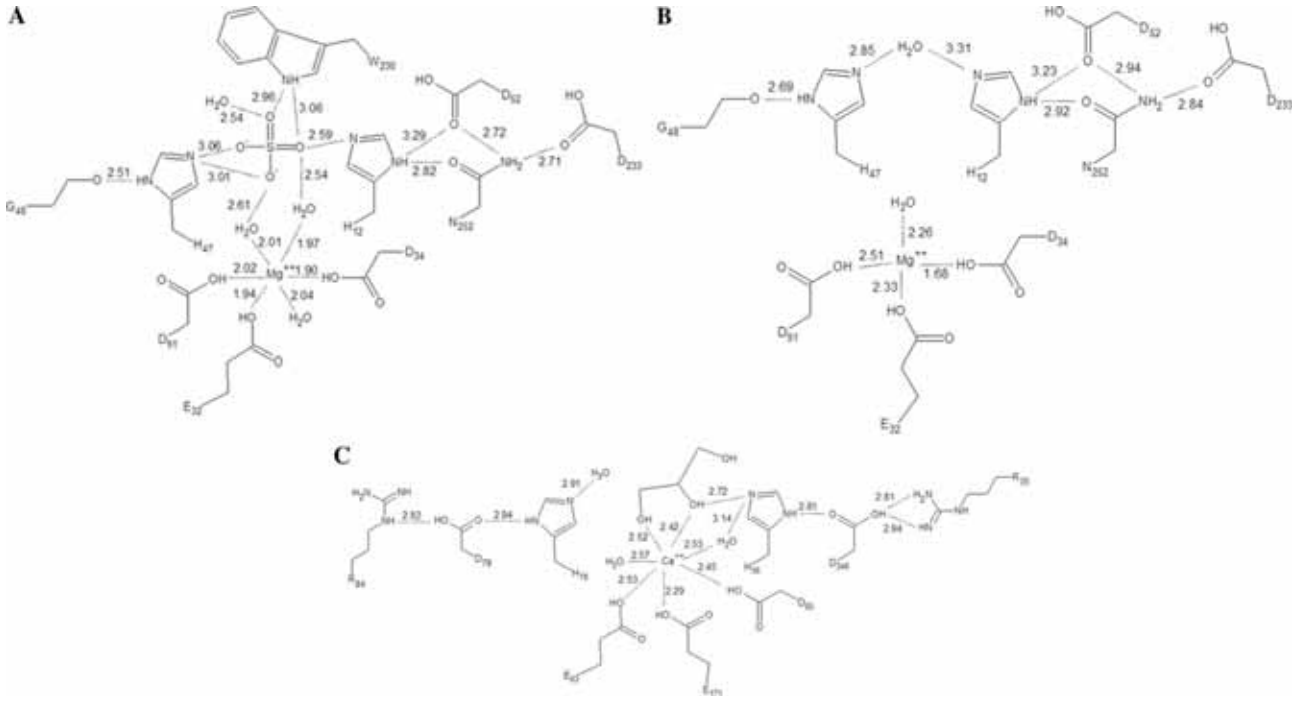

Fig. 3. Network of hydrogen bonds in the active-site pockets of (A) sulfate bound form of SMase I, (B) sulfate free form of SMase I, and (C) GDPD from *Escherichia coli* (PDB code: 1YDY).

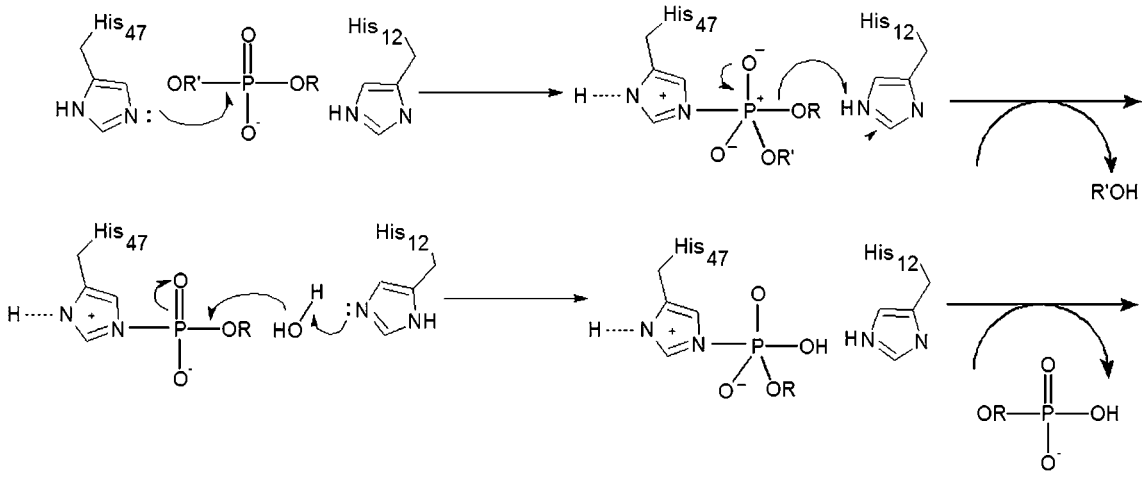

Fig. 4. Catalytic mechanism of SMases D.

data, we propose a classification of spider venom SMases D. The class I enzymes represented by SMase I, a SMase D from *L. laeta* and the H13 isoform possess a single disulphide bridge and contain an extended hydrophobic loop (Fig. 1B; green, amino acid sequence Pro-Tyr-Leu-Pro-Ser). All other SMases D belong to class II, which contains an additional intra-chain disulphide bridge that links the shortened flexible loop (red) with the catalytic loop (blue) (Figs. 1B and 5), and the shortened flexible loop unwinds partially and is involved in dislocating the catalytic loop thus, further shielding the catalytic site.

The class II enzymes can be further subdivided into class IIa and class IIb depending on whether they are capable of hydrolyzing sphingomyelin or not, respectively. In both the class IIa and class IIb SMases D, all the structural elements for metal-ion coordination and catalytic activity are fully conserved, which do not clarify the observed lack of activity of the Class IIb SMases D on sphingomyelin. A detailed structural analysis of a sphere with a radius of 10Å positioned around the active site reveals that all residues important for catalysis are conserved in both sub-classes, except for the dual substitutions at positions 95 (Gly → Asn) and 134 (Pro → Glu), which result in the generation of a hydrophilic environment at the entrance to the active site (Fig. 6) and the presence of a carboxylate group near the active site results in a modification of the local charges maintained mainly by the Mg^{2+} ion. The former region is important in modulating and controlling the approach and also in

Fig. 5. Multiple alignment of SMase I (GenBank Accession No. AY093599 and PDB code: 1XX1), Lb1, and Lb3 SMases D from *Loxosceles bonetti* (Accession Nos. AY559844 and AY559845, respectively) and GDPD from *Thermotoga maritima* (PDB code: 1O1Z). Amino acids involved in metal-ion binding and catalysis are boxed in light gray and cysteines are boxed in yellow. The numbers represent the SMase I sequence. (For interpretation of the references to color in this figure legend, the reader is referred to the web version of this paper.)

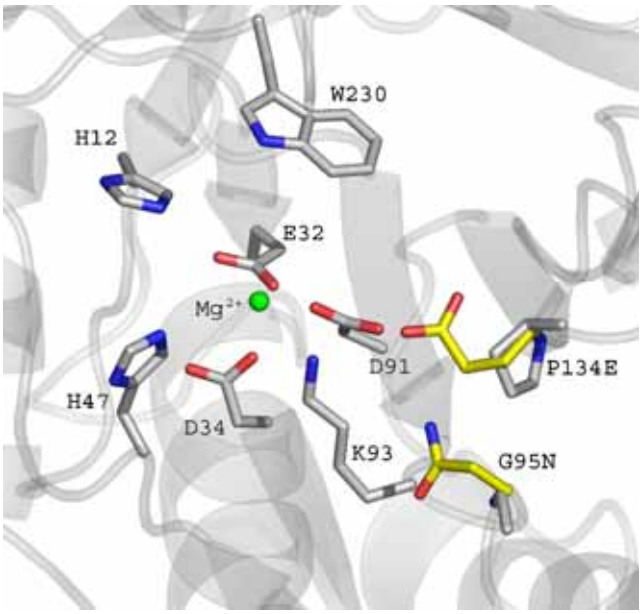

Fig. 6. Amino acid differences at the entrance to the active-site pocket of SMase D Class IIa (carbon atoms in white) and IIb (carbon atoms in yellow). (For interpretation of the references to color in this figure legend, the reader is referred to the web version of this paper.)

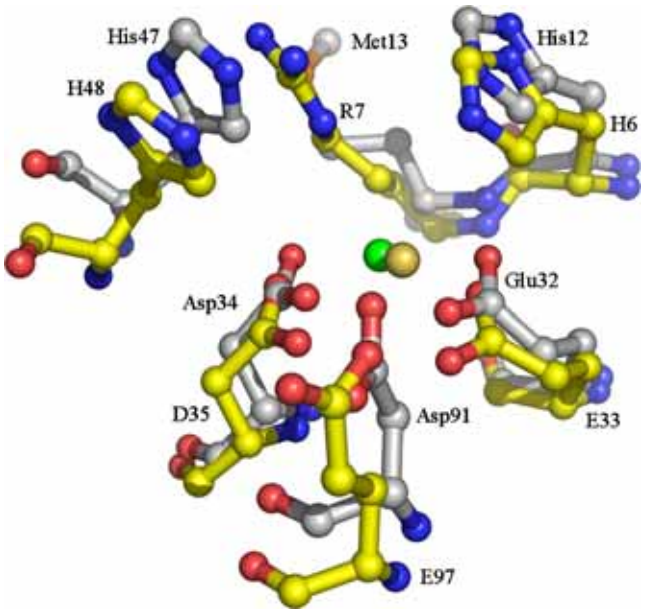

Fig. 7. Amino acid differences in the metal-ion binding and active sites of SMases I (carbon atoms in white; three letter code) and in GDPD from *Escherichia coli* (PDB code:1YDY) (carbon atoms in yellow; one-letter code). Yellow-orange and green spheres represent the Ca^{2+} and Mg^{2+} ions, respectively. (For interpretation of the references to color in this figure legend, the reader is referred to the web version of this paper.)

the stabilization of the substrate hydrocarbon tail during the catalysis event. Thus, the modifications of the local charge and hydrophobicity on the *i*-face, in the vicinity of the entrance to the active site could account for the observed lack of activity upon sphingomyelin by class IIb SMases D.

Common features of the catalytic mechanisms of SMases D and GDPDs

GDPDs encountered in bacteria, higher eukaryotes, and humans are involved in glycerol metabolism and catalyze the reaction of glicerophosphodiester and water to alcohol and *sn*-glycerol-3-phosphate. Structure based sequence alignments indicate that the SMases D and GDPDs are structurally related as pointed out earlier [23] and that the catalytic sites are highly conserved, suggesting that they evolved from a common ancestor and share a similar catalytic mechanism. SMases D are Mg^{2+}-dependent enzymes whereas GDPDs are Ca^{2+}-dependent enzymes due to the substitution of Asp91 by Glu in the latter enzymes (Fig. 7). SMases D bind Mg^{2+} both in the presence and absence of substrate analogues, however, the GDPDs only bind the metal ion simultaneously with the substrate as in the case of the bacterial neutral SMase C [24]. The catalytic mechanism of GDPDs also depend on the acid–base

reactions of two His residues (His6 and His48, based on the numbering of PDB code: 1O1Z) which are assisted by a network of hydrogen bonds in a fashion similar to that observed in the SMases D (Fig. 3C). His47 in the SMase D is hyperpolarized by a short bond to the carbonyl oxygen atom of Gly48, whereas, His48 in GDPD is hyperpolarized by an analogous bond to Asp49 OD1 (Fig. 3C). The proton donor His12 in SMase D is supported by hydrogen bonds to Asp233 and Asn252, whereas His6 in GDPD is hydrogen bonded to Asn195 and Asp213 (Fig. 3C). Additionally, the residues surrounding the catalytic site are conserved between the two enzymes except for the substitution of Met13 by Arg7 which occupies the same relative position (Fig. 7).

Conclusion

SMases D are the principal components responsible for the significant toxicity exhibited by spider venoms of the genus *Loxosceles*. These enzymes belong to the family of phosphodiesterases and serve as structural models to understand lysosomal acid and plasma membrane-bound neutral sphingomyelinases that are encountered in mammalian cells. These two important classes of phosphodiesterases form the principal pathway for sphingomyelin degradation following a reaction analogous to the reaction catalyzed by phospholipases C that yields ceramides and phosphocholine. Whereas SMases D are encountered only in spider venoms and in some bacteria being conspicuously absent in the animal kingdom, the GDPDs are widely distributed in both prokaryotes and eukaryotes and these two functionally different enzymes use the same basic structural and catalytic motifs to hydrolyze different substrates.

Acknowledgments

Financial support by FAPESP, CEPID, SMOLBNet, CNPq, CAPES/PROBAL/DAAD (415-br-probal/ale-03/17635), The Welcome Trust and FUNDUNESP are gratefully acknowledged. M.T.M is the recipient of a FAPESP fellowship.

References

[1] L.A. Van Meeteren, F. Frederiks, B.N. Giepmans, M.F. Pedrosa, S.J. Billington, B.H. Jost, D.V. Tambourgi, W.H. Moolenaar, Spider and bacterial sphingomyelinases D target cellular lysophosphatidic acid receptors by hydrolyzing lysophosphatidylcholine, J. Biol. Chem. 279 (2004) 10833–10836.

[2] A. Gomez-Munoz, Ceramide-1-phosphate: a novel regulator of cell activation, FEBS Lett. 562 (2004) 5–10.

[3] B. Anliker, J. Chun, Lysophospholipid G protein-coupled receptors, J. Biol. Chem. 279 (2004) 20555–20558.

[4] W.H. Moolenaar, L.A. van Meeteren, B.N. Giepmans, The ins and outs of lysophosphatidic acid signaling, BioEssays 26 (2004) 870–881.

[5] J.M. Futrell, Loxoscelism, Am. J. Med. Sci. 304 (1992) 261–267.

[6] M.T. Murakami, M.F. Fernandes-Pedrosa, D.V. Tambourgi, R.K. Arni, Structural basis for metal ion coordination and the catalytic mechanism of sphingomyelinases D, J. Biol. Chem. 280 (2005) 13658–13664.

[7] M.F. Fernandes-Pedrosa, I.L. Junqueira de Azevedo, R.M. Goncalves-de-Andrade, C.W. van den Berg, C.R. Ramos, P.L. Ho, D.V. Tambourgi, Molecular cloning and expression of a functional dermonecrotic and hemolytic factor from *Loxosceles laeta* venom, Biochem. Biophys. Res. Commun. 298 (2002) 638–645.

[8] D.I. Svergun, C. Barbareto, M.H.J. Koch, CRYSOL—a Program to evaluate X-ray solution scattering of biological macromolecules from atomic coordinates, J. Appl. Crystallogr. 28 (1995) 768–773.

[9] Z. Otwinowski, W. Minor, Processing of X-ray diffraction data collection in oscillation mode, Methods Enzymol. 276 (1997) 307–326.

[10] A.A. Vaguine, J. Richelle, S.J. Wodak, SFCHECK: a unified set of procedures for evaluating the quality of macromolecular structure-factor data and their agreement with the atomic model, Acta Crystallogr. D Biol. Crystallogr. 55 (1999) 191–205.

[11] T.O. Yeates, Detecting and overcoming crystal twinning, Methods Enzymol. 276 (1997) 344–358.

[12] J. Navaza, AMoRe: an automated package for molecular replacement, Acta Crystallogr. sect. A 50 (1994) 157–163.

[13] G.N. Murshudov, A.A. Vagin, E.J. Dodson, Refinement of macromolecular structures by the maximum-likelihood method, Acta Crystallogr. Sect. D 53 (1997) 240–255.

[14] T.A. Jones, Interactive computer graphics: FRODO, Methods Enzymol. 115 (1985) 157–171.

[15] P. Emsley, K. Cowtan, Coot: model-building tools for molecular graphics, Acta Crystallogr. Sect. D 60 (2004) 2126–2132.

[16] A. Perrakis, R. Morris, V.S. Lamzin, Automated protein model building combined with iterative structure refinement, Nat. Struct. Biol. 6 (1999) 458–463.

[17] R.A. Laskowski, M.W. MacArthur, D.S. Moss, J.M. Thornton, PROCHECK: a program to check the stereochemical quality of protein structures, J. Appl. Crystallogr. 26 (1993) 283–291.

[18] A. Sali, T.L. Blundell, Comparative protein modelling by satisfaction of spatial restraints, J. Mol. Biol. 234 (1993) 779–815.

[19] A. Fiser, R.K. Do, A. Sali, Modeling of loops in protein structures, Protein Sci. 9 (2000) 1753–1773.

[20] G.N. Ramachandran, C. Ramakrishnan, V. Sasisekharan, Stereochemistry of polypeptide chain configurations, J. Mol. Biol. 7 (1963) 95–99.

[21] G. Newlands, C. Isaacson, C. Martindale, Loxoscelism in the Transvaal. South Africa, Trans. R. Soc. Trop. Med. Hyg. 76 (1982) 610–615.

[22] D.V. Tambourgi, M. Fernandes-Pedrosa, C.W. Van den Berg, R.M. Goncalves-de-Andrade, M. Ferracini, D. Paixao-Calvacante, B.P. Morgan, N.K. Rushmere, Molecular cloning, expression, function and immunoreactivities of members of a gene family of sphingomyelinases from *Loxosceles* venom glands, Mol. Immunol. 41 (2004) 831–840.

[23] M.H. Cordes, G.J. Binford, Lateral gene transfer of a dermonecrotic toxin between spiders and bacteria, Bioinformatics 22 (2005) 264–268.

[24] A.E. Openshaw, P.R. Race, H.J. Monzo, J.A. Vazquez-Boland, M.J. Banfield, Crystal structure of SmcL, a bacterial neutral sphingomyelinase C from Listeria, J. Biol. Chem. 280 (2005) 35011–35017.

ELSEVIER

Toxicon 47 (2006) 380–386

TOXICON

www.elsevier.com/locate/toxicon

Kinetic and mechanistic characterization of the Sphingomyelinases D from *Loxosceles intermedia* spider venom

Sonia A. de Andrade [a], Mario T. Murakami [b], Danielle P. Cavalcante [a], Raghuvir K. Arni [b], Denise V. Tambourgi [a,*]

[a] *Laboratório de Imunoquímica, Instituto Butantan, Av. Prof. Vital Brazil, 1500, CEP 05508-900, São Paulo, SP 05503-900, Brazil*
[b] *Departmento de Física, IBILCE/UNESP, São José do Rio Preto, SP 15054-000, Brazil*

Received 22 August 2005; revised 28 November 2005; accepted 6 December 2005
Available online 2 February 2006

Abstract

Envenomation by arachnids of the genus *Loxosceles* leads to local dermonecrosis and serious systemic toxicity mainly induced by sphingomyelinases D (SMase D). These enzymes catalyze the hydrolysis of sphingomyelin resulting in the formation of ceramide–phosphate and choline as well as the cleavage of lysophosphatidyl choline generating the lipid mediator lysophosphatidic acid. We have, previously, cloned and expressed two functional SMase D isoforms, named P1 and P2, from *Loxosceles intermedia* venom and comparative protein sequence analysis revealed that they are highly homologous to SMase I from *Loxosceles laeta* which folds to form an $(\alpha/\beta)_8$ barrel. In order to further characterize these proteins, pH dependence kinetic experiments and chemical modification of the two active SMases D isoforms were performed. We show here that the amino acids involved in catalysis and in the metal ion binding sites are strictly conserved in the SMase D isoforms from *L. intermedia*. However, the kinetic studies indicate that SMase P1 hydrolyzes sphingomyelin less efficiently than P2, which can be attributed to a substitution at position 203 (Pro–Leu) and local amino acid substitutions in the hydrophobic channel that could probably play a role in the substrate recognition and binding.

Keywords: *Loxosceles* venoms; Sphingomyelinase D; Sphingomyelin; Kinetic parameters; Structure

1. Introduction

Envenomation by spiders belonging to the genus *Loxosceles* commonly results in impressive local necrotic skin lesions and more rarely causes systemic effects, including profound intravascular hemolysis (Barreto et al., 1985; Schenone et al., 1989, Ginsburg and Weinberg, 1988; Sezerino et al., 1998; Gendron, 1990; Futrell, 1992; White et al., 1995; Bey et al., 1997). The predominant clinical sign is a cutaneous reaction characterized by the appearance of necrosis around the wound, resulting in ulceration. Mild systemic effects induced by envenomation, such as fever, malaise, pruritus and exanthema are common, while intravascular haemolyses and coagulation, sometimes accompanied by thrombocytopenia and renal failure, occur in approximately 16% of the victims (Barreto et al., 1985; Schenone et al., 1989; Ginsburg and Weinberg, 1988; Sezerino et al., 1998; Gendron, 1990; Futrell, 1992; White et al., 1995; Bey et al., 1997).

We have recently purified, characterized, cloned and expressed the toxins from *Loxosceles intermedia* venom that are responsible for all the local and systemic effects induced by whole venom (Tambourgi et al., 1995, 1998, 2004). Two highly homologous proteins, termed P1 and P2, with Mr 35 kDa, endowed with sphingomyelinase activity, were both

* Corresponding author. Tel.: +55 11 3726 7222x2231; fax: +55 11 3726 1505.
E-mail address: dvtambourgi@butantan.gov.br (D.V. Tambourgi).

0041-0101/$ - see front matter © 2005 Elsevier Ltd. All rights reserved.
doi:10.1016/j.toxicon.2005.12.005

able to induce dermonecrosis in rabbits, and rendered human erythrocytes susceptible to lysis by complement (C) (Tambourgi et al., 1998, 2000).

Comparative analysis of the P1 and P2 translated protein sequences reveals approximately 85% identity at the level of amino acid and DNA sequence (Tambourgi et al., 2004). Additional comparative analysis between *L. intermedia* P1 and P2 proteins with the SMase I from *Loxosceles laeta* spider venom (Accession number: AY093599; Fernandes Pedrosa et al., 2002), 'sphingomyelinase like proteins H13 and H10' (Accession numbers: AY093600 and AY093601; Fernandes Pedrosa et al., 2002), 'sphingomyelinase D dermonecrotic enzyme precursor' from *Loxosceles arizonica* (Accession number: AF512953; unpublished) and SMase D isoforms from *Loxosceles reclusa* (referred to as Lr1 and Lr2) and *Loxosceles bonetti* venoms (referred to as Lb1 and Lb3; Acession numbers: AAT66075 and AAT66074, respectively; Ramos-Cerrillo et al., 2004) revealed percentages of identity at the amino acid level of 40–85% between and within species.

Spider SMases D catalyze the hydrolysis of sphingomyelin (the major constituent in the outer leaflet of the lipid bilayer of plasma membranes) to yield choline and ceramide 1-phosphate (*N*-acylsphingosine 1-phosphate) (Forrester et al., 1978; Kurpiewski et al., 1981) while mammalian sphingomyelinases converts sphingomyelin (SM) in phosphocholine and ceramide. Previous studies also demonstrated that *Loxosceles* SMase D has an intrinsic lysophospholipase D activity toward lysophosphatidyl choline (LPC). LPC hydrolysis yields the lipid mediator lysophosphatidic acid (LPA), a known inducer of platelet aggregation, endothelial hyperpermeability and proinflammatory responses (van Meeteren et al., 2004).

The crystal structure of a member of the sphingomyelinase D family from *L. laeta* (SMase I: accession number AY093599) has been solved recently and this protein shown to belong to the $(\alpha/\beta)_8$ barrel class of enzymes (Murakami et al., 2005). Structural results indicate that interfacial catalysis is mediated by metal ion binding and that two histidine residues are involved in the stabilization and hydrolysis of sphingomyelin and lysophosphatidyl choline via an acid–base catalytic mechanism.

In the present study, we report the substrate specificity, the kinetic parameters of sphingomyelin hydrolysis and the involvement of histidines residues in the catalytic function of active SMases D isoforms from *L. intermedia* spider venom.

2. Material and methods

2.1. Chemicals, reagents and buffers

Bovine sphingomyelin, bovine phosphatidylcholine, choline oxidase, horseradish peroxidase, 3-(4-hydroxyphenyl propionic acid) were purchased from Sigma (St Louis, MO, USA). Diethylpyrocarbonate (DEPC) was from Aldrich (St Louis, MO, USA). The BCA kit was from Pierce (Rockford, IL, USA). Buffers were: PBS (phosphate buffered-saline) pH 7.2, 10 mM Na Phosphate, 150 mM NaCl; HBS (HEPES buffered saline) pH 7.4, 140 mM NaCl, 5 mM KCl, 1 mM $CaCl_2$, 1 mM $MgCl_2$, 10 mM Hepes; TBS (Tris-buffered saline) pH 7.4, 20 mM Tris, 0.15 M NaCl.

2.2. Recombinant protein expression and purification

Recombinant proteins were produced as described previously (Tambourgi et al., 2004). In brief: pRSETB-*L. intermedia* P1 or P2 cDNAs transformed *Escherichia coli* BL21 (DE3) (Invitrogen, Carlsbad, California, USA) cells were inoculated in 50 mL of 2YT/amp and grown overnight at 37 °C and induced with IPTG. Recombinant proteins (rP1 and rP2) were harvested from the pellet by French pressure and purified on a Ni (II) Chelating Sepharose Fast Flow column (Pharmacia, Sweden, 1.0×6.4 cm). The fractions containing rP1 or rP2 were pooled and concentrated using Centricon-10 (10,000-mw cutoff; Amicon, Inc., Beverly, MA, USA) and rechromatographed on a Superose 12 HR column (HR 10/30, Pharmacia), equilibrated and eluted with TBS at flow rate of 0.4 mL/min. The protein content of the samples was evaluated by the BCA protein kit assay, following the manufacturer's protocol (Pierce, Rockford, USA).

2.3. Sphingomyelinase activity

The SMase enzymatic activity was estimated by determining choline liberated from lipid substrates, using a modified fluorimetric assay (Tokumura et al., 2002). In the standard assay, the lipids were diluted in HEPES-buffered saline (HBS; 140 mM NaCl, 5 mM KCl, 1 mM $CaCl_2$, 1 mM $MgCl_2$, 10 mM Hepes, pH 7.4). SM and PC substrates (50 μM) were applied as liposomes. After SMase D addition, the reaction was developed for 20 min at 37 °C. After incubation, a mixture composed by 1 unit/mL choline oxidase, 0.06-unit/mL of horseradish peroxidase and 50-μM of 3-(4-hydroxy-phenyl) propionic acid in HBS was added and incubated for 10 min. The choline liberated was oxidised to betaine and H_2O_2 and this product determined by fluorimetry at em = 405 nm and ex = 320 nm, using a Perkin–Elmer Spectrofluorimeter. Calculations of K_m and k_{cat} were performed using the Michaelis–Menten equation with GraFit Data Analysis Software.

2.4. pH dependence of the recombinant SMases D

The pH-dependence of the sphingomyelinase activity of rP1 and rP2 was determined at 37 °C over a range of pH from 4.5 to 9.5 (in 20 mM citrate buffer for pH 4.5–5.0; in 20 mM phosphate buffer for pH 5.5–7.5 and in Tris buffer for pH 8.0–9.0). The pH dependent ionizations were determined by a fit of the steady-state parameters according

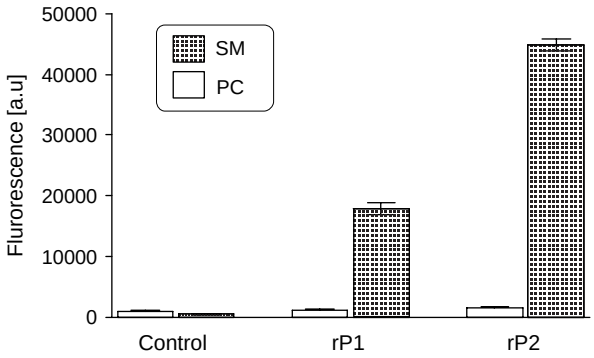

Fig. 1. Choline release from phospholipids induced by recombinant SMase D isoforms from *Loxosceles intermedia*. Choline release was determined fluorimetrically in HEPES-buffered saline, pH 7.4 at 37 °C (see Section 2). SMases rP1 and rP2 were used at 16 nM. 'Control' denotes no enzyme addition. Hydrolysis was determined using 50 μM of PC or SM as multilamellar vesicles (liposomes). Data points are the mean of two independent experiments each performed in triplicate. Error bars represent SD values.

to Eq. (1), where v is the observed rate of the reactions, C is the pH-independent rate, $[H]$ is the concentration of hydrogen ions, and K_a and K_b reflect the ionization constants of the acid and base species, respectively.

$$v = C/(1 + [H]/K_a + K_b/[H]) \quad (1)$$

2.5. Treatment of rP1 and rP2 with diethylpyrocarbonate (DEPC)

In order to inactivate the sphingomyelinase activity, rP1 and rP2 (16 nM) were incubated with increasing concentrations of DEPC in 50 mM sodium phosphate (20–100 μM from a DEPC stock solution diluted in 3% ethanol) at pH 7.4 and room temperature. DEPC was quenched from the samples by using imidazole (250 μM). Control mixtures contained an equivalent amount of ethanol; the amount of ethanol added was less than 3% of the total volume and did not significantly affect the enzymatic activity of rP1 and rP2. The time course of inactivation was determined by monitoring the enzymatic activity retained after determined time interval. Alternatively, rP1 and rP2 (16 nM) were incubated with DEPC (100 μM) in the presence of increasing concentrations of PC and SM (0–2.5 μM) for 20 min at 37 °C. DEPC was quenched and the samples were additionally incubated with SM (50 μM) for 10 min at 37 °C, and the remained sphingomyelinase activity estimated by the fluorimetric method of Tokumura et al. (2002).

2.6. Sequence alignment and structure analysis

Sequences were aligned using Clustal program (Thompson et al., 1994). The rP1 and rP2 structural models were obtained using the webbased utility SWISSMODEL (http://www.expasy.ch/swissmod/SWISS-MODEL.html) and the structure of SMase I from *L. laeta* (PBD 1XX1) as template. The models were selected based on the overall stereochemical quality and subjected to relaxation and energy minimization of the structures using GROMACS molecular dynamics (Lindahl et al., 2001).

3. Results and discussion

3.1. Sphingomyelinase activity

The recombinant sphingomyelinases P1 and P2 were purified from the soluble fraction of cell lysates by Ni^{2+} chelating chromatography and eluted from the resin in an extraction buffer containing 0.8 M imidazole as the initial purification step. The enzymes were further purified by gel filtration and eluted using a Tris buffer pH 7.4, NaCl 0.15 M.

As shown in Fig. 1, the purified recombinant proteins P1 and P2 catalyze choline release from SM, but not from PC. The recombinant SMases P1 and P2 were assayed at various substrate concentrations to determine the kinetic parameters k_{cat} and K_m. As presented in Table 1, the K_m value determined for rP1 are 1.76 times higher than rP2 and the k_{cat} was two times lower than rP2, thus demonstrating that rP2 hydrolyzes sphingomyelin with higher catalytic efficiency than rP1.

Table 1
Comparison of kinetic parameters for rP1 and rP2 sphingomyelinases from *Loxosceles intermedia*

SMases	Sphingomyelin		
	k_{cat} (min^{-1})	K_m (μM)	K_{cat}/K_m (min^{-1} μM^{-1})
rP1	3.50	113 ± 0.03	30097.4
rP2	7.10	64 ± 3.0	110937.8

Rates of choline release from SM are plotted against increasing concentration of the substrate. Data were fitted to the Michaelis–Menten equation, yielding the indicated apparent K_m values. Data points are the mean of two independent experiments each performed in triplicate. Error bars represent SD values.

```
                1                   50                  100
L.laeta SMase I  ADNRRPIWNLAHMVNAVAQIPDFLDLGANALEADVTFKG-SVPTYTYHGTPCDFGRDCIRWEYFNVFLKTLREYTTPGNAKVRDGFILFVLDLKTGSLSND
L.intermedia P1  AGNRRPIWIMGHMVNAIGQIDEFVNLGANSIETDVSFDDNANPEYTYHGIPCDCGRNCKKYENFNDFLKGLRSATTPGNSKYQEKLVLVVFDLKTGSLYDN
L.intermedia P2  ADKRRPIWIMGHMVNAIAQIDEFVNLGANSIETDVSFDDNANPEYTYHGIPCDCGRSCLKWENFNDFLKGLRSATTPGNAKYQAKLILVVFDLKTGSLYDN

                101                 150                 200
L.laeta SMase I  QVRPAGENVAKELLQNYWNNGNNGGRAYVVLSLPDIGHYEFVRGFKEVLKKEGHEDLLEKVGYDFSGPYLPSLPTLDATHEAYKKAGVDGHIWLSDGLTN
L.intermedia P1  QANDAGKKLAKNLLQHYWNNGNNGGRAYIVLSIPDLNHYPLIKGFKDQLTKDGHPELMEKVGHHDFSG-----NDDIGDVGKAYKKAGITGHIWQSDGITN
L.intermedia P2  QANEAGKKLAKNLLKHYWNNGNNGGRAYIVLSIPDLNHYPLIKGFKDQLTQDGHPELMDKVGHHDFSG-----NDAIGDVGNAYKKAGISGHVWQSDGITN

                201                 250                 284
L.laeta SMase I  FSPLGDMARLKEAIKSRDSANGFINKIYYWSVDKVSTTKAALDVGVDGIMTNYPNVLIGVLKESGYNDKYRLATYDDNPWETFKN
L.intermedia P1  CLPRG-LSRVNAAVANRDSANGFINKVYYWTVDKRSTTRDALDAGVDGIMTNYPDVITDVLNEAAYKKKFRVATYDDNPWVTFKK
L.intermedia P2  CLLRG-LDRVKQATANRDSANGFINKVYYWTVDKRATTRDALDAGVDGVMTNYPDVITDVLNESAYKNKFRVASYEDNPWETFKK
```

Fig. 2. Alignment of the complete deduced aminoacid sequences of *Loxosceles* SMases D. The N-terminal amino acid position of the mature toxins P1 and P2 from *L. intermedia* and SMase I from *Loxosceles laeta* (Accession numbers: AY304471, AY304472 and AY093599, respectively), is located at position +1. Histidine and cysteine residues are indicated in gray and underlined, respectively.

3.2. Alignment and prediction of SMase structure

The primary sequence comparison indicates that residues involved in the SMase I catalysis mechanism are completely conserved in *L. intermedia* SMase isoforms (Fig. 2). Previous studies of the secondary structure of the *Loxosceles* SMases D suggest that under physiological conditions the secondary structure elements of rP1, rP2 and SMase I measured by circular dichroism are very similar (Andrade et al., 2005) and agree fairly well with the tertiary structure of SMase I, recently solved by X-crystallography (Murakami et al., 2005). Given the high degree of sequence identity and secondary structure, rP1 and rP2 could adopt a tertiary structure similar to that of SMase I and, therefore, the structures of the rP1 and rP2 were modeled using the SMase I structure as template. Stereochemical parameters of the modeled structure were at or higher than 95% confidence level and no residues were found in the disallowed regions of the Ramachandran plot.

As shown in Fig. 3, rP1 and rP2 also display the $(\alpha/\beta)_8$ barrel fold as described for SMase I (Murakami et al., 2005) with the active site formed by two histidines and the amino acid residues involved in the metal ion coordination and several connecting loops, which support a part of the active site and form the entrance to the catalytic pocket. The major loops are the catalytic loop (which contains the catalytic residue His_{47}-numbering from SMase I), and the flexible loop. However, in this region, rP1 and rP2 have an additional disulfide bridge formed between the tip of catalytic loop and the flexible loop. In the first model the residues Cys_{53} and Cys_{201} (numbering from SMase I), were initially 15 Å apart from each other. After energy minimization and molecular dynamics calculations, the flexible loop region containing Cys_{53} and Cys_{201} was conformationally modified to allow the disulfide bond formation in the catalytic loop at 2.03 Å of the distance in our final model.

The superpositioning of the predicted structures of rP1 and rP2 result in 265 topologically equivalent Cα positions with root mean square (rms) deviation of 0.27 Å, which indicates high structural identity. The major deviations are observed in the flexible loop, which contains a substitution of Pro (rP1) by Leu (rP2) at position 203. The rigidity induced by the presence of an additional disulphide bridge at tip of the loop and the presence of a proline residue at position 203 reduces the accessibility to the active site and could destabilize the enzyme–substrate complex, which could be account for our kinetic results. Additionally, in rP1, the substitution Leu→Lys and Trp→Tyr at positions 58 and 60 reduces the hydrophobicity in the channel composed by Tyr_{44}, Tyr_{46}, Leu_{58} and Trp_{60} (numbering from SMase I). Thus, minor structural modifications, such as substitutions on the surface loops, can affect the hydrolytic activity upon sphingomyelin, suggesting that besides of the active site, these SMases have other structural regions that participate in the recognition, binding and hydrolysis of the substrate.

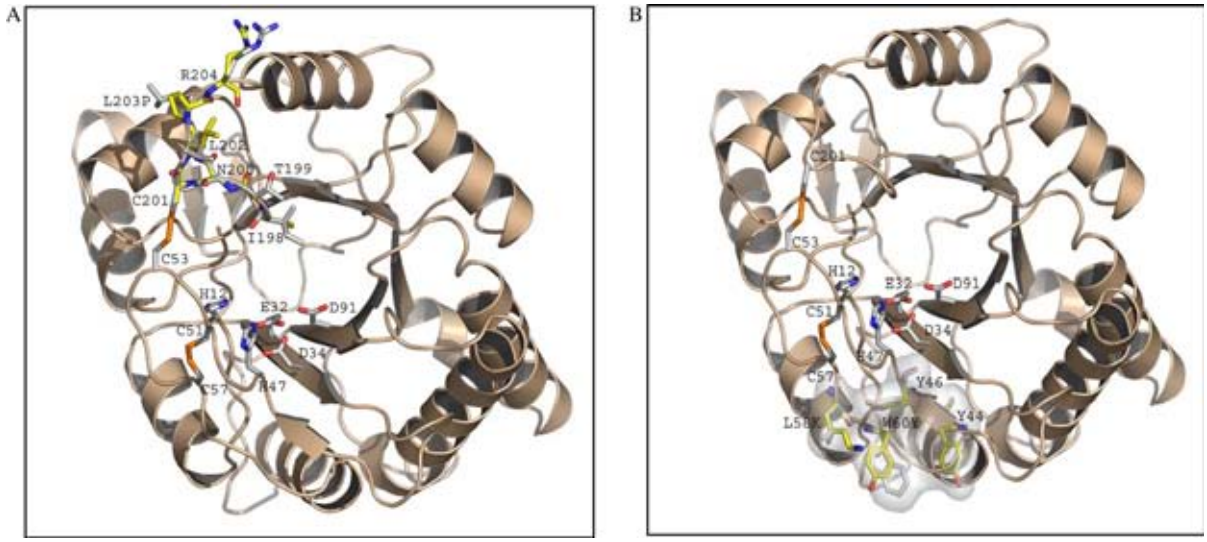

Fig. 3. Stereo-ribbon representation of the overlapped structures of *L. intermedia* active SMase D isoforms, P1 and P2, viewed along the axis of the $(\alpha/\beta)_8$ barrel. The super positioning of the predicted structures of rP1 and rP2 indicates high structural identity. (A) The functionally important His_{12}, Glu_{32}, Asp_{34}, His_{47} and Asp_{91} are included. The major deviations are observed in the flexible loop, which contains a substitution of Pro (rP1) by Leu (rP2) at position 203. (B) Additionally, in rP1, the substitution Leu → Lys and Trp → Tyr at positions 58 and 60 reduces the hydrophobicity in the channel (gray area) composed by Tyr_{44}, Tyr_{46}, Leu_{58} and Trp_{60}.

The parameters of the sphingomyelin hydrolysis by rP1 and rP2 and the assessment of the role of histidine residues in the substrate binding and catalysis were studied by chemical modification and pH dependence to validate the predictions made from the structural homology.

3.3. Effects of pH on kinetic parameters of sphingomyelin hydrolysis by rP1 and rP2

An acid–base mechanism dependent of Mg^{2+} ion has been proposed for the SMase I from *L. laeta* (Murakami et al., 2005). The SMase I mechanism involves two histidines, His_{12} and His_{47}, where His_{12} functions as the nucleophile that initiates the attack on the scissile phosphodiester bond of the sphingomyelin substrate and the His_{47} acts as proton donor destabilizating a shortlived penta-coordinated covalent intermediate to produce choline.

To understand the role of these residues in the interaction of *L. intermedia* SMases rP1 and rP2 to the substrate (SM), the kinetic pH dependent analysis was performed at 37 °C using the substrate at a concentration equivalent to twice the K_m value of the toxins. Based on the acidic limb of the profiles, pK_1 of 6.2 ± 1.2 and 5.8 ± 0.5 to rP1 and rP2 were determined and the basic limb of the profiles shows an ionization pK_2 of 9.5 ± 1.0 and 9.6 ± 0.7. These results indicate that the pK values where the enzymes are inactive are similar to the ionization values for histidine groups (Table 2), which agrees with the catalytic mechanism proposed previously for SMase I (Murakami et al., 2005).

3.4. Chemical modification of the histidines

The kinetic pH dependence of the sphingomyelinases rP1 and rP2 indicates the involvement of histidines residues in their catalytic function. To confirm the functional significance of the histidine(s) for rP1 and rP2, the specific modification of these residues by Diethylpyrocarbonate (DEPC) was accomplished. As shown in Fig. 4(A) and (B) the enzymes were fully inhibited by DEPC at concentrations ranging from 20 to 100 μM. These results indicate that chemical modification of the accessible reactive histidine residues may alter the conformation of both proteins or blocked substrate access to the active site and, thereby, affecting SM hydrolysis.

Since the constant rate of inactivation with DEPC is similar for both rP1 and rP2, it can be suggested that the same histidines are involved in sphingomyelin hydrolysis. However, as both recombinant proteins contain seven

Table 2
pH dependent ionizations of rP1 and rP2 enzymes

Parameter	Measured value	rP1	rP2
V_{max}	pK_1	6.2 ± 1.2	5.8 ± 0.5
	pK_2	9.5 ± 1.0	9.6 ± 0.7

The sphingomyelinasic activities of rP1 and rP2 were determined at 37 °C, using the substrate at a concentration equivalent to twice the K_m value of the toxins, over a range of pH from 4.5 to 9.5 (in 20 mM citrate buffer for pH 4.5–5.0; in 20 mM phosphate buffer for pH 5.5–7.5 and in Tris buffer for pH 8.0–9.0). Data points are the mean of two independent experiments each performed in triplicate.

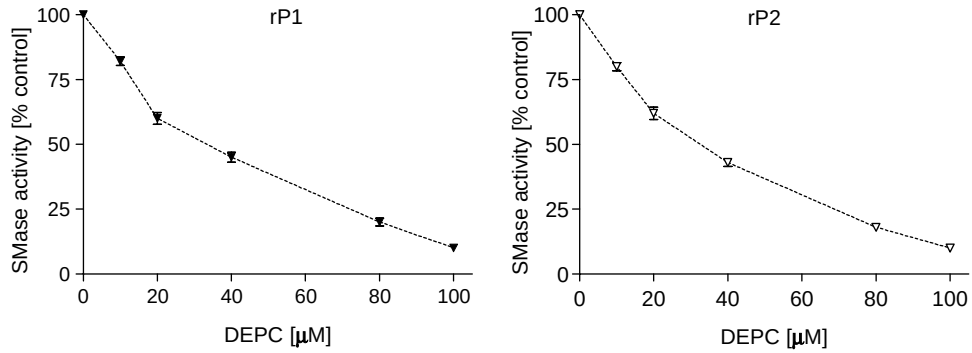

Fig. 4. Effect of chemical modification of histidine on the enzyme activity. SMase D isoforms rP1 and rP2 (16 nM) were preincubated with increased concentrations of DEPC for 20 min at 37 °C and the remaining sphingomyelinase activity was determined fluorimetrically using SM as substrate. Control tubes were prepared in the absence of DEPC or enzyme. Data points are the mean of two independent experiments each performed in triplicate. Error bars represent SD values.

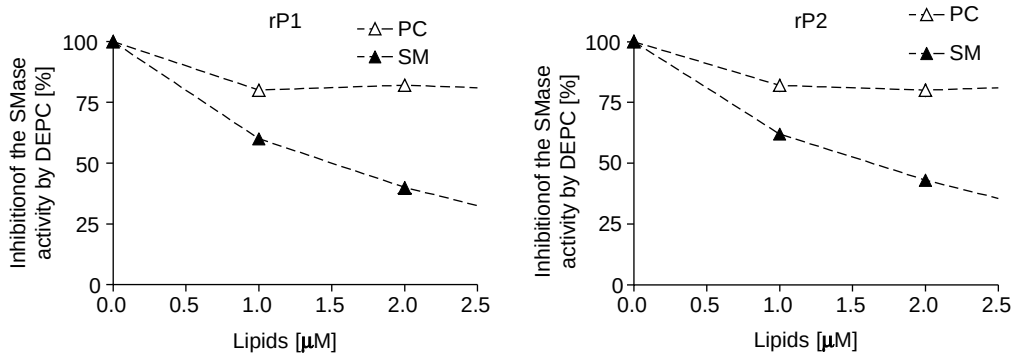

Fig. 5. Substrate protection against the inactivation by DEPC treatment. SMase D isoforms rP1 and rP2 (16 nM) were incubated with DEPC (100 μM) in the presence of increasing concentrations of SM or PC, for 20 min at 37 °C. After this period, SM (50 μM) was added and the remaining sphingomyelinase activity was determined fluorimetrically. Control tubes were prepared in the absence of DEPC or enzyme. Data points are the mean of two independent experiments each performed in triplicate. Error bars represent SD values.

histidine residues, it is also possible that the reactive histidines are not the histidines present in the active site and that they might be necessary for stability. To confirm that essential catalytic histidine residues are within the active site of rP1 and rP2, both proteins were preincubated with DEPC in the presence of increasing concentrations of SM and PC (Fig. 5). In the presence of SM substrate, protection of the enzyme against DEPC inactivation was observed, but under the same condition, no protection was obtained with PC, which is not a substrate for this enzyme as demonstrated in this work.

These results demonstrate that the essential DEPC-sensitive histidine residues are present in the active site. Our structural studies indicate that at least two histidines (His_{12} and His_{47}) are close to the active site(s) and the kinetic pH dependence studies demonstrate that the p*K* values, where the enzymes lose their activity, are similar to the ionization values for histidine groups. These results suggest that these histidine residues are essential for rP1 and rP2 sphingomyelinase activity. The importance of histidine residues was also, recently, demonstrated by Lee and Lynch (2005) through site-directed mutagenesis of a *L. reclusa* recombinant SMase D isoform.

In conclusion, we show here that the amino acids involved in the catalysis and in the metal ion binding sites are strictly conserved in the SMase D isoforms from *L. intermedia* and that SMase P1 hydrolyzes sphingomyelin less efficiently than P2, which can be attributed to a substitution at position 203 (Pro–Leu) and local amino acid substitutions in the hydrophobic channel which could probably play a role in the substrate recognition and binding.

Acknowledgements

This work was supported by FAPESP, CNPq and CAT/CEPID/Butantan.

References

Andrade, S.A., Fernandes Pedrosa, M.F., Gonçalves de Andrade, R.M., Vilela Oliva, M.L., van den Berg, C.W., Tambourgi, D.V., 2005. Conformational changes of *Loxosceles* venom sphingomyelinases monitored by circular dichroism. Biochem. Biophys. Res. Commun. 327, 117–123.

Barreto, C.O., Cardoso, J.L., de Cillo, D., 1985. Viscerocutaneous form of loxocelism and erythrocyte glucose-6-phosphate deficiency. Rev. Inst. Med. Trop. São Paulo 27, 264–267.

Bey, T.A., Walter, F.G., Lober, W., Schmidt, J., Spark, R., Schlievert, P.M., 1997. *Loxosceles arizonica* bite associated with shock. Ann. Emerg. Med. 30, 701–703.

Fernandes Pedrosa, M.F., Junqueira de Azevedo, I.L.M., Gonçalves-de-Andrade, R.M., van den Berg, C.W., Ramos, C.R.R., Ho, P.L., Tambourgi, D.V., 2002. Molecular cloning and expression of a functional dermonecrotic and haemolytic factor from *Loxosceles laeta* venom. Biochem. Biophys. Res. Commun. 298, 638–645.

Forrester, L.J., Barrett, J.T., Campbell, B.J., 1978. Red blood cell lysis induced by the venom of the brown recluse spider: the role of sphingomyelinase D. Arch. Biochem. Biophys. 187, 355–365.

Futrell, J.M., 1992. Loxoscelism. Am. J. Med. Sci. 304, 261–267.

Gendron, B.P., 1990. *Loxosceles reclusa* envenomation. Am. J. Emerg. Med. 8, 51–54.

Ginsburg, C.M., Weinberg, A.G., 1988. Hemolytic anemia and multiorgan failure associated with localized cutaneous lesion. J. Pediatr. 12, 496–499.

Kurpiewski, G., Forrester, L.J., Barrett, J.T., Campbell, B.J., 1981. Platelet aggregation and sphingomyelinase D activity of a purified toxin from the venom of *Loxosceles reclusa*. Biochem. Biophys. Acta 678, 467–476.

Lee, S., Lynch, K.R., 2005. Brown recluse spider (*Loxosceles reclusa*) venom phospholipase D (PLD) generates lysophosphatidic acid (LPA), 2005. Biochem. J. 391, 317–323.

Lindahl, E., Hess, B., van der Spoel, D., 2001. GROMACS 3.0: a package for molecular simulation and trajectoty analysis. J. Mol. Model. 7, 306–317.

Murakami, M.T., Fernandes-Pedrosa, M.F., Tambourgi, D.V., Arni, R.K., 2005. Structural basis for metal ion coordination and the catalytic mechanism of sphingomyelinases D. J. Biol. Chem. 280, 13658–13664.

Ramos-Cerrillo, B., Olvera, A., Odella, G.V., Zamudio, F., Paniagua-Solísb, J., Alagón, A., Stock, R.P., 2004. Genetic and enzymatic characterization of sphingomyelinase D isoforms from the North American fiddleback spiders *Loxosceles boneti* and *Loxosceles reclusa*. Toxicon 44, 507–514.

Schenone, H., Saavedra, T., Rojas, A., Villarroel, F., 1989. Loxoscelism in Chile, epidemiologic, clinical and experimental studies. Rev. Inst. Med. Trop. São Paulo 31, 403–415.

Sezerino, U.M., Zannin, M., Coelho, L.K., 1998. A clinical and epidemiological study of *Loxosceles* spider envenoming in Santa Catarina, Brazil. Trans. R. Soc. Trop. Med. Hyg. 92, 546–548.

Tambourgi, D.V., Magnoli, F.C., Von Eickstedt, V.R., Benedetti, Z.C., Petricevich, V.L., Silva, W.D., 1995. Incorporation of a 35-kilodalton purified protein from *Loxosceles intermedia* spider venom transforms human erythrocytes into activators of autologous complement alternative pathway. J. Immunol. 155, 4459–4466.

Tambourgi, D.V., Magnoli, F.C., van den Berg, C.W., Morgan, B.P., Araújo, P.S., Alves, E.W., Dias da Silva, W., 1998. Sphingomyelinases in the venom of the spider *Loxosceles intermedia* are responsible for both dermonecrosis and complement-dependent hemolysis. Biochem. Biophys. Res. Commun. 251, 366–373.

Tambourgi, D.V., Paul Morgan, B., de Andrade, R.M.G., Magnoli, F.C., van den Berg, C.W., 2000. *Loxosceles intermedia* spider envenomation induces activation of an endogenous metalloproteinase, resulting in cleavage of glycophorins from the erythrocyte surface and facilitating complement-mediated lysis. Blood 95, 683–691.

Tambourgi, D.V., Fernandes Pedrosa, M.F., van den Berg, C.W., Gonçalves-de-Andrade, R.M., Ferracini, M., Paixão-Cavalcante, D., Morgan, B.P., Rushmere, N.K., 2004. Molecular cloning, expression, function and immunoreactivities of members of a gene family of sphingomyelinases from *Loxosceles* venom glands. Mol. Immunol. 41, 831–840.

Thompson, J.D., Higgins, D.G., Gibson, T.J., 1994. CLUSTAL W: improving the sensitivity of progressive multiple sequence alignment through sequence weighting, positions-specific gap penalties and weight matrix choice. Nucleic Acids Res. 22, 4673–4680.

Tokumura, A., Majima, E., Kariya, Y., Tominaga, K., Kogure, K., Yasuda, K., Fukuzawa, K., 2002. Identification of human plasma lysophospholipase D, a lysophosphatidic acid-producing enzyme, as autotaxin, a multifunctional phosphodiesterase K. J. Biol. Chem. 277, 39436–39442.

van Meeteren, L.A., Frederiks, F., Giepmans, B.N., Fernandes Pedrosa, M.F., Billington, S.J., Jost, B.H., Tambourgi, D.V., Moolenaar, W.H., 2004. Spider and bacterial sphingomyelinases D target cellular LPA receptors by hydrolyzing lysophosphatidylcholine. J. Biol. Chem. 279, 10833–10836.

White, J., Cardoso, J.L., Fan, H.W., 1995. Clinical toxinology of spider bites. In: Meier, J., White, J. (Eds.), Handbook of Clinical Toxinology of Animal Venoms and Poisons. CRC Press, Boca Raton, FL, pp. 259–330.

ii. Fosfolipases A_2

As fosfolipases A_2 (PLA_2s) ainda representam um paradigma para os toxinologistas, apesar da vasta caracterização bioquímica e estrutural, devido a sua gama de propriedades farmacológicas contidas no mesmo motivo estrutural. Recentemente, estudos demonstraram que as Lys49 PLA_2s são potentes supressores do fator de crescimento do endotélio vascular e seu receptor KDR (kinase domain-containing receptor), um sistema chave na regulação e formação de vasos sanguíneos (Yamazaki et al., 2005) (Figura 7).

O alvo desse projeto foi delinear os determinantes estruturais da atividade miotóxica de Lys49 PLA_2s através de estudos bioquímicos *in vitro* e *in vivo* e resolução de estruturas tridimensionais de complexos de Lys49 PLA_2s com substâncias polianiônicas como suramina, derivados de heparina e extratos de plantas, as quais são efetivas na inibição da atividade miotóxica. Esse projeto envolveu a atuação de diversos colaboradores como Prof. Dr. Christian Betzel (*University of Hamburg / European Molecular Biology Laboratory*, Alemanha) e o Prof. Dr. Paulo A. Melo (Universidade Federal do Rio de Janeiro). Os resultados provenientes desses estudos estão detalhados em um artigo de revisão e outros manuscritos tratando de diversos aspectos da multi-funcionalidade dessas proteínas.

Como resultado final desse trabalho, foi caracterizada uma potente molécula anti-dermonecrótica que tem aplicação como tratamento complementar ou alternativo para acidentes ofídicos com serpentes do gênero *Bothrops*.

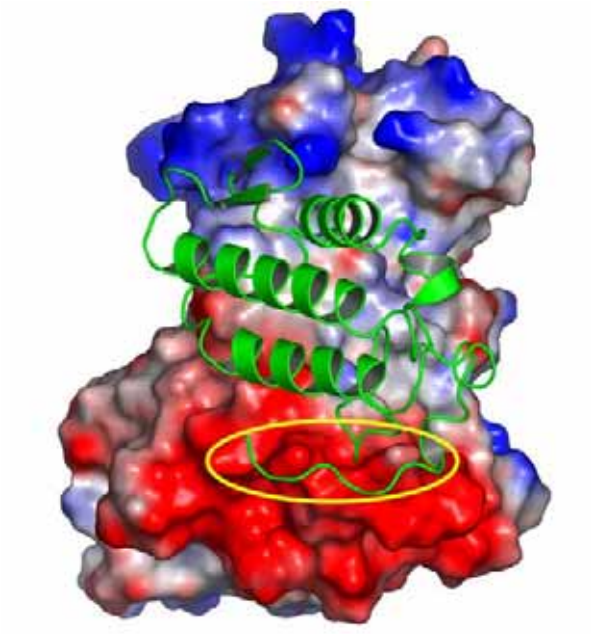

Figura 7: Modo proposto de interação de Lys49 PLA_2 (verde) com receptor KDR (superfície eletrostática) da angiogênese.

ELSEVIER

Toxicon 42 (2003) 903–913

TOXICON

www.elsevier.com/locate/toxicon

A structure based model for liposome disruption and the role of catalytic activity in myotoxic phospholipase A_2s

M.T. Murakami, R.K. Arni*

Department of Biophysics, IBILCE/UNESP, R. Cristovão Colombo 2265, CEP 15054-000, São José do Rio Preto-SP, Brazil

Abstract

Venom phospholipase A_2s (PLA_2s) display a wide spectrum of pharmacological activities and, based on the wealth of biochemical and structural data currently available for PLA_2s, mechanistic models can now be inferred to account for some of these activities. A structural model is presented for the role played by the distribution of surface electrostatic potential in the ability of myotoxic D49/K49 PLA_2s to disrupt multilamellar vesicles containing negatively charged natural and non-hydrolyzable phospholipids. Structural evidence is provided for the ability of K49 PLA_2s to bind phospholipid analogues and for the existence of catalytic activity in K49 PLA_2s. The importance of the existence of catalytic activity of D49 and K49 PLA_2s in myotoxicity is presented.

Keywords: Phospholipase A_2; Lys49 PLA_2; Asp49 PLA_2; Liposomes; Surface electrostatic potential; Catalytic activity

1. Introduction

Phospholipases A_2s (PLA_2, EC 3.1.1.4) are small (~14 kDa), stable, soluble enzymes that are found in a variety of biological fluids and cells, such as synovial fluid, macrophages, platelets, pancreatic secretion, spleen, smooth muscle and placenta. Additional rich sources of PLA_2s are saliva and the venoms of bees, lizards and snakes. The interest in these enzymes stems from the fact that they catalyze the hydrolysis of the *sn-2* ester bonds of phospholipids, liberating free fatty acids and lysophospholipids (van Deenen and de Haas, 1963) which subsequently serve as second messengers or as precursors in a variety of inflammatory reactions (Kudo et al., 1993; Dennis, 1994).

The pharmacological activities exhibited by snake venom PLA_2s vary widely and include neurotoxic, cardiotoxic, haemolytic, myotoxic, anticoagulant, convulsant, hypotensive and oedema-inducing effects (Harris, 1991; Mukherjee et al., 1994). The ability of these proteins to exhibit such a diverse spectrum of activities is intriguing since they share significant sequence and structural homology and since these activities originate from a single structural scaffold (Arni and Ward, 1996).

Structure–function relationships of PLA_2s are important to further our understanding of the stereochemical determinants that are involved in the expression of these activities. There have been a number of attempts to delineate the region or regions critical for the expression of these activities, especially regarding neurotoxicity and myotoxicity. These efforts have been based on sequence homology (Krizaj et al., 1989; Heinrickson, 1991; Ward et al, 1998; Selistre de Araujo et al., 1996), charge distribution (Kini and Iwanaga, 1986; Kini and Evans, 1989; Lomonte et al., 1994b), hydropathy profiles (Kini and Iwanaga, 1986), chemical modification (Dijkstra et al., 1984; Díaz-Oreiro and Gutiérrez, 1997; Andrião-Escarso et al., 2000), peptide synthesis (Lomonte et al., 1999; Núnez et al., 2001), site-directed mutagenesis (Chioato et al., 2002) and structural (Scott and Sigler, 1994) studies.

The catalytic mechanism of PLA_2s have been elucidated based on structural analyses of class I, II and III enzymes in the native state and complexed with transition state analogues (Verheij et al., 1980; Scott et al., 1990). The enzymatic activity of PLA_2s can be inhibited by the addition of chelating agents such as EDTA or *p*-bromophenacylbromide (BPB), which alkylates His48 (Volwerk et al., 1974; Renetseder et al., 1988; Soares et al., 2000).

* Corresponding author. Tel.: +55-1722-12460; fax: +55-1722-12247.

E-mail address: arni@df.ibilce.unesp.br (R.K. Arni).

0041-0101/$ - see front matter © 2003 Elsevier Ltd. All rights reserved.
doi:10.1016/j.toxicon.2003.11.014

Based on structural data of non-myotoxic D49 PLA_2s and myotoxic D49/K49 PLA_2s, we have calculated the surface electrostatic charge distribution of PLA_2s and suggest that this plays an important role in the ability of myotoxic PLA_2s to disrupt the integrity of liposomes containing negatively charged phospholipids without concomitant hydrolysis. Based on structural data, we propose that myotoxic K49 PLA_2s are catalytically active and that hydrolytic activity is important for the expression of myotoxicity by venom class II PLA_2s.

2. Venom myotoxic proteins

2.1. Myotoxic proteins in snake venoms

Myotoxicity has been defined as the ability of proteins to induce skeletal muscle necrosis (myonecrosis) in vivo, upon intramuscular injection, or in vitro, upon incubation with differentiated skeletal muscle (Gutiérrez and Lomonte, 1997). Three distinct groups of proteins are responsible for myotoxic activity in snake venoms (Mebs and Ownby, 1990; Mebs, 1998):

(1) Basic, enzymatically inactive short peptides with 42–45 amino acids, exemplified by crotamine from *Crotalus durissus terrificus* and myotoxin a from *Crotalus viridis viridis*.
(2) Longer chain (60–62 amino acid) cardiotoxins and cytotoxins from some elapid venoms, particularly of *Naja* species.
(3a) Highly toxic, presynaptic PLA_2s that either consist of a single chain or are complexed with other domains or subunits.
(3b) Less toxic PLA_2s which hydrolyze (D49 PLA_2s) or do not hydrolyze (K49 PLA_2 homologues) natural phospholipids.

2.2. Classification of PLA_2s

A number of schemes have been proposed to classify the PLA_2s (Renetseder et al., 1985; Dufton and Hider, 1983; Dennis, 1994). From the point of view of studying secretory PLA_2s, venom PLA_2s belong to one of the three principal classes based on amino acid sequence, secondary structure, insertions, deletions and disulfide bonding pattern (Renetseder et al., 1985; Arni and Ward, 1996; Kini, 1997) (Fig. 1).

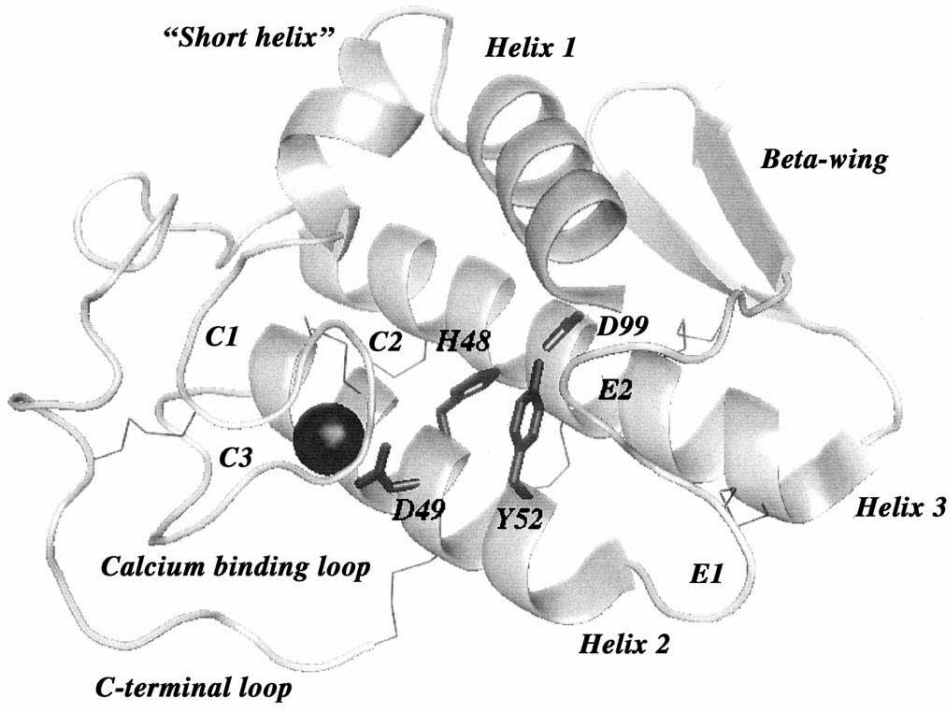

Fig. 1. Ribbon representation of the Class IIA PLA_2, SIISIIB from *Bothrops jararacussu* (unpublished results). Included in the figure are the amino acids important for catalysis (His48, Asp49, Tyr52 and Asp99). The shaded sphere represents the bound calcium ion and thin lines represent disulfide bridges. Sections of the loop (E1 and E2) and 'calcium binding' loop (C1, C2 and C3) are labelled and presented in the discussion.

The discussion in this manuscript is restricted to Class IIA myotoxic PLA_2s found in snake venoms.

2.3. The basic structural motif of class II PLA_2s

The structural aspects of PLA_2s have been reviewed thoroughly (Scott et al., 1990; Arni and Ward, 1996; Scott, 1997) and the following presentation is a brief summary of the principal structural features. Class II PLA_2s contain seven disulfide bridges and between 120 and 125 amino acids. The principal structural feature of class II PLA_2s is a platform formed by the two long anti-parallel disulfide linked α-helices (helices 2 and 3, residues 37–54 and 90–109) with a mean distance of 10 Å between the helical axes (Arni and Ward, 1996). These helices do not display a clear amphiphatic character, as the hydrophilic amino acids are exposed and the hydrophobic amino acids are shielded from the solvent. The amino acids considered important for hydrolysis (His48, Asp49, Tyr52 and Asp99) are located on this structural feature. This structural motif is highly conserved in all class I/II PLA_2s and superpositioning of this region results in a root mean square deviation of only about 0.4 Å.

Other conserved structural features which, however, adopt different relative orientations are the N-terminal helix and reverse turn, the β-wing region, the calcium binding loop, the 'elapid' or 'pancreatic loop' (E-loop), the short helix and the C-terminal extension which is stabilized by a disulfide bond to helix 2.

Class II PLA_2s can be further subdivided into at least two subclasses depending on whether they are D49-PLA_2s or K49-PLA_2 analogues (Ownby et al., 1999). The most abundant protein in some Viperidae snake venoms is a natural mutant where Asp49 previously considered invariant and essential is changed either to Lys (Maraganore and Heinrickson, 1986; Francis et al., 1991; Homsi-Brandenburgo et al., 1988), Ser (Krizaj et al., 1991) or Ala (Liu et al., 1991). The Ser49 PLA_2s have been shown to retain their ability to bind calcium (Polgar et al., 1996). The Asp49 to Lys mutation prevents calcium binding (Maraganore and Heinrickson, 1986); however, the His48/Asp99 diad and the residues Tyr 52 and Tyr73, which form hydrogen bonds to Asp99 and ensure its proper orientation, are considered to form the catalytic network, being strictly conserved (Arni et al., 1999; de Azevedo et al., 1999). These K49 mutants are capable of destroying the integrity of membranes and provoke marker release from liposomes in the absence of calcium without detectable lipid hydrolysis (Rufini et al., 1992) and there exists controversy as to whether these enzymes possess hydrolytic activity (Maraganore and Heinrickson, 1986; Ward et al., 2002).

3. Myotoxicity

A number of reports have attempted to correlate biochemical and biophysical characteristics such as sequence homology (Krizaj et al., 1989; Selistre de Araujo et al., 1996; Ward et al, 1998), charge distribution (Kini and Iwanaga, 1986; Kini and Evans, 1989; Lomonte et al., 1994a,b), hydrophobicity profiles (Kini and Iwanaga, 1986), results of chemical modification (Díaz-Oreiro and Gutiérrez, 1997; Andrião-Escarso et al., 2000; Soares et al., 2001) and structural aspects (Arni and Ward, 1996) of PLA_2s that induce myotoxicity. We briefly summarize the conclusions arrived at in these studies and present details of these structural features.

3.1. N-terminus and reverse turn

The N-terminus of PLA_2s, which includes the short helix and the reverse turn (residues 1–17), forms part of the hydrophobic collar surrounding the hydrophobic channel which provides access to the active site in classes I and II PLA_2s. This region, specifically amino acids at positions 7 and 10 in class I PLA_2s, form the interfacial recognition site and are considered to be involved in substrate binding (Scott and Sigler, 1994; Han et al., 1997).

In the myotoxic K49 PLA_2s, this region is highly conserved with the sequence SLFELGKMILQETGKN. However, some degree of substitution is observed, for example F3Y, E4Q and G6W in myotoxin I (*Bothrops godmani*) (de Sousa et al., 1998). Lys7, Glu12, Thr13 and Lys15 have been suggested to play a role in myotoxicity (Selistre de Araujo et al., 1996).

Cleavage of the N-terminal octapeptide of *B. asper* MTII with cyanogen bromide reduces the myotoxic activity to a third (Díaz et al., 1994; Soares et al., 2001). This region is important for the maintenance of a functional catalytic site (Yang, 1997). As pointed out by Fletcher et al. (1997), the effect of this cleavage on the structural integrity of the protein was not reported (Díaz et al., 1994). Cleavage of the N-terminal octapeptide in *B. pirajai* PrTX-1, a K49 PLA_2, resulted in a wavelength shift in the first minimum to 207 nm and a decreased minimum value at 222 nm in the circular dichroism spectra (Soares et al., 2001), which indicates that structural modification is associated with this cleavage. Cleavage of this octapeptide would expose the amino acids located on helix 3, especially Asp99, which is shielded from the solvent. The short helix would probably not be held in position since class II PLA_2s lack a disulfide bridge in this region. Additionally, loop E2 (Fig. 1) would be destabilized since the hydrogen bonds formed between this region and the N-terminus would be absent. Thus, cleavage of the N-terminal octapeptide could result in a drastic structural re-organization, which may account for its reduced myotoxic activity.

3.2. The short helix

The short helix (Fig. 1), which differs considerably in its relative orientation, is a structurally conserved feature in class II PLA_2s (Arni and Ward, 1996). Except for Tyr21, which is fully conserved and forms a hydrogen bond with the amino acids at the C-terminus of helix 3, there is no charge or sequence pattern that is the exclusive premise of myotoxic PLA_2s and no role in myotoxicity has been attributed to this region.

3.3. The calcium binding loop

Calcium binding is considered to be essential for catalytic activity in D49 PLA_2s, since the calcium ion forms bonds to the bound phospholipid and stabilizes the transition state intermediate (Scott et al., 1990). In the D49 PLA_2s, this region is invariant with the consensus sequence Y25-G-C-Y/F-C-G-X-G-G33. In the K49 PLA_2s, this region does not bind calcium, has a different sequence, and has been observed to adopt different conformations (Scott et al., 1992; Arni et al., 1995, 1999; Arni and Ward, 1996; de Azevedo et al., 1998, 1999;). No role in myotoxic activity has been attributed to this region.

3.4. β-Wing region

The β-wing region (residues 74–84) is structurally conserved and its relative orientation is preserved by two disulfide bridges in class I PLA_2s and only one disulfide bridge in class II PLA_2s. This region adopts different conformations and participates in the formation of dimers in the class II K49 PLA_2s (Arni et al., 1995; da Silva Giotto et al., 1998).

Lys78 and Lys80 in class II myotoxic K49 PLA_2s are conserved and are spatially close to the N-terminal region. Based on molecular modeling of ACL myotoxin (from the venom of *Agkistrodon contortrix laticinctus*), it has been proposed that the amino acids Lys7, Glu12 and Thr13 in myotoxic K49 PLA_2s, which are clustered on the surface of the molecule and are in close proximity to the conserved residues Lys78, Lys80, Lys115 and Lys116, could play a role in determining myotoxicity (Selistre de Araujo et al., 1996).

3.5. Helix 3

Kini and Iwanaga (1986) compared the sequences of a number of neurotoxic and myotoxic PLA_2s with neurotoxic/non-myotoxic PLA_2s. They reported that approximately 15 amino acids in the region between the β-wing and helix 3 were strongly cationic in myotoxic PLA_2s and suggested that this region could form the myotoxic site.

3.6. C-terminus

The C-terminal region (residues 115–134) of myotoxic K49 PLA_2s forms a cationic site which has been implicated in the mediation of electrostatic interactions with negatively charged lipids, forming a cytolytic motif (Lomonte et al., 1994b; Gutiérrez and Lomonte, 1997). Synthetic peptides corresponding to residues 115–129 of *B. asper* MTII induce cytolysis and interfere with the interaction between heparin and *B. asper* MTII (Lomonte et al., 1994b). However, intramuscular injection of 250 μg of this peptide failed to induce myotoxicity in mice (Gutiérrez and Lomonte, 1997). It has been suggested that along with other sites, this could form the molecular region that penetrates and disorganizes membranes (Gutiérrez and Lomonte, 1997; Lomonte et al., 1999; Núnez et al., 2001; Angulo et al., 2002). Selistre de Araujo et al. (1996) also proposed that Lys115 and Lys116 form part of the myotoxic site in K49 PLA_2s. Site directed mutagenesis specifically of cationic and aromatic residues in the C-terminal region (positions 115–129) and substitution of lysines and arginines in the region 117–122 with alanine, except for Lys122, resulted in a significant reduction in myotoxicity (Chioato et al., 2002).

4. Discussion

As presented, various attempts have been made to correlate sequence and structural aspects with myotoxicity in snake venom PLA_2s. However, some of these results contradict each other and no clear picture has emerged concerning the structural basis for the disruption of negatively charged liposomes, the role of hydrolytic activity and the region or regions responsible for myotoxicity in both K49 and D49 PLA_2s.

4.1. Surface charge distribution

The results of the electrostatic surface charge distribution calculations using GRASP (Nicholls, 1993) and potentials in the kT range −4.0 to 4.0 are shown in Fig. 2(a)–(f), with the molecule positioned in the same relative orientation as in Fig. 1. The surface principally encompasses the N-terminal helix, the short helix, the calcium binding loop (C1, C2 and C3), the elapid loop (E1 and E2), the β-wing region, the C-terminal extension and the area around the active site cleft which together form the interfacial activation face or *i*-face.

Calculations performed in the absence of the calcium ion for the non-myotoxic D49 PLA_2 (PDB ID: 1UMV, Murakami et al., unpublished results of this laboratory) indicate that a large part of the surface is uncharged in this PLA_2 and isolated positive regions are observed at the tip of the β-wing and at the end of the C-terminus (Fig. 2(a)). The area around the active site forms a deep channel that is

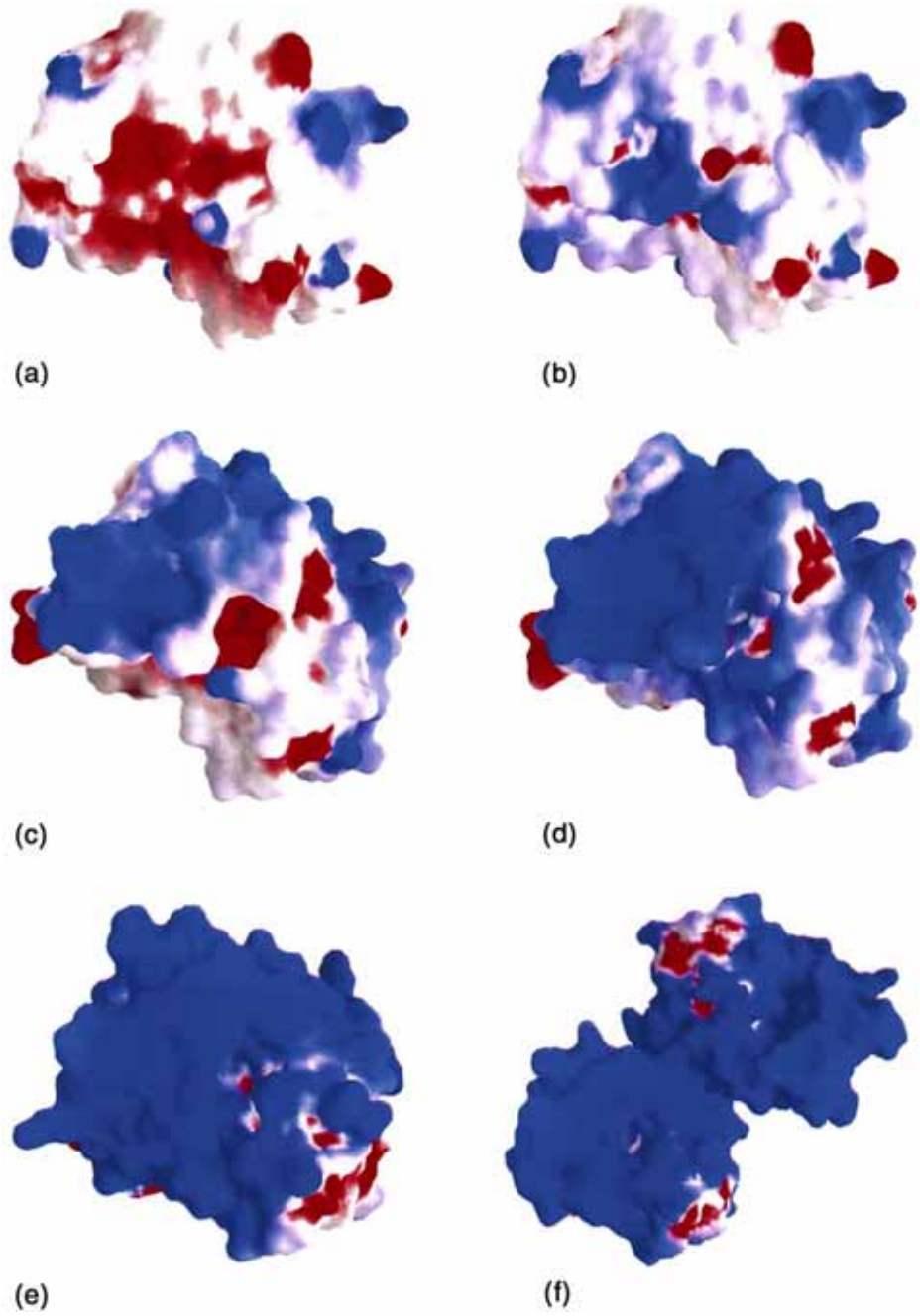

Fig. 2. Electrostatic surface potentials calculated in the same orientation as in Fig. 1 using GRASP (Nicholls, 1993) in the kT range −4.0 to + 4.0. Non-myotoxic D49 PLA_2 from *B. jararacussu* (PDB ID: 1UMV, unpublished results) in the absence (a) and presence (b) of the bound calcium ion. Myotoxic D49 PLA_2 from *A. p. piscivorus* (PDB ID:1VAP) in the absence (c) and presence (d) of the bound calcium ion. Monomer (e) and dimer (f) of *B. asper* MTII K49 PLA_2 (PDB ID:1CLP).

negatively charged. An additional highly charged pocket is observed to the left of this region, in the vicinity of the calcium-binding loop. When the calcium ion, which is coordinated by Asp49 and the putative calcium binding loop (Arni et al., 1995), is included in the calculation, the positively charged region spreads to include the surface of the calcium-binding loop and the region around the active site (Fig. 2(b)).

Similar calculations performed in the absence of the calcium ion with a myotoxic D49 PLA_2 (PDB ID: 1VAP; Han et al., 1997) indicate the presence of a broad positively charged surface in the β-wing region and more noticeably in the loop following the short helix (loop C1), in the calcium binding loop (loop C2) and in loop C3. The negative charge is restricted to the region around the active site cleft. Inclusion of the calcium ion in the calculation (Fig. 2b) dramatically increases the area of the positively charged region, which now spreads to include the major part of the *i*-face. Correspondingly, the negatively charged region shrinks to include, principally, the interior of the active site.

The charge distributions of the K49 PLA_2s from *B. asper*, *B. jararacussu* and *B. nummifer* are strikingly different when compared to the D49 PLA_2s. The positive charge presented for *B. asper* MTII (PDB ID:1CLP; Arni et al., 1995) encompasses the entire *i*-face of the molecule (Fig. 2(e)). Negative charges are not present on the *i*-face and are limited to part of the loop that connects helix 3 to the β-wing region. Formation of the dimer results in a dramatic increase in the area of the positively charged surface (Fig. 2(f)). Calculations performed based on the crystal structures of other myotoxic K49 PLA_2s (Arni et al., 1999; de Azevedo et al., 1999) result in a similar pattern of charge distribution.

In the non-myotoxic D49 PLA_2, access to the active site is through a narrow channel. This channel is much wider in the myotoxic D49 PLA_2, and Trp31 is positioned to enable it to function as a flap to modulate access. In the myotoxic K49 PLA_2, this function is carried out by Phe3 and the amino acids located in loop E2 or Phe102 (Liu et al., 2003) which restricts access to the catalytic site.

These electrostatic potential calculations indicate that in the case of non-myotoxic D49 PLA_2s the predominantly neutral and negatively charged surfaces present on the *i*-face do not permit the approach to negatively charged membranes. However, the myotoxic D49 PLA_2s possess a relatively large positively charged surface, whose area increases significantly with the inclusion of the calcium ion. In the K49 myotoxic PLA_2s, the *i*-face is almost completely positively charged. The large positive surface charge distribution in myotoxic PLA_2s probably plays an important role in the recognition of the muscle membranes and, consequently, in the expression of myotoxic activity. Similar electrostatic surface analysis have been conducted on viperid mytoxins (Falconi et al., 2000).

Liposomes have been used as model systems for the interaction of myotoxins with membranes and the ability of PLA_2s to disrupt negatively charged liposomes that contain markers has been reported (Díaz et al., 1991; Rufini et al., 1992). Catalytically active D49 non-myotoxic PLA_2s hydrolyze lipids only in the presence of calcium with concomitant marker release, and inclusion of EDTA inhibits this activity (Rufini et al., 1992). Myotoxic D49 PLA_2s also require calcium, and the inclusion of EDTA results in a reduction of liposome disrupting activity (Díaz et al., 1991). The myotoxic K49 PLA_2s, on the other hand, disrupt the integrity of liposome in the absence of calcium without concomitant phospholipid hydrolysis (Díaz et al., 1991; Rufini et al., 1992). *B. asper* MTII is also capable of releasing entrapped dyes from liposomes comprised of nonhydrolyzable analogues of phospholipids (Pedersen et al., 1994), and enzymatic activity has been considered non-essential for some myotoxic D49 PLA_2s to lyse liposomes, although it does enhance lytic activity (Díaz et al., 1991; Bultrón et al., 1993).

This liposome disrupting effect by K49 PLA_2s has been observed predominantly for negatively charged phospholipids (Díaz et al., 1991; Rufini et al., 1992; Gutiérrez and Lomonte, 1997). The charge distribution analysis presented above supports the hypothesis that electrostatic interaction between positively charged surfaces on the protein and the negatively charged phospholipids play a crucial role in the disruption of liposomes (Gutiérrez and Lomonte, 1997; Falconi et al., 2000). This would also explain the fact that *B. asper* MTII is capable of disrupting liposomes comprised of negatively charged, nonhydrolyzable phospholipd analogues (Pedersen et al., 1994; Gutiérrez and Lomonte, 1997).

4.2. Is catalytic activity important for myotoxicity?

Based on BPB modification of His48, it has been demonstrated that hydrolytic activity is important for the expression of myotoxicity in D49 PLA_2s (Díaz-Oreiro and Gutiérrez, 1997). In the crystal structure of the acidic class IIA PLA_2 from *Agkistrodon halys pallas* (i.e. *Agkistrodon blomhoffii brevicaudus*) (Zhao et al., 1998; PDB ID: 1BK9), BPB binds to His48 Nδ1 in an analogous manner to that of bovine pancreatic PLA_2 (Renetseder et al., 1988). However, the specific interactions vary considerably (Zhao et al., 1998). In the pancreatic PLA_2, upon inhibitor binding, the 'pancreatic loop' adopts a significantly different conformation and Tyr69 forms extensive contacts while Leu31 does not form contacts with the inhibitor. In the class IIA structure, the shortened, more rigid loop does not change conformation upon BPB binding, and Lys69 does not form contacts whereas Trp31 interacts extensively with the inhibitor.

In the model for catalytic activity of D49 PLA_2s, the calcium ion is essential for the stereospecific orientation of the substrate and it also serves as an electrophile (Scott and Sigler, 1994; Scott, 1997). Exclusion of the calcium ion in D49 PLA_2s results in absence of lipid hydrolysis. There exists considerable controversy as to whether myotoxic K49 PLA_2s possess catalytic activity, since the substitution of Asp49 by Lys prevents Ca^{2+}binding.

In primary cultures of human skeletal muscle, under conditions relevant to myotoxicity, K49 PLA_2s have been shown to be enzymatically active (Rodrigues-Simioni et al., 1995; Fletcher et al., 1996). Highly purified ACLMT was shown to possess significant PLA_2 activity at concentrations relevant to cytotoxicity (Fletcher et al., 1997). It has been

reported that myotoxic K49 PLA_2s are active for β-arachidonoyl phospholipid bilayers (Yamaguchi et al., 1997). However, it cannot be conclusively ruled out that this enzymatic activity is due to trace contamination by D49 PLA_2s or, in the case of cell culture experiments, to the action of intracellular PLA_2s.

Molecular modeling (Fig. 3) of the myotoxic K49 PLA_2 myotoxin II from *B. asper* (Arni et al., 1995, PDB ID:1CLP) with BPB indicates that a covalent bond is formed with His48 Nδ1, as in the structure of the class IIA acidic D49 PLA_2 from *Agkistrodon halys pallas* (i.e. *Agkistrodon blomhoffii brevicaudus*) (Zhao et al., 1998; PDB ID:1BK9). The substitutions Phe5Leu, Trp31/Val, Ala102/Val and Phe106/Leu in the structure of the D49 PLA_2 (PDB ID: 1BK9) when compared with the myotoxic K49 PLA_2 from *B. asper* (PDB ID: 1CLP) result in a modification of the hydrophobic pocket and in a significant perturbation of the stabilizing interactions (Zhao et al., 1998) (Fig. 3).

D49 PLA_2s are less susceptible to inactivation by BPB in the presence of the Ca^{2+} ion due to the position of the equatorial ligand water molecule which would form close contacts with the phenacyl group of the inhibitor (Renetseder et al., 1988; Zhao et al., 1998). In the K49 PLA_2s, Lys49 Nζ occupies the position of the Ca^{2+}ion in D49 PLA_2s (Fig. 3) and is coordinated by two main chain carbonyl oxygen atoms and a solvent water molecule.

Depletion of Ca^{2+}, addition of EDTA or binding of an active site inhibitor such as BPB in D49 PLA_2s abolishes hydrolytic and myotoxic activities. Alkylation of His48 in *B. asper* mytoxin III (D49 PLA_2) with BPB results in reduced enzymatic and myotoxic activities (Bultrón et al., 1993; Díaz-Oreiro and Gutiérrez, 1997). Interestingly, only 30% of the myotoxic activity is retained upon binding of BPB to myotoxic K49 PLA_2s (Soares et al., 2000), indicating that, as in the case of D49 PLA_2s, K49 PLA_2s also require a fully accessible and functional catalytic site for myotoxicity. The absence of stabilizing hydrophobic and aromatic–aromatic interactions in K49 PLA_2s (Fig. 3) results in a weak and partial BPB binding. This reduced binding of BPB could explain the existence of residual myotoxicity in BPB-modified K49 PLA_2s.

Structural studies of the complexes of K49 PLA_2s with phospholipids and fatty acids indicate that these molecules bind at the active site in a manner analogous to the binding of phospholipids in D49 PLA_2s. In the crystal structure of the dimeric myotoxic K49 PLA_2 from *B. moojeni* complexed with stearic acid (unpublished results), two stearic acid molecules are bound in the active site. Based on the structural superpositioning with phospholipd analogues, the two stearic acid molecules can be considered to mimick this binding by occupying the fatty acid and lysophospholipid binding sites. The stearic acid molecules are

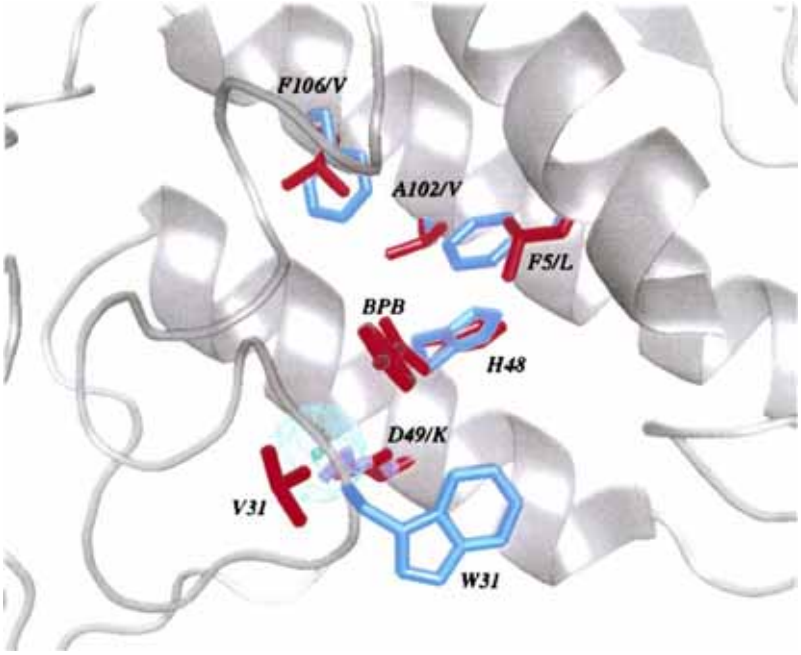

Fig. 3. Details of *p*-bromophenacylbromide (BPB) binding in the structure of *A. h. pallas* (PDB ID:1BK9) in blue. The bound calcium ion is represented in blue and is highlighted by an enclosing mesh. In red, the results of modeling of the binding of BPB in the structure of *B. asper* myotoxin II (PDB ID:1CLP). (For interpretation of the references to colour in this figure legend, the reader is referred to the web version of this article).

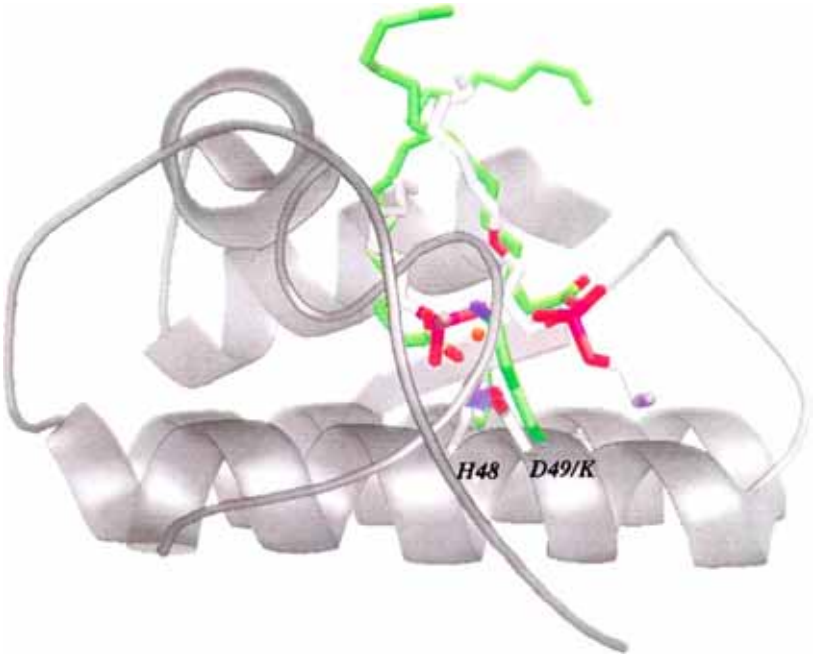

Fig. 4. Ribbon representation of the structure of *B. asper* MTII (PDB ID:1CLP) including His48, Lys49 and the two stearic acid molecules bound in the active site (green). The transition state analogue (L-1-*O*-octyl-2-heptylphosphonyl-*sn*-glycero-3-phosphoethanolamine) and His48 and Asp49 of the class IIA human synovial fluid PLA_2 (PDB ID:1POE) are superimposed in light gray.

hydrogen bonded to the carbonyl oxygen atom of Asn28, the amide nitrogen of Gly30 and His48 Nδ1. The stearic acid molecules occupying the lysophospholipid binding site form only few hydrogen bonds. However, both the fatty acid and lysophospholipid molecules form numerous hydrophobic–hydrophobic and hydrophobic–hydrophilic interactions. Superpositioning of these two stearic acid molecules with the transition state analogue (L-1-*O*-octyl-2-heptylphosphonyl-*sn*-glycero-3-phosphoethanolamine) bound to a catalytically active class II human synovial PLA_2 (Scott et al., 1991; PDB ID:1POE) indicates that the stearic acid molecules occupy a position similar to that of the phospholipid analogue (Fig. 4). Stearic acid is an analogue for arachidonic acid and modeling of the binding of β-arachidonoyl indicates productive mode binding, suggesting that hydrolysis could be possible. Ongoing unpublished structural studies of the binding of dimyristoylphosphatidylcholine (DMPC) also support these results. This indicates that, as in the case of D49 PLA_2s, K49 PLA_2s are catalytically active and such activity is likely to determine myotoxicity.

Rosenberg (1979, 1986, 1997) has pointed out that PLA_2 activity has to be defined against a range of substrates to obtain a clear understanding of the relationship between phospholipid hydrolysis and pharmacological activities. Thus, further studies of K49 PLA_2s have to be conducted and the catalytic activity of K49 PLA_2s has to be determined against different substrates, including phospholipids located in cellular membranes.

In conclusion, we suggest that catalytic activity is essential for myotoxicity in both D49 and K49 PLA_2s and that the surface distribution of charges is important for interaction with membranes and for the disruption of liposomes consisting of negatively charged phospholipids and phospholipid analogues.

Acknowledgements

M.T.M. is the recipient of a FAPESP fellowship. This research was supported by grants from FAPESP and CNPq to RKA. We are grateful to J.R. Giglio, J. M. Gutiérrez, B. Lomonte, A. C. O. Cintra and A. M. Soares for providing us with valuable protein samples. We are also grateful to L. Watanabe and M.R.M. Fontes for their contribution in the crystallographic analysis.

References

Andrião-Escarso, S.H., Soares, A.M., Rodrigues, V.M., Angulo, Y., Díaz, C., Lomonte, B., Gutiérrez, J.M., Giglio, J.R., 2000. Myotoxic phospholipase A_2 in *Bothrops* snake venoms: effect of chemical modification on the enzymatic and pharmacological properties of bothropstoxins from *Bothrops jararacussu*. Biochimie 82, 755–763.

Angulo, Y., Olamendi-Portugal, T., Alape-Girón, A., Possani, L.D., Lomonte, B., 2002. Structural characterization and phylogenetic

relationships of myotoxin II from *Atropoides* (*Bothrops*) *nummifer* snake venom, a Lys49 phospholipase A_2 homologue. Int. J. Biochem. Cell Biol. 34, 1268–1278.

Arni, R.K., Ward, R.J., 1996. Phospholipase A_2—a structural review. Toxicon 34 (8), 827–841.

Arni, R.K., Ward, R.J., Gutiérrez, J.M., Tulinsky, A., 1995. Structure of a calcium-independent phospholipase-like myotoxic protein from *Bothrops asper* venom. Acta Cryst. D51, 311–317.

Arni, R.K., Fontes, M.R., Barberato, C., Gutiérrez, J.M., Díaz, C., Ward, R.J., 1999. Crystal structure of myotoxin II, a monomeric Lys49-phospholipase A_2 homologue isolated from the venom of *Cerrophidion* (*Bothrops*) *godmani*. Arch. Biochem. Biophys. 366 (2), 177–182.

de Azevedo, W.F. Jr, Ward, R.J., Canduri, F., Soares, A., Giglio, J.R., Arni, R.K., 1998. Crystal structure of piratoxin-I: a calcium-independent, myotoxic phospholipase A_2-homologue from *Bothrops pirajai* venom. Toxicon 36 (10), 1395–1406.

de Azevedo, W.F. Jr., Ward, R.J., Gutiérrez, J.M., Arni, R.K., 1999. Structure of a Lys49-phospholipase A_2 homologue isolated from the venom of *Bothrops nummifer* (jumping viper). Toxicon 37 (2), 371–384.

Bultrón, E., Gutiérrez, J.M., Thelestam, M., 1993. Effects of *Bothrops asper* (terciopelo) myotoxin III, a basic phospholipase A_2, on liposomes and mouse gastrocnemius muscle. Toxicon 31, 217–222.

Chioato, L., Oliveira, A.H.C., Ruller, R., Sá, J.M., Ward, R.J., 2002. Distinct sites for myotoxic and membrane-damaging activities in the C-terminal region of a Lys49-phospholipase A_2. Biochem. J. 366, 971–976.

van Deenen, L.L.M., de Haas, G.H., 1963. The substrate specificity of phospholipse A_2. Biochem. Biophys. Acta 70, 538–553.

Dennis, E.A., 1994. Diversity of group types, regulation, and function of phospholipase A_2. J. Biol. Chem. 269, 13057–13060.

Díaz, C., Gutiérrez, J.M., Lomonte, B., Gené, J.A., 1991. The effect of myotoxins isolated from *Bothrops* snake venoms on multilamellar liposomes: relationship to phospholipase A_2, anticoagulant and myotoxic activities. Biochim. Biophys. Acta. 1070 (2), 455–460.

Díaz, C., Alape, A., Lomonte, B., Olamendi, T., Gutiérrez, J.M., 1994. Cleavage of the NH_2-terminal octapeptide of *Bothrops asper* myotoxic lysine-49 phospholipase A_2 reduces its membrane-destabilizing effect. Arch. Biochem. Biophys. 312 (2), 336–339.

Díaz-Oreiro, C., Gutiérrez, J.M., 1997. Chemical modification of histidine and lysine residues of myotoxic phospholipases A_2 isolated from *Bothrops asper* and *Bothrops godmani* snake venoms: effects on enzymatic and pharmacological properties. Toxicon 35, 241–252.

Dijkstra, B.W., Kalk, K.H., Drenth, J., de Haas, G.H., Egmond, M.R., Slotboom, A.J., 1984. Role of the N-terminus in the interaction of pancreatic phospholipase A_2 with aggregated substrates. Properties and crystal structure of transaminated phospholipase A_2. Biochemistry 23 (12), 2759–2766.

Dufton, M.J., Hider, R.C., 1983. Classification of phospholipases A_2 according to sequence. Evolutionary and pharmacological implications. Eur. J. Biochem. 137, 545–551.

Falconi, M., Desideri, A., Rufini, S., 2000. Membrane-perturbing activity of Viperidae myotoxins: an electrostatic surface potential approach to a puzzling problem. J. Mol. Recogn. 13, 14–19.

Fletcher, J.E., Hubert, M., Wieland, S.J., Gong, Q.H., Jiang, M.S., 1996. Similarities and differences in mechanisms of cardiotoxins, melittin and other myotoxins. Toxicon 34 (11–12), 1301–1311.

Fletcher, J.E., Selistre-de-Araújo, H.S., Ownby, C.L., 1997. Molecular events in the myotoxic action of phospholipases. In: Kini, R.M., (Ed.), Venom Phospholipase A_2 Enzymes: Structure, Function and Mechanism, Wiley, Chichester, pp. 455–498.

Francis, B., Gutiérrez, J.M., Lomonte, B., Kaiser, I.I., 1991. Myotoxin II from *Bothrops asper* (Terciopelo) venom is a lysine 49 phospholipase A_2. Arch. Biochem. Biophys. 284, 352–359.

Gutiérrez, J.M., Lomonte, B., 1997. Phospholipase A_2 myotoxins from *Bothrops* snake venoms. In: Kini, R.M., (Ed.), Venom Phospholipase A_2 Enzymes: Structure, Function and Mechanism, Wiley, Chichester, pp. 321–352.

Han, S.K., Yoon, E.T., Scott, D.L., Sigler, P.B., Cho, W., 1997. Structural aspects of interfacial adsorption. J. Biol. Chem. 272 (6), 3573–3582.

Harris, J.B., 1991. Phospholipases in snake venoms and their effects on nerve and muscle. In: Harvey, A.L., (Ed.), Snake Toxins, Pergamon Press, New York, pp. 91–121.

Heinrickson, R.L., 1991. Dissection and sequence analysis of phospholipase A_2. Meth. Enzymol. 197, 201–215.

Homsi-Brandenburgo, M.I., Queiroz, L.S., Santo-Neto, H., Rodrigues-Simioni, L., Giglio, J.L., 1988. Fractionation of *Bothrops jararacussu* snake venom: partial chemical characterization and biological activity of bothropstoxin I. Toxicon 26 (7), 615–627.

Kini, R.M., 1997. Phospholipase A_2—a complex multifunctional protein puzzle. In: Kini, R.M., (Ed.), Venom phospholipase A_2 Enzymes: Structure, Function and Mechanism, Wiley, Chichester, pp. 1–28.

Kini, R.M., Iwanaga, S., 1986. Structure–function relationships of phospholipases II: charge density distribution and the myotoxicity of presynaptically neurotoxic phospholipases. Toxicon 24 (9), 895–905.

Kini, R.M., Evans, H.J., 1989. Role of cationic residues in cytolytic activity: modification of lysine residues in the cardiotoxin from *Naja nigricollis* venom and correlation between cytolytic and antiplatelet activity. Biochemistry 28 (23), 9209–9216.

Krizaj, I., Turk, D., Ritonja, A., Gubensek, F., 1989. Primary structure of ammodytoxin C further reveals the toxic site of ammodytoxin. Biochim. Biophys. Acta 999 (2), 198–202.

Krizaj, R.M., Bieber, A.L., Gubensek, F., 1991. The primary structure of ammodytin L, a myotoxic phospholipase A_2 homologue from *Vipera ammodytes* venom. Eur. J. Biochem. 202, 1165–1168.

Kudo, I., Murakami, M., Hara, S., Inoue, K., 1993. Mammalian nonpancreatic phospholipases A_2. Biochim. Biophys. Acta 117, 217–231.

Liu, C.S., Chen, J.M., Chang, C.H., Chen, S.W., Teng, C.M., Tsai, I.H., 1991. The amino acid sequence and properties of an edema-inducing Lys-49 phospholipase A_2 homolog from the venom of *Trimeresurus mucrosquamatus*. Biochim. Biophys. Acta 1077, 362–370.

Liu, Q., Huang, Q., Teng, M., Weeks, C.M., Jelsch, C., Zhang, R., and Niu, L. 2003. The crystal structure of a novel, inactive, lysine 49 PLA_2 from the *Agkistrodon acutus* venom: an ultrahigh

resolution, ab initio structure determination. J. Biol. Chem. 278, 41400–41408.

Lomonte, B., Tarkowski, A., Hanson, L.A., 1994a. Broad cytolytic specificity of myotoxin II, a lysine-49 phospholipase A_2 of *Bothrops asper* snake venom. Toxicon 32 (11), 1359–1369.

Lomonte, B., Moreno, E., Tarkowski, A., Hanson, L.A., Maccarana, M., 1994b. Neutralizing interaction between heparin and myotoxin II, a Lys49 phospholipase A_2 from *Bothrops asper* snake venom. Identification of a heparin-binding and cytolytic toxin region by the use of synthetic peptides and molecular modelling. J. Biol. Chem. 269, 29867–29873.

Lomonte, B., Pizarro-Cerda, J., Angulo, Y., Gorvel, J.P., Moreno, E., 1999. Tyr → Trp-substituted peptide 115–129 of a Lys49 phospholipase A_2 expresses enhanced membrane-damaging activities and reproduces its in vivo myotoxic effect. Biochim. Biophys. Acta 1461 (1), 19–26.

Maraganore, J.M., Heinrickson, R.L., 1986. The lysine-49 phospholipase A_2 from the venom of *Agkistrodon piscivorus piscivorus*. Relation of structure and function to other phospholipases A_2. J. Biol. Chem. 261, 4797–4804.

Mebs, D., 1998. Phospholipases A_2 that show myotoxic activity. In: Bailey, G.S., (Ed.), Enzymes from Snake Venom, Alaken Inc., Colorado, pp. 451–479.

Mebs, D., Ownby, C.L., 1990. Myotoxic components of snake venoms: their biochemical and biological activities. Pharmacol. Ther. 48 (2), 223–236.

Mukherjee, A.B., Miele, L., Pattabiraman, N., 1994. Phospholipase A_2 enzymes: regulation and physiological role. Biochem. Pharmac. 48, 1–10.

Nicholls, A., 1993. GRASP: graphical representation and analysis of surface properties. Columbia University, New York, NY.

Núnez, C.E., Angulo, Y., Lomonte, B., 2001. Identification of the myotoxic site of the Lys49 phospholipase A_2 from *Agkistrodon piscivorus piscivorus* snake venom: synthetic C-terminal peptides from Lys49, but not from Asp49 myotoxins, exert membrane-damaging activities. Toxicon 39, 1587–1594.

Ownby, C.L., Selistre de Araújo, H.S., White, S.P., Fletcher, J.E., 1999. Lysine 49 phospholipase A_2 proteins. Toxicon 37, 411–445.

Pedersen, J.Z., de Acuri, B.F., Morero, R.D., Rufini, S., 1994. Phospholipase-like myotoxins induce rapid membrane leakage of non-hydrolyzable ether–lipid liposomes. Biochim. Biophys. Acta 1190, 177–180.

Polgar, J., Magnenat, E.M., Peitsch, M.C., Wells, T.N.C., Clemetson, K.J., 1996. Asp-49 is not an absolute prerequisite for the enzymatic acitivity of low-Mr phospholipases A_2: purification, characterization and computer modeling of an enzymatically active Ser-49 phospholipase A_2, ecarpholin S, from the venom of *Echis carinatus sochureki* (saw-scaled viper). Biochem. J. 319, 961–968.

Renetseder, R., Brunie, S., Dijkstra, B.W., Drenth, J., Sigler, P.B., 1985. A comparison of the crystal structures of phospholipase A_2 from bovine pancreas and *Crotalus atrox* venom. J. Biol. Chem. 260, 11627–11636.

Renetseder, R., Dijkstra, B.W., Huizinga, K., Kalk, K.H., Drenth, J., 1988. Crystal structure of bovine pancreatic phospholipase A_2 covalently inhibited by *p*-bromophenacyl-bromide. J. Mol. Biol. 200 (1), 181–188.

Rodrigues-Simioni, L., Prado-Franceschi, J., Cintra, A.C., Giglio, J.R., Jiang, M.S., Fletcher, J.E., 1995. A role for enzymatic activity or dantrolene-sensitive Ca^{2+}stores in the muscular effects of bothropstoxin, a Lys49 phospholipase A_2 myotoxin. Toxicon 33 (11), 1479–1489.

Rosenberg, P., 1979. Pharmacology of phospholipase A_2 from snake venom. In: Lee, C.Y., (Ed.), Snake Venoms, Springer, Berlin, pp. 403–447.

Rosenberg, P., 1986. The relationship between enzymatic activity and pharmacological properties of phospholipases in natural poisons. In: Harris, J.B., (Ed.), Natural Toxins, Oxford University Press, Oxford, pp. 129–174.

Rosenberg, P., 1997. Pitfalls to avoid in the study of correlations between enzymatic activity and pharmacological properties of phospholipase A_2 enzymes. In: Kini, R.M., (Ed.), Venom Phospholipase, Wiley, Chichester, pp. 155–183.

Rufini, S., Cesaroni, P., Desideri, R.F., Gubensek, F., Gutiérrez, J.M., Luly, P., Massoud, R., Morero, R., Pedersen, J.Z., 1992. Calcium ion independent membrane leakage induced by phospholipase-like myotoxins. Biochemistry 31, 12424–12430.

Scott, D.L., 1997. Phospholipase A_2: structure and catalytic properties. In: Kini, R.M., (Ed.), Venom Phospholipase A_2 Enzymes: Structure, Function and Mechanism, Wiley, Chichester, pp. 97–128.

Scott, D.L., Sigler, P.B., 1994. The structural and functional roles of calcium ion in secretory phospholipases A_2. Adv. Inorg. Biochem. 10, 139–155.

Scott, D.L., White, S.P., Otwinowski, Z., Yuan, W., Gelb, M.H., Sigler, P.B., 1990. Interfacial catalysis: the mechanism of phospholipase A_2. Science 250, 1541–1546.

Scott, D.L., White, S.P., Browing, J.L., Rosa, J.J., Gelb, M.H., Sigler, P.B., 1991. Structures of free and inhibited human secretory phospholipase A_2 from inflammatory exudate. Science 254, 1007–1012.

Scott, D.L., Achari, A., Vidal, J.C., Sigler, P.B., 1992. Crytallographical and biochemical studies of the (inactive) Lys49 phospholipase A_2 from the venom of *Agkistrodon piscivorus piscivorus*. J. Biol. Chem. 267, 22645–22657.

Selistre de Araujo, H.S., White, S.P., Ownby, C.L., 1996. cDNA cloning and sequence analysis of a lysine-49 phospholipase A_2 myotoxin from *Agkistrodon contortrix laticinctus* snake venom. Arch. Biochem. Biophys. 326 (1), 21–30.

da Silva Giotto, M.T., Garratt, R.C., Oliva, G., Mascarenhas, Y.P., Giglio, J.R., Cintra, A.C.O., de Azevedo, W.F. Jr., Arni, R.K., Ward, R.J., 1998. Crystallographic and spectroscopic characterization of a molecular hinge: conformational changes in bothropstoxin I, a dimeric Lys49-phospholipase A_2 homologue. Protein Struct. Funct. Genet. 30, 411–445.

Soares, A.M., Guerra-Sá, R., Borja-Oliveira, C.R., Rodrigues, V.M., Rodrigues-Simioni, L., Rodrigues, V., Fontes, M.R.M., Lomonte, B., 2000. Structural and functional characterization of BnSP-7, a Lys49 myotoxic phospholipase A_2 homologue from *Bothrops neuwiedi pauloensis* venom. Arch. Biochem. Biophys. 378 (2), 201–209.

Soares, A.M., Andrião-Escarso, S.H., Bortoleto, R.K., Rodrigues-Simioni, L., Arni, R.K., Ward, R.J., Gutiérrez, J.M., Giglio, J.R., 2001. Dissociation of enzymatic and pharmacological properties of piratoxin-I and -III, two myotoxic phospholipases A_2 from *Bothrops pirajai* snake venom. Arch. Biochem. Biophys. 387 (2), 188–196.

de Sousa, M.V., Morhy, L., Arni, R.K., Ward, R.J., Díaz, C., Gutiérrez, J.M., 1998. Amino acid sequence of a myotoxic Lys49-phospholipase A_2 homologue from the venom of

Cerrophidion (*Bothrops*) *godmani*. Biochim. Biophys. Acta 1384 (2), 204–208.

Verheij, H.M., Volwerk, J.J., Jansen, E.H.J.M., Puyk, W.C., Dijkstra, B.W., Drenth, J., de Haas, G.H., 1980. Methylation of histidine-48 in pancreatic phospholipase A_2. Role of histidine and calcium ion in the catalytic mechanism. Biochemistry 19, 743–750.

Volwerk, J.J., Pieterson, W.A., de Haas, G.H., 1974. Histidine at the active site of phospholipase A_2. Biochemistry 13 (7), 1446–1454.

Ward, R.J., Rodrigues Alves, A., Rugierro Neto, J., Arni, R.K., Casari, J., 1998. A SequenceSpace analysis of Lys 49 phospholipase A_2: clues towards identification of residues involved in a novel mechanism of membrane damage and in myotoxicity. Protein Engng. 11, 285–294.

Ward, R.J., Chioato, L., de Oliveira, A.H.C., Ruller, R., Sá, J.M., 2002. Active-site mutagenesis of a Lys^{49}-phospholipase A_2: biological and membrane-disrupting activities in the absence of catalysis. Biochem. J. 362, 89–96.

Yamaguchi, Y., Shimohigashi, Y., Chiwata, T., Tani, A., Chijiwa, T., Lomonte, B., Ohno, M., 1997. Lys-49-phospholipases A_2 as active enzyme for beta-arachidonoyl phospholipid bilayer membranes. Biochem. Mol. Biol. Int. 43 (1), 19–26.

Yang, C.C., 1997. Chemical modification and functional sites of phospholipases A_2. In: Kini, R.M., (Ed.), Venom Phospholipase A_2 Enzymes: Structure, Function and Mechanism, Wiley, Chichester, pp. 185–204.

Zhao, H., Tang, L., Wang, X., Zhou, Y., Lin, Z., 1998. Structure of a snake venom phospholipase A_2 modified by *p*-bromo-phenacyl-bromide. Toxicon 36 (6), 875–886.

Available online at www.sciencedirect.com
SCIENCE DIRECT®
Biochimie 85 (2003) 983–991
BIOCHIMIE
www.elsevier.com/locate/biochi

Isolation, characterization and biological activity of acidic phospholipase A_2 isoforms from *Bothrops jararacussu* snake venom

D.F.J. Ketelhut [a], M. Homem de Mello [a], E.L.G Veronese [a], L.E. Esmeraldino [a], M.T. Murakami [b], R.K. Arni [b], J.R. Giglio [c], A.C.O. Cintra [a], S.V. Sampaio [a,*]

[a] *Departamento de Análises Clínicas, Toxicológicas e Bromatológicas, Faculdade de Ciências Farmacêuticas, Universidade de São Paulo, Avenida do Café, s/n, Bairro Monte Alegre, Ribeirão Preto, SP 14040-903, Brazil*
[b] *Departamento de Física, IBILCE, Universidade Estadual Paulista, São José do Rio Preto, SP, Brazil*
[c] *Departamento de Bioquímica e Imunologia, Faculdade de Medicina, Universidade de São Paulo, Ribeirão Preto, SP, Brazil*

Received 17 June 2003; accepted 2 September 2003

Abstract

Acidic phospholipase A_2 (PLA_2) isoforms in snake venoms, particularly those from *Bothrops jararacussu*, have not been characterized. This article reports the isolation and partial biochemical, functional and structural characterization of four acidic PLA_2s (designated SIIISPIIA, SIIISPIIB, SIIISPIIIA and SIIISPIIIB) from this venom. The single chain purified proteins contained 122 amino acid residues and seven disulfide bonds with approximate molecular masses of 15 kDa and isoelectric points of 5.3. The respective N-terminal sequences were: SIIISPIIA–SLWQFGKMIDYVMGEEGAKS; SIIISPIIB–SLWQFGKMIFYTGKNEPVLS; SIIISPIIIA–SLWQFGKMILYVMGGEGVKQ and SIIISPIIIB–SLWQFGKMIFYEMTGEGVL. Crystals of the acidic protein SIIISPIIB diffracted beyond 1.8 Å resolution. These crystals are monoclinic with unit cell dimensions of $a = 40.1$ Å, $b = 54.2$ Å and $c = 90.7$ Å. The crystal structure has been refined to a crystallographic residual of 16.1% (R_{free} = 22.9%). Specific catalytic activity (U/mg) of the isolated acidic PLA_2s were SIIISPIIA = 290.3 U/mg; SIIISPIIB = 279.0 U/mg; SIIISPIIIA = 270.7 U/mg and SIIISPIIIB = 96.5 U/mg. Although their myotoxic activity was low, SIIISPIIA, SIIISPIIB and SIIISPIIIA showed significant anticoagulant activity. However, there was no indirect hemolytic activity. SIIISPIIIB revealed no anticoagulant, but presented indirect hemolytic activity. With the exception of SIIISPIIB, which inhibited platelet aggregation, all the others were capable of inducing time-independent edema. Chemical modification with 4-bromophenacyl bromide did not inhibit the induction of edema, but did suppress other activities.

Keywords: Acidic PLA_2s; *Bothrops jararacussu*; N-terminal sequence; Platelet aggregation inhibition; X-ray crystallography

1. Introduction

Extracellular and intracellular phospholipases A_2 (PLA_2s) have been extensively investigated during the last 10 years since they induce a range of important biological effects, some of them showing to be independent of catalytic activity. Extracellular PLA_2s are found in pancreatic tissue, as well as in snake, bee and scorpion venoms. Catalytically active PLA_2s hydrolyze the 2-acyl ester bond of three *sn*-phospholipids releasing fatty acids and lysophosphatides. These PLA_2s display molecular masses from 14 to 21 kDa and have been classified as types I, II or III according to their source, chain length and disulfide bond patterns [1]. Snake venoms are rich in type I and II PLA_2s.

The various pharmacological effects induced by PLA_2s include edema, hemorrhage and inhibition of platelet aggregation, as well as neurotoxic, anticoagulant and myotoxic effects.

It has been shown that myotoxic PLA_2 homologues which, although showing low or no enzymatic activity upon artificial substrates, are able to produce extensive muscle necrosis [2–4]. Experiments using endothelial and skeletal muscle cells in vitro have revealed a cytolytic effect [5]. These myotoxins have an Asp residue at position 49 (D49) showing catalytic activity, or Lys residue (K49), with low or no apparent detectable activity upon artificial substrates.

* Corresponding author. Tel.: +55-16-602-4287; fax: +55-16-633-1936.
E-mail address: suvilela@fcfrp.usp.br (S.V. Sampaio).

doi:10.1016/j.biochi.2003.09.011

The presence of several PLA_2 isoforms in the venom of a single snake species has been shown to be a common feature [6]. The presence of basic and acidic PLA_2s was first reported in the venom of *Bothrops jararacussu* in 1988 by Homsi-Brandeburgo et al. [2], who isolated and partially characterized two of them, later referred to as bothropstoxin-I (BthTX-I) and bothropstoxin-II (BthTX-II). These two basic myotoxic PLA_2s have been sequenced and were shown to be K49 and D49, respectively [7,8]. An acidic platelet aggregation inhibitor and hypotensive PLA_2 has also been isolated from the same venom and sequenced up to the 51st amino acid residue [9].

This article reports the isolation, N-terminal sequencing and partial characterization of four new acidic PLA_2s from *B. jararacussu* snake venom, as well as structural details of one of them (SIIISPIIB).

2. Materials and methods

2.1. Material

The *B. jararacussu* venom was purchased from Instituto Butantan (São Paulo, SP, Brazil). Sephadex G-75, SP-Sephadex C-25 and molecular weight markers were obtained from Pharmacia Fine Chemical Company (St. Louis, USA). All other chemicals and solvents were of analytical grade. 4-Bromophenacyl bromide (BPB) was obtained from Sigma Chemical Company (St. Louis, USA). Male Swiss Wistar mice were used for biological assays.

2.2. Purification procedure

Lyophilized crude venom from *B. jararacussu* (500 mg) was extracted with 5 ml of 0.05 M ammonium bicarbonate buffer, pH 8.0. It was then cleared by centrifugation for 5 min at 480 × *g* and subjected to gel filtration on a Sephadex G-75 column (4.0 × 110.0 cm), which was previously equilibrated and then eluted with the same buffer. Fractions of 5 ml/tube were collected at a flow rate of 30 ml/h.

Fraction SIII (200 mg) from the gel filtration step was dissolved in 3 ml of 0.1 M ammonium acetate buffer, pH 5.0, then cleared by centrifugation as before. Subsequently, this fraction was applied on a 3.0 × 60.0 cm column of SP-Sephadex C-25 with a continuous buffer concentration gradient up to 2.0 M at pH 5.0. Fractions of 5.0 ml were collected at 18 ml/h. Absorbance was monitored at 280 nm and conductivities were measured with a CD-20 (Digimed) conductimeter and converted to concentration values by means of a standard curve.

Pools were collected, dialyzed against water at 5 °C and lyophilized. When necessary, pooled fractions were rechromatographed under the same conditions. Samples of 1 mg were then dissolved in 0.05% (v/v) trifluoroacetic acid (TFA) and rechromatographed on a Shimadzu C_{18} reversed-phase (ODP-50) high performance liquid chromatography (RP-HPLC) column (6.0 × 15.0 cm). Elution followed a 0–100% (v/v) gradient of solvent A [0.05% TFA/acetonitrile (9:1)] and solvent B [0.05% TFA/acetonitrile (4:6) (v/v)] at a flow rate of 1.0 ml/min. All steps of the purification procedure were carried out at room temperature (25 °C).

2.3. Biochemical characterization

Polyacrylamide gel electrophoresis (PAGE) for acidic proteins and sodium dodecyl sulfate PAGE (SDS-PAGE) followed the methods of Davis [10] and Laemmli [11], respectively. Isoelectric focusing was performed according to Vesterberg [12]. Buffalyte, pH range 5.0–8.5 (Pierce), was used to generate the pH gradient. The following p*I* standards were used: methyl-red p*I* 3.8; trypsin inhibitor p*I* 4.6; myoglobin p*I* 6.8 and 7.2, lecithin p*I* 8.2, 8.6 and 8.8.

Sequencing of the N-terminal amino acid residues of the toxins was performed using an Applied Biosystem sequencer, model C 477A.

For protein determination, the micro-biuret method developed by Itzhaki and Gill [13] was followed.

2.4. Crystallization of SIIISPIIB

A lyophilized sample of SIIISPIIB was dissolved in bidistilled water at a concentration of 10 mg/ml. Crystallization was performed by the hanging-drop vapor diffusion method using 24 well tissue culture plates. Initial trials were carried out with a screen similar to the one described by Jancarik and Kim [14]. Typically, 1 µl drops of protein solution were mixed with an equal volume of the screening solution and equilibrated over 1 ml of the latter as reservoir solution. Large single crystals were obtained when a 2 µl protein droplet was mixed with an equal volume of reservoir solution consisting of 0.1 M sodium acetate (pH 4.6) and 28% polyethylene glycol (PEG) 4000.

2.4.1. X-ray diffraction data collection and structure determination

The crystals were flash frozen (15% glycerol) and diffraction data was collected at the Laboratório Nacional de Luz Síncroton (Campinas, Brazil). Diffraction intensities were measured using a MAR 345 imaging-plate detector and were reduced and processed using the HKL suite of programs [15]. The crystal diffracted X-rays to a maximum resolution of 1.8 Å. Data-processing statistics are presented in Table 2.

The crystal structure was solved by molecular replacement techniques using the atomic coordinates of the D49 PLA_2 from *Agkistron piscivorus piscivorus* (PDB code 1VAP) [16] and the program AmoRe [17]. Refinement was carried out using CNS [18] and REFMAC 5.0 as implemented in the CCP4 package [19]. Model building and map interpretation was performed using TurboFrodo.

2.5. Chemical modification

Modification of His48 with BPB from Sigma Chemical Company was carried out as previously described by Díaz-

Table 1
Enzymatic and biological activity of crude *B. jararacussu* venom and isolated acidic PLA_2 isoforms compared with myotoxins BthTX-I and -II

Sample	Activity							
	Indirect hemolytic (%) [a]		Catalytic (U/mg) [b]		Anticoagulant (min) [c]		Platelet aggregation inhibition (%) [d]	
	Native	Modified	Native	Modified	Native	Modified	Native	Modified
Crude venom	23.0	–	290.3	–	–	–	ND	ND
SIIISPIIA	–	–	279.0	–	21 min 10 s	–	–	–
SIIISPIIB	–	–	270.7	–	26 min 13 s	–	100	–
SIIISPIIIA	–	–	254.0	–	30 min 10 s	–	–	–
SIIISPIIIB	95.4	–	96.5	–	10 min 15 s	–	–	–
BthTX-I	–	ND	–	ND	>45 min	–	–	ND
BthTX-II	98.6	–	79.9	–	>45 min	–	–	ND

ND, not determined. –, no activity.
[a] Percentage hemolysis by 200 μg toxin incubated with rat erythrocytes (11 300 cells/ml).Control: 100% hemolysis, $A_{540\ nm} = 0.470$.
[b] Specific activity defined as μmol of acid released/min/mg of protein.
[c] To 250 μl of platelet poor plasma + 50 μl saline or toxin (1 mg/ml), incubated for 10 min at 37 °C, 50 μl of 0.25 M $CaCl_2$ were added and time for clotting was measured up to 45 min.
[d] Native and modified PLA_2s were assayed for inhibitory effect on ADP induced aggregation by 50 μg of PLA_2.

Table 2
Data collection and processing statistics

Space group	$C222_1$
Unit cell parameters (Å)	$a = 40.1$, $b = 54.2$ and $c = 90.7$
Maximum resolution (Å)	1.8
Resolution of data set (Å)	19.6–1.8
Number of observations	28 979
Number of unique reflections	8959
R_{merge} (%) [a]	4.9
Completeness (%) (1.85–1.79 Å)	92.9 (74.2)
V_M (Å^3/Da)	1.8
Number of molecules per asymmetric unit	1
Refinement *R*-factor (%)	16.1
Refinement *R*-free (%)	22.9
Bond length deviation (Å)	0.02
Bond angle deviation (°)	2.0

[a] $R_{merge} = \Sigma|I(h)i - \{I(h)\}|/\Sigma\{I(h)\}$; $I(h)$ is the observed intensity of the ι measurement of reflection h and $\iota\{I(h)\}$ is the mean intensity of reflection h calculated after scaling.

Oreiro and Gutiérrez [20]. Approximately 3 mg of the protein was dissolved in 1 ml of 0.1 M ammonium bicarbonate buffer containing 0.7 mM EDTA, pH 8.0, and then 150 μl of BPB (1.5 mg/ml ethanol) was added. The mixture was incubated for 24 h at 25 °C.

Excess reagent was removed from toxin preparations by chromatography on a Shimadzu C_{18} reversed-phase (CLC-ODS) RP-HPLC column (6.0 × 25.0 cm). Elution followed a 0–100% (v/v) gradient of solvent A (0.1% TFA, v/v) and solvent B (60% acetonitrile, v/v) at a flow rate of 1.0 ml/min, followed by lyophylization.

2.6. Phospholipase A_2 activity

Phospholipase A_2 activity was determined as described by de Haas et al. [21], at pH 8.0 and 25 °C, using a lecithin source of an emulsion of one chicken egg yolk/300 ml distilled water containing 3 mM sodium cholate and 6 mM calcium cholate. Fatty acids were potentiometrically titrated with 0.0818 N NaOH, using a Gilmont micro-biuret assembled with an expanded scale pH meter (Digimed). Phospholipase activity was expressed as the number of microequivalents of fatty acids released/min at 25 °C.

2.7. Hemolytic activity

Indirect hemolytic activity was assayed as described by Jeng et al. [22]. Red blood cells from freshly collected rat blood were used for the assays. Activity was expressed as percentage of hemolysis.

2.8. Anticoagulant activity

Sheep citrated plasma was centrifuged at 1000 × *g* at 4 °C and the anticoagulant effect was assessed as described by Gutiérrez et al. [23]. Subsequently, 0.25 ml aliquots of plasma were incubated with the toxins dissolved in phosphate buffered saline (PBS, pH 7.5) for 10 min at 37 °C. Then, 0.05 ml of a solution of 0.25 M $CaCl_2$ was added and the clotting time determined. Control tubes contained only PBS incubated plasma, while $CaCl_2$ was added as described above.

2.9. In vivo myotoxicity

Groups of five Swiss mice (25–30 g body weight) received an injection of 50 μg PLA_2/50 μl PBS, in the right gastrocnemius muscle. Three hours later, blood was collected from the inferior vena cava and centrifuged. The resulting plasma was submitted to creatine kinase (CK) assay.

Control animals received injections of PBS. Activity was expressed in U/l, 1 U defined as the amount of enzyme that produces 1 μmol of NADH/min at 30 °C.

2.10. In vitro myotoxicity

Swiss mice were sacrificed by cervical dislocation and the soleus muscle (red muscle) of each leg was immediately and

carefully removed. Using a previously described technique, the muscles were then fixed on an aluminum support by their tendons so that their resting length was maintained and the catabolic effect and alterations characteristic of anoxia occurring in central muscle fibers were prevented [24]. The Krebs–Ringer bicarbonate buffer incubation medium containing 0.120 mol/l NaCl; 0.025 mol/l $NaHCO_3$; 4.83 mol/l KCl; 1.2 mol/l $MgSO_4$; 1.2 mol/l KH_2PO_4 and 2.4 mol/l $CaCl_2$ was aerated for 20 min with 95% O_2–5% CO_2 (pH 7.3–7.4). The medium (3 ml) was then transferred to 25 ml Erlenmeyer flasks and the isolated muscles were added. This was followed by another 1-min aeration with 95% O_2–5% CO_2 in a water bath at 37 °C for 1 h under constant agitation.

After an 1-h equilibrium period, the medium was changed and the muscles were incubated for 2 h with either Krebs (control) or toxins (20 μg/ml). Following the incubation period, aliquots were refrigerated for 12 h for later CK activity determination.

2.11. Edema-inducing activity

Groups of five Swiss mice (18–22 g) received, in the subplantar region, injections of 50 μg/50 μl PBS containing either native or treated PLA_2. Control animals received PBS injections only. At 0.5, 1, 2, 4, 24 and 48 h, the progression of edema was evaluated with a low-pressure pachymeter (Mitutoyo, Japan).

The increase paw volume induced by PBS was considered as 0% and the edema induced by toxins at 30 min was considered as 100% in order to obtain the level of edematogenic activity inhibition after BPB treatment.

2.12. Platelet aggregation inhibition effect

The following experiments are identical to those carried out and described by Fuly et al. [25]. Platelet-rich plasma (PRP) was prepared from citrated human blood (0.31% w/v) by centrifugation (360 × *g* for 12 min) at room temperature. PRP samples obtained as above were centrifuged at 1370 × *g* for 20 min, and the platelet pellets were suspended in a calcium free Tyrode solution containing 0.35% (w/v) bovine serum albumin (BSA) and 0.1 mM EDTA (final concentration), pH 6.5, and washed twice by centrifugation (1370 × *g* for 20 min at 0 °C).

The final pellet was then suspended in Tyrode–BSA, pH 7.5, without EDTA. The suspension was adjusted to give 3–4 × 10^5 platelets/μl. Platelet aggregation was measured turbidimetrically using a whole blood Lumi-aggregometer (Chrono-log Corp.). Assays were performed at 37 °C in siliconized glass cuvettes using 400 μl of PRP with stirring, and aggregation was triggered after pre-incubation for 5 min with 50 μl (50 μg) of the acidic PLA_2 isoforms (native or modified). Control experiments were performed using platelets against ADP alone (50 μl).

Percentage of inhibition was evaluated considering the control ADP (50 μl) as 100% aggregation and control PRP (400 μl) as 0%.

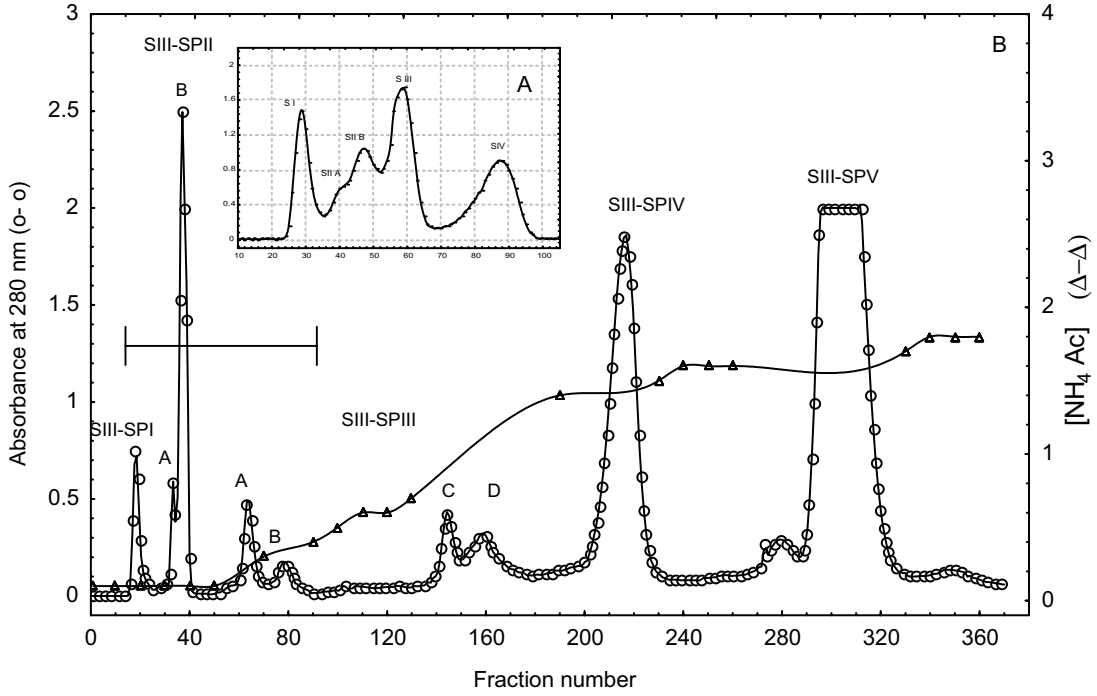

Fig. 1. (A) (Insert) Gel filtration of *B. jararacussu* venom (500 mg) on a 4 × 110 cm column of Sephadex G-75 equilibrated and eluted with 0.05 M ammonium bicarbonate buffer, pH 8.0, flow rate: 30 ml/h. (B) Ion-exchange chromatography of fraction SIII (200 mg) from the above column, on a 3 × 60 cm of SP-Sephadex C-25, previously equilibrated with 0.1 M, pH 5.0 ammonium acetate buffer and then eluted with a concentration gradient of the same buffer up to 2.0 M. Flow rate: 18 ml/h. Subfractions SIIISPIIA, SIIISPIIB, SIIISPIIIA and SIIISPIIIB were further purified by HPLC (not shown).

2.13. Statistical analysis

Results were expressed as the arithmetic mean ± standard deviation (S.D.). Differences between two groups in the same experiment were analyzed by the Student's *t*-test using the Statsoft statistic, version 4.5. The level of significance was $P < 0.05$.

3. Results

Fig. 1A (insert) presents the gel filtration profile of the crude venom on Sephadex G-75. Fraction SIII, which showed PLA_2 activity, was further fractionated into five subfractions on SP-Sephadex C-25 (Fig. 1B), which were designated SIIISPI through SIIISPV. In subfractions SIIISPIIA to SIIISPIIIB (horizontal bar), PLA_2 catalytic activity was detected. Subfractions SIIISPIIB and SIIISPIIIC were shown to be platelet aggregation inhibitors, while SIIISPIV and SIIISPV were identified as BthTX-II and BthTX-I, respectively, both known to be potent basic myotoxins [2,7,8]. Table 1 displays enzymatic and biological activity data related to the four isolated acidic PLA_2 isoforms compared with myotoxins BthTX-I and -II. Subfractions SIIISPIIA, SIIISPIIB and SIIISPIIIA showed very high PLA_2 catalytic activities when compared with BthTX-II, namely: 279.0, 270.7 and 254.0 versus 79.9 U/mg, respectively. The exception was SIIISPIIIB (96.5 U/mg).

In Fig. 2, PAGE and SDS-PAGE of SIII and the subsequent subfractions are presented. Evaluation of these subfractions was performed after re-purification by reverse phase chromatography on C_{18} HPLC column. All subfractions electrofocused at a pH of approximately 5.3. Their homogeneity was further demonstrated by native-PAGE (Fig. 2A), SDS-PAGE (Fig. 2B) and N-terminal sequencing (Table 3).

SIIISPIIB crystals belong to space group $C222_1$, with unit-cell parameters $a = 40.1$ Å, $b = 54.2$ Å and $c = 90.7$ Å. Assuming the presence of one molecule of SIIISPIIB in the asymmetric unit, a Matthews parameter value [26] of 1.8 Å^3/Da was obtained, with a corresponding solvent content of 30.6%. Processing of the 28 979 measured reflections led to 8959 unique reflections with an R_{merge} of 4.9% for the data to 1.8 Å resolution (Table 2). The crystallographic refinement converged to a residual of 16.1% ($R_{free} = 22.9\%$) with excellent stereochemistry (Table 2) and no outliers in the Ramachandran diagram. The structure presented in Fig. 3 where the disulfide bridges are drawn in thin lines demonstrates that this protein is a group IIa PLA_2 with Asp at position 49 which coordinates the bound calcium ion.

The corresponding N-terminal sequences are presented in Table 3. When compared with basic PLA_2s (BthTX-I and -II) from the same venom, the four isolated PLA_2s showed low myotoxic activity both in vivo and in vitro (Fig. 4A,B).

Compared to PBS-injected animals, those which received subplantar injections of the native PLA_2s (50 μg/paw) presented marked paw edema, with no visible hemorrhage

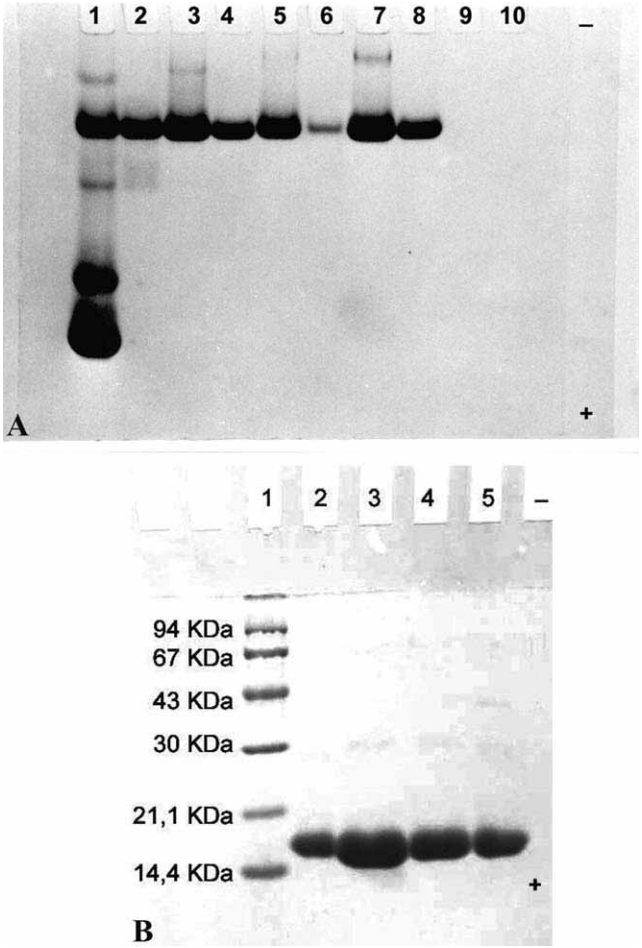

Fig. 2. (A) PAGE for acidic proteins on a 10% (w/v) gel, pH 8.3, 15 mA, 87 V for 3 h 10 min. Lane (1) SIII; (2) SIIISPIIA–HPLC; (3) SIIISPIIB; (4) SIIISPIIB–HPLC; (5) SIIISPIIIA; (6) SIIISPIIIA–HPLC; (7) SIIISPIIIB; (8) SIIISPIIIB–HPLC. Staining was performed with 0.2% (w/w) Coomassie brilliant blue R-250 and destaining with 7% (v/v) acetic acid. (B) SDS-PAGE on a 13.5% (w/v) gel polyacrylamide, containing 0.1% SDS. Lane (1) Mr markers (phosphorylase b, 94 000; BSA 67 000; ovalbumin 43 000; carbonic anhydrase 30 000; soybean trypsin inhibitor 20 100; α-lactalbumin 14 400). (2) SIIISPIIA; (3) SIIISPIIB; (4) SIIISPIIIA; (5) SIIISPIIIB. Approximate Mr of the isolated toxins was 15 000.

(Fig. 5). Maximal response was attained 30 min after injection and receded to normal levels after 4 h, with exception of SIIISPIIB, whose response returned to normal levels after 48 h.

The results obtained with 50 μg/paw demonstrated that, 30 min after administration, SIIISPIIA, SIIISPIIB, SIIISPIIIA and SIIISPIIIB induced edema of 29.91%, 80.89%, 29.91% and 34.58%, respectively. After alkylation of His 48 with BPB, there was a reduction of edema: for SIIISPIIA (29.91–23.11%); for SIIISPIIB (80.89–39.30%); for SIIISPIIIA (29.91–15.11%) and for SIIISPIIIB (34.58–27.79%).

All of the PLA_2 isoforms (with the exception of SIIISPIIIB) exhibited high PLA_2 specific activity and low anticoagulant activity on platelet-poor plasma. In addition, none (with exception of SIIISPIIIB) revealed any indirect hemolytic activity. SIIISPIIB (50 μg/ml) inhibited 100% of

Table 3
Amino terminal protein sequence of PLA_2 acidic isoforms from *B. jararacussu* venom and comparison with PLA_2 and myotoxins from various sources

PLA_2	N-terminal sequence																			
	1									10			↓							20
SIIISPIIA [a]	S	L	W	Q	F	G	K	M	I	D	Y	V	M	G	E	E	G	A	K	S
SIIISPIIB [a]	S	L	W	Q	F	G	K	M	I	F	Y	T	G	K	N	E	P	V	L	S
SIIISPIIIA [a]	S	L	W	Q	F	G	K	M	I	L	Y	V	M	G	G	E	G	V	K	Q
SIIISPIIIB [a]	S	L	W	Q	F	G	K	M	I	F	Y	E	M	T	G	E	G	V	L	
BthTX-I	S	L	F	E	L	G	K	M	I	L	Q	E	T	G	K	N	P	A	K	S
BthTX-II	D	L	W	Q	W	G	Q	M	I	L	K	E	Y	G	K	L	P	F	P	Y
(a)	G	L	W	Q	F	E	N	M	I	I	K	V	V	K	K	S	G	I	L	S
(b)	G	L	W	Q	F	E	N	M	I	I	K	V	V	K	K	S	G	I	L	S
(c)	G	L	W	Q	F	E	N	M	I	I	K	V	V	K	K	S	G	I	L	S
LM-PLA_2-I	H	L	L	Q	F	E	Q	L	I	R	K	I	A	G	R	G	F	R	Y	Y
LM-PLA_2-II	H	L	L	Q	F	G	D	L	I	D	K	I	I	A	G	R	S	G	F	W

BthTX-I and -II: *B. jararacussu* myotoxins I and II. (a, b, c): *Trimeresurus flavoviridis* isoforms of PLA_2s. LM-PLA_2-I and -II: PLA_2 isoenzymes isolated from *Lachesis muta* snake venom [35] and platelet aggregation inhibitors. Note: For homology studies, it is usual to introduce a gap between residues 13 and 14 (arrow). Therefore, numbering from this point is one unit higher and the last residue becomes 21.
[a] N-terminal sequence of PLA_2 acidic isoforms as determined in this work.

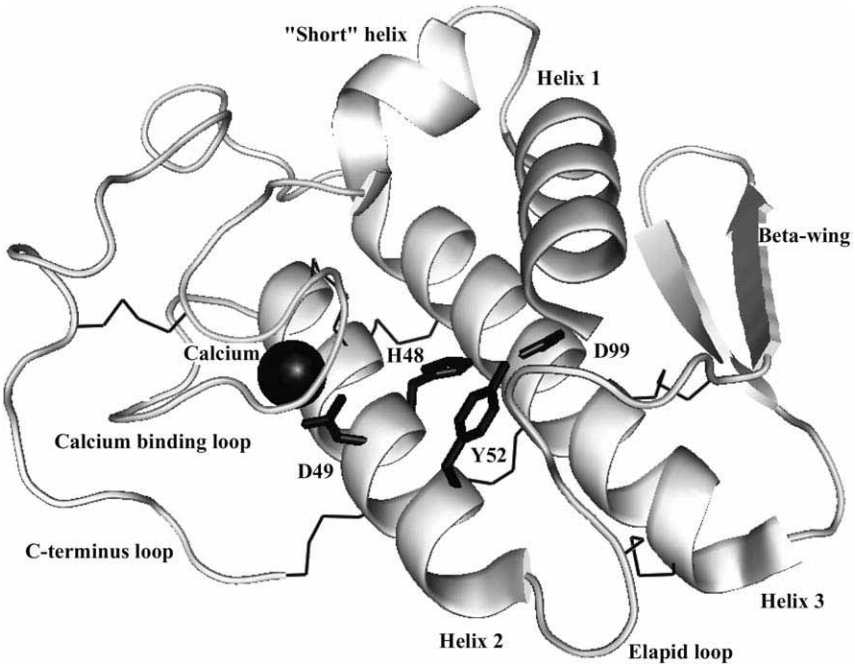

Fig. 3. Ribbon representation of the structure of *B. jararacussu* SIIISPIIB. The amino acids considered important for catalysis and calcium ion binding (H48, D49, Y52 and D99) are included. The large gray sphere represents the calcium ion. The disulfide bonds are drawn as thin lines.

ADP-induced platelet aggregation. After alkylation with BPB, no catalytic activity or indirect hemolytic activity was observed in any of the four isolated PLA_2s (Table 1).

4. Discussion

A previous study has shown that the occurrence of multiple PLA_2 isoforms in snake venom is a common event [27]. This article reports the purification of four acidic PLA_2s isoforms, isolated from *B. jararacussu* venom using a combination of gel filtration, ion-exchange chromatography and HPLC. Evidence pointing to the presence of isoforms is supported by high similarities in N-terminal sequences (20 first aminoacid residues), molecular masses and p*I*s, although significant differences were detected in their pharmacological activities. Differences related to the chromatographic behavior may be partially due to variances in the distribution of aromatic residues on the isoform surfaces [28] as well as probable extra charges provided by differences in aminoacid composition.

Venom PLA_2s usually show indirect hemolytic activity because they promote hydrolysis of lecithins to lysolecithins able to lyze red blood cell membranes. Only SIIISPIIIB revealed indirect hemolytic activity, although its catalytic

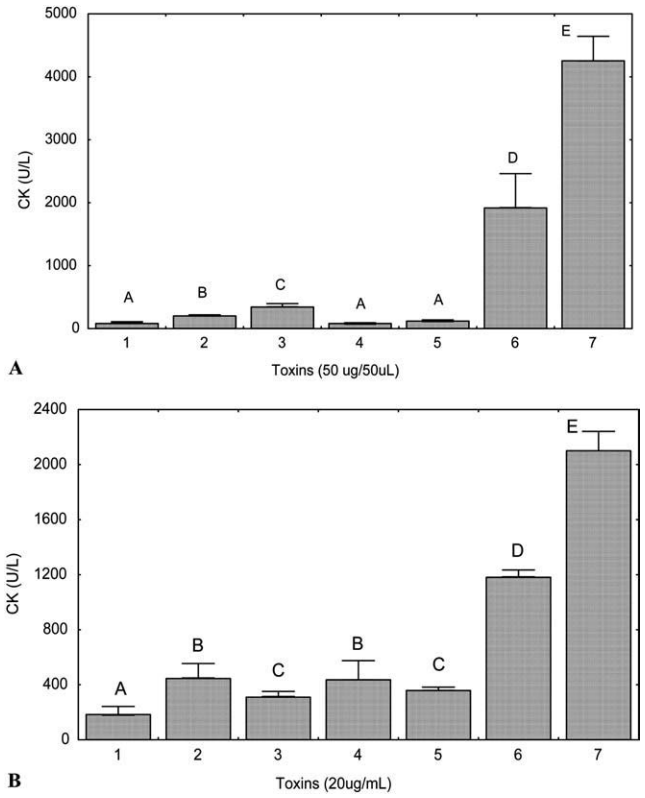

Fig. 4. Determination of blood plasma levels of CK released by PLA_2s. (A) In vivo assay, i.m., 50 μg PLA_2/30 g body weight in 50 μl PBS, 3 h after injection. 1, PBS; 2, SIIISPIIA; 3, SIIISPIIB; 4, SIIISPIIIA; 5, SIIISPIIIB; 6, BthTX-I; 7, BthTX-II. Control animals received buffer alone. (B) In vitro assay in soleus muscle incubated with 20 μg PLA_2/ml for 2 h. Same letters were used for statistically equal groups ($P < 0.05$). (1) Krebs; (2) SIIISPIIA; (3) SIIISPIIB; (4) SIIISPIIIA; (5) SIIISPIIIB; (6) BthTX-I; (7) BthTX-II.

activity was relatively low. Lack of direct hemolytic activity (not shown) is probably due to the inability of SIIISPIIIB to hydrolyze erythrocyte membrane phospholipids. The fact that SIIISPIIA, SIIISPIIB and SIIISPIIIA show high PLA_2 activity upon artificial substrates, although deprived of indirect hemolytic activity, suggests that phospholipids were not hydrolyzed. Therefore, catalytic activity upon artificial substrates is apparently not correlated with indirect hemolytic activity.

In order to confirm this hypothesis, we assayed BthTX-I and -II for indirect hemolytic activity. No catalytic or hemolytic activity was observed in BthTX-I, thus simulating an eventual dependence, but BthTX-II presented high hemolytic activity and low catalytic activity, both of them approximating those of SIIISPIIIB.

The four isolated PLA_2s showed low myotoxic activity, both in vivo and in vitro. Once again, this effect was not correlated with the observed high catalytic activity. This observation favors the hypothesis that myotoxicity is an indirect consequence of the perturbing action of PLA_2s, which leads to increased permeability to Ca^{2+} ions and activation of extracellular proteases. This could explain why *B. jararacussu* acidic PLA_2s are less myotoxic than basic PLA_2s (BthTX-I and -II) although much more active on artificial phospholipids. Acidic PLA_2s are, as a rule, less myotoxic despite being enzymatically more active than basic PLA_2s [29].

The four isolated PLA_2s also induced edema, an activity known to be characteristic of other venom PLA_2s [30–32]. Development of edema is a common feature of the cutaneous inflammatory response and is dependent on a synergism between mediators that increase vascular permeability and those that increase blood flow. This activity was time-dependent and the most active were SIIISPIIB and SIIISPIIIB (the least catalytically active), suggesting that this effect is again not correlated with catalytic activity. This observation was confirmed by alkylation of His from the active site, which completely suppressed PLA_2 activity with no significant change in the edema-inducing effect. Since these four PLA_2s showed low myotoxic activity, the possibility that edema appears in response to muscle fiber necrosis seems improbable.

Daniele et al. [32] demonstrated that the inflammatory response elicited by P3, one of the PLA_2 isoforms from *B. neuwiedi* venom, involves release of heparin and histamine from mast cells. Heparin is known to interact in a non-covalent way with basic PLA_2s, provoking inhibition of their enzymatic and biological activities, such as that caused by bee venom or myotoxin II, a K49 PLA_2 from *B. asper*, or even by a neutral pancreatic PLA_2 [33]. Since this is a charge rather than a covalent type of interaction, it is not surprising that acidic PLA_2s lack this ability to be complexed by an acidic polysaccharide such as heparin and this fact may, at least in part, explain why acidic PLA_2s have higher levels of catalytic activity.

In addition to the potential role that snake venom PLA_2 enzymes play in the digestion of prey, they exhibit a wide variety of pharmacological effects, including platelet aggregation.

Several platelet aggregation inhibitors have been purified and characterized from the venom of various snakes, but data on *Bothrops* snake venom with respect to platelet aggregation inhibitors are still scant. The acidic PLA_2 SIIISPIIB is a new antiplatelet agent. Its N-terminal sequence analysis showed substitutions in the hydrophobic channel where Trp18 (which is also reported to be part of the interfacial binding surface) is replaced by a Val18 residue [34]. A comparison of the N-terminal sequence of SIIISPIIB with other snake venom class II PLA_2s exhibiting platelet-inhibiting activity showed a moderate degree of similarity (68–72%).

In conclusion, isolation and N-terminal sequencing of, four acidic PLA_2s homologues from *B. jararacussu* snake venom, in addition to the evaluation of their catalytic, indirect hemolytic, edema inducing, anticoagulant and myotoxic activities, made their partial characterization possible. These results show that neither the hemolytic nor the myotoxic effects can be correlated with the catalytic activity.

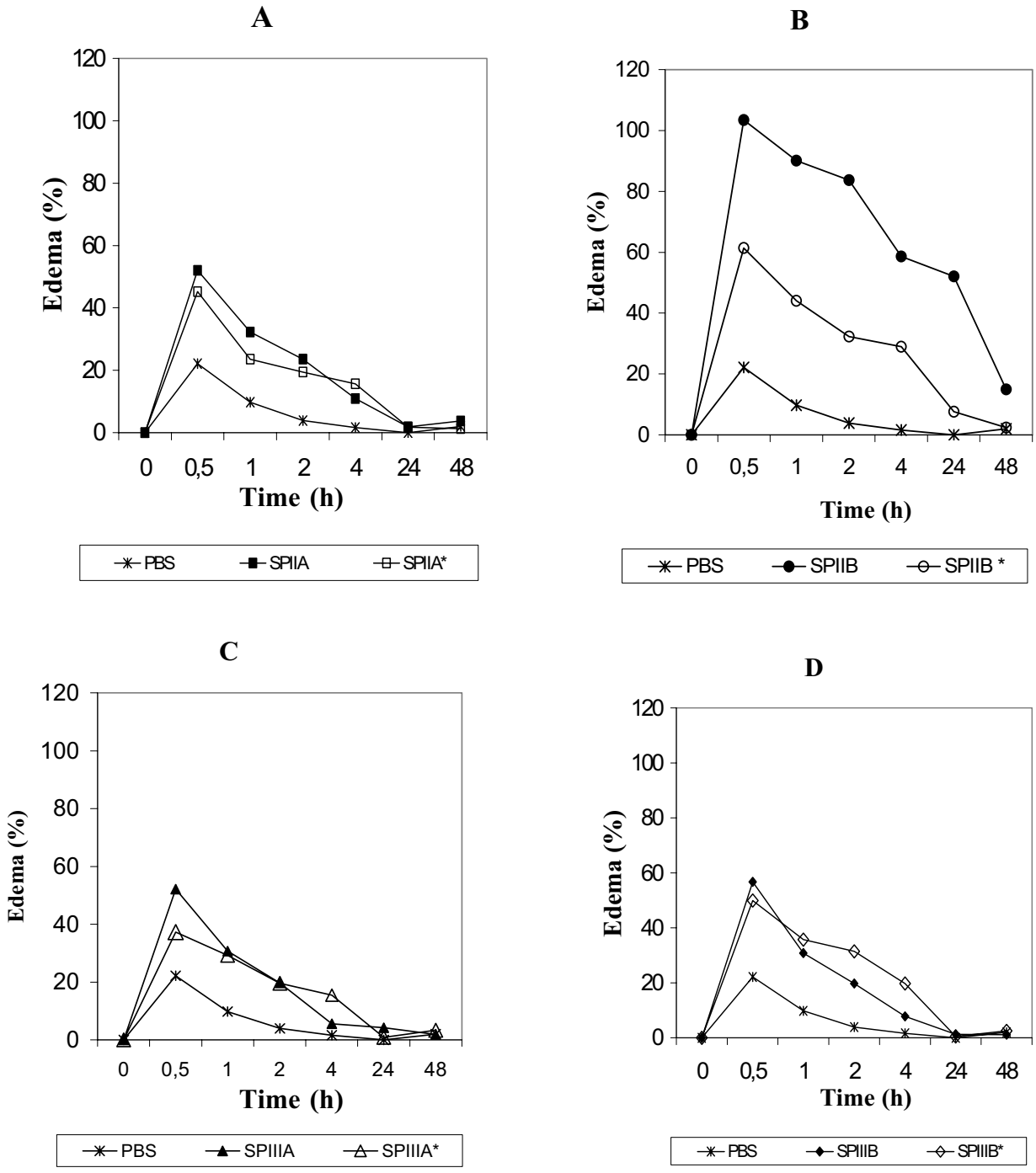

Fig. 5. Time-course of paw edema induced by PLA_2s in 18–22 g male Swiss mice. PBS was used as a control. Each bar represents median values for five mice. SIIISPIIA*, SIIISPIIB*, SIIISPIIIA* and SIIISPIIIB* represent the modified toxins. (A) Edema induced by native (⫆̸) or modified (□) SIIISPIIA, (B) edema induced by native (●) or modified (○) SIIISPIIB, (C) edema induced by native (▲) or modified (△) SIIISPIIIA and (D) edema induced by native (◆) or modified (◇) SIIISPIIIB.

Acknowledgements

The authors wish to express their gratitude to FAPESP and CNPq for their financial support, to Ingrid Ferreira Metzger, Flávia Bonfietti Izidoro and João José Franco for their helpful technical assistance and to Professor E.C. Arantes for carrying out the p*I* determination.

References

[1] E.A. Dennis, Diversity of groups types, regulation and function of phospholipases A_2, J. Biol. Chem. 269 (1994) 13057–13060.

[2] M.I. Homsi-Brandeburgo, L.S. Queiroz, H. Santo-Neto, L. Rodrigues-Simioni, J.R. Giglio, Fractionation of *Bothrops jararacussu* snake venom: partial chemical characterization and biological activity of bothropstoxin, Toxicon 26 (1988) 615–627.

[3] D. Mebs, C.L. Ownby, Myotoxic components of snake venoms their biochemical and biological activities, Pharm. Ther. 48 (1990) 223–236.

[4] J.M. Gutiérrez, B. Lomonte, Phospholipase A_2 myotoxins from *Bothrops* snake venoms, in: R.M. Kini (Ed.), Venom Phospholipases A_2 Enzymes, Structure, Function and Mechanism, Wiley, Chichester, 1997, pp. 321–352.

[5] B. Lomonte, Y. Angulo, S. Rufini, W.W. Cho, J.R. Giglio, M. Ohno, J.J. Daniele, P. Georghegan, J.M. Gutiérrez, Comparative study of the cytolytic activity of myotoxic phospholipases A_2 on mouse endothelial (tend) and skeletal muscle (C_2C_{12}) cells in vitro, Toxicon 37 (1999) 145–158.

[6] T. Fukagawa, T. Nose, J. Shimohigashi, T. Ogawa, N. Oda, K. Nakashima, C. Chang, M. Ohno, Purification sequencing and characterization of single amino acid substituted phospholipase A_2 isoenzymes from *Trimeresurus gramineus* (green habu snake) venom, Toxicon 31 (1993) 957–967.

[7] A.C.O. Cintra, S. Marangoni, B. Oliveira, J.R. Giglio, Bothropstoxin-I: amino acid sequence and function, J. Protein Chem. 12 (1993) 57–64.

[8] M.F. Pereira, J.C. Novelho, E.T. Landucci, J.R. Giglio, A.C.O. Cintra, B. Oliveira, S. Marangoni, The amino acid sequence of bothropstoxin-II, an Asp_{49} myotoxin from *Bothrops jararacussu* snake venoms, J. Protein Chem. 17 (1998) 381–386.

[9] S.H. Andrião-Escarso, A.M. Soares, M.R.M. Fontes, A.L. Fuly, F.M.A. Corrêa, J.C. Rosa, L.J. Greene, J.R. Giglio, Structural and functional characterization of an acidic platelet aggregation inhibitor and hypotensive phospholipase A_a from *Bothrops jararacussu* snake venom, Biochem. Pharmacol. 64 (2002) 723–732.

[10] B.J. Davis, Disc electrophoresis II. Method and application to human serum proteins, Ann. N. Y. Acad. Sci. 121 (1964) 404.

[11] U.K. Laemmli, Cleavage of structural proteins during the assembly of the head of bacteriophage T_4, Nature 227 (1970) 680–685.

[12] O. Vesterberg, Isoelectric focusing of protein, Biophys. Acta 257 (1972) 11–19.

[13] R.F. Itzhaki, D.M. Gill, A micro-biuret method for estimating proteins, Anal. Biochem. 9 (1964) 401–410.

[14] J. Jancarik, S.H. Kim, Sparse matrix sampling: a screening method for crystallization of proteins, J. Appl. Crystallogr. 24 (1991) 409–411.

[15] Z. Otwinowski, W. Minor, Processing of X-ray diffraction data collected in oscillation mode, Methods Enzymol. 276 (1997) 307–326.

[16] S.K. Han, E.T. Yoon, D.L. Scott, P.B. Sigler, W. Cho, Structural aspects of interfacial adsorption. A crystallographic and site-directed mutagenesis study of the phospholipase A2 from the venom of *Agkistrodon piscivorus piscivorus*, J. Biol. Chem. 272 (1997) 3573–3582.

[17] J. Navaza, AmoRe: an automated package for molecular replacement, Acta Crystallogr. 50 A (1994) 157–163.

[18] A.T. Brünger, P.D. Adams, L.M. Rice, Recent developments for the efficient crystallographic refinement of macromolecular structures, Curr. Opin. Struct. Biol. 8 (1998) 606–611.

[19] Collaborative Computational Project Member 4, The CCP4 suite: programs for protein crystallography, Acta Crystallogr. D50 (1994) 760–763.

[20] C. Díaz-Oreiro, J.M. Gutiérrez, Chemical modification of histidine and lysine residues of myotoxic phospholipases A_2 isolated from *Bothrops asper* and *Bothrops godmani* snake venoms, Toxicon 35 (1997) 241–252.

[21] G.H. de Haas, N.M. Postema, W. Nieuwenhuizen, L.L.M. Van Deenen, Purification and properties of phospholipase A from porcine pancreas, Biochem. Biophys. Acta 159 (1968) 103.

[22] T.W. Jeng, R.A. Hendon, H. Fraenkel-Conrat, Search for relationships among the hemolytic, phospholytic and neurotoxin activities of snake venoms, Proc. Natl. Acad. Sci. USA 75 (1978) 600.

[23] J.M. Gutiérrez, B. Lomonte, L. Cerdas, Isolation and partial characterization of a myotoxin from the venom of the snake *Bothrops nummifer*, Toxicon 24 (1986) 885–894.

[24] I.C. Kettelhut, S.W. Simon, A.L. Goldberg, Endocrine regulation of protein breakdown in skeletal muscle, Diabetes 8 (1988) 751–772.

[25] A.L. Fuly, O.L.T. Machado, E.W. Alves, C.R. Carlini, Mechanism of inhibitory action on platelet activation of a phospholipase A_2 isolated from *Lachesis muta* (Bushmaster snake) venom, Thromb. Haemost 78 (1997) 1372–1380.

[26] B.W. Matthews, Solvent content of protein crystals, J. Mol. Biol. 33 (1968) 491–497.

[27] F.F. Davidson, E.A. Dennis, Structure, function and mode of action of snake venom and other phospholipase A_2s, in: A.T. Tu (Ed.), Handbook of Natural Toxins, Peptide Venom, Toxins, vol. 5, Marcel Dekker, New York, 1991, pp. 107–145.

[28] J.J. Daniele, I.D. Bianco, C. Delgado, D. Briones Carrillo, G.D. Fidelio, A new phospholipase A_2 isoform isolated from *Bothrops neuwiedii* (jarara chica) venom with novel kinetic and chromatographic properties, Toxicon 35 (1997) 1205–1215.

[29] D. Rosemberg, The relationship between enzymatic activity and pharmacological properties of phospholipases in natural poisons, in: J.B. Harris (Ed.), Natural Toxins Animal, Plant and Microbial, Oxford Science Publications, Oxford, 1986, pp. 129–174.

[30] H.S. Selistre, L.S. Queiroz, O.A.B. Cunha, G.E.P. Desbuz, J.R. Giglio, Isolation and characterization of hemorrhagic, myonecrotic and edema-inducing toxins from *Bothrops insularis* (jaraca ilhoa) snake venom, Toxicon 28 (1990) 261–273.

[31] K. Kemparaju, B.N. Prasad, T.U. Gowda, Purification of a basic phospholipase A_2 from Indian saw-scaled viper (*Echis carinatus*) venom: characterization of antigenic, catalytic and pharmacological properties, Toxicon 32 (1994) 1187–1196.

[32] J.J. Daniele, I.D. Bianco, G.D. Fidelio, Kinetic and pharmacologic characterization of phospholipases A_2 from *Bothrops neuwiedii* venom, Arch. Biochem. Biophys. 318 (1995) 65–70.

[33] B. Lomonte, A. Tarkowishi, U. Bagge, L.A. Hanson, Neutralization of the cytolitic and myotoxic activities of phospholipases A_2 from *Bothrops asper* snake venom by glycosaminoglycans of the heparin/heparan sulfate family, Biochem. Pharmacol. 47 (1994) 1509–1518.

[34] D.L. Scott, S.P. While, Z. Otwinowski, W. Yuan, M.H. Gelb, P.B. Sigler, Interfacial catalysis: the mechanism of phospholipase A_2, Science 250 (1990) 1541–1546.

[35] A.L. Fuly, A.L.P. de Miranda, R.B. Zingali, J.A. Guimarães, Purification and characterization of a phospholipase A_2 isoenzyme isolated from *Lachesis muta* snake venom, Biochem. Pharmacol. 63 (2002) 1589–1597.

Available online at www.sciencedirect.com
SCIENCE DIRECT
Biochimica et Biophysica Acta 1703 (2004) 79–81
BIOCHIMICA ET BIOPHYSICA ACTA BBA
http://www.elsevier.com/locate/bba

Short crystallization paper

Crystallization and high-resolution X-ray diffraction data collection of an Asp49 PLA_2 from *Bothrops jararacussu* venom both in the presence and absence of Ca^{2+} ions

Mário T. Murakami[a], Simone Michelan-Duarte[a], Adélia C.O. Cintra[b], Raghuvir K. Arni[a,*]

[a]*Departamento de Física, IBILCE, Universidade Estadual Paulista, R. Cristóvão Colombo 2265, Nazareth, CEP 15054-000, São José do Rio Preto, SP, Brazil*
[b]*Departamento de Análises Clínicas, Toxicológicas e Bromatológicas, Faculdade de Ciências Farmacêuticas, Universidade de São Paulo, Ribeirão Preto, SP, Brazil*

Received 18 June 2004; received in revised form 13 August 2004; accepted 18 August 2004
Available online 9 September 2004

Abstract

Snake venom PLA_2s have been extensively studied due to their role in mediating and disrupting physiological processes such as coagulation, platelet aggregation and myotoxicity. The Ca^{2+} ion bound to the putative calcium-binding loop is essential for hydrolytic activity. We report the crystallization in the presence and absence of Ca^{2+} and X-ray diffraction data collection at 1.60 Å (with Ca^{2+}) and 1.36 Å (without Ca^{2+}) of an Asp49 PLA_2 from *Bothrops jararacussu* venom. The crystals belong to orthorhombic space group $C222_1$. Initial refinement and electron density analysis indicate significant conformational changes upon Ca^{2+} binding.

Keywords: Calcium-binding loop; Asp49 PLA_2; Crystallization; X-ray diffraction

Class II snake venom PLA_2s have been the focus of research due to their important role in several pharmacological effects such as anticoagulant, hypotensive, haemolytic, platelet aggregation, convulsant, myotoxic, neurotoxic and oedema-inducing effects [1,2]. Class II PLA_2s can be subdivided in two groups based on their activity: (i) Asp49 PLA_2s, which specifically hydrolyze the *sn*-2 ester bond of phospholipids releasing lysophospholipids and fatty acids [3], and (ii) natural Lys49 PLA_2s mutants, which display low or no apparent hydrolytic activity. Calcium is an essential cofactor in Asp49 PLA_2s and residues 26–34 and 49 form the calcium-binding loop. Amino acids Tyr28, Gly30, Gly32 and Asp49, which are directly involved in calcium binding, are highly conserved in PLA_2s [4–6]. Substitutions of Ca^{2+} for other divalent ions such as Mg^{2+}, Sr^{2+} and Ba^{2+} cause a decrease in PLA_2 activity [7]. These results indicate that the binding of Ca^{2+} to PLA_2s induces a conformational change at the active and substrate-binding sites [8,9]. However, the smaller atomic radius of Mg^{2+} or the larger atomic radius of Sr^{2+} and Ba^{2+} could result in a significantly altered conformation of this region, thus modifying the binding of phospholipids to PLA_2s [7]. Structural analysis of the same Asp49 PLA_2 in the presence and absence of Ca^{2+} should be extremely useful in clarifying the conformational changes in the catalytic site induced upon Ca^{2+} ion binding. We report the crystallization of an acidic isoform (p*I*=5.3) of an Asp49 PLA_2 from *Bothrops jararacussu* venom in the presence and absence (with EDTA) of Ca^{2+} and the preliminary high resolution X-ray diffraction analysis.

A lyophilized sample was dissolved in 20 mM Tris–HCl (pH 8.0) at 10 mg ml^{-1}. The protein was crystallized by the hanging-drop vapor diffusion method at 18 °C. Small crystals appeared in the initials crystallization trials with the well solution containing 30% (w/v) PEG4000, 0.1 M

* Corresponding author. Tel.: +55 17 221 2247; fax: +55 17 221 2247.
E-mail address: arni@df.ibilce.unesp.br (R.K. Arni).

1570-9639/$ - see front matter © 2004 Elsevier B.V. All rights reserved.
doi:10.1016/j.bbapap.2004.08.008

Tris–HCl (pH 8.0), 0.2 M $CaCl_2$. Significant improvement in the crystal quality was obtained by lowering the molecular weight of the precipitant to PEG3350. The best crystals were obtained from a solution containing 25% (w/v) PEG3350, 100 mM Tris–HCl (pH 8.0), 200 mM $CaCl_2$ (Fig. 1). The crystals grew to maximum dimensions of 0.1–0.2 mm within 3 days. Calcium-free crystals were obtained when $CaCl_2$ was substituted by NaCl and 5 mM EDTA was included in the well solution.

The diffraction data were collected at a synchrotron source (Laboratório Nacional de Luz Síncrotron, Brazil) where the wavelength was set to 1.427 Å. Diffraction intensities were recorded at 100 K using a MAR CCD detector. X-ray diffraction data were collected at 1.6 Å (with Ca^{2+}) and at 1.36 Å (Ca^{2+}-free). Data were processed and scaled with the programs DENZO and SCALEPACK [10]. The crystals belong to the orthorhombic space group $C222_1$ with unit cell dimensions a=39.09, b=53.05 and c=89.79 Å (with Ca^{2+}) and a=39.61, b=53.21 and c=88.99 Å (Ca^{2+}-free). The asymmetric unit contains one molecule corresponding to a V_M [11] of 1.7 $Å^3$ Da^{-1} (solvent content of 26.0%) in the presence of Ca^{2+} and 1.7 $Å^3$ Da^{-1} (solvent content of 25.4%) in the absence of Ca^{2+}. The crystallographic parameters and data processing statistics are summarized in Table 1. The crystal structures of this acidic isoform of an Asp49 PLA_2 were determined by molecular replacement with the program AMoRe [12] and using the atomic coordinates of the hypotensive PLA_2 from *B. jararacussu* (Murakami et al., unpublished data, PDB code 1UMR) as a search model. The rotation and translation functions indicated the clear orientation of the molecules in the asymmetric units. The positioning of the molecules was improved by rigid body refinement that resulted in correlation coefficients of 81.2 (80.4, Ca^{2+}-free) and R_{factor} 28.4% (29.5%, Ca^{2+}-free) for data between 30.0 and 1.6 Å (30.0 and 1.36 Å, without Ca^{2+}). The crystallographic refinement of both the structures is currently in progress. The results of this study should provide detailed information of the conformational changes induced upon Ca^{2+} ion binding in Asp49 PLA_2s.

Table 1
X-ray data collection and processing statistics

Isoform acidic PLA_2	Presence of Ca^{2+}	Absence of Ca^{2+}
Data collection		
Temperature (K)	100	100
Wavelength used (Å)	1.427	1.427
Detector	MARCCD	MARCCD
Space group	$C222_1$	$C222_1$
Unit cell parameters (Å)	a=39.09, b=53.05 and c=89.79	a=39.61, b=53.21 and c=88.99
Resolution range (Å)	30.00–1.60	30.00–1.36
No. of observed reflections	85,819	215,134
Data completeness (%)	99.4 (98.4)	97.9 (95.7)
No. of unique reflections	12,658	20,197
I/sigma(I)	29.1 (3.3)	21.05 (6.4)
R_{merge} (%)[a]	4.3 (37.9)	7.3 (28.1)
Molecule per asymmetric unit	1	1
V_M ($Å^3$ Da^{-1})	1.7	1.7
Solvent content (%)	25.4	26.0

Values in parentheses are for the high-resolution bin.

[a] $R_{merge}=\Sigma(\Sigma|I(h)_i-\{I(h)\}|)/\Sigma\{I(h)\}$, where $I(h)_i$ is the observed intensity of the ith measurement of reflection h and $\{I(h)\}$ is the mean intensity of reflection h calculated after scaling.

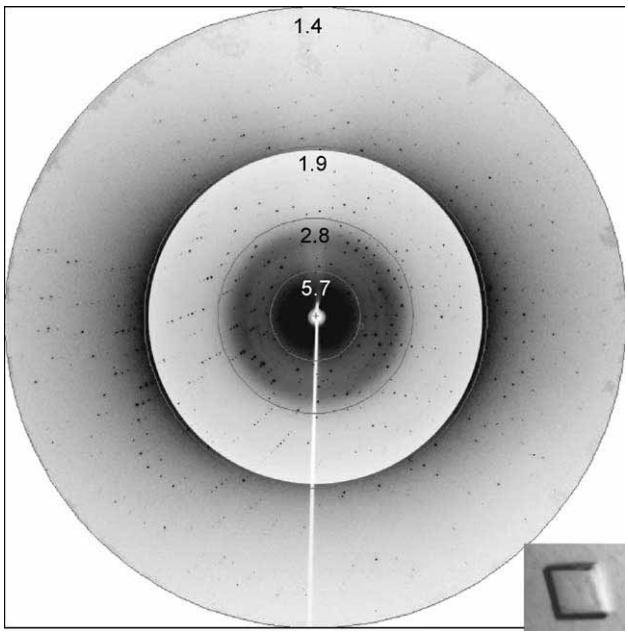

Fig. 1. X-ray diffraction pattern of the calcium-free crystal; inner and outer patterns on different intensity scales represent the low-resolution and high-resolution diffractions (inset: photomicrography of the crystal).

Acknowledgements

Financial support by FAPESP/SMOLBNet, CNPq, CAPES/DAAD is gratefully acknowledged. MTM is recipient of a FAPESP fellowship.

References

[1] J.B. Harris, Phospholipases in snake venoms and their effects on nerve and muscle, in: A.L. Harvey (Ed.), Snake Toxins, Pergamon Press, New York, 1991, pp. 91–121.
[2] A.B. Mukherjee, L. Miele, N. Pattabiraman, Phospholipase A_2 enzymes: regulation and physiological role, Biochem. Pharmacol. 48 (1994) 1–10.
[3] L.L.M. van Deenen, G.H. Haas, The substrate specificity of phospholipse A2, Biochem. Biophys. Acta 70 (1963) 538–553.
[4] B.W. Dijkstra, K.H. Kalk, W.G.J. Hol, J. Drenth, Structure of bovine pancreatic phospholipase A2 at 1.7Å resolution, J. Mol. Biol. 147 (1981) 97–123.
[5] D.L. Scott, S.P. White, Z. Otwinowski, W. Yuan, M.H. Gelb, P.B. Sigler, Interfacial catalysis: the mechanism of phospholipase A2, Science 250 (1990) 1541–1546.
[6] S.P. White, D.L. Scott, Z. Otwinowski, M.H. Gelb, P.B. Sigler, Crystal structure of cobra-venom phospholipase A2 in a complex with a transition-state analogue, Science 250 (1990) 1560–1563.

[7] L.S. Chang, S.R. Lin, C.C. Chang, The essentiality of calcium ion in the enzymatic activity of Taiwan cobra phospholipase A2, J. Protein Chem. 15 (1996) 701–707.
[8] D.N. Georgieva, C. Betzel, B. Aleksiev, N. Genov, Spectroscopic investigation of calcium binding sites in the neurotoxin vipoxin and its components—relation with the X-ray structure, Spectrochim. Acta, A Mol. Biomol. Spectrosc. 56 (2000) 2811–2816.
[9] D.N. Georgieva, N. Genov, K. Hristov, K. Dierks, C. Betzel, Interactions of the neurotoxin vipoxin in solution studied by dynamic light scattering, Biophys. J. 86 (2004) 461–466.
[10] Z. Otwinowski, W. Minor, Processing of X-ray diffraction data collected in oscillation mode, Methods Enzymol. 276 (1997) 307–326.
[11] B.W. Matthews, Solvent content of protein crystals, J. Mol. Biol. 33 (1968) 491–497.
[12] J. Navaza, AmoRe: an automated package for molecular replacement, Acta Crystallogr. A50 (1994) 157–163.

Available online at www.sciencedirect.com
SCIENCE DIRECT
Biochimica et Biophysica Acta 1703 (2004) 83–85
BIOCHIMICA ET BIOPHYSICA ACTA BBA
http://www.elsevier.com/locate/bba

Short crystallization paper

Crystallization and preliminary X-ray diffraction analysis of suramin, a highly charged polysulfonated napthylurea, complexed with a myotoxic PLA_2 from *Bothrops asper* venom

Mário T. Murakami[a], Lisandra M. Gava[a], Sandro P. Zela[a], Emerson Z. Arruda[b], Paulo A. Melo[b], José M. Gutierrez[c], Raghuvir K. Arni[a,*]

[a]*Departamento de Física, IBILCE, Universidade Estadual Paulista, Cristóvão Colombo, 2265, Nazareth, 15054-000, São José do Rio Preto, SP, Brazil*
[b]*Departamento de Farmacologia Básica e Clínica, IBC, Universidade Federal do Rio de Janeiro, Rio de Janeiro, RJ, Brazil*
[c]*Instituto Clodomiro Picado, Facultad de Microbiología, Escuela de Medicina, Universidad de Costa Rica, San José, Costa Rica*

Received 18 June 2004; received in revised form 13 August 2004; accepted 18 August 2004
Available online 9 September 2004

Abstract

Suramin is a highly charged polysulfonated napthylurea that interferes in a number of physiologically relevant processes such as myotoxicity, blood coagulation and several kinds of cancers. This synthetic compound was complexed with a myotoxic Lys49 PLA_2 from *Bothrops asper* venom and crystallized by the hanging-drop vapor diffusion method at 18 °C. The crystals belong to the orthorhombic space group $P2_12_12_1$, with unit cell parameters a=49.05, b=63.84 and c=85.67 Å. Diffraction data was collected to 1.78 Å.

Keywords: Suramin; Myotoxicity; Snake venom; Lys49 PLA_2s; X-ray diffraction

Suramin (Fig. 1) is a highly charged polysulfonated napthylurea that was originally developed for the treatment of African trypanosomiasis and onchocerciasis. It is capable of binding a number of proteins such as platelet-derived growth factors [1,2], fibroblast growth factors [3] and other cellular receptors. Suramin also plays a role in follicular lymphoma [4], angiogenesis [5], AIDS [6] and several kinds of cancers such as prostate [7], renal cells [8] and breast [9]. Suramin has received much attention because of its ability to inhibit the myotoxic activity of different Crotalidae venoms [10,11]. Basic Lys49 phospholipases A_2 (PLA_2) induce skeletal muscle necrosis (myonecrosis) in vivo, upon intramuscular injection, or in vitro, upon incubation [12]. These Lys49 PLA_2s exhibit a wide spectrum of pharmacological activities such as anticoagulant, hypotensive, haemolytic and oedema-inducing effects [13,14]. There have been a number of attempts to delineate the region or regions critical for the expression of these activities based on sequence homology [15,16], charge distribution [17,18], hydropathy profiles [17], chemical modification [19,20], peptide synthesis [21,22], site-directed mutagenesis [23] and structural [24,25] studies. However, the mechanisms involved in the expression of these pharmacological activities are unclear, particularly the myotoxic effect. The structural results of the suramin-Lys49 PLA_2 complex will serve as a model to improve our understanding of the mechanism involved in the expression and inhibition of myotoxicity. We report the crystallization and X-ray diffraction data collection of the complex of suramin with a myotoxic Lys49 PLA_2 from *Bothrops asper* venom.

The purified Lys49 PLA_2 from *B. asper* at 10 mg ml^{-1} in 0.02 M HEPES at pH 7.5 was complexed with suramin at a

* Corresponding author. Tel./fax: +55 17 221 2247.
E-mail address: arni@df.ibilce.unesp.br (R.K. Arni).

1570-9639/$ - see front matter © 2004 Elsevier B.V. All rights reserved.
doi:10.1016/j.bbapap.2004.08.009

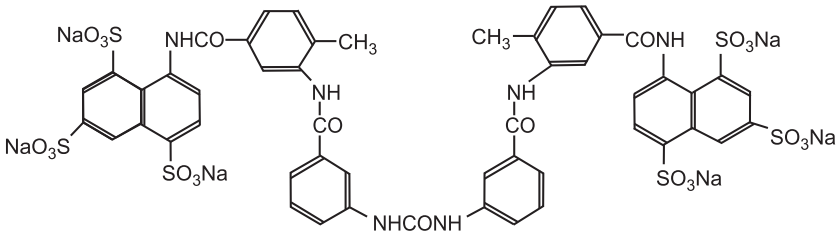

Fig. 1. Structure of suramin, a polysulfonated naphthylurea (molecular weight 1429).

molar ratio of 1:1.2. Crystallization trials were performed by the hanging-drop vapor diffusion method at 18 °C. Optimized crystallization conditions led to the formation of a single crystal after 6 months when 2 μl of the complex was mixed with 2 μl of a reservoir solution containing 0.1 M sodium acetate at pH 4.6, 15% PEG 3350 and 20% isopropanol (Fig. 2). In comparison, the native protein was crystallized from a solution containing 0.1 M sodium citrate (pH 5.6), 20% isopropanol, 20% PEG 4000 and 1 mM sodium azide.

X-ray diffraction data were collected at the protein crystallography beamline (CPR) at the Laboratório Nacional de Luz Síncrotron, Brazil (Fig. 2). A single crystal with a maximum dimension of 0.5 mm was transferred to a solution containing 20% glycerol and flash-frozen at 100 K. The data were integrated with DENZO and scaled with SCALEPACK [26] to a resolution of 1.78 Å. The crystal belongs to the orthorhombic space group $P2_12_12_1$ with unit cell parameters of a=49.05, b=63.84 and c=85.67 Å. Packing considerations based on the molecular weight of 14 kDa and the self-rotation function indicate the presence of two monomers in the crystallographic asymmetric unit. This corresponds to a Matthews's coefficient Vm of 2.4 $Å^3$ Da^{-1} and a solvent content of 48.2% [27]. The statistics of the data processing are summarized in Table 1. Molecular replacement was carried out with the program AmoRe [28]. A model based on the atomic coordinates of Myotoxin-II, a Lys49 PLA_2 from *B. asper* venom [29] (PDB code 1CLP) and stripped of solvent molecules, was used for molecular replacement. A clear solution was obtained for the orientation of the two molecules present in the asymmetric unit.

Rigid-body refinement of the solution using data in the resolution range of 30.0–1.78 Å resulted in a correlation coefficient of 80.1% and an R_{factor} of 27.5%. An examination of the electron density maps indicated clear density for the bound suramin molecule. Restrained refinement with REFMAC5 [30] and model building using TURBO FRODO (Biographics, Marseille, France) are currently in progress.

This work presents the first structure of suramin complexed with a protein as determined by X-ray crystallography. The three-dimensional structure of the suramin–PLA_2 complex should be useful for structure-based drug design and to understand the mechanism of inhibition of myotoxicity in snake venom Lys49 PLA_2s.

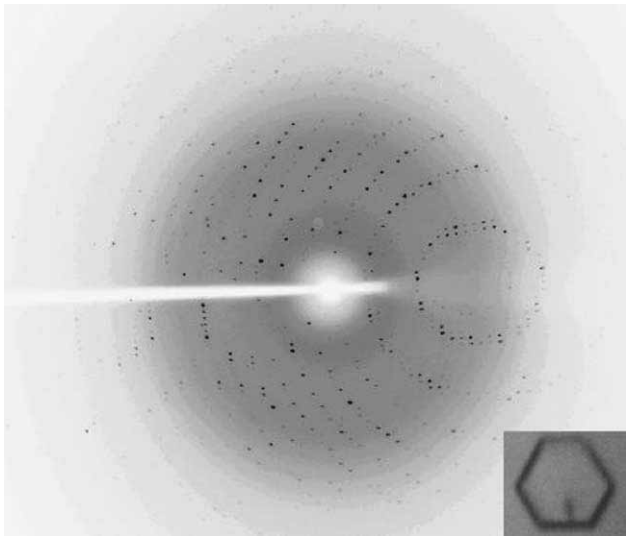

Fig. 2. X-ray diffraction pattern obtained at the Laboratório Nacional de Luz Síncrotron using a MARCCD detector of the PLA_2–suramin complex crystal. Photomicrograph of the crystal (inset).

Table 1
Data collection and processing statistics

Data collection	
Temperature (K)	100
Wavelength used (Å)	1.427
Detector	MARCCD
Space group	$P2_12_12_1$
Unit cell parameters (Å)	a=49.05, b=63.84 and c=85.67
Resolution range (Å)	30.00–1.78
No. of observed reflections	297,425
Data completeness (%)	99.7 (99.7)
No. of unique reflections	26,395
I/sigma(I)	28.5 (5.1)
R_{merge} (%)[a]	4.8 (31.7)
Molecule per asymmetric unit	2
Vm ($Å^3$ Da^{-1})	2.4
Solvent content (%)	48.2

Values in parentheses are for the high-resolution bin.

[a] $R_{merge}=\Sigma(\Sigma|I(h)_I-\{I(h)\}|)/\Sigma\{I(h)\}$, where $I(h)_i$ is the observed intensity of the ith measurement of reflection h and $\{I(h)\}$ is the mean intensity of reflection h calculated after scaling.

Acknowledgements

Financial support by FAPESP/SMOLBNet, CNPq, CAPES/DAAD is gratefully acknowledged. MTM is recipient of a FAPESP fellowship.

References

[1] M. Hosang, Suramin binds to platelet-derived growth factor and inhibits its biological activity, J. Cell. Biochem. 29 (1985) 265–273.
[2] S.S. Huang, J.S. Huang, Rapid turnover of the platelet-derived growth factor receptor in cis-transformed cells and reversal by suramin: Implications for the mechanism of autocrine transformation, J. Biol. Chem. 263 (1988) 12608–12618.
[3] D.B. Rifkin, D. Moscatelli, Recent developments in the cell biology of basic fibroblast growth factor, J. Cell Biol. 109 (1989) 1–6.
[4] S.G. Arbuck, J.M. Sorensen, M.C. Christian, P. Ho, J.M. Pluda, B.D. Cheson, New drugs in non-Hodgkin's lymphoma, Ann. Oncol. Suppl. 1 (1997) 119–128.
[5] C.E. Hensey, D. Boscoboinik, A. Azzi, Suramin, anti-cancer drug, inhibits protein kinase C and induces differentiation in neuroblastoma cell clone NB2A, FEBS Lett. 258 (1989) 156–158.
[6] B.D. Cheson, A.M. Levine, D. Mildvan, L.D. Kaplan, P. Wolfe, A. Rios, J.E. Groopman, P. Gill, P.A. Volberding, B.J. Poiesz, et al., Suramin therapy in AIDS and related disorders. Report of the US Suramin Working Group, JAMA 258 (1987) 1347–1351.
[7] M.A. Eisenberger, L.M. Reyno, D.I. Jodrell, V.J. Sinibaldi, K.H. Tkaczuk, R. Sridhara, E.G. Zuhowski, M.H. Lowitt, S.C. Jacobs, M.J. Egorin, Suramin, an active drug for prostate cancer: Interim observations in a phase I trial, J. Natl. Cancer Inst. 85 (1993) 611–621.
[8] R. Dreicer, D.C. Smith, R.D. Williams, W.A. See, Phase II trial of suramin in patients with metastatic renal cell carcinoma, Invest. New Drugs 17 (1999) 183–186.
[9] W.J. Gradishar, G. Soff, J. Liu, A. Cisneros, S. French, A. Rademaker, A.B. Benson, N. Bouck, A pilot trial of suramin in metastatic breast cancer to assess antiangiogenic activity in individual patients, Oncology-Basel 58 (2000) 324–333.
[10] E.Z. Arruda, N.M.V. Silva, R.A.M. Moraes, P.A. Melo, Effect of suramin on myotoxicity of some crotalid snake venoms. Antimyotoxic effect of suramin, Braz. J. Med. Biol. Res. 35 (2002) 723–726.
[11] M. Oliveira, W.L.G. Cavalcante, E.Z. Arruda, P.A. Melo, M.D. Silva, M. Gallaccia, Antagonism of myotoxic and paralyzing activities of bothropstoxin-I by suramin, Toxicon 42 (2003) 373–379.
[12] J.M. Gutiérrez, B. Lomonte, Phospholipase A_2 myotoxins from *Bothrops* snake venoms, in: R.M. Kini (Ed.), Venom Phospholipase A_2 Enzymes: Structure, Function and Mechanism, Wiley, Chichester, 1997, pp. 321–352.
[13] J.B. Harris, Phospholipases in snake venoms and their effects on nerve and muscle, in: A.L. Harvey (Ed.), Snake Toxins, Pergamon Press, New York, 1991, pp. 91–121.
[14] A.B. Mukherjee, L. Miele, N. Pattabiraman, Phospholipase A_2 enzymes: regulation and physiological role, Biochem. Pharmacol. 48 (1994) 1–10.
[15] R.L. Heinrickson, Dissection and sequence analysis of phospholipase A_2, Methods Enzymol. 197 (1991) 201–215.
[16] R.J. Ward, A. Rodrigues Alves, J. Rugierro Neto, R.K. Arni, J. Casari, A sequence space analysis of Lys49 phospholipase A_2: clues towards identification of residues involved in a novel mechanism of membrane damage and in myotoxicity, Protein Eng. 11 (1998) 285–294.
[17] R.M. Kini, S. Iwanaga, Structure–function relationships of phospholipases: II. Charge density distribution and the myotoxicity of presynaptically neurotoxic phospholipases, Toxicon 24 (1986) 895–905.
[18] R.M. Kini, H.J. Evans, Role of cationic residues in cytolytic activity: modification of lysine residues in the cardiotoxin from *Naja nigricollis* venom and correlation between cytolytic and antiplatelet activity, Biochemistry-US 28 (1989) 9209–9216.
[19] C. Díaz-Oreiro, J.M. Gutiérrez, Chemical modification of histidine and lysine residues of myotoxic phospholipases A_2 isolated from *Bothrops asper* and *Bothrops godmani* snake venoms: effects on enzymatic and pharmacological properties, Toxicon 35 (1997) 241–252.
[20] S.H. Andrião-Escarso, A.M. Soares, V.M. Rodrigues, Y. Angulo, C. Díaz, B. Lomonte, J.M. Gutiérrez, J.R. Giglio, Myotoxic phospholipase A_2 in *Bothrops* snake venoms: effect of chemical modification on the enzymatic and pharmacological properties of bothropstoxins from *Bothrops jararacussu*, Biochimie 82 (2000) 755–763.
[21] B. Lomonte, J. Pizarro-Cerda, Y. Angulo, J.P. Gorvel, E. Moreno, Tyr→Trp-substituted peptide 115–129 of a Lys49 phospholipase A_2 expresses enhanced membrane-damaging activities and reproduces its in vivo myotoxic effect, Biochim. Biophys. Acta 1461 (1999) 19–26.
[22] C.E. Núnez, Y. Angulo, B. Lomonte, Identification of the myotoxic site of the Lys49 phospholipase A_2 from *Agkistrodon piscivorus piscivorus* snake venom: synthetic C-terminal peptides from Lys49, but not from Asp49 myotoxins, exert membrane-damaging activities, Toxicon 39 (2001) 1587–1594.
[23] L. Chioato, R.J. Ward, Mapping structural determinants of biological activities in snake venom phospholipases A_2 by sequence analysis and site directed mutagenesis, Toxicon 42 (2003) 869–883.
[24] M.T. Murakami, R.K. Arni, A structure based model for liposome disruption and the role of catalytic activity in myotoxic phospholipase A2s, Toxicon 42 (2003) 903–913.
[25] D.L. Scott, P.B. Sigler, The structural and functional roles of calcium ion in secretory phospholipases A_2, Adv. Inorg. Biochem. 10 (1994) 139–155.
[26] Z. Otwinowski, W. Minor, Processing of X-ray diffraction data collected in oscillation mode, Methods Enzymol. 276 (1997) 307–326.
[27] B.W. Matthews, Solvent content of protein crystals, J. Mol. Biol. 33 (1968) 491–497.
[28] J. Navaza, AmoRe: an automated package for molecular replacement, Acta Crystallogr. A50 (1994) 157–163.
[29] R.J. Ward, W.F. Azevedo, R.K. Arni, At the interface: crystal structures of phospholipases A_2, Toxicon 36 (1998) 1623–1633.
[30] G.N. Murshudov, A.A. Vagin, E.J. Dodson, Refinement of macromolecular structure by the maximum-likelihood method, Acta Crystallogr. D53 (1997) 240–255.

Available online at www.sciencedirect.com
SCIENCE DIRECT®
Biochemical and Biophysical Research Communications 323 (2004) 24–31
BBRC
www.elsevier.com/locate/ybbrc

Crystal structure of an acidic platelet aggregation inhibitor and hypotensive phospholipase A_2 in the monomeric and dimeric states: insights into its oligomeric state☆

Angelo J. Magro[a,1], Mário T. Murakami[b,1], Silvana Marcussi[c], Andreimar M. Soares[c], Raghuvir K. Arni[b], Marcos R.M. Fontes[a,*]

[a] *Departamento de Física e Biofísica, Instituto de Biociências, UNESP, Botucatu-SP, Brazil*
[b] *Departamento de Física, IBILCE, UNESP, São José do Preto-SP, Brazil*
[c] *Unidade de Biotecnologia, UNAERP, Ribeirão Preto-SP, Brazil*

Received 4 August 2004
Available online 21 August 2004

Abstract

Phospholipases A_2 belong to the superfamily of proteins which hydrolyzes the *sn*-2 acyl groups of membrane phospholipids to release arachidonic acid and lysophospholipids. An acidic phospholipase A_2 isolated from *Bothrops jararacussu* snake venom presents a high catalytic, platelet aggregation inhibition and hypotensive activities. This protein was crystallized in two oligomeric states: monomeric and dimeric. The crystal structures were solved at 1.79 and 1.90 Å resolution, respectively, for the two states. It was identified a Na^+ ion at the center of Ca^{2+}-binding site of the monomeric form. A novel dimeric conformation with the active sites exposed to the solvent was observed. Conformational states of the molecule may be due to the physicochemical conditions used in the crystallization experiments. We suggest dimeric state is one found in vivo.

Keywords: X-ray crystallography; Acidic phospholipase A_2; *Bothrops jararacussu* venom; Platelet aggregation and hypotensive effects; Crystal structure; Oligomeric state; Dimeric phospholipase A_2

Phospholipases A_2 (PLA_2, EC 3.1.1.4) belong to the superfamily of proteins which hydrolyzes the *sn*-2 acyl groups of membrane phospholipids to release arachidonic acid and lysophospholipids. The superfamily of PLA_2s is divided into 11 classes [1], of which five (I, II, III, V, and X) are abundant in a variety of biological fluids, particularly pancreatic secretions, inflammatory exudates, and reptile and arthropod venoms [2]. PLA_2s are the major components of snake venoms, being those of group IIA predominant in *Bothrops* venoms. In addition to their primary catalytic role, snake venoms PLA_2s show other important toxic/pharmacological effects including myonecrosis, neurotoxicity, cardiotoxicity, and hemolytic, hemorrhagic, hypotensive, anticoagulant, platelet aggregation inhibition, and edema-inducing activities [3–5]. Some of these activities correlate with the enzymatic activity and others are completely independent [6,7].

PLA_2s are also one of the enzymes involved in the production of eicosanoids. These molecules have physiological effects at very low concentrations; however, the increasing of their concentration can lead to the state of

☆ *Abbreviations:* PLA_2, phospholipase A_2; BthA-I, acidic phospholipase A_2 from *Bothrops jararacussu* venom; m-BthA-I, monomeric acidic phospholipase A_2 from *Bothrops jararacussu* venom; d-BthA-I, dimeric acidic phospholipase A_2 from *Bothrops jararacussu* venom.

* Corresponding author. Fax: +55 14 38153744.
E-mail address: fontes@ibb.unesp.br (M.R.M. Fontes).

[1] These authors contributed equally to this work.

0006-291X/$ - see front matter © 2004 Elsevier Inc. All rights reserved.
doi:10.1016/j.bbrc.2004.08.046

inflammation [8]. Then, the study of specific PLA_2s inhibitors can be important in the production of structure-based anti-inflammatory agents.

A group of myotoxic Phospholipases A_2 homologues present in the venoms of some species of *Agkistrodon*, *Bothrops*, and *Trimeresurus* (family Viperidae) is characterized by a Lys to Asp substitution of residue 49 [9,10]. The coordination of the Ca^{2+} ion in the PLA_2 calcium-binding loop includes an Asp at position 49 which plays a crucial role in the stabilization of the tetrahedral transition state intermediate in catalytically active phospholipases A_2 [11]. Therefore, the Asp49 to Lys substitution drastically affects the calcium-binding ability of these Lys49-PLA_2 homologues and, as a consequence, they present a very limited catalytic activity.

Many basic Lys49-PLA_2s have been purified from *Bothrops* snake venoms and structurally and functionally characterized [12–18]. However, little is known about the bothropic Asp49-PLA_2s [19–21]. Two basic myotoxic phospholipases A_2, the bothropstoxin-I (Lys49-BthTX-I—catalytic inactive) and II (Asp49-BthTX-II—low catalytic activity), have been isolated from *Bothrops jararacussu* venom and characterized [15,18,22,23]. BthA-I is three to four times more active catalytically than BthTX-II and other basic Asp49 PLA_2 from *Bothrops* venoms, however, it is not myotoxic, cytotoxic or lethal. Although it showed no toxic activity, it was able to induce time-independent edema. In addition, BthA-I caused a hypotensive response in rats and inhibited platelet aggregation [24]. Catalytic, desintegrin, and pharmacological activities were abolished by chemical modification with *p*-bromophenacyl bromide, which covalently binds to His48 of the catalytic site [24]. In order to better understand the structure–function relationship of these bothropic proteins, the cDNA sequence cloning, functional expression crystallization, and X-ray diffraction data of BthA-I-PLA_2 were recently described [24–26].

In this paper, we described the high resolution crystal structures of BthA-I-PLA_2 in two oligomeric states: monomeric and dimeric.

Table 1
X-ray data collection and refinement statistics

	d-BthA-I	m-BthA-I
Unit cell (Å)	$a = 33.19$ $b = 63.14$ $c = 47.40$ $\beta = 102.3$	$a = 39.98$ $b = 53.99$ $c = 90.46$
Space group	$P2_1$	$C222_1$
Resolution (Å)	29.7–1.9 (2.02–1.9)[a]	30.0–1.79 (1.84–1.79)[a]
Unique reflections	14,151 (2084)[a]	9034 (507)[a]
Completeness (%)	93.3 (87.7)[a]	94.3 (80.1)[a]
R_{merge}[b] (%)	4.5 (29.3)[a]	4.6 (15.3)[a]
$I/\sigma(I)$	20.1 (5.0)[a]	22.1 (6.0)[a]
Redundancy	3.5 (3.4)[a]	5.7(1.2)[a]
R_{Cryst}[c] (%)	19.0 (23.8)[a]	18.6 (24.6)[a]
R_{free}[d] (%)	24.7 (28.5)[a]	25.5 (33.8)[a]
Number of non-hydrogen atoms:		
Protein	1900	949
Water	381	144
Mean *B* factor (Å^2)[e]		
Overall	27.8	23.2
Main chain atoms	34.6	17.4
Side chain atoms	35.6	19.4
Water molecules	49.0	27.9
Na^+ ion	38.1	—
R.m.s deviations from ideal values[e]		
Bond lengths (Å)	0.005	0.018
Bond angles (°)	1.3	1.9
Ramachandran plot[f] (%)		
Residues in most favored region	90.7	92.2
Residues in additional allowed region	9.3	7.8
Residues in generously/disallowed regions	0.0	0.0
Coordinate error (Å)[e]		
Luzzati plot (cross-validated Luzzati plot)	0.20 (0.28)	0.18 (0.38)
SIGMAA (cross-validated SIGMAA)	0.22 (0.22)	0.11 (0.11)

[a] Numbers in parentheses are for the highest resolution shell.

[b] $R_{merge} = \sum_{hkl}(\sum_i(|I_{hkl,i} - \langle I_{hkl}\rangle|))/\sum_{hkl,i}\langle I_{hkl}\rangle$, where $I_{hkl,i}$ is the intensity of an individual measurement of the reflection with Miller indices h, k, and l, and $\langle I_{hkl}\rangle$ is the mean intensity of that reflection. Calculated for $I > -3\sigma(I)$.

[c] $R_{cryst} = \sum_{hkl}(||\text{Fobs}_{hkl}| - |\text{Fcalc}_{hkl}||)/|\text{Fobs}_{hkl}|$, where $|\text{Fobs}_{hkl}|$ and $|\text{Fcalc}_{hkl}|$ are the observed and calculated structure factor amplitudes.

[d] R_{free} is equivalent to R_{cryst} but calculated with reflections (5%) omitted from the refinement process.

[e] Calculated with the program CNS [30].

[f] Calculated with the program PROCHECK [34].

Materials and methods

Isolation, cDNA cloning, and sequencing. BthA-I-PLA_2 was isolated from *B. jararacussu* snake venom by ion-exchange chromatography on CM-Sepharose followed by reverse phase chromatography on a RP-HPLC C-18 column [24]. The amino acid sequence of BthA-I-PLA_2 was deduced from the cDNA sequence and deposited in GenBank (AY145836) [25,26].

Crystallization and data collection. BthA-I-PLA_2 was crystallized in two different conditions: 0.2 M ammonium sulfate and 22% (w/v) polyethylene glycol 6000 (d-BthA-I) [24]; and 0.1 M sodium acetate (pH 4.6) and 28% polyethylene glycol 4000 (m-BthA-I). Lyophilized sample of BthA-I-PLA_2 was dissolved in ultra-pure water at a concentration of 10 and 12 mg/mL, respectively, for crystals of m-BthA-I and d-BthA-I. The crystals were flash-frozen (15% glycerol for m-BthA-I) and diffraction data were collected at a wavelength of 1.38 Å (at 100 K) using a Synchrotron Radiation Source (LNLS, Campinas, Brazil). Diffraction intensities were measured using a MAR 345 imaging-plate detector and were reduced and processed using the HKL suite [27]. The data sets are 94.3% and 93.3% complete at 1.79 and 1.9 Å resolution with R_{merge} = 4.6% and 4.5% for m-BthA-I and d-BthA-I, respectively. The m-BthA-I crystals belong to the space group $C222_1$ and for m-BthA-I to the space group $P2_1$. Data processing statistics are presented in Table 1.

Structure determination and refinement. The crystal structures of m-BthA-I and d-BthA-I were solved by the Molecular Replacement Method using the program AMoRe [28] and the coordinates of the Lys49-PLA_2 from *Agkistron piscivorus piscivorus* (PDB code 1VAP) [29]. The model choice was based on the best results of correlation and *R* factor from the AMoRe program. After a cycle of simulated annealing refinement using the CNS program [30], the electron densities were inspected and the amino acid sequence as obtained from the cDNA of BthA-I [25,26] was inserted for both m-BthA-I and d-BthA-I. The modeling process was always performed by manually rebuilding with the "O" program [31]. Electron density maps calculated with coefficients $3|F_{obs}| - 2|F_{calc}|$ and simulated annealing omit maps calculated with analogous coefficients were generally used. The model was improved, as judged by the free *R* factor [32], through rounds of crystallographic refinement (positional and restrained isotropic individual *B* factor refinement, with an overall anisotropic temperature factor and bulk solvent correction) using the CNS program [30], and manual rebuilding with the "O" program [31]. Solvent molecules were added and refined also with the program CNS [30]. In the last stages of refinement of m-BthA-I the program REFMAC 5.0 was used [33].

The refinement converged to *R* and free *R* factors of 18.3% and 24.3%; 19.0% and 24.7%, respectively, for m-BthA-I and d-BthA-I (see Table 1 for explanation of *R* factors). The final models comprise 950 protein atoms and 144 water molecules for m-BthA-I, and 1900 protein atoms and 381 water molecules for d-BthA-I. The refinement statistics are shown in Table 1. For molecular comparisons of the Lys49-PLA_2 structures, the "O" program [31] was used with only the C^{α} coordinates. The quality of the model was checked with the PROCHECK program [34]. The coordinates have been deposited in the RCSB Protein Data Bank with ID code 1UMV and 1U73, respectively, for m-BthA-I and d-BthA-I.

Results

The structures showed overall stereochemistry better than expected for an average structure at the same resolution, where no residue was found in the disallowed or generously allowed regions of Ramachandran plot, and with the overall Procheck *G* factor of 0.4 and −0.1 for d-BthA-I and m-BthA-I, respectively [34].

The m-BthA-I and d-BthA-I monomers are very similar to other class IIA PLA_2 structures. As is usual for other proteins of this class, there are seven disulfide bridges and the main secondary structural elements are conserved. The structure is composed of: (i) N-terminal α-helix 1, (ii) Ca^{2+}-binding loop, (iii) two anti-parallel α-helixes 2 and 3, (iv) short two-stranded anti-parallel β-sheet (β-wing), and (v) C-terminal loop (Fig. 1A).

The monomers of m-BthA-I and d-BthA-I are essentially identical, where the r.m.s. deviation of C^{α} atoms is 0.49 Å for both superposition of d-BthA-I monomer A and m-BthA-I, and d-BthA-I monomer B and m-BthA-I. The average *B* factors for m-BthA-I and d-BthA-I are 25.6 and 18.6 $Å^2$, respectively (calculated without solvent molecules).

In the active site for both structures, there is just a water molecule bound to His48 and Lys49 residues.

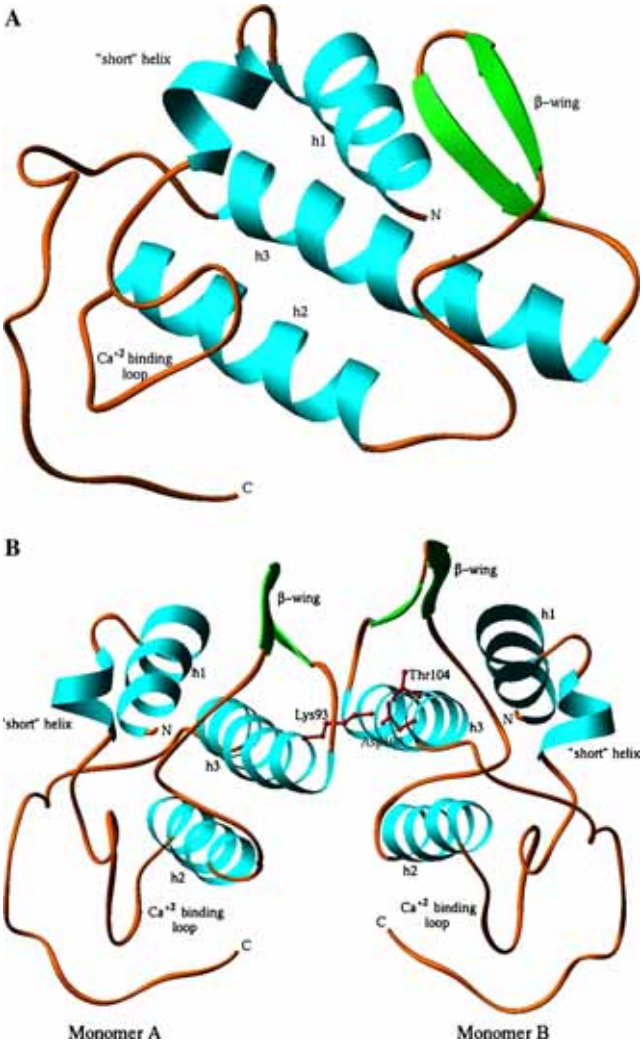

Fig. 1. Structures of (A) m-BthA-I and (B) d-BthA-I are showed as a ribbon diagram [35]. The residues Thr104, Asp108, and Lys93 of interface of monomers of d-BthA-I are shown in a ball-stick representation.

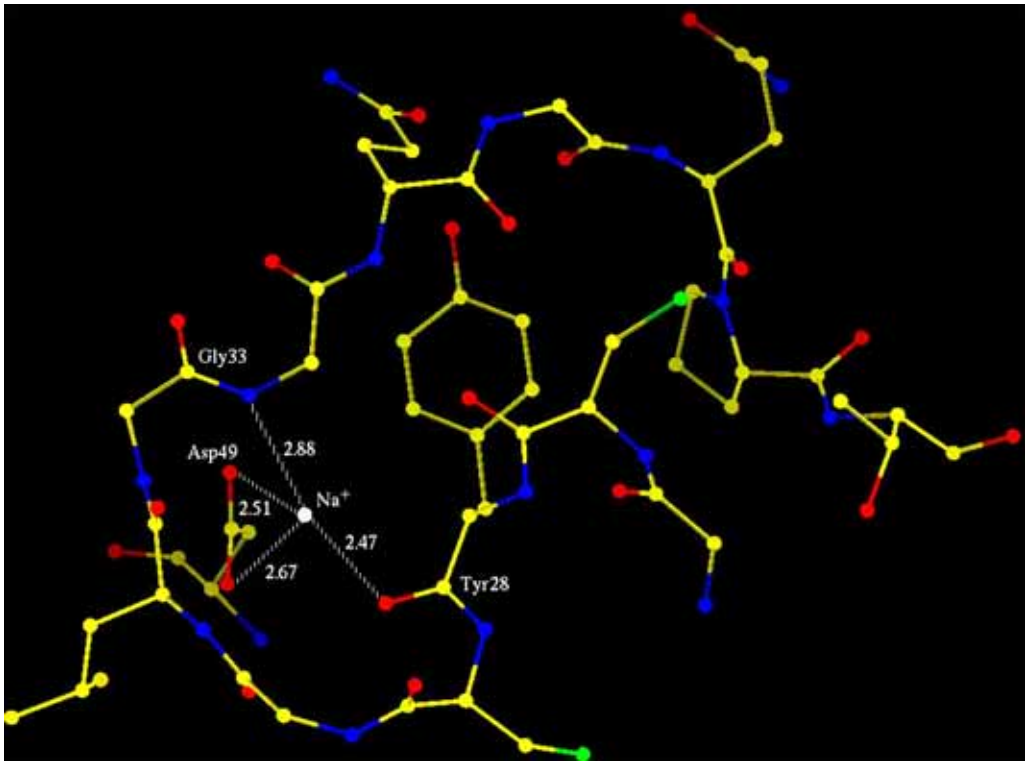

Fig. 2. Ca^{2+}-binding loop interactions with Na^{+} ion in the m-BthA-I structure [31].

The electron density map for m-BthA-I structure shows a single prominent peak at the center of Ca^{2+}-binding site, which was identified as Na^{+} ion rather than Ca^{2+} ion for three main reasons. (i) The protein was crystallized in the presence of sodium acetate. (ii) The *B* factor of Na^{+} is 38.1 $Å^2$, which is reasonably close to the value of the average *B* factor (23.2 $Å^2$). If the position was occupied by Ca^{2+} ion, its *B* factor would be 60.3 $Å^2$. (iii) All PLA_2s solved to this time with the presence of Ca^{2+} present this ion coordinated by carboxyl group of residues 28, 30, 32, and Asp49 and two (or one) water molecules [36]. However, the Na^{+} ion of m-BthA-I just interacts with the Tyr28 carboxyl group (2.47 Å), Gly32 N (2.88 Å), and Asp49 Oδ1 and Oδ2 (2.67 and 2.51 Å, respectively) (Fig. 2). Additionally, the distance between the closest water molecule and the Na^{+} ion is about 4 Å, which makes impossible the essential role of a water molecule presence in the catalytic mechanism [37].

No strong densities were found at the center of Ca^{2+}-binding loops of d-BthA-I monomers. However, water molecules were found in both sites of d-BthA-I in the similar position to the Na^{+} ion of m-BthA-I (*B* factors are 33.9 and 43.5 $Å^2$ which are comparable with the average value of 40.9 $Å^2$ for water molecules). Despite the lack of Na^{+} ion in the d-BthA-I, the conformations of Ca^{2+}-binding loops are similar with m-BthA-I molecule (superposition between the m-BthA-I

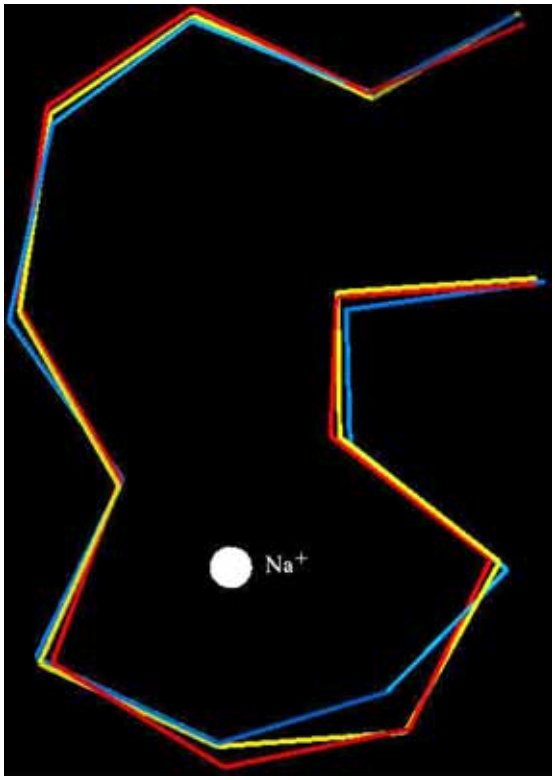

Fig. 3. Superposition of C^{α} atoms of Ca^{2+}-binding loop of each one monomer of d-BthA-I (red, monomer A; blue, monomer B) and m-BthA-I. Na^{+} ion is shown like a white sphere [31]. (For interpretation of the references to color, the reader is referred to the web version of this paper.)

loop and d-BthA-I monomers A and B loops resulted in C^{α} atom r.m.s. deviation of 0.26 and 0.46 Å, respectively) (Fig. 3).

The monomers of d-BthA-I are related by twofold axis perpendicular to h3 α-helix (Fig. 1B). Hydrophobic contacts, one intermolecular hydrogen bond, and one

```
                                10        20        30        40        50        60          Identity (%)
B. taurus (1bp2)                ALWQFNGMIKCKIPSSEPLLDFNNYGCYCGLGGSGTPVDDLDRCCQTHDNCYKQAKKLDSCKVLVDNPY      41.6
B. jararacussu (1umv)           SLWQFGKMINYVM-GESGVLQYLSYGCYCGLGGQGQPTDATDRCCFVHDCCYG---KVTGC-----NPK      -
A. p. piscivorus (1vap)         NLFQFEKLIKKMT-GKSGMLWYSAYGCYCGWGGQGRPKDATDRCCFVHDCCYG---KVTGC-----DPK      71.5
D. acutus (1ijl)                SLIQFETLIMKVV-KKSGMFWYSAYGCYCGWGGHGRPQDATDRCCFVHDCCYG---KVTGC-----NPK      66.7
C. atrox (1pp2)                 SLVQFETLIMKIA-GRSGLLWYSAYGCYCGWGGHGLPQDATDRCCFVHDCCYG---KATDC-----DPK      63.1
A. h. pallas (1jia)             HLLQFRKMIKKMT-GKEPVVSYAFYGCYCGSGGRGKPKDATDRCCFVHDCCYE---KVTGC-----KPK      62.8
B. pirajai (1gmz)               DLWQFGKMILKET-GKLPFPYYVTYGCYCGVGGRGGPKDATDRCCFVHDCCYG---KLTSC-----NPK      59.5
D. r. pulchella (1fb2)          SLLEFGKMILEET-GKLAIPSYSSYGCYCGWGGKGTPKDATDRCCFVHDCCYG---NLPDC-----NPK      54.3
N. n. sagittifera (1mh2)        NTWQFKNMISCTVPSR-SWWDFADYGCYCGRGGSGTPSDDLDRCCQTHDNCYNEAEKISGC-VLVDNPR      41.8

                                70        80        90        100       110       120
B. taurus (1bp2)                TNNYSYSCSNNEITCSS-ENNACEAFICNCDRNAAICF-----SKVPYNKE-HKNLDKKNC-------      41.6
B. jararacussu (1umv)           IDSYTYSKKNGDVVCGG-DN-PCKKQICECDRVATTCFRD---NKDTYDIK-YWFYGAKNCQEKSEPC      -
A. p. piscivorus (1vap)         MDIYTYSVDNGNIVCGG-TN-PCKKQICECDRAAAICFRD---NLKTYDSKTYWKYPKKNCKEESEPC      71.5
D. acutus (1ijl)                MDSYTYSEENGDIVCGG-DD-PCKREICECDRVAADCFRD---NLDTYNSDTYWRYPRQDCEESPEPC      66.7
C. atrox (1pp2)                 TVSYTYSEENGEIICGG-DD-PCGTQICECDKAAAICFRD---NIPSYDNK-YWLFPPKDCREEPEPC      63.1
A. h. pallas (1jia)             WDDYTYSWKNGTIVCGG-DD-PCKKEVCECDKAAAICFRD---NLKTYKKR-YMAYPDILCSSKSEKC      62.8
B. pirajai (1gmz)               TDRYSYSRKDGTIVCGE-D--PCRKEICECDKAAAVCFRE---NLDTYNKK-YMSYLKSLCK-KADDC      59.5
D. r. pulchella (1fb2)          SDRYKYKRVNGAIVCEK-GT-SCENRICECDKAAAICFRQ---NLNTYSKK-YMLYPDFLCKGELKC-      54.3
N. n. sagittifera (1mh2)        FRTYSYACTAGTLTCTGRNN-ACAASVCDCDRNAAICFAGAPYNDSNYNID-LQARCN----------      41.8

Key: red = helix, blue = strand, green = turn, black = coil.
```

Fig. 4. Amino acid sequence alignments of Asp49-PLA_2s monomers A from *B. jararacussu* (1u73), *A. p. piscivorus* (1vap) [29], *D. acutus* (1ijl) [39], *C. atrox* (1pp2) [40], *A. h. pallas* (1jia) [41], *D. r. pulchella* (1fb2) [42], and *N. n. sagittifera* (1mh2—monomer B) [43]. The sequences have been numbered according to Renetseder et al. [44]. Identity values related to BthA-I are shown at the right column. Produced by the FASTA program [45]. PDB ID codes are shown in parentheses.

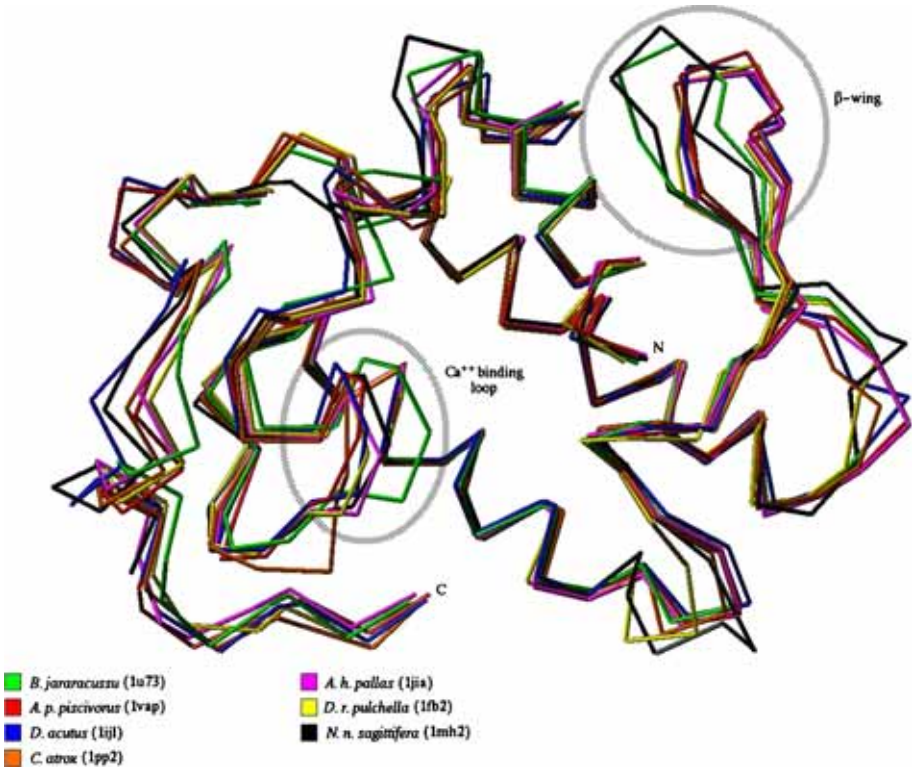

Fig. 5. Superposition of monomers A Asp49-PLA_2s from *B. jararacussu* (1u73), *A. p. piscivorus* (1vap) [29], *D. acutus* (1ijl) [39], *C. atrox* (1pp2) [40], *A. h. pallas* (1jia) [41], *D. r. pulchella* (1fb2) [42], and *N. n. sagittifera* (1mh2—monomer B) [43]—performed using only C^{α} atoms from h1, h2, and h3 α-helixes [31]. Asp49-PLA_2 from the *N. n. sagittifera* venom belongs to group I while the others to the group IIA. Drawn using RIBBONS [35]. PDB ID codes are shown in parentheses.

salt-bridge contribute to the stabilization of the dimer. All contacts involve the residues of h3 α-helix, including the salt bridge between the Nε atom of Lys83 (monomer A) and Oδ2 of Glu98 (monomer B) (2.56 Å).

Discussion

It was identified to be a Na^+ ion rather of a Ca^{2+} ion for m-BthA-I at the center of Ca^{2+}-binding site. Similar fact was observed in the acidic PLA_2 structure from *Agkistrodon halys pallas* complexed with *p*-bromo-phenacyl (BPB) [38], which was crystallized in the presence of Na^+ ions. Zhao et al. [38] noted the strong interaction of Na^+ ion with three carbonyl oxygen atoms of residues Tyr28, Gly 30, and Gly32 while for Asp49 Oδ1 and Oδ2 these interactions are longer than usual. In the case of m-BthA-I, Na^+ ion interacts with Tyr28 carboxyl, Gly32 N, and Asp49 Oδ1 and Oδ2. These differences are likely to be due to the *p*-bromo-phenacyl group interacting with Gly30 and Asp49 in the PLA_2 structure from *A. h. pallas* complexed with BPB [38].

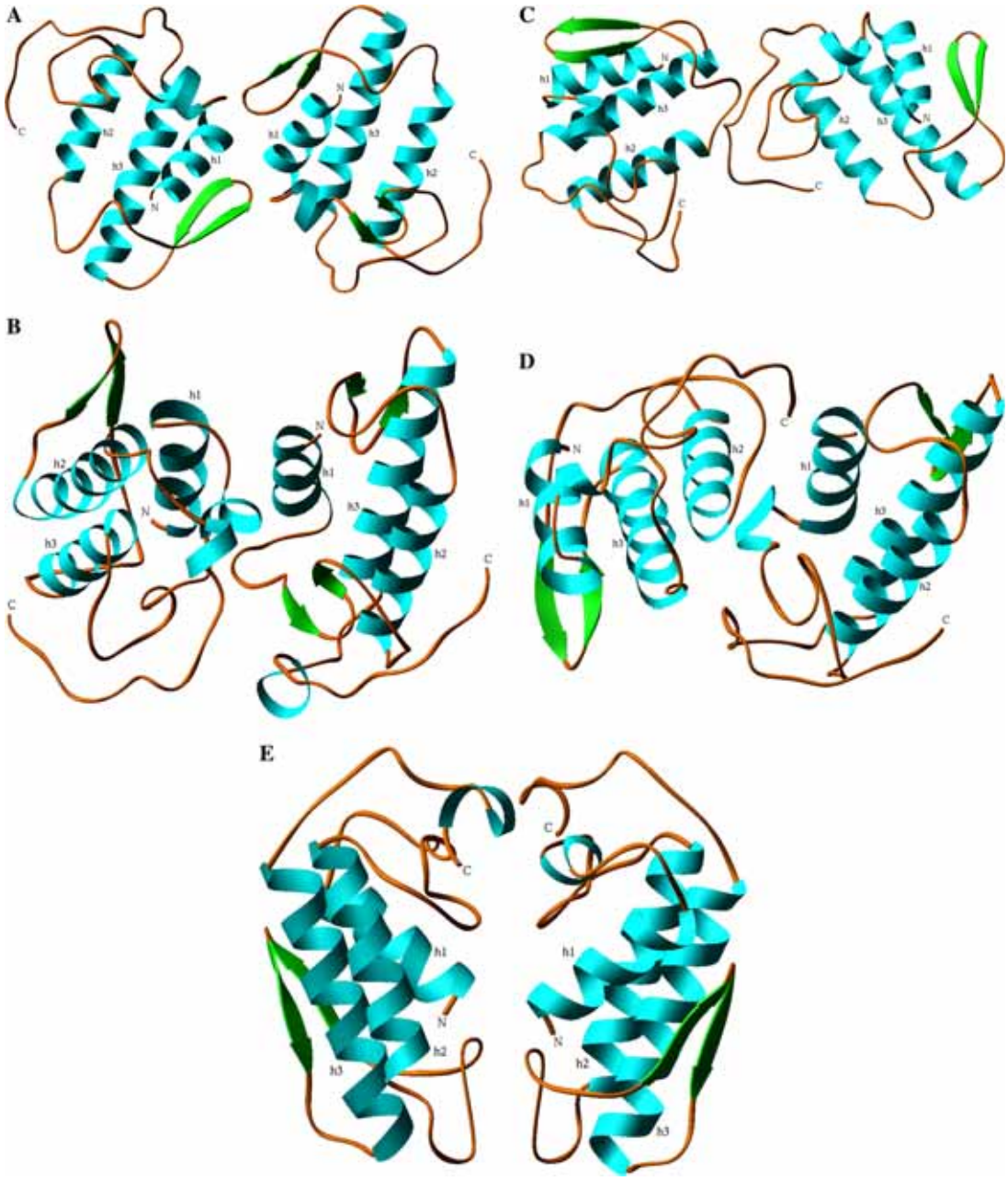

Fig. 6. Structure of dimeric PLA_2s: (A) *Bothrops neuwiedi pauloensis* (1pa0) [12]; (B) *Deinagkistrodon acutus* (1ijl) [39]; (C) *Agkistrodon halys pallas* (1jia) [41]; (D) *Daboia russeli pulchella* (1fb2) [42]; and (E) *Naja naja sagittifera* (1mh2) [43]. Drawn using RIBBONS [35]. PDB ID codes are shown in parentheses.

The d-BthA-I structure shows the lack of Ca^{2+} or Na^{+} ions at the Ca^{2+}-binding loops, however, a water molecule was found in similar position for both monomers. The Ca^{2+}-binding loops do not show important structural differences by occupation of this site by water or Na^{+} ion (Fig. 3).

Fig. 4 shows the alignment of the class I or IIA Asp49-PLA_2s from different species (*B. jararacussu*, *A. p. piscivorus* [29], *Deinagkistrodon acutus* [39], *Crotalus atrox* [40], *A. h. pallas* [41], *Daboia russeli pulchella* [42], and *Naja naja sagittifera* [43]) produced using only the secondary structure residues. The sequence identity related to BthA-I varies from 71.5% (*A. p. piscivorus*) to 41.8% (*N. n. sagittifera*). In contrast, the C^{α} atom's superposition of secondary structure elements between monomers (Fig. 5) shows conformations to be very similar. As seen in Fig. 5, the main structural differences are in the Ca^{2+}-binding loop and β-wing regions. BthA-I presents these regions as slightly altered compared to other class IIA PLA_2 (all structures of Fig. 5, except the class I Asp49-PLA_2 from the *N. n. sagittifera*). In contrast, in the Asp49-PLA_2 piratoxin III structure [18], Ca^{2+}-binding loop presents high structural distortion when compared with other PLA_2s due to an extreme diversion taken by the main chain of residues 30–31 associated with a change in the backbone dihedral angles of Cys29. The authors support this distortion may be due to an alternative conformation of enzyme (T-state). In that case, the structures of BthA-I and other PLA_2s presented here should be in the R-state conformation.

The oligomeric state is an important issue for many of phospholipase A_2 structures solved [12,37,46–49]. A comparison of d-BthA-I with all class IIA PLA_2 structures available at the RCSB Protein Data Bank reveals this structure adopts a novel oligomeric conformation whereas the active site of both monomers can be reached by a hydrophobic channel exposed to the solvent. Fig. 6 shows some examples of oligomeric conformations of PLA_2s.

BthA-I was crystallized in two conformational states: monomeric and dimeric. This is likely to be due to the physicochemical conditions used in the crystallization experiments. The crystals of m-BthA-I were grown at pH 4.6 and those of d-BthA-I were grown at pH 3.5. Then, the m-BthA-I molecules are in the condition very close to their p$I \sim 5.0$ [24], whereas the molecules are in charge equilibrium leading to their dissociation. Consequently, we suggest dimeric state of BthA-I could be that found predominately in vivo.

It has been shown dimeric is the most favorable or active state for Lys49-PLA_2 [12,46] and for outer membrane phospholipases (OMPLA) [47,48]. However, *C. atrox* PLA_2 is dimeric in the absence of lipids and monomeric when interacting with lipids [49]. Then, clearly, deep structural studies must be done to better understanding of oligomeric mechanism Asp49-PLA_2s.

Acknowledgments

The authors gratefully acknowledge the financial support from Fundação de Amparo à Pesquisa do Estado de São Paulo (FAPESP), Conselho Nacional de Desenvolvimento Científico e Tecnológico (CNPq), Fundação para o Desenvolvimento da UNESP (FUNDUNESP), Laboratório Nacional de Luz Síncrontron (LNLS, Campinas-SP), and Universidade de Ribeirão Preto (UNAERP, Ribeirão Preto-SP).

References

[1] D.A. Six, E.A. Dennis, The expanding superfamily of phospholipase A_2 enzymes: classification and characterization, Biochim. Biophys. Acta 1488 (2000) 1–19.
[2] P. Rosenberg, in: W. Shier, D. Mebs (Eds.), Handbook of Toxinology, Marcel Dekker, New York, 1990, pp. 67–277.
[3] J.M. Gutiérrez, B. Lomonte, Phospholipase A_2 myotoxins from *Bothrops* snake venoms, in: R.M. Kini (Ed.), Venom Phospholipase A_2 Enzymes: Structure, Function and Mechanism, Wiley, Chichester, 1997, pp. 321–352.
[4] C.L. Ownby, Structure, function and biophysical aspects of the myotoxins from snake venoms, J. Toxicol. Toxin Rev. 17 (1998) 1003–1009.
[5] E. Valentin, G. Lambeau, What can venom phospholipase A_2 tell us about the functional diversity of mammalian secreted phospholipase A_2, Biochimie 82 (2000) 815–831.
[6] R.M. Kini, H.J. Evans, A model to explain the pharmacological effects of snake venom phospholipases A_2, Toxicon 27 (1989) 613–635.
[7] A.M. Soares, J.R. Giglio, Chemical modifications on phospholipases A_2 from snake venoms: effects on catalytic and pharmacological properties. Review, Toxicon 42 (2004) 855–868.
[8] P. Needleman, J. Turk, B.A. Jakschik, A.R. Morrison, J.B. Lefkowith, Arachidonic acid metabolism, Annu. Rev. Biochem. 55 (1986) 69–102.
[9] B. Francis, J.M. Gutierrez, B. Lomonte, I.I. Kaiser, Myotoxin II from *Bothrops asper* (terciopelo) venom in a lysine-49 phospholipase A_2, Arch. Biochem. Biophys. 284 (1991) 352–359.
[10] C.L. Ownby, H.S. Selistre de Araújo, S.P. White, J.E. Fletcher, Lysine 49 phospholipases A2 proteins. Review, Toxicon 37 (1999) 411–445.
[11] D.L. Scott, A. Achari, J.C. Vidal, P.B. Sigler, Crystallographic and biochemical studies of the (inactive) Lys49 phospholipase A_2 from the venom of *Agkistrodon piscivorus piscivorus*, J. Biol. Chem. 267 (1992) 22645–22657.
[12] A.J. Magro, A.M. Soares, J.R. Giglio, M.R.M. Fontes, Crystal structures of BnSP-7 and BnSP-6, two Lys49-phospholipases A_2: quaternary structure and inhibition mechanism insights, Biochem. Biophys. Res. Commun. 311 (2003) 713–720.
[13] A.M. Soares, M.R. Fontes, J.R. Giglio, Phospholipase A_2 myotoxins from *Bothrops* snake venoms: structure–function relationship, Curr. Org. Chem. 8 (2004) in press.
[14] W.F. de Azevedo Jr., R.J. Ward, F.R. Lombardi, J.R. Giglio, A.M. Soares, M.R.M. Fontes, R.K. Arni, Crystal structure of myotoxin-II: a myotoxic phospholipase A2 homologue from *Bothrops moojeni* venom, Protein Pept. Lett. 4 (1997) 329–334.
[15] M.T. da Silva-Giotto, R.C. Garrat, G. Oliva, Y.P. Mascarenhas, J.R. Giglio, A.C.O. Cintra, W.F. de Azevedo Jr., R.K. Arni, R.J. Ward, Crystallographic and spectroscopic characterization of a molecular hinge: conformational changes in bothropstoxin I, a

dimeric Lys49-phospholipase A_2 homologue, Proteins: Struct. Funct. Genet. 30 (1998) 442–454.
[16] W.H. Lee, M.T. da Silva-Giotto, S. Marangoni, M.H. Toyama, I. Polikarpov, R.C. Garratt, Structural basis for low catalytic activity in Lys49-phospholipase A_2—a hypothesis: the crystal structure of piratoxin II complexed to fatty acid, Biochemistry 40 (2001) 28–36.
[17] R.K. Arni, M.R.M. Fontes, C. Barberato, J.M. Gutiérrez, C. Díaz-Oreiro, R.J. Ward, Crystal structure of myotoxin II, a monomeric Lys49-phospholipase homologue isolated from the venom of *Cerrophidion* (*Bothrops*) *godmani*, Arch. Biochem. Biophys. 366 (1999) 177–182.
[18] S.H. Andrião-Escarso, A.M. Soares, V.M. Rodrigues, Y. Angulo, C. Diaz, B. Lomonte, J.M. Gutiérrez, J.R. Giglio, Myotoxic phospholipases A_2 in *Bothrops* snake venoms: effect of chemical modifications on the enzymatic and pharmacological properties of bothropstoxins from *Bothrops jararacussu*, Biochimie 82 (2000) 755–763.
[19] D.J. Rigden, L.W. Hwa, S. Marangoni, M.H. Toyama, I. Polikarpov, The structure of the D49 phospholipase A_2 piratoxin III from *Bothrops pirajai* reveals unprecedented structural displacement of the calcium-binding loop: possible relationship to cooperative substrate binding, Acta Crystallogr. D 59 (2003) 255–262.
[20] J.J. Daniele, I.D. Bianco, G.D. Fidelio, Kinetic and pharmacological characterization of phospholipases A_2 from *Bothrops neuwiedii* venom, Arch. Biochem. Biophys. 318 (1995) 65–70.
[21] S.M.T. Serrano, A.P. Reichl, R. Mentele, E.A. Auerswald, M.L. Santoro, C.A.M. Sampaio, A.C.M. Camargo, M.T. Assakura, A novel phospholipase A2, BJ-PLA2, from the venom of the snake *Bothrops jararaca*: purification, primary structure analysis, and its characterization as a platelet-aggregation-inhibiting factor, Arch. Biochem. Biophys. 367 (1999) 26–32.
[22] M.I. Homsi-Brandeburgo, L.S. Queiroz, H. Santo-Neto, L. Rodrigues-Simioni, J.R. Giglio, Fractionation of *Bothrops jararacussu* snake venom: partial chemical characterization and biological activity of bothropstoxin, Toxicon 26 (1988) 615–627.
[23] M.F. Pereira, J.C. Novello, A.C.O. Cintra, J.R. Giglio, E.C.T. Landucci, B. Oliveira, S. Marangoni, The amino acid sequence of bothropstoxin-II, an Asp-49 myotoxin from *Bothrops jararacussu* (jararacucu) venom with low phospholipase A_2 activity, J. Protein Chem. 17 (1998) 381–386.
[24] S.H. Andrião-Escarso, A.M. Soares, M.R.M. Fontes, A.L. Fuly, F.M.A. Corrêa, J.C. Rosa, L.J. Greene, J.R. Giglio, Structural and functional characterization of an acidic platelet aggregation inhibitor and hypotensive phospholipase A_2 from *Bothrops jararacussu* snake venom, Biochem. Pharmacol. 64 (2002) 723–732.
[25] P.G. Roberto, S. Kashima, S. Marcussi, J.O. Pereira, S. Astolfi-Filho, A. Nomizo, J.R. Giglio, M.R.M. Fontes, A.M. Soares, S.C. França, Cloning and identification of a complete cDNA coding for a bactericidal and antitumoral acidic phospholipase A_2 from *Bothrops jararacussu* venom, Protein J. 23 (2004) 273–285.
[26] P.G. Roberto, S. Kashima, A.M. Soares, L. Chioato, V.M. Faça, A.L. Fuly, S. Astolfi-Filho, J.O. Pereira, S.C. França, Cloning and expression of an acidic platelet aggregation inhibitor phospholipase A_2 cDNA from *Bothrops jararacussu* venom gland, Protein Expr. Purif. 37 (2004) 102–108.
[27] Z. Otwinowski, W. Minor, Processing of X-ray diffraction data collected in oscillation mode, Methods Enzymol. 276 (1997) 307–326.
[28] J. Navaza, AMoRe: an automated package for molecular replacement, Acta Crystallogr. A50 (1994) 157–163.
[29] S.K. Han, E.T. Yoon, D.L. Scott, P.B. Sigler, W. Cho, Structural aspects of interfacial adsorption. A crystallographic and site-directed mutagenesis study of the phospholipase A2 from the venom of *Agkistrodon piscivorus piscivorus*, J. Biol. Chem. 272 (1997) 3573–3582.
[30] A.T. Brünger, P.D. Adams, G.M. Clore, W.L. DeLano, P. Gros, R.W. Grosse-Kunstleve, J.S. Jiang, J. Kuszewski, M. Nilges, N.S. Pannu, R.J. Read, L.M. Rice, T. Simonson, G.L. Warren, Crystallography and NMR system (CNS): a new software system for macromolecular structure determination, Acta Crystallogr. D54 (1998) 905–921.
[31] T.A. Jones, M. Bergdoll, M. Kjeldgaard, O: a macromolecule modeling environment, in: C.E. Bugg, S.E. Ealick (Eds.), Crystallographic and Modeling Methods in Molecular Design, Springer-Verlag, New York, 1990, pp. 189–195.
[32] A.T. Brünger, X-PLOR Version 3.1: A System for Crystallography and NMR, Yale University Press, New Haven, 1992.
[33] Collaborative Computing Project No. 4 (CCP4), The CCP4 suite: programs for protein crystallography, Acta Crystallogr. D 50 (1994) 760–763.
[34] R.A. Laskowski, M.W. MacArthur, D.S. Moss, J.M. Thornton, Procheck: a program to check the stereochemical quality of protein structures, J. Appl. Crystallogr. 26 (1993) 283–291.
[35] M. Carson, Ribbons, Methods Enzymol. 277 (1997) 493–505.
[36] S. Xu, L. Gu, T. Jiang, Y. Zhou, Z. Lin, Structures of cadmium-binding acidic phospholipase A_2 from the venom of *Agkistrodon halys* Pallas at 1.9 Å resolution, Biochem. Biophys. Res. Commun. 300 (2003) 271–277.
[37] Y.H. Pan, T.M. Epstein, M.K. Jain, B.J. Bahnson, Five coplanar anion binding sites on one face of phospholipase A_2: relationship to interface binding, Biochemistry 40 (2001) 609–617.
[38] H. Zhao, T. Liang, W. Xiaoqiang, Z. Yuancong, L. Zhengjiong, Structure of a snake venom phospholipase A_2 modified by *p*-bromo-phenacyl-bromide, Toxicon 36 (1998) 875–886.
[39] L. Gu, H. Zhang, S. Song, Y. Zhou, Z. Lin, Structure of an acidic phospholipase A2 from the venom of *Deinagkistrodon acutus*, Acta Crystallogr. D 58 (2002) 104–110.
[40] S. Brunie, J. Bolin, D. Gewirth, P.B. Sigler, The refined crystal structure of dimeric phospholipase A2 at 2.5 Å. Access to a shielded catalytic center, J. Biol. Chem. 260 (1985) 9742–9749.
[41] V. Chandra, P. Kaur, J. Jasti, C. Betzel, T.P. Singh, Regulation of catalytic function by molecular association: structure of phospholipase A2 from *Daboia russelli pulchella* (DPLA2) at 1.9 Å resolution, Acta Crystallogr. D 57 (2001) 1793–1798.
[42] K. Zhao, S. Song, Z. Lin, Y. Zhou, Structure of a basic phospholipase A2 from *Agkistrodon halys* Pallas at 2.13 Å resolution, Acta Crystallogr. D 510 (1998) 510–521.
[43] T. Jabeen, A.K. Varma, M. Paramasivam, N. Singh, R.K. Singh, S. Sharma, A. Srinivasan, T.P. Singh, Crystal structure of a zinc containing dimer of phospholipase A2 from the venom of Indian cobra (*Naja naja saggittifera*), to be published.
[44] R. Renetseder, S. Brunie, B.W. Dijkstra, J. Drenth, P.B. Sigler, A comparison of the crystal structures of phospholipases A_2 from bovine pancreas and *Crotalus atrox* venom, J. Biol. Chem. 260 (1985) 11627–11636.
[45] W.R. Pearson, Rapid and sensitive sequence comparison with FASTP and FASTA, Methods Enzymol. 183 (1990) 63–98.
[46] A.H. de Oliveira, J.R. Giglio, S.H. Andrião-Escarso, A.S. Ito, R.J. Ward, A pH-induced dissociation of the dimeric form of a lysine 49-phospholipase A_2 abolishes Ca^{2+}-independent membrane damaging activity, Biochemistry 40 (2001) 6912–6920.
[47] N. Dekker, Outer-membrane phospholipase A: known structure, unknown biological function, Mol. Microbiol. 35 (2000) 711–717.
[48] H.J. Snijder, I. Ubarretxena-Belandia, M. Blaauw, K.H. Kalk, H.M. Verheij, M.R. Egmond, N. Dekker, B.W. Dijkstra, Structural evidence for dimerization-regulated activation of an integral membrane phospholipase, Nature 401 (1999) 717–721.
[49] S.A. Sanchez, Y. Chen, J.D. Muller, E. Gratton, T.L. Hazlett, Solution and interface aggregation states of *Crotalus atrox* venom phospholipase A_2 by two-photon excitation fluorescence correlation spectroscopy, Biochemistry 40 (2001) 6903–6911.

doi:10.1016/j.jmb.2005.04.072 J. Mol. Biol. (2005) 350, 416–426

JMB

Available online at www.sciencedirect.com

SCIENCE DIRECT®

ELSEVIER

Inhibition of Myotoxic Activity of *Bothrops asper* Myotoxin II by the Anti-trypanosomal Drug Suramin

Mário T. Murakami[1], Emerson Z. Arruda[2], Paulo A. Melo[2] Ana B. Martinez[2], Sabriña Calil-Eliás[2], Marcelo A. Tomaz[2] Bruno Lomonte[3], José M. Gutiérrez[3] and Raghuvir K. Arni[1,4]*

[1]*Departament of Physics IBILCE/UNESP, São José do Rio Preto, SP, Brazil*

[2]*Departamento de Farmacologia Básica e Clínica, IBC/UFRJ Rio de Janeiro, RJ, Brazil*

[3]*Instituto Clodomiro Picado Facultad de Microbiología Universidad de Costa Rica San José, Costa Rica*

[4]*Center for Applied Toxinology Instituto Butantan, São Paulo SP, Brazil*

**Corresponding author*

Suramin, a synthetic polysulfonated compound, developed initially for the treatment of African trypanosomiasis and onchocerciasis, is currently used for the treatment of several medically relevant disorders. Suramin, heparin, and other polyanions inhibit the myotoxic activity of Lys49 phospholipase A_2 analogues both *in vitro* and *in vivo*, and are thus of potential importance as therapeutic agents in the treatment of viperid snake bites. Due to its conformational flexibility around the single bonds that link the central phenyl rings to the secondary amide backbone, the symmetrical suramin molecule binds by an induced-fit mechanism complementing the hydrophobic surfaces of the dimer and adopts a novel conformation that lacks C2 symmetry in the dimeric crystal structure of the suramin–*Bothrops asper* myotoxin II complex. The simultaneous binding of suramin at the surfaces of the two monomers partially restricts access to the nominal active sites and significantly changes the overall charge of the interfacial recognition face of the protein, resulting in the inhibition of myotoxicity.

Keywords: suramin; heparin; myotoxicity; inhibition; crystal structure

Introduction

Suramin (8,8′-[carbonylbis [imino-3,1-phenylene-carbonylimino (4-methyl-3,1-phenylene) carbonylimino]] bis-1,3,5-naphtalenetrisulfonic acid hexasodium salt), a highly charged polysulfonated compound, is one of the first successful synthetic therapeutic agents developed and is used clinically in the treatment of African trypanosomiasis and onchocerciasis.[1–4] The spectrum of suramin applications now includes the clinical treatment of angiogenesis, carcinomas of the kidney and prostate gland, breast cancer, inhibition of growth factor/receptor interactions, inhibition of human α-thrombin, protein-tyrosine phosphatases, G proteins, merozoite surface protein-1, and acidic and basic fibroblast growth factors.[5–14] Suramin prevents the development of muscle necrosis induced by some snake venoms, since it inhibits the myotoxic and *in vitro* neuromuscular blocking activities of Lys49 phospholipases A_2 from *Bothrops* species.[15,16]

Phospholipases A_2 (PLA_2s: EC 3.1.1.4) are key enzymes in the control, regulation, production and release of lipid mediator precursors that serve as messengers in fundamental, highly regulated processes such as growth, adhesion, apoptosis, secretion, hemostasis and immune regulation. The group II PLA_2s encountered in viperid snake venoms and mammalian fluids share significant sequence homology, and are based on a single structural motif or scaffold.[17] Snake venom PLA_2s exhibit a wide spectrum of activities including myotoxic, neurotoxic, cardiotoxic, anticoagulant, platelet-aggregating, hypotensive and inflammatory effects.[18] On the basis of sequence and structural similarities, the snake venom group II PLA_2s can be subdivided into (a) the catalytically active Asp49 enzymes and (b) the basic, myotoxic Lys49 proteins, which possess no catalytic activity.[17] Myotoxicity

Abbreviations used: Basp-II, *Bothrops asper* myotoxin II; PLA_2s, phospholipases A_2; suramin, 8,8′-[carbonylbis [imino-3,1-phenylenecarbonylimino (4-methyl-3,1-phenylene) carbonylimino]] bis-1,3,5-naphtalenetrisulfonic acid hexasodium salt; CK, creatine kinase; PEG, polyethylene glycol; *i*-face, interfacial recognition face; EDL, extensor digitorum longus; PSS, physiological saline solution; Hepes, 4-(2-hydroxyethyl)-1-piperazineethanesulfonic acid; i.m., intramuscular.

E-mail address of the corresponding author: arni@df.ibilce.unesp.br

affects only muscle fibers without damaging other tissue structures such as connective tissue, nerves and vessels,[19] and can lead to permanent tissue loss, disability, amputation and death.[20]

Suramin binds to a surprisingly wide variety of proteins of different function, structure and size due to its torsional flexibility and ability to stretch or compress itself, which results in the two naphthyl rings with the sulfonate groups being able to interact simultaneously with a number of structurally distinct sites. Due to a lack of structural information, the target sites, conformational flexibility and mode of binding of suramin to proteins are still unclear at the atomic level.

The crystal structure of the complex between suramin and *Bothrops asper* myotoxin II represents the first crystal structure of suramin bound to a protein. The structural details presented here should be of relevance in understanding the steric requirements of suramin binding to proteins, and should shed light on the mechanism of myotoxicity displayed by Lys49 phospholipases A_2 and their inhibition by polyanionic compounds.

Results

In vitro myotoxicity

As illustrated in Figure 1(a), *B. asper* myotoxin II caused a time-dependent increase in the rate of creatine kinase release from isolated extensor digitorum longus muscles. A more pronounced effect is observed after 90 minutes with 25 μg/ml of *B. asper* myotoxin II alone. The presence of suramin (10 μM) together with the toxin markedly inhibits the creatine kinase release induced by the *B. asper* myotoxin II (Basp-II). After 90 minutes of exposure to the toxin, in the presence of suramin, the creatine kinase release was less than 15% of the value measured in the absence of suramin.

In vivo myotoxicity

Intramuscular (i.m.) injections of Basp-II alone increased plasma creatine kinase (CK) activity in a dose and time-dependent fashion. Figure 1(b) indicates that an i.m. injection of Basp-II (2.0 μg/g) induced a significant increase in plasma CK activity compared to physiological saline solution. CK levels increased from 65($\pm$42) units/l (mean$\pm$SEM, $n=4$) to 1368($\pm$386) units/l ($n=4$) after two hours. These values of plasma CK activity are in agreement with previously reported observations.[21] Preincubation with suramin significantly ($p<0.05$) inhibits the increase in plasma CK activity induced by Basp-II. Experiments performed following protocol B (see Materials and Methods) indicate that suramin also significantly inhibits ($p<0.05$) the plasma CK activity increment induced by Basp-II. However, under these conditions, suramin was less effective in antagonizing myotoxicity than when incubated with Basp-II prior to injection. Figure 2 presents light micrographs of extensor digitorum longus muscle exposed to either Basp-II (Figure 2(b) and (b′)), Basp-II pre-incubated with suramin (1 mg/kg) (Figure 2(c) and (c′)) or post-treated with suramin (1 mg/kg) 15 minutes after Basp-II injection. In all samples, normal muscle cells were observed in the central region of the muscle, whereas the peripheral fibers were in different stages of necrosis, characterized by densely clumped myofibrils and swollen cells. Pre-incubation or post-treatment with suramin resulted in a reduction in the number of necrotic fibers (Figure 2(c) and (d)).

Crystal structure

Data collection and processing statistics are presented in Table 1. Molecular replacement using a single molecule of native Basp-II (PDB ID, 1CLP) as the search model resulted in clear rotation and translation solutions for the two molecules in the asymmetric unit, with a correlation coefficient of

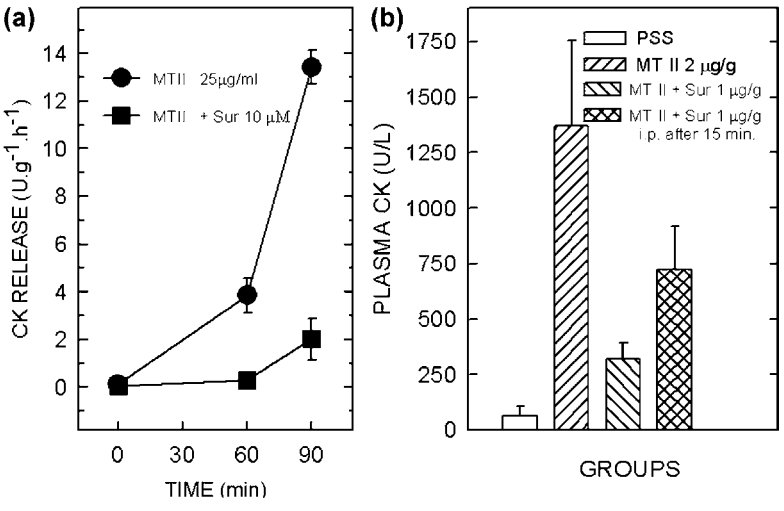

Figure 1. *In vitro* and *in vivo* inhibition of myotoxicity of Basp-II by suramin. (a) Experiments performed on isolated EDL mouse muscle exposed to Basp-II (25 μg/ml) alone or with 10 μM suramin. The toxin was applied at time zero in the absence (filled circles) or in the presence of suramin (filled squares). (b) The effect of i.m. injection of Basp-II alone (2.0 μg/g), pre-incubated with suramin (1.0 mg/kg), or post-treated with the same dose of suramin (1.0 mg/kg; intraperitoneal route), 15 minutes after the venom i.m. injection. In (a) and (b), the data represent the mean values$\pm$SEM ($n=4$).

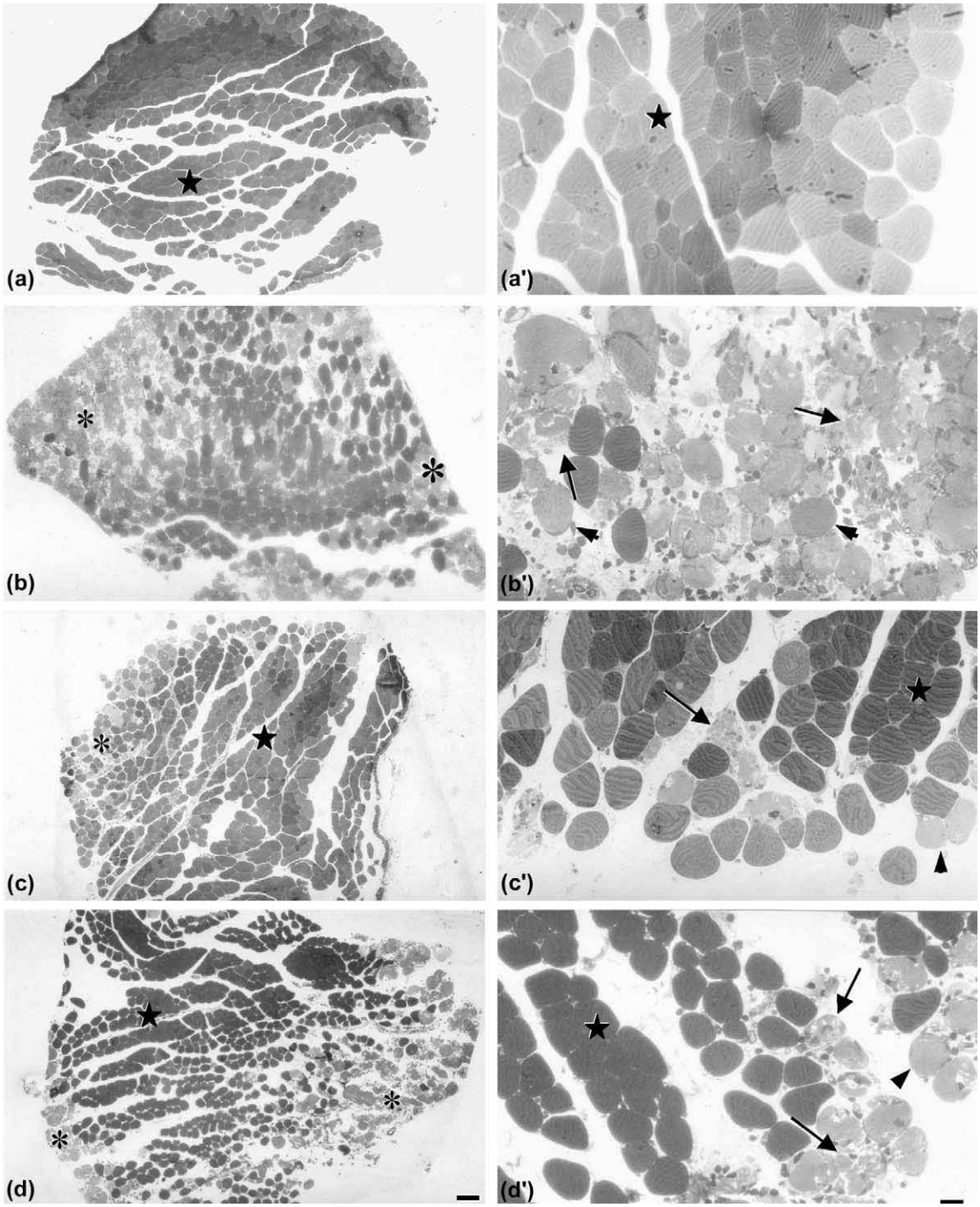

Figure 2. Light micrographs of cross-sections of mouse EDL muscle 24 hours after the injection of PSS or Basp-II. (a) and (a′) Panoramic and close-up views of the control muscle showing normal muscle cells (star) and muscle structure, respectively. (b) and (b′) Intense degeneration of the peripheral muscle cells (asterisk), and the details of the lesion induced by the Basp-II 24 hours after injection, respectively. Swollen cells (arrowhead) and clumped myofibrils (arrow) are indicated. (c) A section of muscle from the group that received Basp-II pre-incubated with suramin (1 mg/kg). (d) Tissue from the group treated with suramin (1 mg/kg) 15 minutes after injection of Basp-II. There are normal muscle cells in the central region (star) and an inflammatory reaction at the periphery (asterisk). Swollen cells (arrowhead) and clumped myofibrils (arrow) are shown in detail in (c′) and (d′). Scale bars represent: (a), (b) and (c) 200 μm; (a′), (b′) and (c′) 50 μm.

75.8% and an *R*-factor of 30.5% after rigid-body refinement. After four cycles of refinement and model building, the electron density peaks above 2σ in the Fourier difference maps were examined and the additional electron density present in the vicinity of the calcium-binding loop was identified as belonging to the trisulphonate naphthalene ring of the suramin molecule. At all stages of the

Table 1. Data collection, refinement statistics and hydrogen bond distances between Basp-II and suramin (atom numbering scheme based on the deposited atomic coordinates 1Y4L)

	Basp-II+suramin		
A. Crystal preparation			
Cryoprotectant solution	Mother liquor+25% glycerol		
Soaking time	30 seconds		
B. Data collection			
Wavelength (Å)	1.437		
Temperature (K)	100		
Detector	MARCCD		
Synchrotron radiation source	CPr beamline/LNLS-Brazil		
Space group	$P2_12_12_1$		
Unit cell parameters			
a (Å)	49.20		
b (Å)	64.04		
c (Å)	85.99		
Resolution (Å)	30.0–1.70 (1.74–1.70)		
No. molecules in the asymmetric unit	2		
Solvent content (%, v/v)	56		
V_M (Å^3 Da^{-1})	2.8		
No. reflections	253,143		
No. unique reflections[a]	15,224 (907)		
$I/\sigma(I)$	26.0 (2.8)		
Multiplicity	6.5 (5.5)		
Completeness (%)	99.3 (97.4)		
R_{merge}[b] (%)	4.9 (50.7)		
C. Structure refinement statistics			
R_{factor} (%)	20.6		
R_{free} (%)	24.0		
rmsd from ideal			
Bond distances (Å)	0.012		
Bond angles (deg.)	1.663		
Average *B*-factors (Å^2)	26.0		
Ramachandran plot analysis			
Most favoured regions (%)	91.5		
Additional allowed regions (%)	7.5		
Generously allowed regions (%)	1.0		
Hydrogen bonds			
Protein		Suramin	
Residue	Atom	Atom	Distance (Å)
Arg34 (A)	N	O29	2.97
Arg34 (A)	N^{ε}	O30	2.53
Arg34 (A)	NH2	O30	3.33
Lys53 (A)	N^{ζ}	O28	3.00
Lys53 (A)	N^{ζ}	O30	3.15
Arg34 (B)	NH1	O82	3.06
Lys53 (B)	N^{ζ}	O80	2.64
Lys53 (B)	N^{ζ}	O82	3.34
Lys69 (B)	N^{ζ}	O54	2.75

Statistical values for the highest-resolution shells are given in parentheses.

[a] Multiplicities of the derivative data sets were calculated with the Friedel-related reflections treated separately. Multiplicity of the native data set was calculated with the Friedel-pairs treated as equivalent.

[b] $R_{merge} = \Sigma|I(h)_l - \{I(h)\}|/\Sigma\{I(h)\}$, where I_h is the observed intensity of the *i*th measurement of reflection *h* and $\{I(h)\}$ is the mean intensity of reflection *h* calculated after scaling.

refinement, the electron density maps indicated the presence of a bound polyethylene glycol (PEG) molecule in both the monomers in the hydrophobic channels that leads to the active sites. As in the crystal structure of the highly homologous Bothropstoxin-I, a Lys49 phospholipase A_2 (PLA_2) from the venom of *Bothrops jararacussu*, the hydroxyl groups of PEG form hydrogen bonds to His48 $N^{\delta1}$ (Figure 3) and the extended tails of the bound PEG molecules occupy the positions of the fatty acids (Figure 4(a)) of the phospholipid analogue (PDB ID, 1POE).[22] The refinement converged to a crystallographic residual of 20.5% (R_{free}=24.0%) for all data between 30.0 Å and 1.70 Å (Table 1). The final model consists of the 242 amino acid residues, 170 solvent molecules, five isopropanol molecules, two fragments of PEG 3350 and a suramin molecule. The crystal structure is characterized by excellent stereochemistry, as indicated by an analysis of the deviations from ideal values of the bond lengths, bond angles, planarity and non-bonded contacts (Table 1). The two molecules in the asymmetric unit are related by a 2-fold axis of rotation, and the hydrophobic surfaces surrounding the entrance to the active sites form the dimer interface, resulting in the burial of 3446 Å^2 of the surface area of each molecule (30.9%).

The structure of group IIA PLA_2s has been reviewed extensively,[17,23] and consists of three α-helices, a short β-wing and connecting loops (Figure 3). The principal, highly conserved structural feature is a platform formed by the two long anti-parallel disulfide-linked (Cys29-Cys45 and Cys51-Cys98) α-helices (helices 2 and 3, residues 37–54 and 90–109) on which are located the amino acid residues considered important for catalytic activity (His48, Asp49, Tyr52, Tyr73 and Asp99). The interfacial recognition surface contains a wide hydrophobic collar and provides access to the catalytic site. In the case of catalytically active Asp49 PLA_2s, His48 and Asp99 together with a structurally conserved water molecule (hydrogen bonded to His48 $N^{\delta1}$) participate in the nucleophilic attack at the sn-2 position of the phospholipid substrate. The tetrahedral transition state intermediate is stabilized by a calcium ion and is coordinated by Asp49 and the main-chain atoms located in the calcium-binding loop. In the subgroup of Lys49 PLA_2 analogues, substitution of Asp49 by Lys results in the N^{ζ} atom of Lys49 occupying the position of the calcium ion in Asp49 PLA_2s.[17,24] These Lys49 PLA_2s are capable of binding fatty acids,[25] stearic acid[26] and PEG. The controversy as to whether these enzymes possess catalytic activity[27–29] has been clarified, since no substrate hydrolysis was detected with the wild-type recombinant protein.[30]

Suramin-binding site

NMR experiments indicate that the conformational flexibility at α3/α3′ and α4/α4′ and the *C*2 symmetry enable suramin to adopt multiple conformations wherein the two sulfonated naphthyl rings are separated by distances between 16 Å and 30 Å in the compact and fully extended conformations, respectively (Figure 5).[9] In this structure, suramin adopts a novel conformation that lacks *C*2 symmetry, with an overall

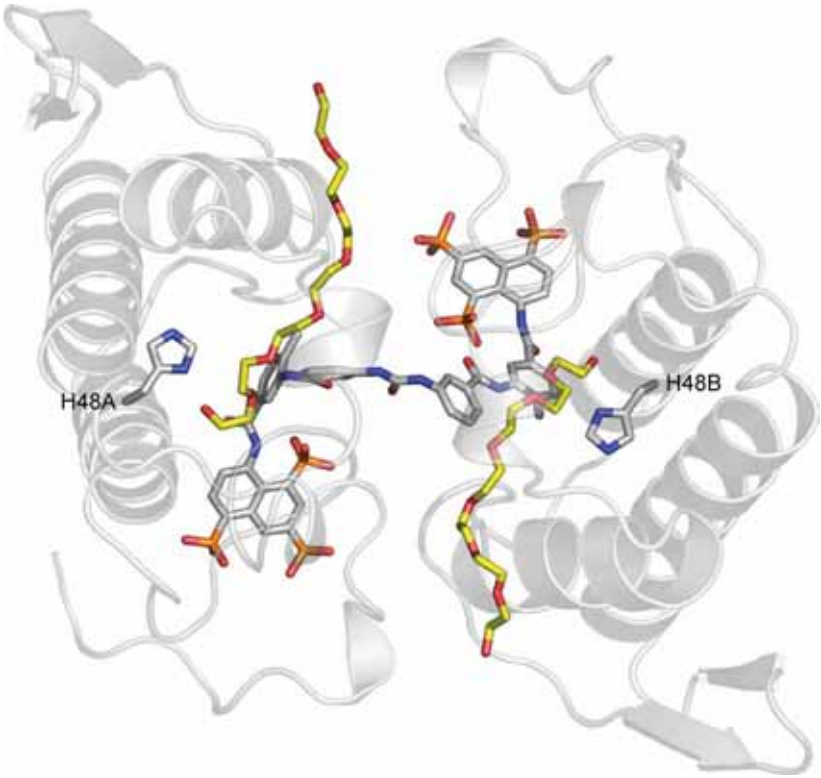

Figure 3. Ribbon representation of the Basp-II dimer, suramin and PEG (atom colors) bound to His48. Figures 3 and 4 were generated using PYMOL (http://www.pymol.org).

length of 24.7 Å and dihedral angles of $\alpha1 = 22.8°$, $\alpha2 = -4.0°$, $\alpha3 = 91.5°$, $\alpha4 = 148.8°$, $\alpha5 = 136.9°$, $\alpha1' = 24.3°$, $\alpha2' = 53.3°$, $\alpha3' = -93.2°$, $\alpha4' = -128.9°$ and $\alpha5' = 177.2°$.

In the protein molecule A, the hydrophobic naphthalene ring is very clearly defined in the electron density maps (Figure 6), aligns itself in relation to the putative calcium-binding loop

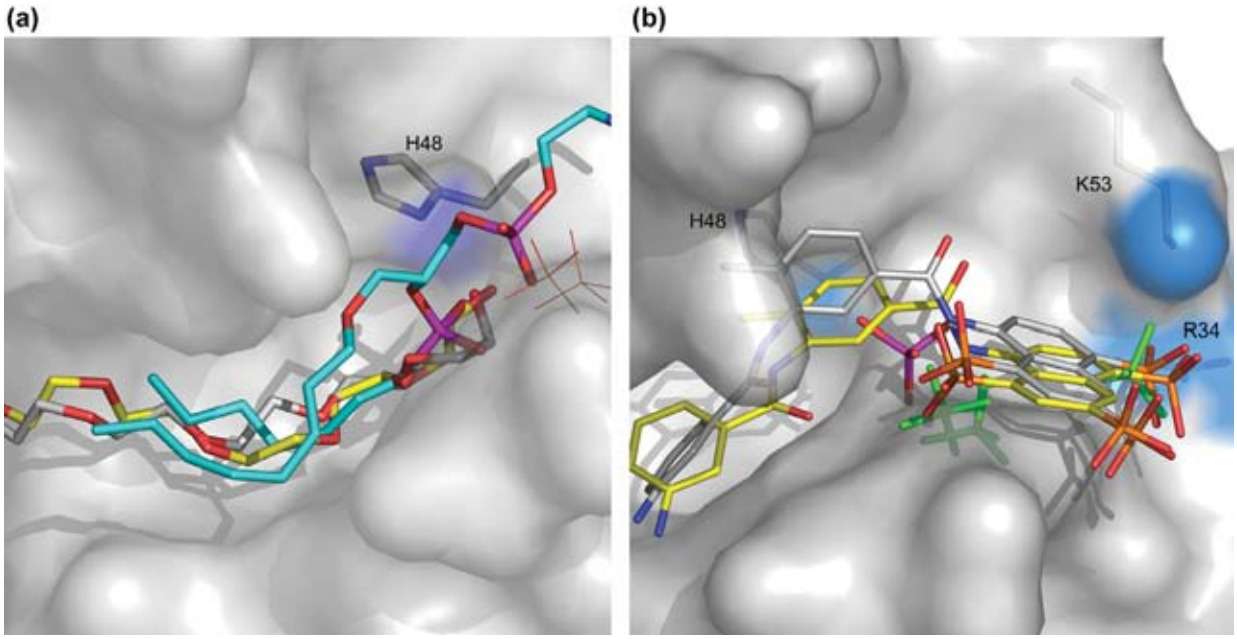

Figure 4. Specific interactions in the putative catalytic and calcium binding sites. (a) Binding of PEG molecules in the active-site cleft, molecule A (grey/red) and molecule B (yellow/red). The transition-state analogue (PDB ID, 1POE) presented with the carbon atoms in cyan. Thin lines indicate the positions of the sulfate ions (PDB ID, 1S8H and 1S8I). (b) Suramin binding near the putative calcium-binding loop. The carbon atoms from the naphthalene rings of suramin bound to molecules A and B are presented in grey and yellow, respectively. The position of the phosphate moiety of the transition-state inhibitor is presented in magenta (PDB ID, 1POE) and the sulfate ions encountered in the crystal structures of ACL myotoxin (PDB ID, 1S8G, 1S8H and 1S8I) are presented in green.

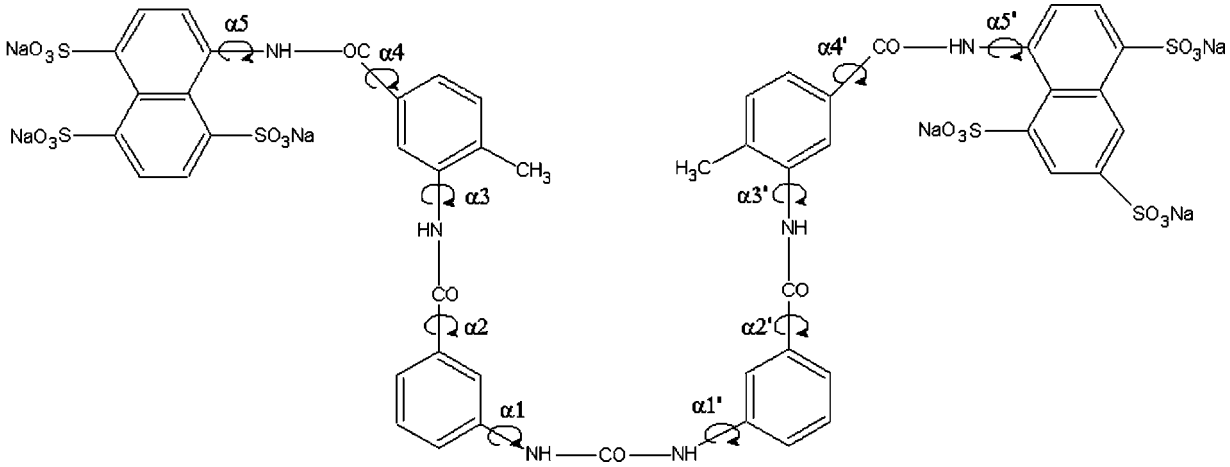

Figure 5. Chemical structure and torsion angles of suramin. This Figure was generated using ChemSketch version 5.0 (http://www.acdlabs.com/).

(residues 27–35) and is additionally stabilized by hydrogen bonds to Arg34 and Lys53 (Figures 4(b) and 6; and Table 1). The adjacent phenyl ring interacts with hydrophobic amino acid residues in the loop that links helix 2 with the β-wing (residues 65–71), whereas the central phenyl ring is stabilized by hydrophobic interactions with residues surrounding the active site and the N terminus. The distal or second naphthalene ring of suramin, which is less well defined in the electron density maps, binds in a similar fashion between loops C and E to the second protein molecule interacting with Arg34B and Lys53B (Table 1).

Discussion

Myonecrosis is a major event in envenomation by snakes and compounds such as suramin, heparin, heparin-like glycosaminoglycans and related polyanions inhibit the activity of myotoxic PLA_2s both *in vitro* and *in vivo*.[31–35] A number of studies have

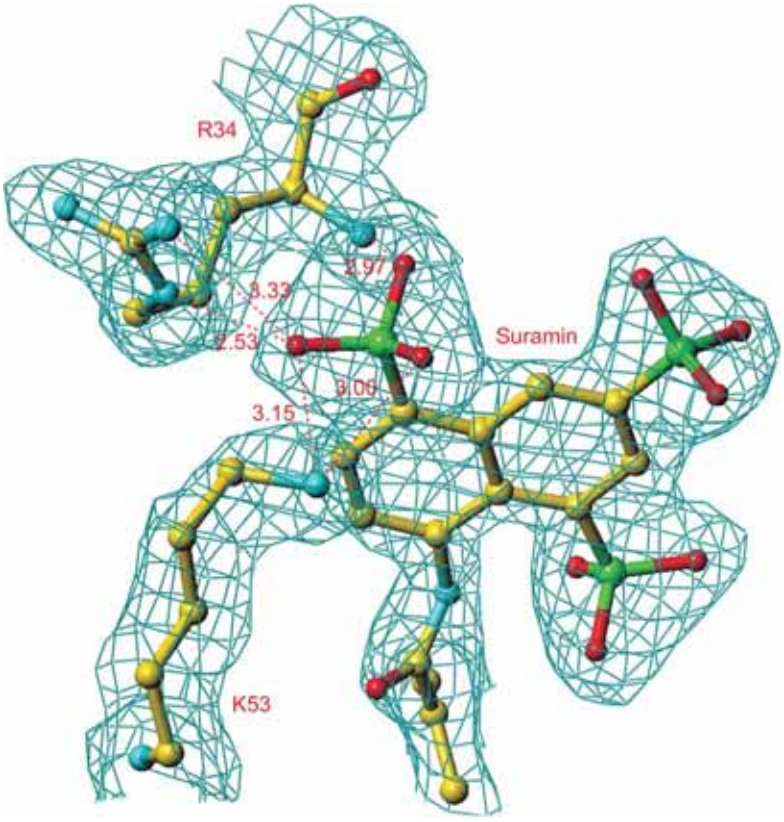

Figure 6. Electron density contoured at 1.5σ around the suramin molecule. Hydrogen bonds between suramin and Arg34 and Lys53 are in red (broken lines).

attempted to identify and to delineate the region or regions important for the expression of myotoxicity in PLA_2s,[23] on the basis of sequence homology,[36–38] charge distribution,[39–41] hydrophobicity profiles,[39] chemical modification,[42,43] use of synthetic peptides,[34,44,45] and site-directed mutagenesis.[30,46]

With the biochemical and structural information currently available we are now able to probe the structure–function relationship, and the mode of action and inhibition of Lys49 PLA_2 analogues by addressing the roles of the C-terminal region and the nominal active site in myotoxicity.

Suramin and its inhibitory effects

Since the conformational flexibility of suramin is restricted to rotations around the single bonds, the simultaneous binding of the naphthalene rings to the two protein molecules perturbs the putative calcium-binding loop and the C-terminal extensions.

The interfacial recognition face (*i*-face) of myotoxic Lys49 PLA_2s contains a high density of positive charges, a structural feature that has been associated with the ability of these proteins to interact with phospholipid bilayers.[23,41] The induced-fit binding of suramin results in the burial of 102.1 $Å^2$ (total surface area of suramin = 335.1 $Å^2$), does not directly involve amino acid residues in the putative catalytic site but modifies the surface charge significantly (Figure 7). This change in the charge on the *i*-face plays a crucial role in the inhibition of myotoxicity, since Basp-II would now be unable to bind to the negatively charged membrane target in muscle cells.

The heparin-binding site

The positions of the sulfonate groups of suramin and the sulfate ions encountered in the crystal structure of Lys49 PLA2s[25] were used as a guide to overlay the atomic coordinates of heparin (PDB ID, 1XMN). This leads us to speculate that this highly conserved sulfate-binding site could represent the primary heparin-binding site in Basp-II. In this orientation, the heparin molecule could extend towards the C-terminal region, interacting with residues 115–129, which contain the motif B–B–X–B (where B denotes a basic amino acid) and a total of six basic residues out of 13.[34] This is analogous to the interaction in the suramin–bFGF complex model, where the induced-fit binding of suramin sterically blocks the receptor-binding region of bFGF and competes for the binding of heparin.[47]

The role of the C terminus

The C-terminal region (residues 115–134) of myotoxic Lys49 PLA_2s forms a cationic/hydrophobic site that has been suggested to play a role in the mediation of electrostatic interactions with negatively charged acceptors, acting as a cytolytic motif.[34,44,45,48] A synthetic peptide corresponding to residues 115–129 of Basp-II induces cytolysis, interferes with the interaction between heparin and Basp-II, and binds directly to radiolabeled heparin in solution.[34] Although the i.m. injection of this peptide failed to induce myotoxicity in mice,[28,49] the corresponding analogous peptides of related Lys49 PLA_2s from *Agkistrodon piscivorus piscivorus*[45] and *Agkistrodon contortrix laticinctus*[28] venoms are myonecrotic. Site-directed mutagenesis has further demonstrated the importance of specific residues in the C-terminal region for the development of myotoxic activity in another Lys49 PLA_2 from *B. jararacussu* venom, bothropstoxin-I.[46] Substitution of Lys and Arg residues with Ala in the C terminus results in a significant loss of myotoxic activity of the recombinant bothropstoxin-I.[46]

The crystal structure of Basp-II (PDB code, 1CLP) determined in the absence of a ligand results in the exposure of the hydrophobic residues in the C-terminal region, which are referred to collectively

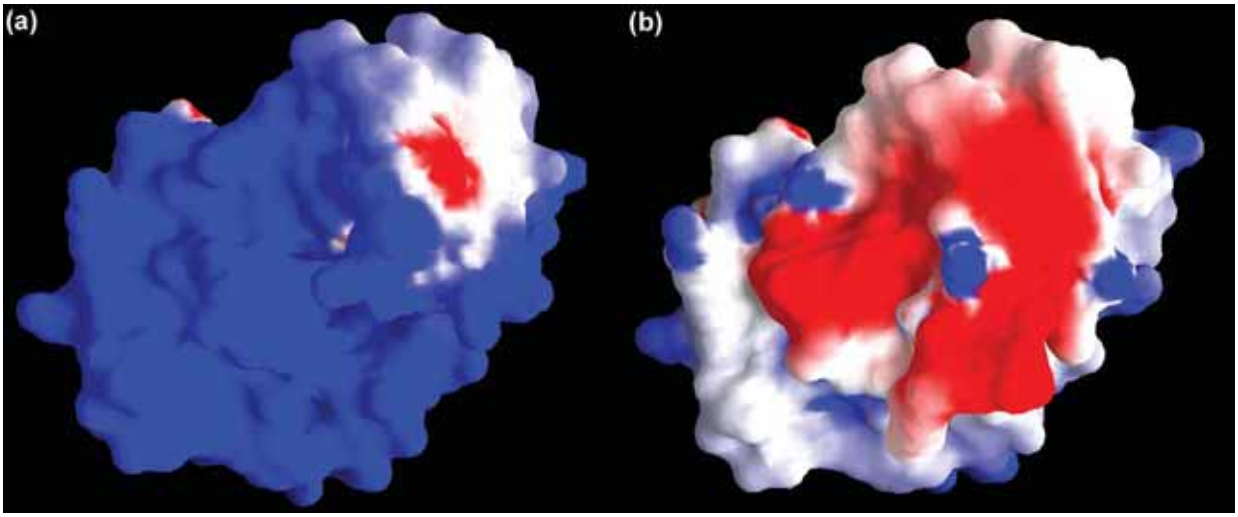

Figure 7. Surface charge distribution (red negative and blue positive) of the monomers, (a) of Basp-II and (b) of the Basp-II + suramin complex in the same orientation.

as the hydrophobic knuckle (residues Leu121 and Leu124), due to the interaction of Lys122 with the peptide bond formed between Cys29 and Gly30.[25] Superpositioning the structures of this protein in the ligand-free state and when bound to suramin results in an overall rmsd of 0.6 Å. The largest deviations are observed in the putative calcium-binding loop (rmsd 0.9 Å for residues 28–35), at the base of the β-wing, which is generally disordered (rmsd greater than 1.5 Å for residues 86–87) and in the C-terminal region (rmsd between 0.9 Å and 1.8 Å for residues 120–129). An analysis of these deviations indicates that the binding of suramin does not alter the interactions that are responsible for maintaining the conformation of the hydrophobic knuckle but results in a rigid-body shift of the motif formed by the putative calcium-binding loop and C terminus.

In our X-ray model, the C-terminal region does not form part of the suramin-binding site of the dimer, but contributes significantly to the maintenance of the positive charge on the *i*-face, which is important for the binding of the myotoxin to the phospholipid bilayers. Thus, the C terminus, besides being involved in the development of myonecrosis, also likely plays a dual role by maintaining the positive charge on the *i*-face and interacting with the putative calcium-binding loop.

The putative active site

Lys49 PLA_2s are capable of binding fatty acids,[25,50] stearic acid,[26] and PEG at the nominal catalytic site. The induced-fit binding of suramin at the surface does not completely block access to the nominal active site. Thus, the active site is still accessible to fatty acids, as evidenced by the presence of PEG molecules bound to His48, which occupy positions analogous to lysophospholipids in the structure of human group IIA PLA_2 (PDB ID, 1POE; Figure 4(a)) complexed with the transition-state analogue (L1-O-octyl-2-heptylphosphonyl-sn-glycero-3-phosphoethanolamine). A direct relationship between the active site and the C terminus in a Lys49 PLA_2 has been proposed by the hyperpolarization of the hydrogen bond formed by Lys122 NE and the peptide bond between residues Cys29 and Gly30.[25]

Concluding remarks

These results suggest strongly that suramin is a potentially useful drug in the prevention of acute muscle toxicity associated with *Bothrops* sp. snakebite envenomation, since it is highly effective in inhibiting the myotoxic activity of Basp-II *in vitro* and *in vivo*, pre-incubated or administered alone after injection of the toxin. The structural results indicate that the relative orientation of the putative calcium-binding loop and C-terminal regions together with the maintenance of the charge pattern on the *i*-face could be important for myotoxicity in Lys49 PLA_2s. Due to the diversity of proteins that suramin can bind to, it is tempting to speculate that it may interact with other PLA_2s from venoms and other sources including mammalian group IIA PLA_2s, thus suggesting a wider pharmacological potential for this inhibitor and these structural results should serve as the basis for the development of novel naphthalene sulfonate derivatives.

Materials and Methods

Basp-II and suramin

Basp-II was isolated by two cycles of cation-exchange chromatography on CM-Sephadex C-25, as described.[51] Suramin was obtained from Sigma Chemical Co. (St. Louis, MO, USA). All other reagents were of analytical grade.

In vitro myotoxicity

In vitro myotoxicity experiments were performed at room temperature.[31,32] The extensor digitorum longus muscles from mice were removed, blotted, weighed immediately and then transferred to sample-collecting units of 2.5 ml capacity, where they were superfused continuously at a flow-rate of 3.0 ml/minute with a physiological saline solution equilibrated with 95% (v/v) O_2, 5% (v/v) CO_2. Perfusing physiological saline solution contained 135 mM NaCl, 5 mM KCl, 2 mM $CaCl_2$, 1 mM $MgCl_2$, 15 mM $NaHCO_3$, 1 mM NaH_2PO_4, 11 mM glucose. The final pH was adjusted to 7.3 after physiological saline solution (PSS) equilibration with the gaseous mixture. After 60 minutes equilibration, Basp-II alone (25 μg/ml) or the Basp-II plus suramin (10 μM) were added to the solution containing the extensor digitorum longus (EDL) muscles and then the perfusates were collected and replaced with fresh PSS. The collected samples were stored at 4 °C. CK activity was determined by using a diagnostic kit (Sigma Chemical Co., USA). The rate of CK release from the isolated muscles was expressed as the increase in CK release compared to control values. Basal release rate refers to the enzyme loss from the muscles into the PSS medium during the equilibration period of perfusion (one hour), starting immediately after the preparation had been mounted in the sample-collection unit. The CK activity was expressed in international units (U), where 1 U is the amount that catalyzes the transformation of 1 μmol of substrate at 25 °C. The rate of CK release from the isolated muscle was expressed as enzyme units released into the medium per gram per one hour of collection ($U\ g^{-1}\ h^{-1}$).[31,32]

In vivo myotoxicity

Changes in plasma CK activity

Basp-II was dissolved in 0.1 ml of PSS and injected by the i.m. route into the thighs of Swiss mice (20–25 g body weight). The amounts of toxin or suramin administered were adjusted taking into account the weight of each animal and injected in doses of 2.0 μg/g for the toxin and 1.0 μg/g for suramin. Previous studies indicate that i.m. injection of 0.1 ml of PSS has no effect on plasma CK activity.[21,32] Two different experimental protocols were used; in protocol A, Basp-II and suramin were incubated for 15 minutes at 37 °C, and then injected i.m. into each

animal. In protocol B, Basp-II was administered i.m. to the animals 15 minutes before the intraperitoneal injection of suramin (1.0 μg/g). In both protocols, the final volume of toxin injected, either alone or with suramin, was 0.1 ml. The animals were anesthetized lightly with diethyl ether immediately before and two hours after the injection of the toxin for blood collection, in accordance with guidelines for care and use of laboratory animals.[52] Plasma was separated by centrifugation and stored at 4 °C for subsequent determination of CK activity as described above.

Histological alterations

Mice, weighing 25.0(±5.0) g, were assembled into four groups of three mice each. Animals were anesthetized with ether, and subsequently injected with Basp-II (2.5 μg/g in 50 μl of PSS). Injection was performed just over the EDL muscle of the right limb, as described.[53] The control group was injected only with PSS in the right paw (50 μl). Two different experimental protocols were used for the study of suramin antimyotoxic effect. In the first protocol, the Basp-II was incubated with suramin (1 mg/kg) for 15 minutes prior to the injection of the mixture. In the second protocol, suramin (1 mg/kg) was injected i.v. 15 minutes after the injection of Basp-II. The mice were anesthetized with ether and sacrificed by cervical dislocation 24 hours after the injection of the toxin. The EDL muscles were dissected and fixed for two to three hours in 2.5% (v/v) glutaraldehyde, 4% (v/v) paraformaldehyde in 0.1 M sodium cacodylate (pH 7.4). They were subsequently washed thrice in the same buffer and post-fixed for one hour in 1% (w/v) osmium tetroxide. The tissue was then dehydrated in increasing concentrations of acetone (30–100%, v/v) and embedded in Polybed 812 resin. Sections (400–600 nm) for light microscopic examination were obtained using an RMC ultramicrotome and stained with 1% (w/v) toluidine blue dye.

Crystallization and X-ray diffraction data collection

Basp-II was dissolved at a concentration of 10 mg/ml in 0.02 M Hepes (pH 7.5) and suramin was added at a molar ratio of 1:1.2. This complex was crystallized from a solution containing 0.1 M sodium acetate (pH 4.6), 15% (w/v) PEG 3350, 20% (v/v) isopropanol at 291 K by the hanging-drop, vapor-diffusion method as described.[54]

X-ray diffraction data were collected at 100 K from a single crystal at a synchrotron radiation source (PCr beamline, Laboratório Nacional de Luz Sincrotron, LNLS, Campinas, Brazil) where the wavelength was set to 1.427 Å. Diffraction intensities were measured using a MARCCD detector (MAR Research), and the diffraction data were integrated, reduced and processed using the DENZO/SCALEPACK suite of programs.[55]

Structure determination and refinement

The atomic coordinates of Basp-II[24] (PDB ID, 1CLP) were utilized to solve the structure by molecular replacement with the program package AMoRe.[56] Non-crystallographic symmetry restraints were imposed in the early cycles of refinement and the translation-libration-screw, positional and restrained isotropic *B*-factor refinements were carried out using REFMAC5,[57] and the electron density maps were examined after each round of refinement with TURBO-FRODO.[58] The stereochemistry of the final structure was evaluated using PROCHECK.[59]

Protein Data Bank accession code

The atomic coordinates and structure factors of the Basp-II+suramin complex have been deposited with the Protein Data Bank (accession code: 1Y4L).

Acknowledgements

This research was supported by grants from Fundação de Amparo à Pesquisa do Estado de São Paulo (FAPESP), Structural Molecular Biology Network (SMOLBNet), Conselho Nacional de Desenvolvimento Científico e Tecnológico (CNPq), Coordenação de Aperfeiçoamento de Pessoal de Nível Superior (CAPES/DAAD) and Centros de Pesquisa, Inovação e Difusão (CEPID) to R.K.A., Fundação de Amparo à Pesquisa do Estado do Rio de Janeiro (FAPERJ) and Programa de Apoio a Núcles de Excelência (PRONEX) to P.A.M., as well as from Vicerrectoría de Investigación, University of Costa Rica, to B.L. and to J.M.G. M.T.M. is the recipient of a FAPESP doctoral fellowship.

References

1. Burch, T. A. & Ashburn, L. L. (1951). Experimental therapy of onchocerciasis with suramin and hetrazan; results of a three-year study. *Am. J. Trop. Med. Hyg.* **31**, 617–623.
2. Williamson, J. & Desowitz, R. S. (1956). Prophylactic activity of suramin complexes in animal trypanosomiasis. *Nature*, **177**, 1074–1075.
3. Cherry, J. K. (1960). The treatment of onchocerciasis. *East. Afr. Med. J.* **37**, 550–558.
4. Schneider, J. (1963). Treatment of human African trypanosomiasis. *Bull. World Health Organ.* **28**, 763–786.
5. LaRocca, R. V., Cooper, M. R., Uhrich, M., Danesi, R., Walther, M. M., Linehan, W. M. & Myers, C. E. (1991). Use of suramin in treatment of prostatic carcinoma refractory to conventional hormonal manipulation. *Urol. Clin. North Am.* **18**, 123–129.
6. van Oosterom, A. T., ten Bokkel Huinink, W. W., van der Burg, M. E., Vermorken, J. B., Willemse, P. H. & Neijt, J. P. (1991). Phase II clinical trial of doxifluridine in patients with advanced ovarian cancer. *Eur. J. Cancer*, **27**, 747–749.
7. Waltenberger, J., Mayr, U., Frank, H. & Hombach, V. (1996). Suramin is a potent inhibitor of vascular endothelial growth factor. A contribution to the molecular basis of its antiangiogenic action. *J. Mol. Cell Cardiol.* **28**, 1523–1529.
8. Cadene, M., Duranton, J., North, A., Si-Tahar, M., Chignard, M. & Bieth, J. G. (1997). Inhibition of neutrophil serine proteinases by suramin. *J. Biol. Chem.* **272**, 9950–9955.
9. Raj, P. A., Marcus, E. & Rein, R. (1998). Conformational requirements of suramin to target angiogenic growth factors. *Angiogenesis*, **2**, 183–199.

10. Hermans, J. M., Haines, D. S., James, P. S. & Jones, R. (2003). Kinetics of inhibition of sperm beta-acrosin activity by suramin. *FEBS Letters*, **544**, 119–222.
11. Jennings, F. W., Rodgers, J., Bradley, B., Gettinby, G., Kennedy, P. G. & Murray, M. (2002). Human African trypanosomiasis: potential therapeutic benefits of an alternative suramin and melarsoprol regimen. *Parasitol. Int.* **51**, 381–388.
12. Fleck, S. L., Birdsall, B., Babon, J., Dluzewski, A. R., Martin, S. R., Morgan, W. D. *et al*. (2003). Suramin and suramin analogues inhibit merozoite surface protein-1 secondary processing and erythrocyte invasion by the malaria parasite *Plasmodium falciparum*. *J. Biol. Chem.* **278**, 47670–47677.
13. McCain, D. F., Wu, L., Nickel, P., Kassack, M. U., Kreimeyer, A., Gagliardi, A. *et al*. (2004). Suramin derivatives as inhibitors and activators of protein-tyrosine phosphatases. *J. Biol. Chem.* **279**, 14713–14725.
14. Fernandez-Tornero, C., Lozano, R. M., Redondo-Horcajo, M., Gomez, A. M., Lopez, J. C., Quesada, E. *et al*. (2003). Leads for development of new naphthalenesulfonate derivatives with enhanced antiangiogenic activity: crystal structure of acidic fibroblast growth factor in complex with 5-amino-2-naphthalene sulfonate. *J. Biol. Chem.* **278**, 21774–21781.
15. Arruda, E. Z., Silva, N. M., Moraes, R. A. & Melo, P. A. (2002). Effect of suramin on myotoxicity of some crotalid snake venoms. *Braz. J. Med. Biol. Res.* **35**, 723–726.
16. de Oliveira, M., Cavalcante, W. L., Arruda, E. Z., Melo, P. A., Dal-Pai Silva, M. & Gallacci, M. (2003). Antagonism of myotoxic and paralyzing activities of bothropstoxin-I by suramin. *Toxicon*, **42**, 373–379.
17. Arni, R. K. & Ward, R. J. (1996). Phospholipase A2—a structural review. *Toxicon*, **34**, 827–841.
18. Kini, R. M. (2003). Excitement ahead: structure, function and mechanism of snake venom phospholipase A2 enzymes. *Toxicon*, **42**, 827–840.
19. Mebs, D. & Ownby, C. L. (1990). Myotoxic components of snake venoms: their biochemical and biological activities. *Pharm. Ther.* **48**, 223–236.
20. da Silva Giotto, M. T., Garratt, R. C., Oliva, G., Mascarenhas, Y. P., Giglio, J. R., Cintra, A. C. *et al*. (1998). Crystallographic and spectroscopic characterization of a molecular hinge: conformational changes in bothropstoxin I, a dimeric Lys49-phospholipase A2 homologue. *Proteins: Struct. Funct. Genet.* **30**, 442–454.
21. Melo, P. A., Nascimento, M. C., Mors, W. B. & Ownby, C. L. (1994). Inhibition of the myotoxic and hemorrhagic activities of crotalid venoms by *Eclipta prostrata* (Asteraceae) extracts and constituents. *Toxicon*, **32**, 595–603.
22. Scott, D. L., Otwinowski, Z., Gelb, M. H. & Sigler, P. B. (1990). Crystal structure of bee-venom phospholipase A2 in a complex with a transition-state analogue. *Science*, **250**, 1563–1566.
23. Murakami, M. T. & Arni, R. K. (2003). A structure based model for liposome disruption and the role of catalytic activity in myotoxic phospholipase A2s. *Toxicon*, **42**, 903–913.
24. Arni, R. K., Ward, R. J., Gutierrez, J. M. & Tulinsky, A. (1995). Structure of a calcium-independent phospholipase-like myotoxic protein from *Bothrops asper* venom. *Acta Crystallog. sect. D*, **51**, 311–317.
25. Ambrosio, A. L., Nonato, M. C., Selistre-de-Araujo, H. S., Arni, R. K., Ward, R. J., Ownby, C. L. *et al*. (2005). A molecular mechanism for Lys49-phospholipase A2 activity based on ligand-induced conformational change. *J. Biol. Chem.* **280**, 7326–7335.
26. Watanabe, L., Soares, A. M., Ward, R. J., Fontes, M. R. M. & Arni, R. K. (2005). Structural insights for fatty acid binding in a Lys49-phospholipase A(2): crystal structure of myotoxin II from *Bothrops moojeni* complexed with stearic acid. *Biochimie*, **87**, 161–167.
27. Lee, W. H., da Silva Giotto, M. T., Marangoni, S., Toyama, M., Polikarpov, I. & Garrat, R. C. (2001). Structural basis for low catalytic activity in Lys49 phospholipases A2—a hypothesis: the crystal structure of piratoxin II complexed to fatty acid. *Biochemistry*, **40**, 28–36.
28. Lomonte, B., Angulo, Y. & Santamaría, C. (2003). Comparative study of synthetic peptides corresponding to region 115–129 in Lys49 myotoxic phospholipases A2 from snake venoms. *Toxicon*, **42**, 307–312.
29. Lomonte, B., Angulo, Y. & Calderón, L. (2003). An overview of lysine-49 phospholipase A2 myotoxins from crotalid snake venoms and their structural determinants of myotoxic action. *Toxicon*, **42**, 885–901.
30. Ward, R. J., Chioato, L., de Oliveira, A. H., Ruller, R. & Sa, J. M. (2002). Active-site mutagenesis of a Lys49-phospholipase A2: biological and membrane-disrupting activities in the absence of catalysis. *Biochem. J.* **362**, 89–96.
31. Melo, P. A. & Suarez-Kurtz, G. (1988). Release of creatine kinase from skeletal muscles by *Bothrops* venoms: heparin potentiation of inhibition by antivenin. *Braz. J. Med. Biol. Res.* **21**, 548–558.
32. Melo, P. A. & Suarez-Kurtz, G. (1988). Release of sarcoplasmic enzymes from skeletal muscle by *Bothrops jararacussu* venom: antagonism by heparin and by the serum of South American marsupials. *Toxicon*, **26**, 87–95.
33. Lomonte, B., Tarkowski, A., Bagge, U. & Hanson, L. A. (1994). Neutralization of the cytolytic and myotoxic activities of phospholipases A2 from *Bothrops asper* snake venom by glycosaminoglycans of the heparin/heparan sulfate family. *Biochem. Pharmacol.* **47**, 1509–1518.
34. Lomonte, B., Moreno, E., Tarkowski, A., Hanson, L. A. & Maccarana, M. (1994). Neutralizing interaction between heparins and myotoxin II, a lysine 49 phospholipase A2 from *Bothrops asper* snake venom. Identification of a heparin-binding and cytolytic toxin region by the use of synthetic peptides and molecular modeling. *J. Biol. Chem.* **269**, 29867–29873.
35. Melo, P. A., Homsi-Brandeburgo, M. I., Giglio, J. R. & Suarez-Kurtz, G. (1993). Antagonism of the myotoxic effects of *Bothrops jararacussu* venom and bothropstoxin by polyanions. *Toxicon*, **31**, 285–291.
36. Krizaj, I., Turk, D., Ritonja, A. & Gubensek, F. (1989). Primary structure of ammodytoxin C further reveals the toxic site of ammodytoxin. *Biochim. Biophys. Acta*, **999**, 198–202.
37. Selistre de Araujo, H. S., White, S. P. & Ownby, C. L. (1996). Sequence analysis of Lys49 phospholipase A2 myotoxins: a highly conserved class of proteins. *Arch. Biochem. Biophys.* **326**, 21–30.
38. Ward, R. J., Rodrigues Alves, A., Rugierro Neto, J., Arni, R. K. & Casari, J. A. (1998). Sequence space analysis of Lys49 phopholipases A2: clues towards identification of residues involved in a novel mechanism of membrane damage and in myotoxicity. *Protein Eng.* **11**, 285–294.
39. Kini, R. M. & Iwanaga, S. (1986). Structure-function relationships of phospholipases. II: charge density distribution and the myotoxicity of presynaptically neurotoxic phospholipases. *Toxicon*, **24**, 895–905.
40. Kini, R. M. & Evans, H. J. (1989). Role of cationic residues in cytolytic activity: modification of lysine

residues in the cardiotoxin from *Naja nigricollis* venom and correlation between cytolytic and anti-platelet activity. *Biochemistry,* **28**, 9209–9216.
41. Falconi, M., Desideri, A. & Rufini, S. (2000). Membrane-perturbing activity of Viperidae myotoxins: an electrostatic surface potential approach to a puzzling problem. *J. Mol. Recogn.* **13**, 14–19.
42. Andrião-Escarso, S. H., Soares, A. M., Rodrigues, V. M., Angulo, Y., Díaz, C., Lomonte, B. *et al*. (2000). Myotoxic phospholipases A(2) in *Bothrops* snake venoms: effect of chemical modifications on the enzymatic and pharmacological properties of bothropstoxins from *Bothrops jararacussu*. *Biochimie*, **82**, 755–763.
43. Soares, A. M., Andrião-Escarso, S. H., Bortoleto, R. K., Rodrigues-Simioni, L., Arni, R. K., Ward, R. J. *et al*. (2001). Dissociation of enzymatic and pharmacological properties of piratoxins-I and -III, two myotoxic phospholipases A2 from *Bothrops pirajai* snake venom. *Arch. Biochem. Biophys.* **387**, 188–196.
44. Calderón, L. & Lomonte, B. (1998). Immunochemical characterization and role in toxic activities of region 115–129 of myotoxin II, a Lys49 phospholipase A2 from *Bothrops asper* snake venom. *Arch. Biochem. Biophys.* **358**, 343–350.
45. Núñez, C. E., Angulo, Y. & Lomonte, B. (2001). Identification of the myotoxic site of the Lys49 phospholipase A(2) from *Agkistrodon piscivorus piscivorus* snake venom: synthetic C-terminal peptides from Lys49, but not from Asp49 myotoxins, exert membrane-damaging activities. *Toxicon*, **39**, 1587–1594.
46. Chioato, L., Oliveira, A. H. C., Ruller, R., Sá, J. M. & Ward, R. J. (2002). Distinct sites for myotoxic and membrane-damaging activities in the C-terminal region of a Lys49-phospholipase A2. *Biochem. J.* **366**, 971–976.
47. Fernandez-Tornero, C., Lozano, R. M., Redondo-Horcajo, M., Gomez, A. M., Lopez, J. C., Quesada, E. *et al*. (2003). Leads for development of new naphthalenesulfonate derivatives with enhanced antiangiogenic activity: crystal structure of acidic fibroblast growth factor in complex with 5-amino-2-naphthalene sulfonate. *J. Biol. Chem.* **278**, 21774–21781.
48. Páramo, L., Lomonte, B., Pizarro-Cerdá, J., Bengoechea, J. A., Gorvel, J. P. & Moreno, E. (1998). Bactericidal activity of Lys49 and Asp49 myotoxic phospholipases A2 from *Bothrops asper* snake venom-synthetic Lys49 myotoxin II-(115–129)-peptide identifies its bactericidal region. *Eur. J. Biochem.* **253**, 452–461.
49. Gutiérrez, J. M. & Lomonte, B. (1997). Phospholipase A_2 myotoxins from *Bothrops* snake venoms. In *Venom Phospholipase A_2 Enzymes: Structure, Function and Mechanism* (Kini, R. M., ed.), p. 321, Wiley, Chichester.
50. Lee, W. H., Toyama, M. H., Soares, A. M., Giglio, J. R., Marangoni, S. & Polikarpov, I. (1999). Crystallization and preliminary X-ray diffraction studies of piratoxin III, a D-49 phospholipase A2 from the venom of *Bothrops pirajai*. *Acta Crystallog. sect. D*, **55**, 1229–1230.
51. Lomonte, B. & Gutiérrez, J. M. (1989). A new muscle damaging toxin, myotoxin II, from the venom of the snake *Bothrops asper* (terciopelo). *Toxicon*, **27**, 725–733.
52. Mass, J., Heling, W. & Seeger, K. (1997). Anesthesia of experimental animals. In *Drug Discovery and Evaluation: Pharmacological Assays* (Vogel, H. G. & Vogel, W., eds), p. 732, Spring-Verlag, Berlin.
53. Melo, P. A. & Ownby, C. L. (1999). Ability of wedelolactone, heparin, and *para*-bromophenacyl bromide to antagonize the myotoxic effects of two crotaline venoms and their PLA2 myotoxins. *Toxicon*, **37**, 199–192.
54. Murakami, M. T., Gava, L. M., Zela, S. P., Arruda, E. Z., Melo, P. A., Gutierrez, J. M. & Arni, R. K. (2004). Crystallization and preliminary X-ray diffraction analysis of suramin, a highly charged polysulfonated napthylurea, complexed with a myotoxic PLA2 from *Bothrops asper* venom. *Biochim. Biophys. Acta*, **1703**, 83–85.
55. Otwinowski, Z. & Minor, W. (1997). Processing of X-ray diffraction data collection in oscillation mode. *Methods Enzymol.* **276**, 307–326.
56. Navaza, J. (1994). AMoRe: an automated package for molecular replacement. *Acta Crystallog. sect. A*, **50**, 157–163.
57. Murshudov, G. N., Vagin, A. A. & Dodson, E. J. (1997). Refinement of macromolecular structures by the maximum-likelihood method. *Acta Crystallog. sect. D*, **53**, 240–255.
58. Roussel, A. & Cambillau, C. (1989). Turbo-Frodo. In *Silicon Graphics Geometry Partner Directory* (Silicon Graphics, ed.), p. 77, Mountain View, CA.
59. Laskowski, R. A., MacArthur, M. W., Moss, D. S. & Thornton, J. M. (1993). PROCHECK: a program to check the stereochemical quality of protein structures. *J. Appl. Crystallog.* **26**, 283–291.

Edited by I. Wilson

(Received 23 March 2005; received in revised form 23 April 2005; accepted 27 April 2005)

Available online at www.sciencedirect.com
SCIENCE DIRECT®
Biochimie 88 (2006) 543–549
BIOCHIMIE
www.elsevier.com/locate/biochi

Insights into metal ion binding in phospholipases A_2: ultra high-resolution crystal structures of an acidic phospholipase A_2 in the Ca^{2+} free and bound states

M.T. Murakami [a], A. Gabdoulkhakov [b], N. Genov [c], A.C.O. Cintra [d], C. Betzel [e], R.K. Arni [a,f,*]

[a] *Department of Physics, IBILCE/UNESP, Cristovão Colombo 2265, São José do Rio Preto, SP 15054-000, Brazil*
[b] *Institute of Protein Research RAS, Puschino, Moscow Region 142290, Russia*
[c] *Institute of Organic Chemistry, Bulgarian Academy of Sciences, Sofia 1113, Bulgaria*
[d] *Department of Biochemistry, USP, Ribeirão Preto 14040902, Brazil*
[e] *Institute of Medical Biochemistry and Molecular Biology, 22603 Hamburg, Germany*
[f] *Center for Applied Toxinology, Butantan Institute, São Paulo 05503900, Brazil*

Received 15 July 2005; accepted 28 October 2005
Available online 05 December 2005

Abstract

The electrophile Ca^{2+} is an essential multifunctional co-factor in the phospholipase A_2 mediated hydrolysis of phospholipids. Crystal structures of an acidic phospholipase A_2 from the venom of *Bothrops jararacussu* have been determined both in the Ca^{2+} free and bound states at 0.97 and 1.60 Å resolutions, respectively. In the Ca^{2+} bound state, the Ca^{2+} ion is penta-coordinated by a distorted pyramidal cage of oxygen and nitrogen atoms that is significantly different to that observed in structures of other Group I/II phospholipases A_2. In the absence of Ca^{2+}, a water molecule occupies the position of the Ca^{2+} ion and the side chain of Asp49 and the calcium-binding loop adopts a different conformation.

Keywords: Snake venom; Phospholipases A_2; Ca^{2+} coordination; Anticoagulant activity; X-ray analysis

1. Introduction

Phospholipases A_2s (PLA_2s; E.C. 3.1.1.4) constitute a large class of intracellular and extracellular enzymes that hydrolyze the 2-acyl ester bond of 1,2-diacyl-3-*sn*-phosphoglycerides. The most well studied enzymes of this group are the small (~14 kDa), stable, calcium-dependent enzymes encountered in a wide range of biological fluids, such as saliva, venom, synovial fluid, macrophages, platelets, pancreas, spleen and placenta [1,2] that are involved in phospholipid digestion and metabolism, host defense, signal transduction [3] and play important roles in inflammatory diseases [4] since the hydrolysis products may subsequently be utilized for the synthesis of eicosanoids, which serve as secondary messengers, or as metabolic precursors in a variety of inflammatory reactions. Snake venom PLA_2s display a wide spectrum of additional pharmacological activities such as neurotoxicity, myotoxicity, cardiotoxicity, anti-platelet aggregation, hypotensive, haemolytic, coagulant, anticoagulant and edema-inducing effects [5].

The mechanism of lipid hydrolysis by these enzymes was initially proposed by Verheij et al., and subsequently modified based on the crystal structure of the PLA_2 from *Naja naja atra* venom complexed with a transition state analogue [6,7]. In this model, His48 and Asp99 function in conjunction to abstract a proton from a structurally conserved solvent water molecule thus facilitating the nucleophilic attack on the *sn*-2 bond of the bound phospholipid substrate to form a tetrahedral oxyanion reaction intermediate. Alternate mechanisms have been proposed wherein two solvent water molecules participate in the formation and subsequent breakdown of the tetrahedral intermediate [8,9]. In both these mechanisms Ca^{2+} is coordinated by the carboxyl oxygen atoms of Asp49 and the carbonyl main chain oxygen atoms of the calcium-binding loop and serves as an electrophile during catalysis by polarizing the scissile bond and stabilizing the transition state during phospholipid hydro-

* Corresponding author. Tel.: +55 17 3221 2460; fax:+55 17 3221 2247.
E-mail address: arni@ibilce.unesp.br (R.K. Arni).

0300-9084/$ - see front matter © 2005 Elsevier SAS. All rights reserved.
doi:10.1016/j.biochi.2005.10.014

lysis [10]. Catalysis by secretory PLA_2s can be considered to involve four basic steps: (i) binding of Ca^{2+} and substrate, (ii) general base-mediated catalysis, (iii) formation and collapse of the tetrahedral intermediate and (iv) release of the reaction products. The bound Ca^{2+} ion also supports the interactions of secreted PLA_2s with aggregated micelles, vesicles, monolayers and membranes since electrostatic forces play critical roles in the binding of these substrates [11].

A number of basic and acidic PLA_2s have been isolated from the venom of *Bothrops* sp. [12,13] and references therein, whereas the basic enzymes are well characterized, little is known about the structure and calcium binding to their acidic counterparts. In order to clarify the structural changes induced by Ca^{2+} ion, we determined the crystal structures of an acidic Group II PLA_2 from the venom of *Bothrops jararacussu* (BthA-I-PLA_2), in the Ca^{2+} bound and free states at high-resolution (1.60 Å) and at atomic resolution (0.97 Å), respectively. BthA-I-PLA_2 is acidic (pI ~ 4.5), catalytically active, and lacks myotoxic, neurotoxic or cytotoxic activities, but, induces oedema, inhibits platelet aggregation and possesses hypotensive as well as anticoagulant activities [12]. Additionally, new insights into the anticoagulant site and hydrophobic channel are presented based on the atomic resolution data.

2. Materials and methods

2.1. Purification, crystallization and data collection

BthA-I-PLA_2 was purified from the crude venom of *B. jararacussu* by gel filtration, followed by anionic exchange chromatography as previously described [13]. The protein was crystallized by the hanging-drop vapor diffusion method at 18 °C both in the presence and absence of Ca^{2+} ions [14]. The crystals of the Ca^{2+} free and bound states belong to the same space group, $C222_1$, with similar unit cell dimensions of $a = 39.21$ Å, $b = 53.21$ Å and $c = 90.05$ Å (Ca^{2+} bound state), and $a = 39.96$ Å, $b = 53.79$ Å and $c = 89.82$ Å (Ca^{2+} free state). Diffraction data for the Ca^{2+} bound PLA_2 were collected to 1.60 Å at the synchrotron Beamline CPr (Laboratório Nacional de Luz Síncrotron, Brazil). The X-ray data for the Ca^{2+} free state were collected at atomic resolution of 0.97 Å at the consortium's Beamline X13 at HASYLAB/DESY–Hamburg. Data were processed and scaled with the programs DENZO and SCALEPACK [15]. X-ray data collection and refinement statistics are presented in Table 1.

2.2. Structure determination and refinement

The crystal structures were solved by the molecular replacement technique using the program *AMoRe* [16] and the atomic coordinates of the phospholipase A_2 from the venom of *B. jararacussu* refined at 1.79 Å (PDB code 1UMV) [17]. The isotropic and restrained refinements for both the crystal structures were carried out by using the program REFMAC5 [18] and were interspersed with cycles of manual model building using the program TURBO FRODO [19]. The crystal structure of the Ca^{2+} bound state was refined at 1.60 Å and inspection of the difference electron-density maps indicated an alternate conformation for the backbone between Cys29 and Gly32. The clear electron density ($> 3\sigma$) in the F_o–F_c map around the active site was considered to represent a glycerol molecule and the density observed in the calcium-binding loop was attributed to the presence of a Ca^{2+} ion. The structure of the Ca^{2+} free state was initially refined at 1.50 Å by anisotropic and restrained refinement, solvent water molecules were added using the program ARP/wARP [20] and the resolution was extended stepwise to 0.97 Å. Clear signs of anisotropy present in the electron density for several residues suggested possible alternate side chain conformations. The side chains of Gln21, Asp49, Thr56, Lys69 and Thr103 were modeled with more than one side chain position. The conjugate-gradient least-squares minimization against an intensity based residual target function that includes distance, planarity, chiral restraints and bulk solvent correction (SWAT) was applied using SHELXL [21]. New ordered solvent molecules were located in the difference Fourier map. $2F_o$–F_c and F_o–F_c electron-density maps were calculated after each step, and the model was checked and rebuilt. The final model has been analyzed using the program PROCHECK [22] and the stereochemical parameters of the two structures are presented in Table 1.

2.3. Protein Data Bank accession number

The atomic coordinates and structure factors for the structures of Ca^{2+} bound and free states of the BthA-I-PLA_2 have

Table 1
Data collection and refinement statistics. Values in parentheses are for the highest resolution shell

Parameter	Ca^{2+} bound BthA-I-PLA_2	Ca^{2+} free BthA-I-PLA_2
Data collection		
Space group	$C222_1$	$C222_1$
Unit-cell dimensions (Å, °)	$a = 39.21$, $b = 53.21$, $c = 90.05$ $\alpha = \beta = \gamma = 90.00$	$a = 39.96$, $b = 53.79$, $c = 89.82$ $\alpha = \beta = \gamma = 90.00$
V_M (Å^3 Da^{-1})	1.56	1.52
Solvent content (%)	21.01	19.2
Resolution range (Å)	30.00–1.60 (1.63–160)	10.00–0.97 (0.99–0.97)
Number of observations	128986	784618
Number of unique reflections	12748 (793)	57413 (2818)
Completeness (%)	99.2 (98.9)	99.3 (97.8)
R_{merge} (%)	4.7 (48.2)	6.8 (47.7)
$I/\sigma(I)$	23.07 (3.37)	17.09 (2.61)
Redundancy	8.0 (7.0)	7.5 (4.5)
Refinement		
Protein atoms	962	962
Water O atoms	106	262
Calcium ions	1	0
Glycerol atoms	6	0
R factor (%)	17.62	15.07
R_{free} (%)	23.21	20.11
r.m.s.d. in bond length (Å)	0.016	0.014
r.m.s.d. in bond angles (°)	1.731	0.040

been deposited with the RCSB Protein Data Bank and have assigned accession codes of 1ZL7 and 1ZLB, respectively.

3. Results and discussion

3.1. Overall structure

Both the structures contain one protein molecule (122 amino acids; 963 non-H atoms) in the asymmetric unit. The final model of the Ca^{2+} bound state additionally contains one calcium ion, one glycerol molecule and 106 solvent water molecules whereas, the Ca^{2+} free state contains 262 water molecules. The final *R*-factor and R_{free} values are 17.62% and 23.21% for the structure containing Ca^{2+} (resolution range 30.00 Å–1.60 Å) and 15.07% and 20.11% for the Ca^{2+} free state (resolution range 10.00 Å–0.97 Å), respectively. The data reduction, refinement statistics and the stereochemical parameters of the final model are presented in Table 1.

The overall fold of the BthA-I-PLA_2 in the Ca^{2+} free and bound states is similar to that of other Group II PLA_2s (Fig. 1A, B) and has been extensively reviewed [23,24]. Briefly, the principal structural features include an N-terminal α-helix, Leu2–Met14, two antiparallel α-helices, Ala40–Gly53 and Pro90–Asp108, one small α-helix, Gly18–Leu23, three 3_{10} helices (Lys110–Thr112, Ile115–Tyr117 and Ala122–Asn125), and a section of antiparallel β-sheet (β-wing, Tyr75–Cys84). A disulfide bridge formed between Cys43 and Cys95 links the two antiparallel helices. The structures are stabilized by six additional disulfide bonds: Cys25–Cys115, Cys28–Cys44, Cys49–Cys122, Cys50–Cys88, Cys57–Cys81 and Cys75–Cys86. Three salt bridges that are formed between Glu87–Arg90, Glu120–Arg42 and Asp104–Lys106 further stabilize the Ca^{2+} bound state. However, the third salt bridge is absent in the Ca^{2+} free state due to minor changes in the mutual orientation of the charged residues. The N-terminal helix includes residues Leu2, Phe5, Met8 and Ile9, forms one face of the hydrophobic channel, which is occupied by the substrate during catalysis and leads to the catalytic site. The channel is also lined with the side chains of Tyr22, Cys29, Cys45, Ala102, Thr103 and Phe106. The catalytic site which is located at the base of this hydrophobic channel is conserved in the Group I/II PLA_2s and consists of His48, Asp99, Tyr52 and Tyr73.

A comparison between the structures in the Ca^{2+} free and bound states (Fig. 1C) indicates that the two structures are very similar (r.m.s. deviation of 0.40 Å) and the salient differences are limited to the region of the calcium-binding loop (r.m.s. deviation of 1.1–1.9 Å; Fig. 2). The side chains of Arg106, Glu16, Lys77 and Asp88 adopt different conformations. Thus,

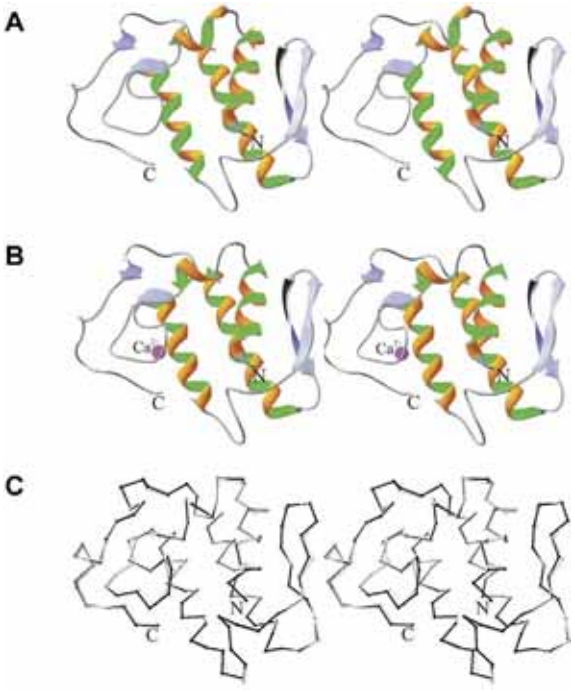

Fig. 1. Ribbon representations of the overall structures of the BthA-I-PLA_2 in the absence (A, resolution of 1.60 Å) and presence (B, resolution of 0.97 Å) of the Ca^{2+} ion. C: superpositioning of the Ca^{2+} bound (in gray) and free (in black) structures of BthA-I-PLA_2. The major difference is in the region of the calcium-binding loop.

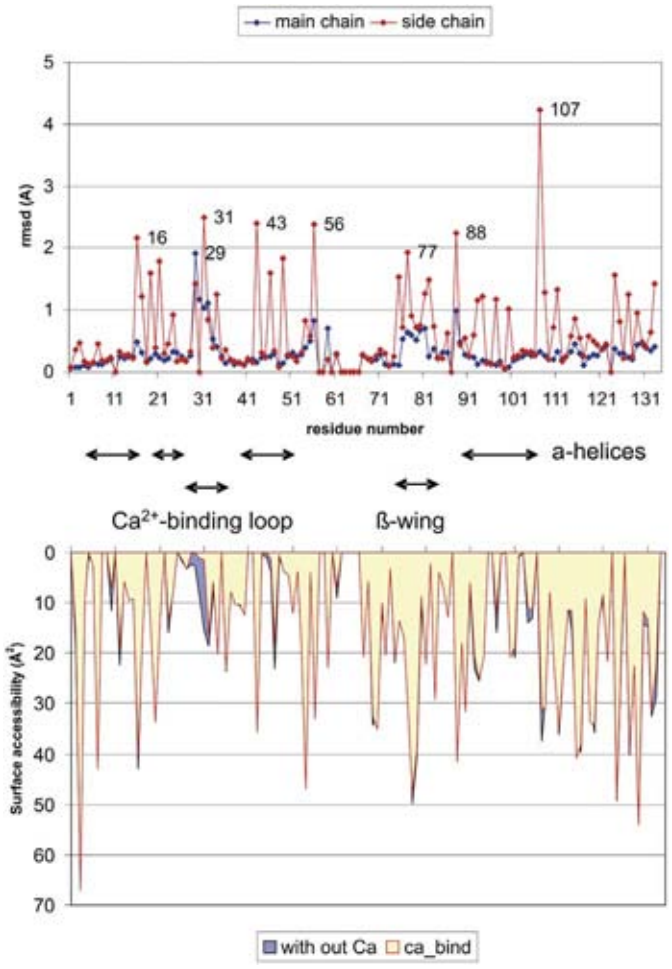

Fig. 2. The r.m.s. deviation of the C_α atoms (in blue) and the side chains (in red) between the Ca^{2+} bound and free structures of the BthA-I-PLA_2 versus the surface accessibility. The major C_α r.m.s. deviations are in the region of the calcium-binding loop. The surface accessibility was calculated using the program WHAT IF [39]. On the *x* axis the α-helices, calcium-binding loop and β-wing are indicated by arrows.

the binding of the Ca^{2+} ion to BthA-I-PLA_2 results in structural changes principally in the region of the metal-binding site.

A glycerol molecule, which is the basic structural element of the natural substrates of PLA_2s, was observed bound at the surface of the protein in the Ca^{2+} bound state, close to the metal-binding site and in van der Waals contact with Phe46. The three oxygen atoms of glycerol are involved in a system of H-bonds: Glycerol O1 ··· OD1 of Asp49 = 2.69 Å, Glycerol O2 ··· HOH = 2.72 Å, Glycerol O2 ··· HOH = 2.83 Å and Glycerol O3 ··· HO-Tyr28 = 2.56 Å.

3.2. Ca^{2+} ion coordination

Ca^{2+} is a functionally important co-factor, stabilizing the oxy-anion of the tetrahedral intermediate during PLA_2 catalyzed hydrolytic reactions [25]. Substrate binding to Group II PLA_2s is facilitated more than 10-fold by the binding of Ca^{2+} to the enzyme [26]. Fig. 3A illustrates the Ca^{2+} coordination by five ligands in BthA-I-PLA_2, the positive charge of Ca^{2+} enhances the interactions between PLA_2 and negatively charged substrates [11], which are particularly important in acidic PLA_2s. The backbone carbonyl oxygen of Tyr28, OD1 and OD2 atoms of Asp49, and the main chain nitrogen atoms of Gly32 and Gly33, respectively, form a pyramidal coordination cage for Ca^{2+}. The latter two ligands are unique in comparison to other Ca^{2+} bound PLA_2 structures since the coordination of Ca^{2+} by amide nitrogen atoms has not previously been observed in the crystal structures of PLA_2s [10,27,28]. In contrast, a bi-pyramidal coordination of the metal ion by seven ligands, formed by the backbone carbonyl oxygen atoms of Tyr28, Gly30 and Gly32, the carboxylate group of Asp49 and two water molecules is observed for both, basic and acidic PLA_2, exemplified by the pancreatic enzyme (Fig. 3B) [27]. However, in the Ca^{2+} bound state the carbonyl oxygen atoms of Gly30 and Gly32 are oriented away from the carboxylic group of Asp49 and the conformation is thus, not optimized for coordination of the metal ion by these ligands. The two water molecules are absent in the coordination sphere of Ca^{2+} in the BthA-I-PLA_2, which was observed in the structure of the human secretory enzyme [29].

In Fig. 4 the catalytic and metal-binding sites in the Ca^{2+} bound and free states are compared and the effect of the absence of Ca^{2+} on the geometry of this region, which is critical for catalytic activity, is illustrated. The active site residues His48, Asp99, Tyr52 and Tyr73 participate in the formation of the "catalytic" H-bonding network. The principal ligand of Ca^{2+}, the Asp49 side chain, is connected to this network via a hydrogen bond formed between the OD1 atom of the carboxylic group and the water molecule bound to His48 (Fig. 4B). In the Ca^{2+} free structure the co-factor is replaced by a water molecule, OW18, which is hydrogen bonded to the two nitrogen ligands and the carbonyl oxygen of Tyr28. The catalytically important water molecule, which is H-bonded to the active site His48 and upon activation to the couple His48–Asp99 serves as a nucleophile during catalysis, is located in exactly the same position in the two structures. This molecule is labeled as OW37 in the structure containing Ca^{2+} and as OW13 in that lacking metal ion. Absence of Ca^{2+} does not disturb the "catalytic" H-bonding network and only the relative orientation of the Asp49 side chain is slightly changed and no changes in the orientation of the imidazol and phenolic rings in the catalytic site are observed.

The conformation of the calcium-binding loop in the BthA-I-PLA_2 is only marginally altered in the absence of the metal ion, and the backbone conformations of the loop in the two structures are virtually identical (Fig. 5). The observed network of hydrogen bonds formed between the water molecule replacing the metal ion and protein ligands play a role in the stabilization. In the Ca^{2+} free state, the loop adopts an open conformation based on the solvent accessibility of the respective residues (Fig. 2). This loop forms part of the opposite wall of the hydrophobic channel where the substrate binds. This small conformational change can likely influence the substrate binding, based on the considerably increased substrate affinity of the channel in Group II PLA_2s upon Ca^{2+} binding [26]. In the majority of the structures determined in the absence of Ca^{2+}, this loop is destabilized [30,31]. Comparisons of the cal-

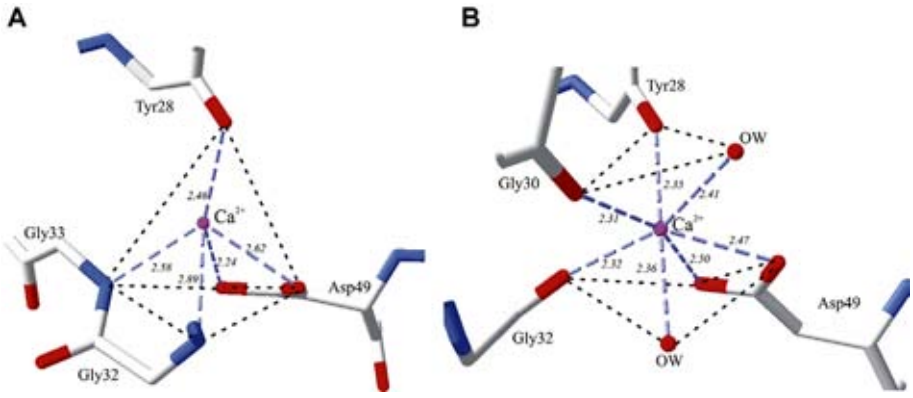

Fig. 3. Ca^{2+} coordination of the BthA-I-PLA_2 (A) compared to the bovine pancreatic PLA_2 (B; PDB code: 1G4I). In BthA-I-PLA_2, Ca^{2+} is pentacoordinated in a pyramidal cage by two main chain nitrogen atoms, a carbonyl oxygen and a carboxylate group. The coordination of the Ca^{2+} in the pancreatic PLA_2 is bipyramidal with seven ligands: three carbonyl oxygens, a carboxylate group and two water molecules.

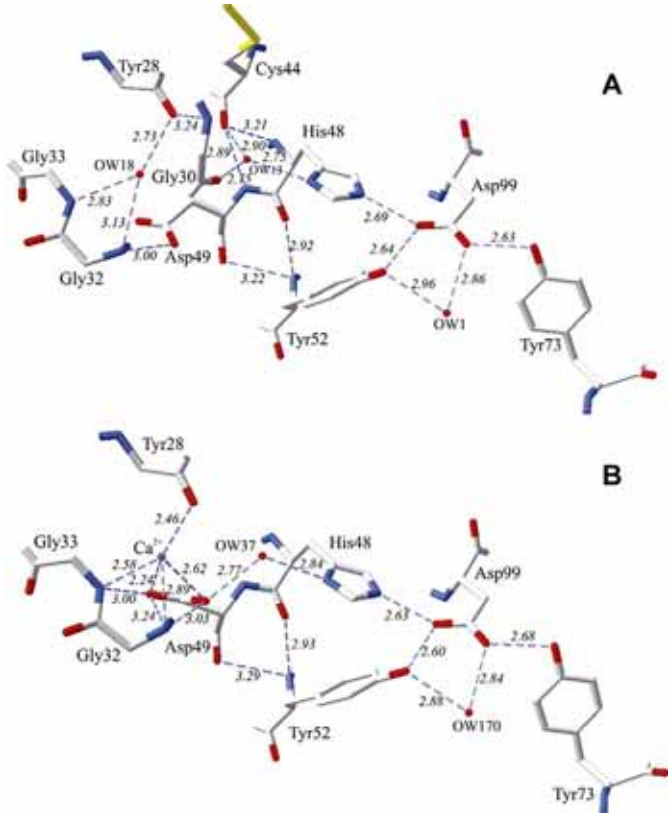

Fig. 4. Hydrogen bonding networks at the catalytic and calcium-binding sites of the BthA-I-PLA2 in the absence (A) and presence (B) of Ca^{2+} ion. The "catalytic" network and the catalytically important water molecule, bound to the active site His48, are preserved in both states. The co-factor is replaced by a water molecule in the Ca^{2+} free state.

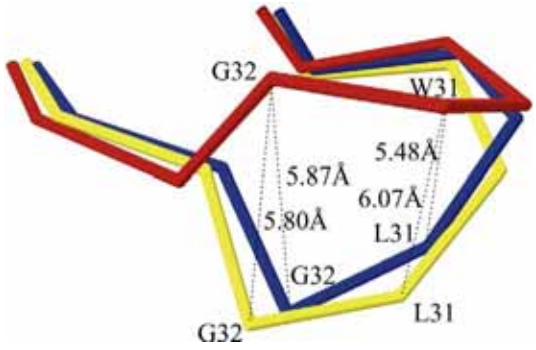

Fig. 5. Superposition of the calcium-binding loops of the Ca^{2+} bound (blue) and free (yellow) states of BthA-I-PLA_2, and of Vipoxin (red). In contrast to BthA-I-PLA_2, the loop of the Vipoxin is considerably destabilized in the absence of the co-factor.

cium-binding loop of BthA-I-PLA_2 with Vipoxin, a basic Ca^{2+} free PLA_2 from the venom of *Vipera ammodytes meridionalis*, indicate that this region of Vipoxin is considerably less well stabilized in the absence of the co-factor (Fig. 5).

3.3. Anticoagulant site

Coagulation is a rapid response of the organism to the loss of blood. This process includes a cascade of zymogen activations with the participation of serine proteinases. Snake venom PLA_2s can block the formation of coagulation complexes through interactions with procoagulant phospholipids [32]. This mechanism is non-enzymatic and the respective pharmacological site in the Group I/II PLA_2s has been identified as a region located between residues 54 and 77 [33]. This region is positively charged in the strongly anticoagulant enzymes and a pair of lysine residues is present at both ends of the site. BthA-I-PLA_2 exhibits significant anticoagulant activity and the part of the polypeptide chain, located between the fore-mentioned residues, fulfill these requirements. There are four lysine residues in the region, Lys54, Lys69, Lys77 and Lys78, two of them located at either end of the polypeptide segment. In this case the anticoagulant site can be considered to include one more residue, to include Lys78. All four lysine residues are located on the protein surface and can interact with phospholipids (Fig. 6).

It has been suggested that the anticoagulant site of Group I/II PLA_2s is negatively charged due to the presence of Glu53 [34] but in the BthA-I-PLA_2 structure, a glycine residue occupies this position. The same residue is encountered at position 53 in the *Daboia russelli pulcella* PLA_2, which also induces anticoagulant reactions in experimental models [35,36]. These findings refute the suggestion that glutamic acid at position 53 is an essential requirement for anticoagulant activity.

3.4. Region of high aromaticity in the vicinity of the entrance of the hydrophobic channel: a possible functional role

The PLA_2 substrate-binding site is a hydrophobic channel that binds alkyl substituents of phospholipids. In BthA-I-PLA_2 this channel includes the residues Leu2, Phe5, Met8,

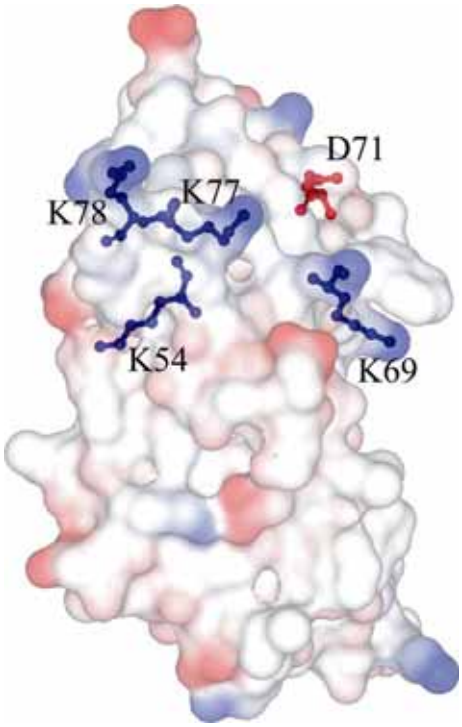

Fig. 6. Surface representation of the anticoagulant site in the BthA-I-PLA_2. There is a pair of lysyl residues at the both ends of the anticoagulant site.

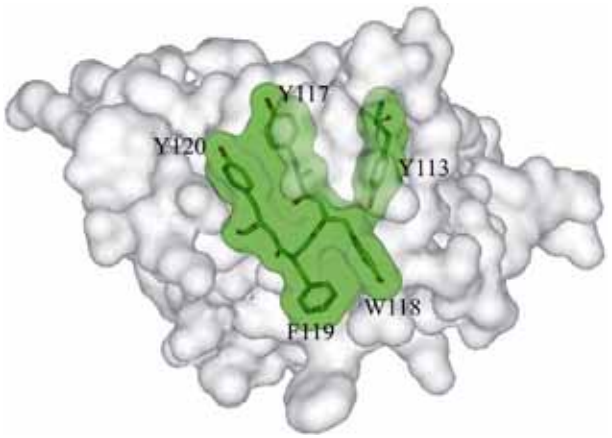

Fig. 7. Region of high aromaticity in the vicinity of the BthA-I-PLA_2 substrate-binding site. Aromatic side chains can interact with a target membrane during catalysis.

Ile9, Tyr22, Cys29, Cys45, Ala102, Thr103 and Phe106, and extends approximately 14 Å from the surface to the catalytic site. Side chains of residues, surrounding the entrance of the channel, form the interfacial-binding surface, which is necessary for interfacial catalysis [37]. Inspection of the BthA-I-PLA_2 model indicates a region with a significant number of aromatic residues (Tyr113, Tyr117, Trp118, Phe119 and Tyr120; Fig. 7) in the vicinity of the entrance to the substrate-binding site. Aromatic residues have been implicated in contributing significantly to interfacial catalysis [38] and the couples Tyr117 – Tyr120 and Trp118 – Phe119 are involved in the formation of van der Waals contacts.

4. Conclusions

A novel coordination for Ca^{2+} ion in Group I/II phospholipases A_2 formed by a distorted pyramidal cage of oxygen and nitrogen atoms was observed in the BthA-I-PLA_2 crystal structure. Ca^{2+} binding induces local structural modifications limited to the calcium-binding site, which demonstrates that binding of the catalytically essential ion does not result in significant changes in others regions of the molecule, excluding possible communication or allosteric effects due to the Ca^{2+} binding. Since BthA-I-PLA_2 displays anticoagulant activity and has a glycine at position 53, the essential requirement of Glu53 for anticoagulant activity is refuted.

Acknowledgements

This research was supported by grants from Fundação de Amparo à Pesquisa do Estado de São Paulo (FAPESP), Structural Molecular Biology Network (SMOLBNet), Conselho Nacional de Desenvolvimento Científico e Tecnológico (CNPq), Coordenação de Aperfeiçoamento de Pessoal de Nível Superior/Deutscher Akademischer Austauschclienst (CAPES/DAAD) and Centros de Pesquisa, Inovação e Difusão (CEPID) to R.K.A. and by a grant from DAAD to C.B. and in part by the Bulgarian Foundation for Scientific Research, Grant X-14 to N.G. M.T.M. is the recipient of a FAPESP doctoral fellowship.

References

[1] L.L.M. Van Deenen, G.H. de Haas, The substrate specificity of phospholipase A_2, Biochim. Biophys. Acta 70 (1963) 538–553.
[2] M. Waite, Phospholipases, enzymes that share a substrate class, Adv. Exp. Med. Biol. 279 (1990) 1–22.
[3] D.A. Six, E.A. Dennis, The expanding superfamily of phospholipase A(2) enzymes: classification and characterization, Biochim. Biophys. Acta 1488 (2000) 1–19.
[4] S. Yedgar, D. Lichtenberg, E. Schnitzer, Inhibition of phospholipase A(2) as a therapeutic target, Biochim. Biophys. Acta 1488 (2000) 182–187.
[5] E. Valentin, G. Lambeau, What can venom phospholipase A_2 tell us about the functional diversity of mammalian secreted phospholipases A_2 ? Biochemie 82 (2000) 815–831.
[6] S.P. White, D.L. Scott, Z. Otwinowski, M.H. Gelb, P.B. Sigler, Crystal structure of cobra venom phospholipase A2 in a complex with a transition state analogue, Science 250 (1990) 1560–1563.
[7] D.L. Scott, S.P. White, Z. Otwinowski, W. Yuan, M.H. Gelb, P. B. Sigler, Interfacial catalysis: the mechanism of phospholipase A2, Science 250 (1990) 1541–1546.
[8] J. Rogers, B.Z. Yu, S.V. Serves, G.M. Tsivgoulis, D.N. Sotiropoulos, P. V. Ioannou, et al., Kinetic basis for the substrate specificity during hydrolysis of phospholipids by secreted phospholipase A2, Biochemistry 35 (1996) 9375–9384.
[9] S.H. Edwards, D. Thompson, S.F. Baker, S.P. Wood, D.C. Wilton, The crystal structure of the H48Q active site mutant of human group IIA secreted phospholipase A2 at 1.5 Å resolution provides an insight into the catalytic mechanism, Biochemistry 41 (2002) 15468–15476.
[10] D.L. Scott, Phospholipase A_2: structure and catalytic properties, in: R. M. Kini (Ed.), Venom Phospholipase A_2 Enzymes: Structure, Function and Mechanism, John Wiley & Sons, Chichester, 1997, pp. 97–128.
[11] D.L. Scott, A.M. Mandel, P.B. Sigler, B. Honig, The electrostatic basis for the interfacial binding of secretory phospholipases A_2, Biophys. J. 67 (1994) 493–504.
[12] S.H. Andrião-Escarso, A.M. Soares, M.R.M. Fontes, A.L. Fuly, F.M. A. Corrêa, J.C. Rosa, et al., Structural and functional characterization of an acidic platelet aggregation inhibitor and hypotensive phospholipase A_2 from *Bothrops jararacussu* snake venom, Biochem. Pharmacol. 64 (2002) 723–732.
[13] D.F.J. Ketelhut, M. Homem de Melo, E.L.G. Veronese, L. E. Esmeraldino, M.T. Murakami, R.K. Arni, et al., Isolation, characterization and biological activity of acidic phospholipase A2 isoforms from *Bothrops jararacussu* snake venom, Biochemie 85 (2003) 983–991.
[14] M.T. Murakami, S. Michelan-Duarte, A.C.O. Cintra, R.K. Arni, Crystallization and high-resolution X-ray diffraction data collection of an Asp49 PLA_2 from *Bothrops jararacussu* venom both in the presence and absence of Ca^{2+} ions, Biochim. Biophys. Acta 1703 (2004) 79–81.
[15] Z. Otwinowski, W. Minor, Processing of X-ray diffraction data collected in oscillation mode, Methods Enzymol. 276 (1997) 307–326.
[16] J. Navaza, AMoRe: an automated package for molecular replacement, Acta Crystallogr. A 50 (2004) 157–163.
[17] A.J. Magro, M.T. Murakami, S. Marcussi, A.M. Soares, R.K. Arni, M. R. Fontes, Crystal structure of an acidic platelet aggregation inhibitor and hypotensive phospholipase A_2 in the monomeric and dimeric states: insights into its oligomeric state, Biochem. Biophys. Res. Commun. 323 (2004) 24–31.
[18] G.N. Murshudov, A.A. Vagin, E.J. Dodson, Refinement of macromolecular structures by the maximum-likelihood method, Acta Crystallogr. D. Biol. Crystallogr. 53 (1997) 240–255.
[19] T.A. Jones, Diffraction methods for biological macromolecules. Interactive computer graphics, FRODO, Methods Enzymol. 115 (1985) 157–171.

[20] V.S. Lamzin, A. Perrakis, K.S. Wilson, A.R.P. The, WARP suite for automated construction and refinement of protein models, in: M. G. Rossman, E. Arnold (Eds.), International Tables for Crystallography, Vol. F: Crystallography of biological macromolecules, 1st ed, Kluwer Academic Publishers, Dordrecht, 2001, pp. 720–7222.

[21] G.M. Sheldrick, T.R. Schneider, SHELXL: high resolution refinement, Methods Enzymol. 277 (1997) 319–343.

[22] R.A. Laskowski, M.W. MacArthur, D.S. Moss, J.M. Thornton, Procheck: a program to check the stereochemical quality of protein structures, J. Appl. Crystallogr. 26 (1993) 283–291.

[23] R.K. Arni, R.J. Ward, Phospholipase A_2—a structural review, Toxicon 34 (1996) 827–841.

[24] M.T. Murakami, R.K. Arni, A structure based model for liposome disruption and the role of catalytic activity in myotoxic phospholipase A2s, Toxicon 42 (2003) 903–913.

[25] M.M.G.M. Thunnissen, A.B. Eiso, K.H. Kalk, J. Drenth, B.W. Dijkstra, O.P. Kuipers, et al., X-ray structure of phospholipase A_2 complexed with a substrate-derived inhibitor, Nature 347 (1990) 689–691.

[26] K. Teshima, Y. Kitagawa, Y. Samejima, S. Kawauchi, S. Fujii, K. Ikeda, et al., Role of Ca^{2+} in the substrate binding and catalytic functions of snake venom phospholipases A_2, Biochem. J. 106 (1989) 518–527.

[27] R.A. Steiner, H.J. Rozeboom, A. de Vries, K.H. Kalk, G.N. Murshudov, K.S. Wilson, et al., X-ray structure of bovine pancreatic phospholipase A_2 at atomic resolution, Acta Crystallogr. D57 (2001) 516–526.

[28] J. Jasti, M. Paramasivam, A. Srinivasan, T.P. Singh, Structure of an acidic phospholipase A_2 from Indian saw-scaled viper (*Echis carinatus*) at 2.6 Å resolution reveals a novel intermolecular interaction, Acta Crystallogr. D60 (2004) 66–72.

[29] D.L. Scott, S.P. White, J.L. Browning, J.J. Rosa, M.H. Gelb, P.B. Sigler, Structures of free and inhibited human secretory phospholipase A_2 from inflammatory exudates, Science 254 (1991) 1007–1010.

[30] B.W. Segelke, D. Nguyen, R. Chee, N.H. Xuong, E.A. Dennis, Structures of two novel crystal forms of *Naja naja naja* phospholipase A_2 lacking Ca^{2+} reveal trimeric packing, J. Mol. Biol. 279 (1998) 223–232.

[31] L. Gu, Z. Wang, S. Song, Y. Shu, Z. Lin, Crystal structures of an acidic phospholipase A_2 from the venom of *Naja kaouthina*, Toxicon 40 (2002) 917–922.

[32] H.J. Evans, R.M. Kini, The anticoagulant effects of snake venom phospholipases A_2, in: R.M. Kini (Ed.), Venom Phospholipase A_2 Enzymes: Structure, Function and Mechanism, John Wiley & Sons, Chichester, 1997, pp. 97–128.

[33] R.M. Kini, H.J. Evans, Effects of phospholipase A_2 enzymes on platelet aggregation, in: R.M. Kini (Ed.), Venom Phospholipase A_2 Enzymes: Structure, Function and Mechanism, John Wiley & Sons, Chichester, 1997, pp. 369–388.

[34] E. Carredano, B. Westerlund, B. Persson, M. Saarinen, S. Ramaswamy, D. Eaker, et al., The three-dimensional structures of two toxins from snake venom throw light on the anticoagulant and neurotoxic sites of Phospholipase A_2, Toxicon 36 (1998) 75–92.

[35] V.T. Gowda, J. Schmidt, J.L. Middlebrook, Primary sequence determination of the most basic myonecrotic phospholipase A_2 from venom of *Vipera russelli*, Toxicon 32 (1994) 665–673.

[36] V. Chandra, P. Kaur, A. Srinivasan, T.P. Singh, Three-dimensional structure of a presynaptic neurotoxic phospholipase A_2 from *Daboia russelli pulcella* at 2.4 Å resolution, J. Mol. Biol. 296 (2000) 1117–1126.

[37] D.L. Scott, S.P. White, Z. Otwinowski, W. Yuan, M.H. Gelb, P. B. Sigler, Interfacial catalysis: the mechanism of phospholipase A_2, Science 250 (1990) 1541–1546.

[38] M. Sumandea, S. Das, C. Sumandea, W. Cho, Roles of aromatic residues in high interfacial activity of *Naja naja atra* phospholipase A_2, Biochemistry 38 (1999) 16290–16297.

[39] R. Rodriguez, G. Chinea, N. Lopez, T. Pons, G. Vriend, Homology modelling, model and software evaluation: three related resources, Cabios 14 (1998) 523–528.

protein structure communications

Acta Crystallographica Section F
Structural Biology and Crystallization Communications
ISSN 1744-3091

Structure of myotoxin II, a catalytically inactive Lys49 phospholipase A_2 homologue from *Atropoides nummifer* venom

Mário T. Murakami,[a] Cristiane C. Melo,[a] Yamileth Angulo,[b,c] Bruno Lomonte[b]* and Raghuvir K. Arni[a,d]*

[a]Department of Physics, IBILCE/UNESP, São José do Rio Preto-SP, Brazil, [b]Instituto Clodomiro Picado, Facultad de Microbiologia, San José, Costa Rica, [c]Departamento de Bioquímica, Escuela de Medicina, Universidad de Costa Rica, San José, Costa Rica, and [d]Center for Applied Toxinology, Butantan Institute, São Paulo-SP, Brazil

Correspondence e-mail: blomonte@cariari.ucr.ac.cr, arni@ibilce.unesp.br

Received 10 February 2006
Accepted 23 March 2006

PDB Reference: myotoxin II, 2aoz, r2aozsf.

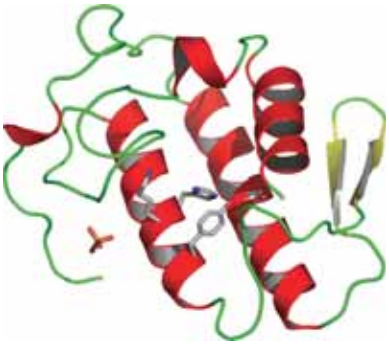

Lys49 snake-venom phospholipase A_2 (PLA_2) homologues are highly myotoxic proteins which, although lacking catalytic activity, possess the ability to disrupt biological membranes, inducing significant muscle-tissue loss and permanent disability in severely envenomed patients. Since the structural basis for their toxic activity is still only partially understood, the structure of myotoxin II, a monomeric Lys49 PLA_2 homologue from *Atropoides nummifer*, has been determined at 2.08 Å resolution and the anion-binding site has been characterized.

1. Introduction

Skeletal muscle necrosis is a frequent consequence of envenomation by snakes of the family Crotalidae and may lead to significant tissue loss and permanent disability (Mebs & Ownby, 1990; Nishioka & Silveira, 1992). The venoms of these snakes contain a number of basic phospholipases A_2 (PLA_2s; EC 3.1.1.4) that play prominent roles in the pathogenesis of myonecrosis (Gutiérrez & Lomonte, 1995). These myotoxic proteins are classified as belonging to the group IIA PLA_2s on the basis of their primary structure and disulfide-bonding pattern (Six & Dennis, 2000). A subgroup of catalytically inactive variants or PLA_2 homologues was initially characterized from the venom of the North American water mocassin *Agkistrodon piscivorus piscivorus*, in which the conserved Asp at position 49 is replaced by Lys (Maraganore *et al.*, 1984; Scott *et al.*, 1992; Arni & Ward, 1996). Homologous 'Lys49 PLA_2 myotoxins' have now been encountered in the venoms of a wide variety of crotalid species (reviewed by Lomonte *et al.*, 2003) and have attracted attention since they serve as models for the investigation of the structural basis of the catalytically independent mechanisms of membrane damage. Recently, it has been demonstrated that these basic Lys49 PLA_2s bind to the extracellular domain of the vascular endothelial growth factor ($VEGF_{165}$) receptor with a sub-nanomolar affinity (Yamazaki *et al.*, 2005).

Two Lys49 PLA_2 homologues have previously been isolated from the venom of *Atropoides nummifer*, a crotalid snake distributed along the Central American isthmus (Taylor *et al.*, 1974; Solórzano, 1989). *A. nummifer* myotoxin I (Gutiérrez *et al.*, 1986) has been crystallized and its structure has been reported at 2.4 Å resolution (Arni & Gutiérrez, 1993; de Azevedo *et al.*, 1999); however, since its amino-acid sequence has not been determined, accurate structural data is as yet unavailable. On the other hand, *A. nummifer* myotoxin II (Anum-II) has been well characterized in terms of its biological activities (Angulo *et al.*, 2000) and its complete amino-acid sequence has been determined (SwissProt code P82950; Angulo *et al.*, 2002). This protein has recently been crystallized (Watanabe *et al.*, 2004) and the present report presents a detailed analysis of its three-dimensional structure, which has been determined at 2.08 Å resolution.

2. Materials and methods

2.1. Purification, crystallization and data collection

A. nummifer venom was obtained from more than 15 specimens collected in Costa Rica. Anum-II was purified by cation-exchange

Table 1
Data-collection and refinement statistics of the Anum-II crystal structure.

Values in parentheses are for the highest resolution shell.

Data collection	
Space group	$P4_32_12$
Unit-cell parameters (Å)	$a = b = 68.94$, $c = 64.07$
V_M (Å^3 Da^{-1})	2.66
Solvent content (%)	53.40
Resolution range (Å)	30.36–2.08 (2.19–2.08)
No. of unique reflections	9671
Completeness (%)	99.3 (94.1)
R_{merge}† (%)	8.9 (48.1)
$I/\sigma(I)$	6.7 (2.3)
Refinement	
R factor‡ (%)	21.9
R_{free}§ (%)	27.0
B values¶ (Å^2)	
Overall	30.48
Main chain	28.64
Side chain	29.2
R.m.s.d. in bond length (Å)	0.021
R.m.s.d. in bond angles (°)	1.868

† $R_{merge} = 100 \times \sum[\sum |I(h) - \langle I(h)\rangle|]/\sum I(h)$, where $I(h)$ is the observed intensity and $\langle I(h)\rangle$ is the mean intensity of reflection h over all measurements of $I(h)$. ‡ R factor = $100 \times \sum(|F_o - F_c|)/\sum(F_o)$, the sums being taken over all reflections with $F/\sigma(F) > 2$ cutoff. § R_{free} = R factor for 5% of the data which were not included during crystallographic refinement. ¶ B values are average B values for all non-H atoms.

chromatography on carboxymethyl-Sephadex C-25 (Pharmacia) (Angulo *et al.*, 2000) and reverse-phase high-performance liquid chromatography (RP-HPLC) on a C4 column (Vydac) which was eluted at a flow rate of 1.0 ml min^{-1} with a gradient ranging from 0 to 60% acetonitrile in 0.1% trifluoroacetic acid, using a Waters 600E instrument (Watanabe *et al.*, 2004).

The Anum-II sample was dissolved in water at a concentration of 10 mg ml^{-1}. Crystallization experiments were carried out by the hanging-drop vapour-diffusion method. Single crystals were obtained when a 2 µl protein droplet was mixed with an equal volume of a solution consisting of 0.1 *M* sodium acetate pH 4.6, 20% PEG 3350 and 0.2 *M* ammonium sulfate and subsequently equilibrated over 1 ml of the latter solution at 291 K (Watanabe *et al.*, 2004). Crystals of Anum-II were flash-cooled in crystallization solution to which 15%(*v*/*v*) glycerol had been added. Diffraction data were collected from a single cryoprotected Anum-II crystal utilizing a wavelength of 1.427 Å (at 100 K) at a synchrotron-radiation source (Laboratório Nacional de Luz Síncrotron, Campinas, Brazil). Intensity data were reduced and processed at 2.08 Å using the program *MOSFLM* (Leslie, 1992). The crystals of Anum-II belong to space group $P4_32_12$ and are compatible with the presence of one protein molecule in the asymmetric unit. The data-collection and processing statistics are summarized in Table 1.

2.2. Structure determination and crystallographic refinement

The crystal structure of Anum-II was determined by molecular replacement using the program *MOLREP* (Vagin & Teplyakov, 1997). The atomic coordinates of a Lys49 PLA_2 isolated from the venom of *Ag. acutus* (PDB code 1mc2), stripped of solvent and ligand atoms, were used to generate the search model. The cross-rotation and translation functions were calculated over the resolution range 20.0–3.0 Å and the rotation angles which produced the peak with the highest correlation and the lowest R factor were applied to the search model for the translation search. The searches were performed for both enantiomorphic space groups ($P4_32_12$ and $P4_12_12$) and the correct solution was selected based on the crystallographic residual and the correlation coefficient. The model was subjected to isotropic restrained refinement using the program *REFMAC*5 (Murshudov *et al.*, 1997) and the structural model was improved based on $2F_o - F_c$ and $F_o - F_c$ electron-density maps, which were examined using the graphics program *TURBO-FRODO* (Roussel & Cambillau, 1991). During the refinement, residual density observed near Arg34 was attributed to a sulfate ion based on the tetrahedral shape of the density and the possible interactions. The refinement converged to an R factor of 22% and an R_{free} of 27% (Table 1).

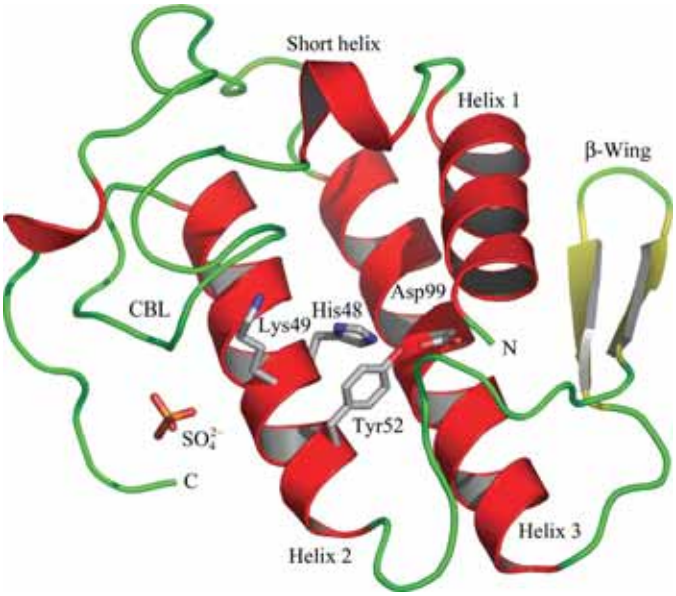

Figure 1
Cartoon representation of the *A. nummifer* myotoxin II (Anum-II) crystal structure. The residues which form the nominal active-site are presented in atom colours. CBL: putative calcium-binding loop.

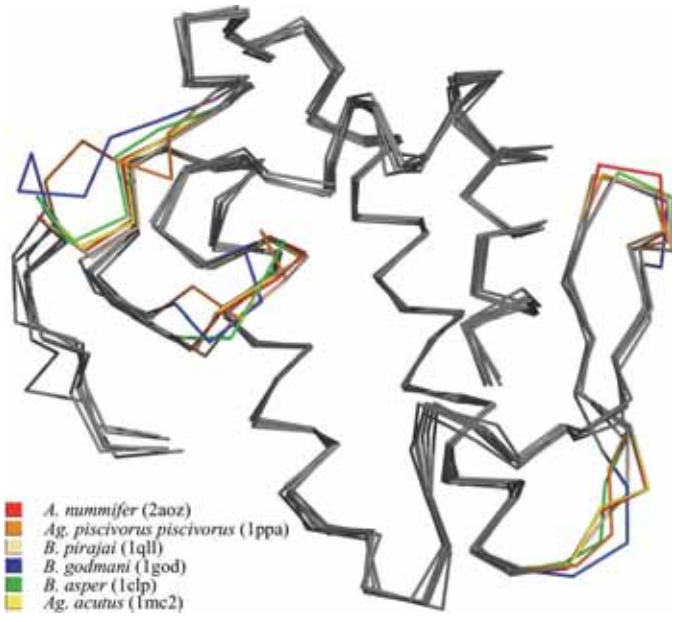

Figure 2
Superpositioning of Anum-II on the structures of *B. godmani* (PDB code 1god), *B. asper* (1clp, chain *A*), *Ag. piscivorus piscivorus* (1ppa), *B. pirajai* (1qll) and *Ag. acutus* (1mc2) Lys49 PLA_2s. The structural differences are highighted by utilizing different colours.

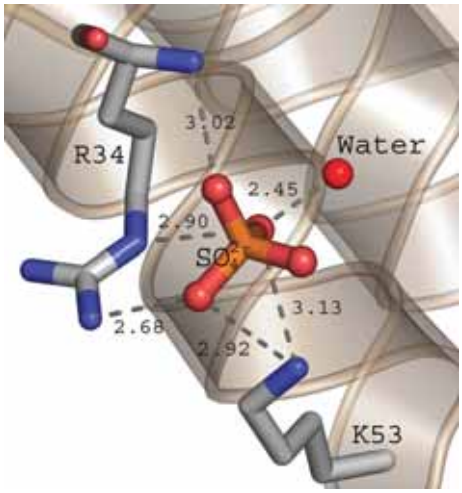

Figure 3
Interactions of the sulfate ion with Arg34 and Lys53 of Anum-II.

3. Results and discussion

3.1. Overall structure

The asymmetric unit of the Anum-II crystals consists of one protein molecule (121 amino-acid residues), one sulfate ion and 71 solvent water molecules. The quality of the model assessed by *PROCHECK* (Laskowski *et al.*, 1993) indicates that the stereochemical parameters lie within the expected range and the overall deviations from ideal stereochemistry are presented in Table 1. The Ramachandran diagram (Ramachandran *et al.*, 1963) indicates that 87% of the main-chain dihedral angles of all non-glycine and non-proline residues are located in the energetically most favoured regions, 12% are located in the additional permitted regions and only 1% lie in the generously permitted region. Based on the nomenclature and numbering scheme suggested by Renetseder *et al.* (1985), Anum-II can be classified as a class II PLA_2 enzyme and is stabilized by seven disulfide bridges (between residues 27 and 125, 29 and 45, 44 and 105, 50 and 133, 51 and 98, 61 and 91, and 84 and 96). The structures of PLA_2s have been extensively reviewed (Arni & Ward, 1996); briefly, the Anum-II structure can be considered to be formed of a short N-terminal α-helix (residues 2–12), a putative Ca^{2+}-binding loop (residues 25–35), a second α-helix (residues 40–55), a two-stranded antiparallel sheet referred to as the β-wing (residues 74–85) and a third α-helix (residues 90–107) that is antiparallel to the second; these two long helices are linked by two disulfide bridges to form a rigid platform. The positions of the amino-acid residues that form the catalytic apparatus (His48, Tyr52, Tyr73 and Asp99, including the catalytic water molecule) are conserved except for Asp49, which is substituted by Lys (Fig. 1). Superpositioning the Anum-II structure onto the structures of other Lys49 PLA_2s indicates that all structural features are conserved, with inherent flexibility observed in the C-terminus, putative calcium-binding loop, β-wing connecting loop and the tip of the β-wing (Fig. 2).

3.2. Anion-binding site

Clear density for a tetrahedral molecule was observed close to Arg34 in both the $2F_o - F_c$ and $F_o - F_c$ electron-density maps. Since the mother solution contains 0.2 *M* ammonium sulfate, this electron density was considered to represent a sulfate ion based on the geometry and possible hydrogen bonds. In this model, the O1 atom of the sulfate ion is anchored by hydrogen bonds to Arg34 N^{ε} (2.90 Å), Lys53 N^{ζ} (3.13 Å) and a solvent water molecule (2.45 Å). The O2 atom interacts with the main-chain NH group of Arg34 (3.02 Å) and the O4 atom with Lys53 N^{ζ} (3.38 Å) and Arg34 $N^{\eta 2}$ (2.68 Å) (Fig. 3). The crystal structure of *Ag. contortrix laticinctus* myotoxin also indicated the presence of a sulfate ion bound to Arg34 and Lys53 (Ambrosio *et al.*, 2005) and the sulfonyl group of the suramin molecule was shown to interact with Arg34 in *Bothrops asper* myotoxin II (Murakami *et al.*, 2005). This indicates that Arg34, which is strictly conserved in all Lys49 PLA_2s (Fig. 4), is likely to play a crucial role in the binding of negatively charged substrates or inhibitors.

3.3. Oligomeric state

The dimerization of Lys49 PLA_2s has been suggested to play an important role in their ability to damage membranes (de Oliveira *et al.*, 2001) and in the expression of cytolytic and myotoxic activities (Angulo *et al.*, 2005). Previous crystallographic results on the Lys49 PLA_2s *B. asper* myotoxin II (Arni *et al.*, 1995), *B. pirajai* piratoxin I (de Azevedo *et al.*, 1998) and *B. jararacussu* bothropstoxin I (Giotto *et al.*, 1998) suggested that the monomers present in the asymmetric unit are related by a twofold axis and that the dimer is stabilized by reciprocal interactions formed at the interface of the N-terminal and β-wing regions that encompass the conserved interfacial residues Glu12, Trp77 and Lys80 (Ward *et al.*, 1998; Ruller *et al.*, 2005). This quaternary arrangement stabilized by the Glu12–Lys80 salt bridge has been considered to represent the biologically relevant form (Ward *et al.*, 1998) and has been shown to be very stable.

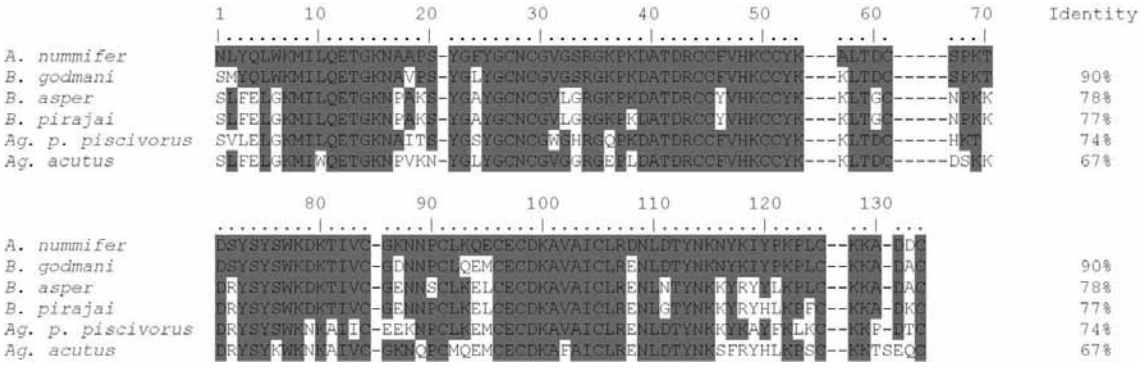

Figure 4
Sequence alignment of Anum-II with other Lys49 PLA_2s from *Cerrophidion (Bothrops) godmani* (PDB code 1god), *B. asper* (1clp), *Ag. piscivorus piscivorus* (1ppa), *B. pirajai* (1qll, chain *A*) and *Ag. acutus* (1mc2).

However, a Lys49 PLA_2 from *Deinagkistrodon acutus* (PDB code 1mg6; Huang *et al.*, unpublished work), myotoxin from *Ag. contortrix laticinctus* (PDB code 1s8g; Ambrosio *et al.*, 2005), myotoxin II from *Cerrophidion (Bothrops) godmani* (Arni *et al.*, 1999) and Anum-II (this work) exist as monomers in the crystalline state. Anum-II is present as a dimer in solution at physiological pH (Angulo *et al.*, 2000). Thus, the monomeric Anum II observed in the asymmetric unit may be an artifact of the crystallization process and the low pH of the solution (pH 5). In the case of bothropstoxin I (BthTX-I), the effect of pH on the monomer–dimer equilibrium was examined based on the fluorescent properties of the single Trp77 and it was shown that the monomeric form of the protein is predominant at acidic pH (de Oliveira *et al.*, 2001). Small-angle X-ray scattering studies currently in progress will be useful in clarifying the parameters that influence the equilibrium between monomers and dimers.

Financial support from FAPESP, CEPID/FAPESP, SMOLBNet (FAPESP), CNPq, CAPES/DAAD, FUNDUNESP and CONICIT (FV-058-02) is gratefully acknowledged. MTM is the recipient of a FAPESP fellowship.

References

Ambrosio, A. L., Nonato, M. C., de Araújo, H. S., Arni, R. K., Ward, R. J., Ownby, C. L., de Souza, D. H. & Garratt, R. C. (2005). *J. Biol. Chem.* **280**, 7326–7335.

Angulo, Y., Gutiérrez, J. M., Soares, A. M., Cho, W. & Lomonte, B. (2005). *Toxicon*, **46**, 291–296.

Angulo, Y., Olamendi-Portugal, T., Alape-Girón, A., Possani, L. D. & Lomonte, B. (2002). *Int. J. Biochem. Cell Biol.* **34**, 1268–1278.

Angulo, Y., Olamendi-Portugal, T., Possani, L. D. & Lomonte, B. (2000). *Int. J. Biochem. Cell Biol.* **32**, 63–71.

Arni, R. K., Fontes, M. R., Barberato, C., Gutiérrez, J. M., Díaz, C. & Ward, R. J. (1999). *Arch. Biochem. Biophys.* **366**, 177–182.

Arni, R. K. & Gutiérrez, J. M. (1993). *Toxicon*, **31**, 1061–1064.

Arni, R. K. & Ward, R. J. (1996). *Toxicon*, **34**, 827–841.

Arni, R. K., Ward, R. J., Gutiérrez, J. M. & Tulinsky, A. (1995). *Acta Cryst.* D**51**, 311–317.

Azevedo, W. F. de, Ward, R. J., Canduri, F., Soares, A., Giglio, J. R. & Arni, R. K. (1998). *Toxicon*, **36**, 1395–1406.

Azevedo, W. F. de, Ward, R. J., Gutiérrez, J. M. & Arni, R. K. (1999). *Toxicon*, **37**, 371–384.

Giotto, M. T. S., Garratt, R. C., Oliva, G., Mascarenhas, Y. P., de Azevedo, W. F., Giglio, J. R., Cintra, A. C. O., Arni, R. K. & Ward, R. J. (1998). *Proteins*, **30**, 442–454.

Gutiérrez, J. M. & Lomonte, B. (1995). *Toxicon*, **33**, 1405–1424.

Gutiérrez, J. M., Lomonte, B. & Cerdas, L. (1986). *Toxicon*, **24**, 885–894.

Laskowski, R. A., MacArthur, M. W., Moss, D. S. & Thornton, J. M. (1993). *J. Appl. Cryst.* **26**, 283–291.

Leslie, A. G. W. (1992). *Jnt CCP4/ESF–EACBM Newsl. Protein Crystallogr.* **26**.

Lomonte, B., Angulo, Y. & Calderón, L. (2003). *Toxicon*, **42**, 885–901.

Maraganore, J. M., Merutka, G., Cho, W., Welches, W., Kézdy, F. J. & Heinrikson, R. L. (1984). *J. Biol. Chem.* **259**, 13839–13843.

Mebs, D. & Ownby, C. L. (1990). *Pharmacol. Ther.* **48**, 223–236.

Murakami, M. T., Arruda, E. Z., Melo, P. A., Martinez, A. B., Calil-Elias, S., Tomaz, M. A., Lomonte, B., Gutierrez, J. M. & Arni, R. K. (2005). *J. Mol. Biol.* **350**, 416–426.

Murshudov, G. N., Vagin, A. A. & Dodson, E. J. (1997). *Acta Cryst.* D**53**, 240–255.

Nishioka, S. A. & Silveira, P. V. P. (1992). *Am. J. Trop. Med. Hyg.* **47**, 805–810.

Oliveira, A. H. C., Giglio, J. R., Andrião-Escarso, S. H., Ito, A. S. & Ward, R. J. (2001). *Biochemistry*, **40**, 6912–6920.

Ramachandran, G. N., Ramakrishnan, C. & Sasisekharan, V. (1963). *J. Mol. Biol.* **7**, 95–99.

Renetseder, R., Brunie, S., Dijkstra, B. W., Drenth, J. & Sigler, P. B. (1985). *J. Mol. Chem.* **260**, 11627–11636.

Roussel, A. & Cambillau, C. (1991). *Silicon Graphics Geometry Partners Directory*, p. 86. Mountain View, CA, USA: Silicon Graphics.

Ruller, R., Aragao, E. A., Chioato, L., Ferreira, T. L., de Oliveira, A. H., Sa, J. M. & Ward, R. J. (2005). *Biochimie*, **87**, 993–1003.

Scott, D. L., Achari, A., Vidal, J. C. & Sigler, P. B. (1992). *J. Biol. Chem.* **267**, 22645–22657.

Six, D. A. & Dennis, E. A. (2000). *Biochim. Biophys. Acta*, **1488**, 1–19.

Solórzano, A. (1989). *Rev. Biol. Trop.* **37**, 133–137.

Taylor, R., Flores, A., Flores, G. & Bolaños, R. (1974). *Rev. Biol. Trop.* **21**, 383–397.

Vagin, A. A. & Teplyakov, A. (1997). *J. Appl. Cryst.* **30**, 1022–1025.

Ward, R. J., de Azevedo, W. F. & Arni, R. K. (1998). *Toxicon*, **36**, 1623–1633.

Watanabe, L., Angulo, Y., Lomonte, B. & Arni, R. K. (2004). *Biochim. Biophys. Acta*, **1703**, 87–89.

Yamazaki, Y., Matsunaga, Y., Nakano, Y. & Morita, T. (2005). *J. Biol. Chem.* **280**, 29989–29992.

8.07f/W(Jul162004) +model | TOXCON : 2824 | Prod.Type:FTP pp.1–10(col.fig.:3,6) | ED:G.JayaL. PAGN:santhamma SCAN:

ARTICLE IN PRESS

ELSEVIER

Toxicon ▮ (▮▮▮▮) ▮▮▮–▮▮▮

TOXICON

www.elsevier.com/locate/toxicon

Interfacial surface charge and free accessibility to the PLA_2-active site-like region are essential requirements for the activity of Lys49 PLA_2 homologues

Mário T. Murakami[a], Magno M. Viçoti[a], José R. B. Abrego[a], Marco R. Lourenzoni[b], Adélia C.O. Cintra[c], Emerson Z. Arruda[d], Marcelo A. Tomaz[d], Paulo A. Melo[d], Raghuvir K. Arni[a,e,*]

[a]*Department of Physics, IBILCE/UNESP, Cristovão Colombo 2265, São José do Rio Preto, SP 15054-000, Brazil*
[b]*Associated Researchers, São Carlos, SP, Brazil*
[c]*Department of Toxicology, USP, Ribeirão Preto, SP, Brazil*
[d]*Department of Basic and Clinical Pharmacology, ICB, CCS, UFRJ, Rio de Janeiro, RJ, Brazil*
[e]*Center for Applied Toxinology, Butantan Institute, São Paulo, SP, Brazil*

Received 14 August 2006; received in revised form 19 October 2006; accepted 23 October 2006

Abstract

Lys49 phospholipase A_2 homologues are highly myotoxic and cause extensive tissue damage but do not display hydrolytic activity towards natural phospholipids. The binding of heparin, heparin derivatives and polyanionic compounds such as suramin result in partial inhibition (up to 60%) of the myotoxic effects due to a change in the overall charge of the interfacial surface. In vivo experiments demonstrate that polyethylene glycol inhibits more than 90% of the myotoxic effects without exhibiting secondary toxic effects. The crystal structure of bothropstoxin-I complexed with polyethylene glycol reveals that this inhibition is due to steric hindrance of the access to the PLA_2-active site-like region. These two inhibitory pathways indicate the roles of the overall surface charge and free accessibility to the PLA_2-active site-like region in the functioning of Lys49 phospholipases A_2 homologues. Molecular dynamics simulations, small angle X-ray scattering and structural analysis indicate that the oligomeric states both in solution and in the crystalline states of Lys49 phospholipases A_2 are principally mediated by hydrophobic contacts formed between the interfacial surfaces. These results provide the framework for the potential application of both clinically approved drugs for the treatment of *Viperidae* snakebites.

Keywords: Lys49 phospholipases A2 homologues; Myonecrosis; Suramin; Polyethylene glycol; Small angle scattering; Crystal structure and molecular dynamics

Abbreviations: PLA_2, phospholipase A_2; BthTX-I, *Bothrops jararacussu* bothropstoxin-I; ACL myotoxin, *Agkistrodon contortrix laticinctus* myotoxin; Basp-II, *Bothrops asper* myotoxin II; CK, creatine kinase; NSD, normalized spatial discrepancy; SAXS, small angle X-ray scattering; PEG-400, polyethylene glycol 400; MD, molecular dynamics; RMSD, root mean square deviations; IIP, intermolecular interaction potential; PISA, Protein, Interfaces, Surfaces and Assemblies.

*Corresponding author. Department of Physics, IBILCE/UNESP, Cristovão Colombo 2265, São José do Rio Preto, SP 15054-000, Brazil. Tel.: +55 17 3321 2460; fax: +55 17 3221 2247.
E-mail address: arni@ibilce.unesp.br (R.K. Arni).

0041-0101/$ - see front matter © 2006 Published by Elsevier Ltd.
doi:10.1016/j.toxicon.2006.10.011

1. Introduction

Envenomation by Viperidae snakes results in acute myonecrosis that provokes permanent tissue loss resulting in disability, amputation and in some cases, death (Gutiérrez and Lomonte, 1995). Myonecrosis is mainly caused by the direct action of catalytically inactive Lys49 phospholipases A_2 (PLA_2) homologues upon the plasma membrane of muscle cells and by the indirect action of metalloproteinases and serine proteinases on the haemostatic system (Gutiérrez and Lomonte, 1995; Ownby et al., 1999). Since the widely used antivenom serum therapy does not address myonecrosis, the inclusion of a supplementary agent for the treatment of Viperidae snakebites is therapeutically relevant.

Heparin and related polyanions are able to inhibit myonecrosis induced by snake venoms that contains myotoxins such as *Bothrops jararacussu* bothropstoxin-I (BthTX-I) (Homsi-Branderburgo et al., 1988), *Agkistrodon contortrix laticinctus* myotoxin (ACL myotoxin) (Johnson and Ownby, 1993) and *Bothrops asper* myotoxin II (Basp-II), both in vivo and in vitro (Lomonte and Gutiérrez, 1989). Suramin, a polysulphonated naphthyl urea derivative used clinically in the treatment of onchocerciasis (Burch and Ashburn, 1951), African trypanosomiasis (Williamson and Desowitz, 1956) and several kinds of cancers (LaRocca et al., 1993; van Oosterom et al., 1991), is also a potential inhibitor of myotoxins both in vivo and in vitro and represents an important therapeutic agent for the treatment of Viperidae snakebites (Arruda et al., 2002; Murakami et al., 2005).

Catalytically inactive Lys49 PLA_2s homologues cause membrane leakage in the absence of Ca^{2+} ions, without concomitant hydrolysis when tested against negatively charged liposomes (Gutiérrez and Lomonte, 1995; Ownby et al., 1999). A number of studies involving different techniques, such as chemical modification, sequence comparison analyses, interaction with neutralizing molecules, synthetic peptide studies, and site-directed mutagenesis, have been used in an attempt to elucidate the structural determinants for myotoxicity of Lys49 PLA_2s homologues (Ownby et al., 1999; Murakami et al., 2005).

Our studies combining small angle X-ray scattering, crystallography, molecular dynamics simulations, inhibition by suramin and polyethylene glycol and in vivo tests, reveal new features of the action mechanism of myotoxins, suggesting a promising supplement of the current serum treatment by the inclusion of potent inhibitors that simultaneously bind both in the putative catalytic and at the interfacial recognition sites.

2. Materials and methods

2.1. Purification and biochemical characterization

Crude dessicated *B. jararacussu* venom was obtained from a local serpentarium and BthTX-I was purified with minor modifications following the published protocol (Spencer et al., 1998). The purity of the samples was confirmed by SDS-PAGE (Laemmli, 1970) and the protein concentrations were determined by the Bradford method (Bradford, 1976).

2.2. In vivo myotoxic assay

In vivo myotoxic assays were carried out as previously described in Murakami et al. (2005) with minor modifications. In accordance with each protocol, the quantity of toxin (50 μg/g) administered was adjusted taking into consideration the individual weight of each animal and different ratios of suramin and polyethylene glycol (1:0.25, 1:0.50, 1:1, 1:2.5, 1:5.0; BthTX-I:inhibitor). Enzyme activity was expressed as international Units per liter (U/L), where 1 U is defined as the amount that catalyzes the transformation of 1 μmol of substrate at 25 °C.

2.3. Scattering data acquisition and analysis

Small angle X-ray scattering (SAXS) measurements were conducted at room temperature utilizing the D11A-SAXS beamline at the Brazilian National Synchrotron Light Source where the wavelength was set to 1.488 Å. A sample concentration of 4–10 mg/mL in a 20 mM, pH 7.0 Tris–HCl buffer was used and serial dilutions were prepared to permit the extrapolation of the SAXS curves to zero concentration. Data acquisitions were performed by taking several 600 s frames of each sample. Data fitting was performed using the GNOM program (Semenyuk and Svergun, 1991) and the radius of gyration (R_g) of the protein in solution was determined from the lowest q values using the Guinier approximation (Guinier and Fournet, 1955). The ab initio shape determination was

Please cite this article as: Murakami, M.T., et al., Interfacial surface charge and free accessibility to the PLA_2-active site-like region are essential requirements for the activity of Lys49 PLA_2.... Toxicon (2006), doi:10.1016/j.toxicon.2006.10.011

performed by the dummy atom model method, using the program DAMMIN (Svergun, 1999) and the independent ab initio reconstructions were averaged with program DAMAVER. The shape reconstruction and the crystallographic atomic coordinates were superimposed (SUPCOMB 2.0) (Kozin and Svergun, 2001). The superpositioning was assessed by normalized spatial discrepancy (NSD or parameter *d*), which estimates the similarity between two different three-dimensional objects. NSD values <1.5 indicate high correlation of the surface complementarity and is typical for the comparisons between an atomic model and the corresponding DAMMIN model. The theoretical SAXS pattern based on the atomic coordinates was calculated using the program CRYSOL (Svergun et al., 1995).

2.4. Crystallization, data collection, structure determination and refinement

Crystallization was performed by the hanging-drop vapour diffusion method and large single crystals (0.4 mm in each dimension) were obtained when a 2-μL protein droplet (protein concentration 12 mg/mL) was mixed with an equal volume of reservoir solution consisting of 0.1 M Hepes (pH 7.5), 2.0 M ammonium sulphate and 20% polyethylene glycol 400 (PEG-400). The crystals were transferred to a cryo-protectant solution containing 20% glycerol and were flash frozen, diffraction intensities were recorded utilizing a MAR-CCD detector at the D03B/MX1 Beamline at the Brazilian National Synchrotron Light Source where the wavelength of the incident radiation was set to 1.47 Å. The diffraction intensities were integrated, scaled and merged using the HKL suite of programs (Otwinowski and Minor, 1997).

The crystal structure of the BthTX-I was solved by molecular replacement techniques with the AMoRe package (Navaza, 1994) using the atomic coordinates of the Basp-II (PDB code 1Y4L) (Murakami et al., 2005) as the search model. Positional and individual isotropic thermal factor refinements were carried out using REFMAC5 (Murshudov et al., 1997) as incorporated in the CCP4 suite. The $2F_o–F_c$ and $F_o–F_c$ electron density maps were examined, the protein model was manually adjusted after each refinement cycle using TURBO FRODO (Jones, 1985) and COOT (Emsley and Cowtan, 2004) and the stereochemistry of the final model was analyzed using PROCHECK (Laskowski et al., 1993). The atomic coordinates and structure factors of BthTX-I have been deposited with the Protein Data Bank (acession code 2H8I).

2.5. Molecular dynamics

Explicit solvent molecular dynamics (MD) simulations were performed using the GROMACS 3.2 software package and the GROMOS-96 (43a1) force field (Lindahl et al., 2001). Two different systems were simulated, (i) the BthTX-I dimer and (ii) BthTX-I complexed with suramin. The topology of suramin was obtained from the Dundee PRODRG Server (http://davapc1.bioch.dundee.ac.uk/cgi-bin/prodrg_beta). All MD simulations were performed in an isothermal–isobaric ensemble, using the "leapfrog" algorithm (Hockney and Goel, 1974) and the temperature and pressure were controlled using the Berendsen method (Berendsen et al., 1981). The long-range interactions were treated using the particle-mesh Ewald sum method (Darden et al., 1993). The LINCS algorithm (Hess et al., 1997) was used to constrain protein covalent bonds involving hydrogen atoms, and the SETTLE algorithm (Miyamoto and Kollman, 1992) was used to constrain water molecules. The BthTX-I/suramin complex simulations were performed in three phases. In the first phase (Phase I) a short simulation was performed with BthTX-I by imposing restraints on atomic positions during 100 ps in order to equilibrate the system. In the second phase (Phase II), the atomic positions of BthTX-I atoms were not restrained in order to relax the protein structure, enabling the determination of the relaxed solution structure. In the final phase (Phase III), the complete system was simulated without imposing positional restraints. The root mean square deviations (RMSD) and intermolecular interaction potential (IIP) were monitored.

3. Results

3.1. Effect of suramin or/and polyethylene glycol on myotoxicity in vivo

Intramuscular injections of BthTX-I (50 μg/g) increased plasma CK activity from 85 ± 41 to 3950 ± 248 U/L after 2 h (Figs. 1A and B). Pre-incubation of BthTX-I with suramin for 15 min significantly inhibits the increase in plasma CK activity in a dose-dependent fashion with maximum

Please cite this article as: Murakami, M.T., et al., Interfacial surface charge and free accessibility to the PLA_2-active site-like region are essential requirements for the activity of Lys49 PLA_2.... Toxicon (2006), doi:10.1016/j.toxicon.2006.10.011

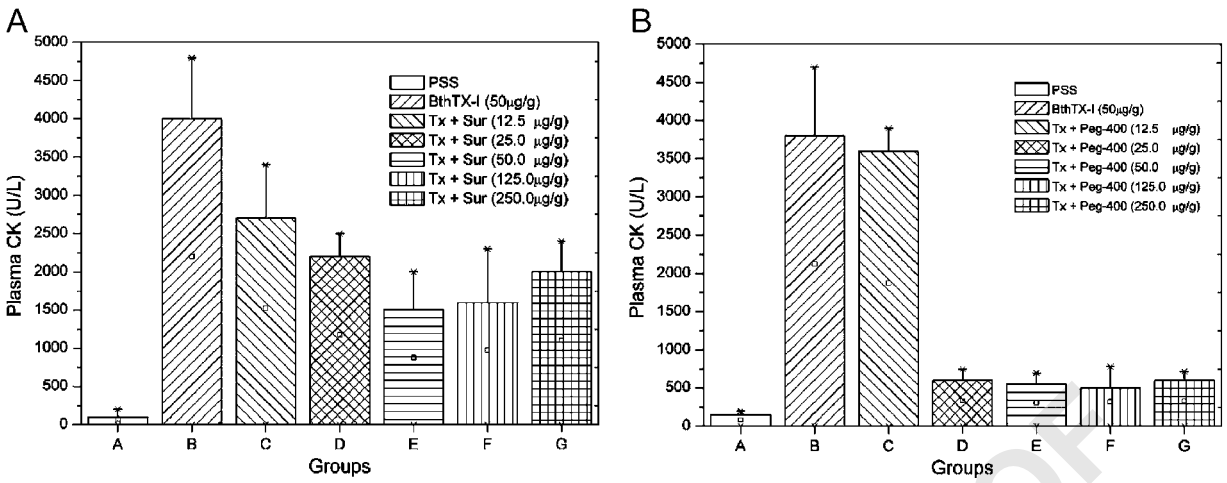

Fig. 1. Experimental scattering intensity and $p(r)$ distribution curves.

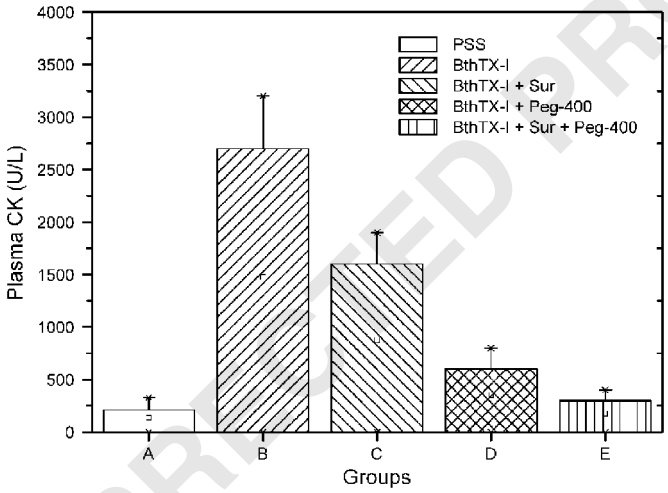

Fig. 2. In vivo dose-dependent effect of suramin (A) or PEG-400 (B) on CK release.

inhibition observed when the ratio is 1:1 (w/w; BthTX-I:suramin) (Fig. 2A). These values of plasma CK activity are in agreement with previously reported values for other homologous Lys49 PLA_2s such as ACL myotoxin (Melo et al., 1994) and Basp-II (Murakami et al., 2005). Experiments with PEG-400 were conducted under the same conditions (Fig. 2B). PEG-400 proved to be 30% more potent than suramin resulting in approximately 92% inhibition of myotoxicity, whereas the maximum inhibition by suramin is 40% (Figs. 1A and B). The effect of the simultaneous inclusion of both compounds was tested in vivo (Fig. 2) and displayed enhanced inhibition, dramatically decreasing the CK activity to insignificant levels.

3.2. Crystal structure of BthTX-I complexed with PEG-400

The final model consists of two molecules of BthTX-I forming a homodimer, two PEG-400 fragments and 86 solvent water molecules. The refinement converged to a crystallographic residual of 22.5% (R_{free} = 27.6%) for 18,722 reflections in the resolution range of 10.0–1.9 Å. The electron density in the $2F_o$–F_c Fourier maps was continuous and well defined for both monomers in the asymmetric unit, except for the C-terminii, which are typically disordered as in other structures. The model displays good overall stereochemistry with RMSD values of 0.02 Å and 2.1° for bond lengths

Please cite this article as: Murakami, M.T., et al., Interfacial surface charge and free accessibility to the PLA_2-active site-like region are essential requirements for the activity of Lys49 PLA_2.... Toxicon (2006), doi:10.1016/j.toxicon.2006.10.011

and bond angles, respectively and the average *B*-value for all atoms is 41.5 Å^2 (Table 1). The Ramachandran plot demonstrates that 88.5% of the dihedral angles are situated in the most favored regions, while the remaining 10.5% of residues are in the additionally permitted regions. The molecular topology of BthTX-I conserves all the main features of PLA_2s containing an N-terminal α-helix (H1) (residue 2–12) and the two long anti-parallel disulphide linked α-helices (H2 from residue 40 to residue 55 and H3 from residue 86 to residue 103) with a mean distance of 10 Å between the helical axes and two short helical turns (residues 19–22; SH4 and 108–110; SH5) (Arni and Ward, 1996). The *β*-wing region (residues 74–84) is structurally conserved and a disulphide bridge preserves its relative orientation. The total dimeric interface area between the two molecules was calculated to be approximately 3598 Å^2 occluding the whole hydrophobic channel and the entrance to both the active-site pockets.

Table 1
Data collection and refinement statistics

PDB code	2H8I
Data-collection statistics	
Space group	P 3_1 2 1
Unit-cell parameters (Å)	$a = b = 56.02$; $c = 127.57$
Resolution range (Å)	9.96–1.90
Unique reflections	18,722
Redundancy	10.5 (8.5)
Completeness (%)	99.3 (98.8)
$I/\sigma(I)$	32.81 (4.33)
R_{merge} (%)[a]	5.3 (41.0)
V_M (Å^{3}Da^{-1})	2.02
Solvent content (%)	38.58
Refinement statistics	
R_{factor} (%)[b]	22.5
R_{free} value (%)[c]	27.6
No. of amino acid residues	242
No. of solvent molecules	122
No. of polyethylene glycol molecules	2
Mean temperature factor (Å^2)[d]	41.5
R.m.s.d. bond lengths (Å)	0.020
R.m.s.d. bond angles (°)	2.145
Ramachandran plot	
Most favoured region (%)	88.5
Additionally allowed regions (%)	10.5
Generously allowed regions (%)	0.5
Disallowed regions (%)	0.5

Values in parentheses are for the highest resolution shell.
[a] $R_{merge} = 100 \times \Sigma|I(h) - \langle I(h)\rangle|/\Sigma I(h)$, where $I(h)$ is observed intensity and $\langle I(h)\rangle$ is mean intensity of reflection h over all measurements of $I(h)$.
[b] $R_{factor} = 100 \times \Sigma|F_o - F_c|/\Sigma(F_o)$ the sums being taken over all reflections with $F/\sigma(F) > 2$ cutoff.
[c] $R_{free} = R_{factor}$ for 5% of the data, which were not included during crystallographic refinement.
[d] *B*-values are average *B*-values for all non-hydrogen atoms.

3.3. PEG-binding site

In both monomers, the electron density maps indicated the presence of a PEG-400 molecule bound in the hydrophobic channels that lead to the PLA_2-active site-like regions (Fig. 3A). The PEG-400 molecules interact with the putative calcium-binding loop and the residues considered important for catalysis. The O1 atoms from the tails of the PEG-400 fragments simultaneously interact with the amide bonds between Cys29–Gly30 and His48ND1 atom via a water molecule (Fig. 3B). Similar interactions were observed in the crystal structure of piratoxin II, a Lys49 PLA_2 from *Bothrops pirajai*, which contains a fatty acid bound at the entrance to the active-site cavity (Lee et al., 2001) and in the crystal structure of Basp-II complexed with stearic acid (Watanabe et al., 2005). The crystal structure of Basp-II complexed with suramin also contains a PEG molecule bound at the active-site cavity concomitantly with suramin (Murakami et al., 2005) bound at the interfacial recognition face.

3.4. Suramin-binding site

In the MD simulations of BthTX-I with suramin, the structural stability was monitored by the RMSDs of the protein atoms in phases II and III (Fig. 4A), which undergo small positional shifts (around 1.4 Å) and a corresponding reduction in the IIP from −145 to −233 kcal mol^{-1} (Fig. 4B), indicating that the hydrated structure of BthTX-I is similar to the crystallographic model. The resulting BthTX-I/suramin complex model obtained from the MD simulations demonstrate a similar mode of binding to that described for the crystal structure of the Basp-II/suramin complex, where the residues Arg34 and Lys53 play key roles in the interaction with the sulphonated naphthyl rings (Fig. 3C). The central phenyl rings embrace the putative calcium-binding loop and the short helical turn (SH4) shields the whole hydrophobic surface, inducing a drastic change in the overall charge of the interfacial recognition face of the protein.

Please cite this article as: Murakami, M.T., et al., Interfacial surface charge and free accessibility to the PLA_2-active site-like region are essential requirements for the activity of Lys49 PLA_2.... Toxicon (2006), doi:10.1016/j.toxicon.2006.10.011

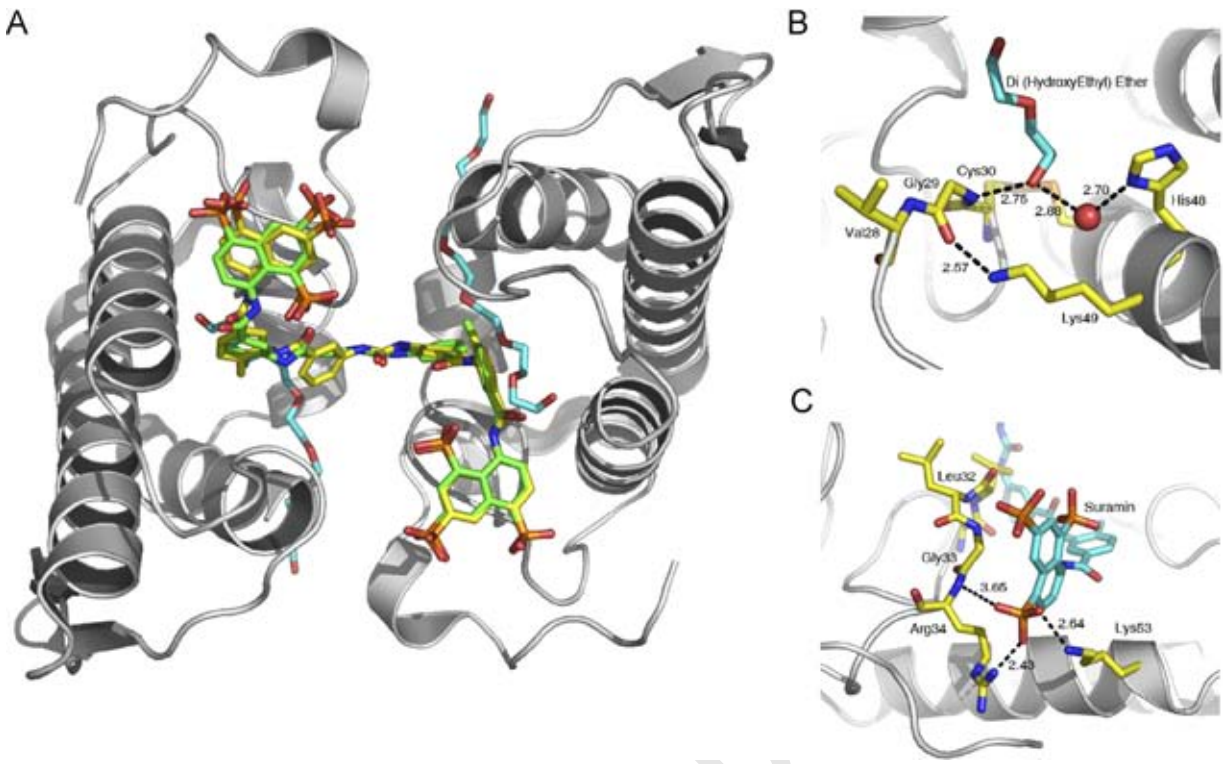

Fig. 3. In vivo effects of suramin and/or PEG-400 on the CK release.

3.5. Oligomeric state

Electrophoretic and spectroscopic techniques indicate that a number of Lys49 PLA_2s homologues exist as dimers in solution (Arni et al., 1995). Previous crystallographic and spectroscopic results suggest that these molecules adopt an extended conformation with a radius of gyration of 20.2 Å, maintained by diad, polar interactions formed between the β-wing and N-terminal helix regions that involve the strictly conserved residues: Gln11, Glu12, Trp77 and Lys80. In this conformation, the hydrophobic channels and interfacial surfaces are exposed to the solvent (Ward et al., 1998; da Silva-Giotto et al., 1998). Based on this, a model for the disruption of membranes by Lys49 PLA_2 homologues has been proposed (Lomonte et al., 2003).

However, the SAXS results show that the radius of gyration (R_g) of BthTX-I is 17.5 Å indicating that this molecule adopts a more compact dimeric conformation as observed in the crystal structure of the suramin/Basp-II complex (Murakami et al., 2005) (Fig. 3A) that displays a R_g of 17.9 Å. The profiles of the scattering curve and distance distribution function $p(r)$ are presented in Figs. 5A and B, respectively. Re-examination of the molecules forming the asymmetric unit of a numerous dimeric Lys49 PLA_2 homologues indicates that this conformation is equally likely depending on the criteria used for the selection of the symmetry mates. The averaged ab initio shape of BthTX-I was superposed on the atomic coordinates of the extended (Figs. 6D–F) and compact dimers (Figs. 6A–C), resulting in NSD values of 1.85 and 1.21, respectively, indicating high shape complementarity between the ab initio solution envelope and the surface envelope of the compact dimer (Fig. 6G).

In this compact model, the interface consists of non-polar contacts formed between the interfacial surfaces connecting the PLA_2-active site-like regions, shielding the whole hydrophobic faces of Lys49 PLA_2s homologues from the solvent. Analysis of the protein interfaces of several Lys49 PLA_2s homologues with the Protein, Interfaces, Surfaces and Assemblies (PISA) software (http://www.ebi.ac.uk/msd-srv/prot_int/pistart.html) suggests that the compact dimeric conformation is more likely. Additionally, MD simulations of the compact dimer for 9 ns indicated small increments in the RMSD (Fig. 4C) and a reduction in the IIP from −45 to

Please cite this article as: Murakami, M.T., et al., Interfacial surface charge and free accessibility to the PLA_2-active site-like region are essential requirements for the activity of Lys49 PLA_2.... Toxicon (2006), doi:10.1016/j.toxicon.2006.10.011

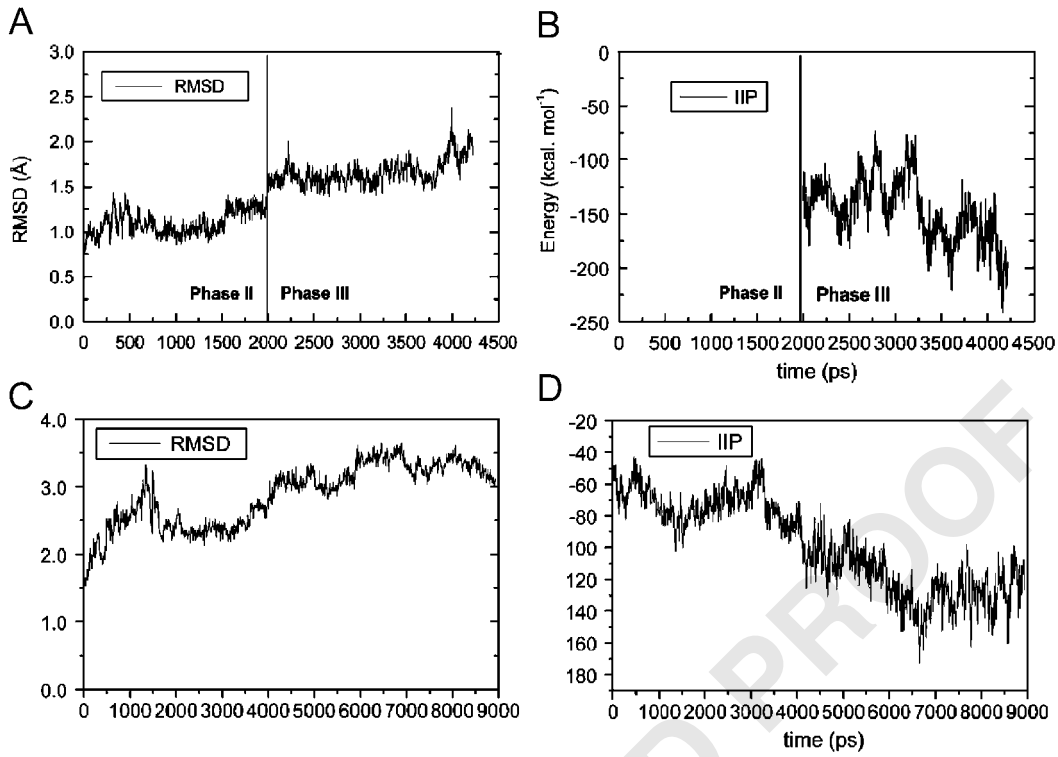

Fig. 4. (A) Simultaneous binding of suramin in the crystal structure of Basp-II (carbon atoms in yellow; PDB entry: 14YL) and in MD simulations of BthTX-I (carbon atoms in green, this work) and PEG of Basp-II (carbon atoms in blue). (B) Interactions of PEG (carbon atoms in blue) at the putative catalytic active of BthTX-I (this work). (C) Interactions resulting from the MD simulations between suramin (carbon atoms in blue) and BthTX-I (carbon atoms in yellow).

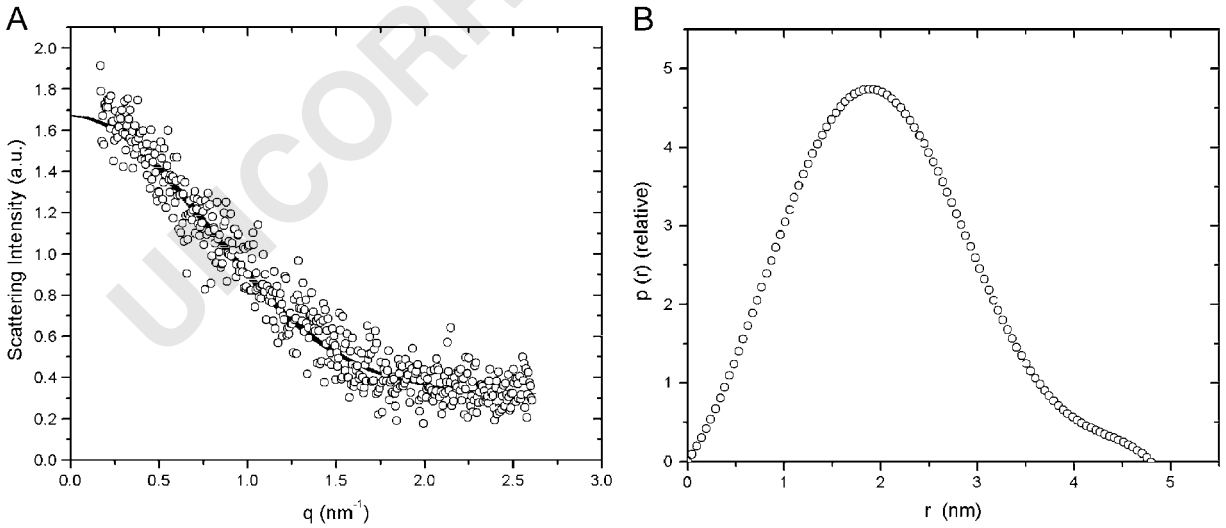

Fig. 5. Results of the MD simulations. (A) RMSD and IIP values during phases II and III of BthTX-I plus suramin and (B) RMSD and IIP for 9 ns of the compact dimer.

Please cite this article as: Murakami, M.T., et al., Interfacial surface charge and free accessibility to the PLA_2-active site-like region are essential requirements for the activity of Lys49 PLA_2.... Toxicon (2006), doi:10.1016/j.toxicon.2006.10.011

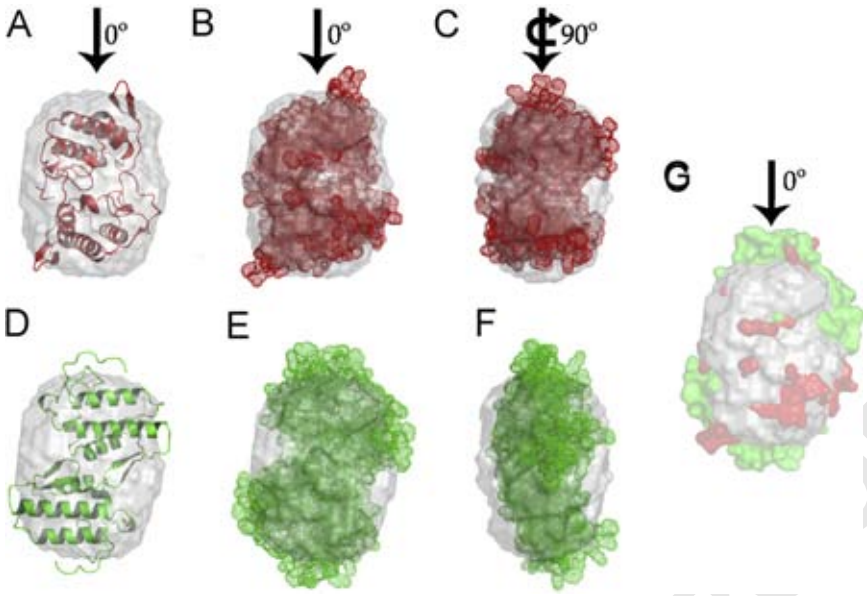

Fig. 6. Superpositioning of the atomic coordinates of the compact (A), (B) and (C) and extended (D), (E) and (F) oligomeric states on the SAXS ab initio envelope (gray transparent surface). Ribbon and space filling representations of the compact (A), (B) and (C) and extended (D), (C) and (E) dimers in the same orientation and 90° rotation of *B*/*E* along the vertical axis. (G) Surface representation of the compact (red) and extended (green) dimers on the SAXS envelope.

$-125\,\mathrm{kcal\,mol^{-1}}$ (Fig. 4D), indicating that this conformation is stable in aqueous solution.

4. Discussion

The capacity of polyanionic compounds to neutralize the myotoxic effects of snake venoms PLA_2s has been extensively studied, especially in view of the limited efficacy of antisera in antagonizing these effects (Melo and Suarez-Kurtz, 1988b; Melo and Ownby, 1999; Calil-Elias et al., 2002; Murakami et al., 2005) and the fact that they constitute useful tools for investigating the mechanisms of action of myotoxins (Gutiérrez and Lomonte, 1995).

The mechanism of inhibition of Lys49 PLA_2s homologues by suramin, which involves an induced-fit binding at the hydrophobic surface of the dimer significantly changing the overall charge on the interfacial recognition face and the resulting partial blockage of the PLA_2-active site-regions, has been reported (Melo et al., 1993; Calil-Elias et al., 2002; de Oliveira et al., 2003; Murakami et al., 2005). In vivo experiments with polyethylene glycol, a water-soluble waxy solid that is used extensively in the cosmetic, toiletry industry and as a medication for osmotic laxatives, indicates that is a more potent inhibitor of myotoxicity induced by Lys49 PLA_2s homologues than suramin. Polyethylene glycol inhibits more than 90% of the myotoxic activity and does not display any secondary toxic effects. In the crystal structure of BthTX-I complexed with PEG, the PEG molecules are bound in the hydrophobic channels that lead to the PLA_2-active site-like region, interacting simultaneously with the amide bonds formed between Cys29–Gly30 and ND1 of His48 via a water molecule. This result indicates an alternative, more efficient pathway for the inhibition of myotoxicity by blocking the PLA_2-active site-like region, without altering the overall surface charge. Since both suramin and PEG use different sites, the combination of suramin and polyethylene glycol was tested and almost complete inhibition of the myotoxic activity of Lys49 PLA_2s homologues was observed, thus representing a possible utility for the complementary treatment of *Viperidae* snakebites.

5. Concluding remarks

The action mechanism of myotoxic homologues Lys49 PLA_2s is a paradigm for toxinologists and a number of different strategies, such as chemical modification, sequence comparison analyses, inter-

Please cite this article as: Murakami, M.T., et al., Interfacial surface charge and free accessibility to the PLA_2-active site-like region are essential requirements for the activity of Lys49 PLA_2.... Toxicon (2006), doi:10.1016/j.toxicon.2006.10.011

action with neutralizing molecules, synthetic peptide studies, and site-directed mutagenesis analyses have attempted to elucidate the structural determinants for myotoxicity of Lys49 PLA_2s. Our results indicate that (i) the molecules that bind at the PLA_2-active site-like region inhibit the myotoxic activity of Lys49 PLA_2; (ii) PEG derivatives represent attractive targets for drug design aimed at the treatment of Viperidae snakebites since they are non-toxic; (iii) binding of suramin and heparin analogues at the hydrophobic interfacial surface also inhibit myotoxic activity albeit at a lower level and (iv) the inclusion of molecules that bind both at the PLA_2-active site-like region and at the hydrophobic interfacial surface reduces myonecrosis to extremely low levels.

These biochemical, physiological and structural findings suggest a new promising therapeutic utility for the clinically approved drugs, suramin and PEG, which interact at two distinct sites, for the treatment of myonecrosis induced by Viperidae snakebites.

6. Uncited references

Myers (1991); Lomonte et al. (1994); Melo and Suarez-Kurtz (1988a).

Acknowledgements

Financial support by FAPESP, CEPID, SMOLB-Net, CNPq and CAPES/DAAD is gratefully acknowledged. MTM is recipient of a FAPESP fellowship.

References

Arni, R.K., Ward, R.J., Gutiérrez, J.M., Tulinsky, A., 1995. Structure of a calcium-independent phospholipase-like myotoxic protein from *Bothrops asper* venom. Acta Crystallogr. D 51, 311–317.

Arni, R.K., Ward, R.J., 1996. Phospholipase A2—a structural review. Toxicon 34, 827–841.

Arruda, E.Z., Silva, N.M., Moraes, R.A., Melo, P.A., 2002. Effect of suramin on myotoxicity of some crotalid snake venoms. Braz. J. Med. Biol. Res. 35, 723–726.

Berendsen, H.J.C., Postma, J.P.M., van Gunsteren, W.F., Hermans, J., 1981. Interactions models for water in relation to protein hydration. In: Pullman, B. (Ed.), Intermolecular Forces. Reidel Publishing Company, Dordrecht, pp. 331–342.

Bradford, M.M., 1976. A rapid and sensitive method for the quantitation of microgram quantities of protein utilizing the principle of protein dye binding. Anal. Biochem. 72, 248–254.

Burch, T.A., Ashburn, L.L., 1951. Experimental therapy of onchocerciasis with suramin and hetrazan; results of a three-year study. Am. J. Trop. Med. Hyg. 31, 617–623.

Calil-Elias, S., Martinez, A.M., Melo, P.A., 2002. Effect of heparin and antivenom on skeletal muscle damage produced by *Bothrops jararacussu* venom. Histol. Histopathol. 17, 463–470.

Darden, T., York, D., Pedersen, L., 1993. Particle mesh Ewald. An $N\log(N)$ method for Ewald sumsin large systems. J. Chem. Phys. 98, 10089–10092.

da Silva-Giotto, M.T., Garrat, R.C., Oliva, G., Mascarenhas, Y.P., Giglio, J.R., Cintra, A.C.O., de Azevedo, W.F., Arni, R.K., Ward, R.J., 1998. Crystallographic and spectroscopic characterization of a molecular hinge: conformational changes in bothropstoxin I, a dimeric Lys49-phospholipase A2 homologue. Prot. Struct. Funct. Gen. 30, 442–454.

de Oliveira, M., Cavalcante, W.L., Arruda, E.Z., Melo, P.A., Dal-Pai Silva, M., Gallacci, M., 2003. Antagonism of myotoxic and paralyzing activities of bothropstoxin-I by suramin. Toxicon 42, 373–379.

Emsley, P., Cowtan, K., 2004. Coot: model-building tools for molecular graphics. Acta Crystallogr. Sect. D 60, 2126–2132.

Guinier, A., Fournet, G., 1955. Small Angle Scattering of X-rays, first ed. Wiley, New York, pp. 17–19.

Gutiérrez, J.M., Lomonte, B., 1995. Phospholipase A_2 myotoxins from *Bothrops* snake venons. Toxicon 33, 1405–1424.

Hess, B., Becker, H., Berendsen, H.J., Fraaije, J.G.E.M., 1997. Lincs: a linear constraint solver for molecular simulations. J. Comput. Chem. 18, 1463–1472.

Hockney, R.W., Goel, S.P., 1974. Quiet high-resolution computer models of a plasma. J. Comput. Phys. 14, 148–158.

Homsi-Brandeburgo, M.I., Queiroz, L.S., Santo-Neto, H., Rodrigues-Simioni, L., Giglio, J.R., 1988. Fractionation of *Bothrops jararacussu* snake venom: partial chemical characterization and biological activity of bothropstoxin. Toxicon 26, 615–627.

Johnson, E.K., Ownby, C.L., 1993. Isolation of a myotoxin from the venom of *Agkistrodon contortrix laticinctus* (broad-banded copperhead) and pathogenesis of myonecrosis induced by it in mice. Toxicon 31, 243–255.

Jones, T.A., 1985. Interactive computer graphics: FRODO. Methods Enzymol. 115, 157–171.

Kozin, M.B., Svergun, D.I., 2001. Automated matching of high- and low-resolution structural model. J. Appl. Crystallogr. 34, 33–41.

Laemmli, U.K., 1970. Cleavage of structural proteins during the assembly of head of bacteriophage T4. Nature 227, 680–685.

LaRocca, R.V., Cooper, M.R., Uhrich, M., Danesi, R., Walther, M.M., Linehan, W.M., Laskowski, R.A., Moss, D.S., Thornton, J.M., 1993. Main-chain bond lengths and bond angles in protein structures. J. Mol. Biol. 231, 1049–1067.

Laskowski, R.A., Moss, D.S., Thornton, J.M., 1993. Main-chain bond lengths and bond angles in protein structures. J. Mol. Biol. 231, 1049–1067.

Myers, C.E., 1991. Use of suramin in treatment of prostatic carcinoma refractory to conventional hormonal manipulation. Urol. Clin. North Am. 18, 123–129.

Lee, W.H., da Silva Giotto, M.T., Marangoni, S., Toyama, M.H., Polikarpov, I., Garratt, R.C., 2001. Structural basis for low catalytic activity in Lys49 phospholipases A2—a hypothesis: the crystal structure of piratoxin II complexed to fatty acid. Biochemistry 40, 28–36.

Lindahl, E., Hess, B., van der Spoe, D.L., 2001. Gromacs 3.0: a package for molecular simulation and trajectory analysis. J. Mol. Model. 7, 306–317.

Lomonte, B., Gutiérrez, J.M., 1989. A new muscle damaging toxin, myotoxin II, from the venom of the snake *Bothrops asper* (terciopelo). Toxicon 27, 725–733.

Lomonte, B., Moreno, E., Tarkowski, A., Hanson, L.A., Maccarana, M., 1994. Neutralizing interaction between heparins and myotoxin II, a lysine 49 phospholipase A2 from Bothrops asper snake venom. Identification of a heparin-binding and cytolytic toxin region by the use of synthetic peptides and molecular modeling. J. Biol. Chem. 269, 29867–29873.

Lomonte, B., Angulo, Y., Calderon, L., 2003. An overview of lysine-49 phospholipase A2 myotoxins from crotalid snake venoms and their structural determinants of myotoxic action. Toxicon 42, 885–901.

Melo, P.A., Ownby, C.L., 1999. Ability of wedelolactone, heparin and para-bromophenacyl bromide to antagonize the myotoxic effects of two crotaline venoms and their PLA_2 myotoxins. Toxicon 37, 199–215.

Melo, P.A., Suarez-Kurtz, G., 1988a. Release of sarcoplasmic enzymes from skeletal muscle by *Bothrops jararacussu* venom: antagonism by heparin and by the serum of South American marsupials. Toxicon 26, 87–95.

Melo, P.A., Suarez-Kurtz, G., 1988b. Release of creatine kinase from skeletal muscle by *Bothrops* venoms: heparin potentiation of inhibition by antivenin. Braz. J. Med. Biol. Res. 21, 548–558.

Melo, P.A., Homsi-Brandemburgo, M.I., Giglio, J.R., Ownby, G., 1993. Antagonism of the myotoxic effects of *Bothrops jararacussu* venom and bothropstoxin by polyanions. Toxicon 31, 285–291.

Melo, P.A., Nascimento, M.C., Mors, W.B., Ownby, G., 1994. Inhibition of the myotoxic and hemorrhagic activities of crotalid venoms by *Eclipta prostrata* (asteraceae) extracts and constituents. Toxicon 32, 595–603.

Miyamoto, S., Kollman, P.A., 1992. SETTLE: an analytical version of the SHAKE and RATTLE algorithm for rigid water models. J. Comput. Chem. 13, 952–962.

Murakami, M.T., Arruda, E.Z., Melo, P.A., Martinez, A.B., Calil-Elias, S., Tomaz, M.A., Lomonte, B., Gutiérrez, J.M., Arni, R.K., 2005. Inhibition of myotoxic activity of *Bothrops asper* myotoxin II by the anti-trypanosomal drug suramin. J. Mol. Biol. 350, 416–426.

Murshudov, G.N., Vagin, A.A., Dodson, E.J., 1997. Refinement of macromolecular structures by the maximum-likelihood method. Acta Crystallogr. Sect. D 53, 240–255.

Navaza, J., 1994. AMoRe: an automated package for molecular replacement. Acta Crystallogr. A 50, 157–163.

Ownby, C.L., Selistre de Araujo, H.S., White, S.P., Fletcher, J.E., 1999. Lysine 49 phospholipase A_2 proteins. Toxicon 37, 441–445.

Otwinowski, Z., Minor, W., 1997. Processing of X-ray diffraction data collected in oscillation mode. Methods Enzymol. 276, 307–326.

Semenyuk, A.V., Svergun, D.I., 1991. Gnom—a program package for small-angle scattering data-processing. J. Appl. Crystallogr. 24, 537–540.

Spencer, P.J., Aird, S.D., Boni-Mitake, M., Nascimento, N., Rogero, J.R., 1998. A single-step purification of bothropstoxin-I. Braz. J. Med. Biol. Res. 31, 1125–1127.

Svergun, D.I., 1999. Restoring low resolution structure of biological macromolecules from solution scattering using simulated annealing. Biophys. J. 76, 2879–2886.

Svergun, D.I., Barberato, C., Koch, M.H., 1995. Crysol—a program to evaluate X-ray solution scattering of biological macromolecules from atomic coordinates. J. Appl. Crystallogr. 28, 768–773.

van Oosterom, A.T., ten Bokkel Huinink, W.W., van der Burg, M.E., Vermorken, J.B., Willemse, P.H., Neijt, J.P., 1991. Phase II clinical trial of doxifluridine in patients with advanced ovarian cancer. Eur. J. Cancer 27, 747–749.

Ward, R.J., de Azevedo, W.F., Arni, R.K., 1998. At the interface: crystal structures of phospholipases A2. Toxicon 36, 1623–1633.

Watanabe, L., Soares, A.M., Ward, R.J., Fontes, M.R., Arni, R.K., 2005. Structural insights for fatty acid binding in a Lys49-phospholipase A2: crystal structure of myotoxin II from Bothrops moojeni complexed with stearic acid. Biochimie 87, 161–167.

Williamson, J., Desowitz, R.S., 1956. Prophylacticactivity of suramin complexes in animal trypanosomiasis. Nature 177, 1074–1075.

Please cite this article as: Murakami, M.T., et al., Interfacial surface charge and free accessibility to the PLA_2-active site-like region are essential requirements for the activity of Lys49 PLA_2.... Toxicon (2006), doi:10.1016/j.toxicon.2006.10.011

c. Termoestabilidade de Proteínas

A maioria das formas vivas na terra suportam temperaturas menores a 50ºC e, acima dessa temperatura, a energia térmica pode causar o desenovelamento da estrutura nativa das proteínas de forma irreversível, resultando na perda de suas funções biológicas. Entretanto, certos organismos termofílicos podem suportar temperaturas superiores a 90ºC e suas proteínas apresentam diferentes estratégias para garantir resistência térmica sem sofrer alteração na sua funcionalidade. Técnicas *in vitro* são extensivamente usadas para gerar proteínas termoestáveis através de adição de pontes salinas, pontes dissulfeto e ligações de hidrogênio permitindo delinear os determinantes estruturais da termoestabilidade e os mecanismos envolvidos em catálises a altas temperaturas. Estudos espectroscópicos e bioquímicos combinados com métodos cristalográficos podem fornecer informações essenciais para compreensão da termoestabilidade de proteínas. As enzimas termofílicas têm grande importância industrial, principalmente no ramo de branqueamento de papel e indústrias alimentícias.

Neste trabalho foram estudadas as xilanases da família G/11 que são excelentes modelos de estudo da termoestabilidade, pois apresenta alta variação na termoestabilidade e termofilicidade por meio de modificações locais num arcabouço estrutural altamente conservado (Figura 9). Técnicas de evolução molecular *in vitro* estão sendo utilizadas para gerar mutantes termoestáveis pelo grupo do Prof. Richard John Ward e estes foram caracterizadas por métodos cristalográficos, bioquímicos e espectroscópicos. Detalhes desse trabalho são apresentados nos artigos a seguir.

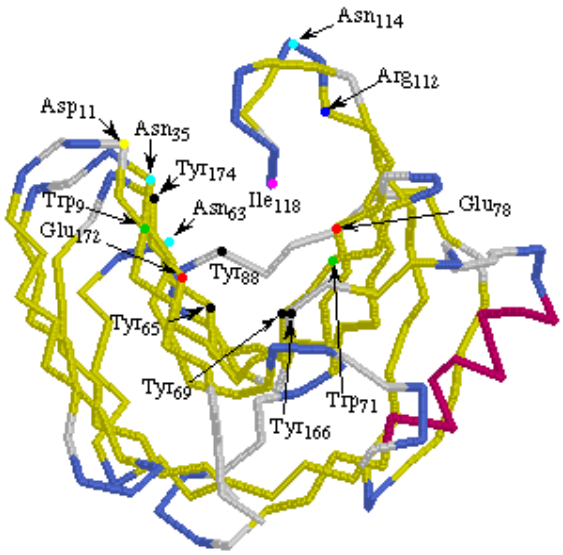

Figura 9: Representação esquemática da estrutura de uma xilanase G/11 com setas indicando os resíduos relevantes para a atividade catalítica.

Acta Crystallographica Section F
Structural Biology and Crystallization Communications
ISSN 1744-3091

Crystallization and preliminary X-ray crystallographic studies of the mesophilic xylanase A from *Bacillus subtilis* 1A1

M. T. Murakami,[a] R. Ruller,[b] R. J. Ward[b] and R. K. Arni[a]*

[a]Department of Physics, IBILCE/UNESP, Cristovao Colombo 2265, 15054-000 Sao Jose do Rio Preto, Sao Paulo, Brazil, and [b]Department of Chemistry, Avenida do Cafe 1544, USP, Ribeirao Preto, Sao Paulo, Brazil

Correspondence e-mail: arni@df.ibilce.unesp.br

Received 29 October 2004
Accepted 10 January 2005
Online 20 January 2005

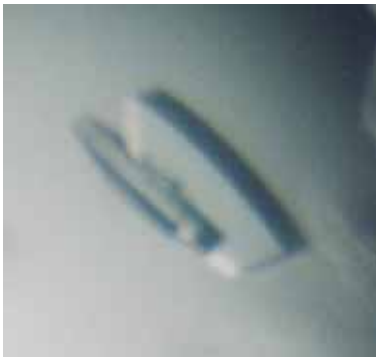

Xylanases have been the focus of research owing to their industrial potential in animal feed production, food processing and pulp and paper processes. In order to obtain insight into the structural stability of family 11 xylanases, the mesophilic family 11 xylanase (β-1,4-xylan xylanohydrolase; EC 3.2.1.8) from *Bacillus subtilis* 1A1 has been crystallized and diffraction data have been collected to 1.7 Å. The crystals belong to the orthorhombic space group $P2_12_12$, with unit-cell parameters $a = 50.93$, $b = 70.50$, $c = 40.05$ Å. The structure has been determined by molecular replacement, resulting in a crystallographic residual of 36.4% after rigid-body refinement.

1. Introduction

Xylanases (β-1,4-xylan xylanohydrolases; EC 3.2.1.8) cleave the β-1,4-xylosidic linkages of xylans and are of interest to the animal-feed, food-processing, and pulp and paper industries, where the use of xylanase has been found to be effective in reducing chlorine-dosage requirements in the Kraft pulp-bleaching process. Because of the industrial potential of these enzymes, a large number of bacterial and fungal xylanase genes have been isolated, sequenced and expressed as heterologous proteins.

On the basis of amino-acid sequence similarities, xylanases are classified into glycosyl hydrolase families 10 and 11 (Henrissat, 1991). The family 10 enzymes have an $(\alpha/\beta)_8$-barrel fold with a molecular weight of approximately 35 kDa. Family 11 xylanases are somewhat smaller, approximately 20 kDa, and their fold contains an α-helix and two β-sheets packed against each other, forming a so-called β-sandwich. Family 11 xylanases have been well studied because of their direct use in bio-bleaching in the paper industry (Gilkes *et al.*, 1991; Henrissat & Bairoch, 1993; Wakarchuk, Sung *et al.*, 1994; Törrönen *et al.*, 1994; Gruber *et al.*, 1998; McCarthy *et al.*, 2000; Wouters *et al.*, 2001; Oakley *et al.*, 2003; Moiseeva & Allaire, 2004), especially the mesophilic xylanases expressed by *Bacillus circulans* (PDB code 1xnb) and *Trichoderma longibrachiatum* (PDB codes 1enx and 1xyn). These enzymes are gaining importance since they serve as model enzymes for investigating protein folding, thermal stability, pH stability, enantiospecificity and stereospecificity (Wakarchuk, Campbell *et al.*, 1994; Törrönen & Rouvinen, 1995; Krengel & Dijkstra, 1996; Törrönen & Rouvinen, 1997; Fushinobu *et al.*, 1998; Sabini *et al.*, 1999). We present the results of the crystallization, data collection to 1.7 Å and initial structure determination of the mesophilic family 11 xylanase from *B. subtilis*. Comparative studies of this data and thermostable mutants generated by *in vitro* molecular evolution will be employed to obtain insight as to the structural basis of the thermostability of family 11 xylanases.

2. Methods

2.1. Dynamic light scattering and crystallization

Recombinant family 11 xylanase from *B. subtilis* strain 1A1 was expressed in *Escherichia coli* DH5α and purified from culture supernatants by cation-exchange chromatography as described elsewhere (Ruller *et al.*, 2005). Dynamic light-scattering experiments were carried out at 293 K using a DynaPro 810 (Protein Solutions Co.) equipped with a temperature stabilizer. A 3.4 mg ml^{-1} protein solution was prepared in 20 m*M* HEPES buffer pH 7.5. Standard

curves of bovine serum albumin were used for calibration and the experiments were conducted at 291 K. For crystallization, the protein was dialyzed and concentrated to 4.5 mg ml^{-1} against 20 m*M* HEPES pH 7.5. The protein was crystallized by the hanging-drop vapour-diffusion method at 291 K. HR2-110 and HR2-112 screens (Hampton Research) were used initially. Irregular and highly twinned crystals were obtained after 3 d in 2 µl droplets (1 µl protein solution and 1 µl reservoir solution) which contained 0.9 *M* potassium sodium tartrate tetrahydrate (Fig. 1*a*). Crystals suitable for X-ray diffraction were obtained using the same conditions upon addition of 1%(*v*/*v*) dioxane, a reagent commonly used to overcome twinning (Bergfors, 1999) (Fig. 1*b*).

2.2. X-ray diffraction analysis

X-ray diffraction data were collected at the CPr beamline of the synchrotron source at the Laboratório Nacional de Luz Síncrotron, Brazil. A single crystal with a maximum dimension of 0.3 mm was soaked in mother liquor containing 25% glycerol and flash-frozen at 100 K. The diffraction data were processed with *DENZO* and scaled with *SCALEPACK* (Otwinowski & Minor, 1997) to a resolution of 1.7 Å. Molecular replacement was carried out using the program *AMoRe* (Navaza, 1994) and a model based on the atomic coordinates of the xylanase from *B. circulans* (PDB code 1hv0).

3. Results

The structural homogeneity of the xylanase from *B. subtilis* in solution was verified by dynamic light scattering, which demonstrated a monomodal distribution with a hydrodynamic radius of 1.7 nm, corresponding to a molecular weight of 22 kDa. Suitable crystals for X-ray diffraction analysis with a maximum dimension of 0.3 mm (Fig. 1*b*) were obtained in the presence of 1%(*v*/*v*) dioxane and diffraction data were collected to 1.7 Å at cryogenic temperature (100 K). The diffraction data were indexed in the orthorhombic space group $P2_12_12$, with unit-cell parameters a = 50.93, b = 70.50, c = 40.05 Å. Processing the 21 487 measured reflections to 1.7 Å resulted in a data set containing 14 449 unique reflections, with an $R_{\rm merge}$ of 9.2% (26.9% in the last shell) and a completeness of 83.5% (81.3% in the last shell). The Merohedral Crystal Twinning Server (Yeates, 1997) clearly indicated that the data were not twinned ($\langle I^2\rangle/\langle I\rangle^2 > 1.95$ in all resolution shells). Data-processing statistics are summarized in Table 1.

Assuming a molecular weight of 20.38 kDa, calculation of the Matthews coefficient resulted in a $V_{\rm M}$ value of 1.7 Å^3 Da^{-1} for the presence of one molecule in the asymmetric unit, corresponding to a solvent content of 27.7% (Matthews, 1968). Molecular replacement was carried out using the program *AMoRe* (Navaza, 1994) and the atomic coordinates of a xylanase from *B. circulans* (PDB code 1hv0). A unique rotation and translation solution was obtained for the single molecule in the asymmetric unit. Rigid-body refinement of the solution using data in the resolution range 41.9–1.7 Å resulted in a correlation coefficient of 65.4% and an *R* factor of 36.4% (Table 1). The structure of the xylanase A from *B. subtilis* 1A1 contains an α-helix and two β-sheets packed against each other, indicating that it belongs to the β-sandwich class of proteins.

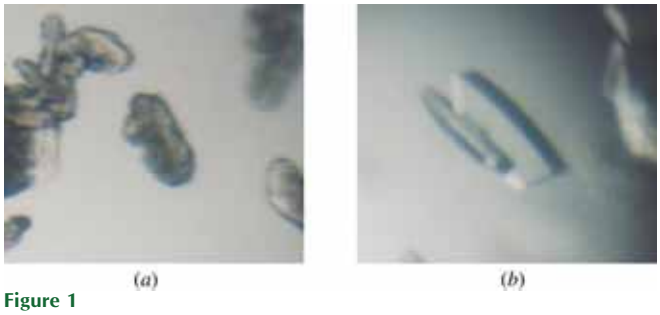

Figure 1
Photomicrographs of crystals of mesophilic xylanase A from *B. subtilis* (*a*) in the absence and (*b*) in the presence of 1%(*v*/*v*) dioxane.

Table 1
Data-collection and structure-determination statistics for *B. subtilis* xylanase A.

Values in parentheses are for the high-resolution bin.

Data collection	
Synchrotron-radiation source	LNLS Brazil, beamline CPr
Temperature (K)	100
Wavelength used (Å)	1.427
Detector	MAR CCD
Space group	$P2_12_12$
Unit-cell parameters (Å)	a = 50.93, b = 70.50, c = 40.05
Resolution range (Å)	41.9–1.7
No. observed reflections	21487 (1850)
Data completeness (%)	83.5 (81.3)
No. unique reflections	14449 (1364)
$I/\sigma(I)$	7.16 (2.5)
$R_{\rm merge}$† (%)	9.2 (26.9)
Molecules per asymmetric unit	1
Molecular replacement	
Correlation coefficients (%)	
Rotation	33.7
Translation	52.3
Rigid-body refinement	65.4
Rigid-body refinement *R* factor (%)	36.4

† $R_{\rm merge} = \sum|I(h)_i - \langle I(h)\rangle|/\sum\langle I(h)\rangle$, where $I(h)_i$ is the observed intensity of the ith measurement of reflection h and $\langle I(h)\rangle$ is the mean intensity of reflection h calculated after scaling.

This study was supported by FAPESP, SMOLBNet, CAPES/DAAD and CNPq. We are grateful to Dr J. Medrano and the staff at LNLS-Campinas (Brazil) for expert assistance.

References

Bergfors, T. M. (1999). Editor. *Protein Crystallization*, p. 245. La Jolla, CA, USA: International University Line.
Fushinobu, S., Ito, K., Konno, M., Wakagi, T. & Matsuzawa, H. (1998). *Protein Eng.* **11**, 1121–1128.
Gilkes, N. R., Henrissat, B., Kilburn, D. G., Miller, R. C. Jr & Warren, R. A. J. (1991). *Microbiol. Rev.* **55**, 303–515.
Gruber, K., Klintschar, G., Hayn, M., Schlacher, A., Steiner, W. & Kratky, C. (1998). *Biochemistry*, **37**, 13475–13485.
Henrissat, B. (1991). *Biochem. J.* **280**, 309–316.
Henrissat, B. & Bairoch, A. (1993). *Biochem. J.* **293**, 781–788.
Krengel, U. & Dijkstra, B. W. (1996). *J. Mol. Biol.* **263**, 70–78.
McCarthy, A. A., Morris, D. D., Bergquist, P. L. & Baker, E. N. (2000). *Acta Cryst.* D**56**, 1367–1375.
Matthews, B. W. (1968). *J. Mol. Biol.* **33**, 491– 497.
Moiseeva, N. & Allaire, M. (2004). *Acta Cryst.* D**60**, 1275–1277.
Navaza, J. (1994). *Acta Cryst.* A**50**, 157–163.
Oakley, A., Heinrich, T., Thompson, C. & Wilce, M. (2003). *Acta Cryst.* D**59**, 627–636.
Otwinowski, Z. & Minor, W. (1997). *Methods Enzymol.* **276**, 307–326.
Ruller, R., Rosa, J. C., Faça, V. M., Greene, L. J. & Ward, R. J. (2005). Submitted.
Sabini, E., Sulzenbacher, G., Dauter, M., Dauter, Z., Jorgensen, P. L., Schulein, M., Dupont, C., Davies, G. J. & Wilson, K. S. (1999). *Chem. Biol.* **6**, 483–492.
Törrönen, A., Harkki, A. & Rouvinen, J. (1994). *EMBO J.* **13**, 2493–2501.
Törrönen, A. & Rouvinen, J. (1995). *Biochemistry* **34**, 847–856.
Törrönen, A. & Rouvinen, J. (1997). *J. Biotechnol.* **57**, 137–149.
Wakarchuk, W. W., Campbell, R. L., Sung, W. L., Davoodi, J. & Yaguchi, M. (1994). *Protein Sci.* **3**, 467–475.
Wakarchuk, W. W., Sung, W. L., Campbell, R. L., Cunningham, A., Watson, D. C. & Yaguchi, M. (1994). *Protein Eng.* **7**, 1379–1386.
Wouters, J., Georis, J., Engher, D., Vandenhaute, J., Dusart, J., Frere, J. M., Depiereux, E. & Charlier, P. (2001). *Acta Cryst.* D**57**, 1813–1819.
Yeates, T. O. (1997). *Methods Enzymol.* **276**, 344–358.

FEBS 30131 FEBS Letters 579 (2005) 6505–6510

Correlation of temperature induced conformation change with optimum catalytic activity in the recombinant G/11 xylanase A from *Bacillus subtilis* strain 168 (1A1)

Mário T. Murakami[a], Raghuvir K. Arni *,[a], Davi S. Vieira[c], Léo Degrève *,[c], Roberto Ruller[b], Richard J. Ward[c,*]

[a] *Department of Physics, IBILCE/UNESP, Cristovão Colombo 2265, São José do Rio Preto, São Paulo, Brazil*
[b] *Department of Cellular and Molecular Biology, FMRP, Universidade de São Paulo, Avenida Bandeirantes 3900, Ribeirão Preto, São Paulo, Brazil*
[c] *Department of Chemistry, FFCLRP, Universidade de São Paulo, Avenida Bandeirantes 3900, Ribeirão Preto, São Paulo, Brazil*

Received 9 September 2005; revised 30 September 2005; accepted 19 October 2005

Available online 2 November 2005

Edited by Miguel De la Rosa

Abstract The 1.7 Å resolution crystal structure of recombinant family G/11 β-1,4-xylanase (rXynA) from *Bacillus subtilis* 1A1 shows a jellyroll fold in which two curved β-sheets form the active-site and substrate-binding cleft. The onset of thermal denaturation of rXynA occurs at 328 K, in excellent agreement with the optimum catalytic temperature. Molecular dynamics simulations at temperatures of 298–328 K demonstrate that below the optimum temperature the thumb loop and palm domain adopt a closed conformation. However, at 328 K these two domains separate facilitating substrate access to the active-site pocket, thereby accounting for the optimum catalytic temperature of the rXynA.

Keywords: Thermostable enzyme; Crystal structure; Molecular dynamics

1. Introduction

Xylan is the most abundant hemicellulose in plant cell walls, and is comprised of a β-(1,4)-D-xylopyranoside backbone which is generally substituted by acetyl, arabinose and 4-*O*-methyl-glucuronose residues. A wide variety of microorganisms produce xylan-degrading enzymes, and the enzymatic cleavage of β-1,4-xylosidic linkages is performed by β-1,4-xylan xylanohydrolase (EC 3.2.1.8). Xylanases have been grouped into families F/10 and G/11 on the basis of amino acid sequence homology, hydrophobic cluster and three-dimensional structural analysis [1]. The structures of the family G/11 xylanases contain an α-helix and two twisted β-sheets forming a jellyroll fold [2,3], yet despite the high similarity of amino acid sequences and structural homology, the G/11 xylanases exhibit a wide range of temperature optima of catalytic activity.

A common approach to address the question as to the structural basis of thermostability uses the comparison between the crystal structures of mesophilic and thermophilic homologues. Superposition of the crystal structures of thermostable xylanases from *Thermoanaerobacterium saccharoclyticum* [4] and *Clostridium thermocellum* [5] reveals that an N-terminal extension forms an additional β-strand that increases the number of hydrogen bonds in the β-sandwich finger domain, and has led to the suggestion that the N-terminal regions of these enzymes contribute to their thermostability. Hydrophobic interactions and salt bridges have also been suggested to be important structural features for thermostability [6,7]. The hydrophobic core of G/11 xylanases extends along the entire length of the internal surface of the β-sandwich and is rich in highly conserved tyrosine and tryptophan residues, and indeed the thermostability of family G/11 xylanases has been improved through the introduction of aromatic interactions by site-directed mutagenesis [7]. Salt bridges are distributed over the whole surface of the protein, and mutagenesis of His149 (located on the opposite side of the active site) to Phe or Gln did not modify the catalytic activity, but significantly improved the thermal stability [8]. Furthermore, the thermostability of family G/11 xylanases has been improved by the inclusion of additional surface charges [9], arginine residues [10] and disulphide bonds [11,12].

Several experimental approaches have been used to improve the thermostability and thermophilicity of xylanases including chemical modification, cross-linking, immobilization, treatment with additives and protein engineering [13], and the results of these studies suggest that multiple factors may contribute to the structural basis of thermostability. In an effort to identify the structural basis of thermostability, we have focused on understanding the structural changes in the G/11 xylanases at various temperatures leading up to the optimum temperature for catalysis. With the aim of identifying and delineating the structural basis for the catalytic activity at elevated temperature of these industrially relevant enzymes, we report the crystal structure at 1.7 Å resolution and molecular dynamics studies in the range of temperature of a recombinant thermophilic family G/11 xylanase from *Bacillus subtilis* 1A1 (rXynA).

2. Materials and methods

2.1. Expression, purification, crystallization and data collection

The gene encoding XynA was expressed in *Escherichia coli* strain DH5α and the recovered protein was purified as described previously [14]. The expression system yields 26 mg L^{-1} of culture of

*Corresponding authors. Fax: +55 0 16 36338151.
E-mail address: rjward@fmrp.usp.br (R.J. Ward).

Abbreviations: rXynA, recombinant family G/11 β-1,4-xylan xylanohydrolase from *Bacillus subtilis* strain 1A1; RMSD, root mean square deviation

0014-5793/$30.00
doi:10.1016/j.febslet.2005.10.039

protein (7.7% total yield), and N-terminal sequencing and mass-spectrometry have confirmed that the signal peptide has been correctly processed to give as the final product the expected 185 amino acid protein [14]. Crystals suitable for X-ray diffraction experiments were obtained from 2 μL droplets containing 2.8 mg mL^{-1} of protein, 1.2 M sodium tartrate and 1% dioxane [15]. The data were collected to 1.7 Å using synchrotron radiation and a MARCCD detector at the CPr beam line, LNLS (Laboratorio Nacional de Luz Sincrotron, Campinas, Brazil). Intensity data were integrated, scaled and reduced to obtain structure factor amplitudes with the HKL package [16].

2.2. Structure solution and refinement

The crystal structure of the rXynA was solved by molecular replacement techniques with the AMoRe package [17] using the atomic coordinates of the G/11 xylanase from *Bacillus circulans* (PDB code 1XNB, [18]) as the search model. Positional and individual isotropic thermal factor refinements were carried out using REFMAC5 [19] as incorporated in the CCP4 suite (Collaborative Computational Project Number 4, 1994). The $2F_{ob} - F_c$ and $F_{ob} - F_c$ electron density maps were examined and the protein model was manually adjusted after each refinement cycle using the TURBO FRODO program [20]. The stereochemistry of the final model was analyzed using PROCHECK [21]. The atomic coordinates and structure factors of XynA have been deposited with the Protein Data Bank (code: 1XXN).

2.3. Thermal denaturation monitored by circular dichroism

Thermal denaturation experiments were performed using a J-810 spectropolarimeter equipped with a Peltier-type temperature controller (PTC423S-JASCO Inc., Tokyo, Japan) with a heating rate of 1 °C min^{-1} using 1 cm path-length cuvettes and a protein concentration of 100 μg mL^{-1} in 20 mM phosphate buffer at pH 6.0. The change in the ellipticity signal at 216 nm was monitored over the temperature range of 25–75 °C (298–348 K). The fitting of the thermal denaturation curve assumed a two-state mechanism and used a least squares fitting routine derived from the van't Hoff equation as described previously [22,23].

2.4. Sequence alignment and structural analysis

The alignment of 5 amino acid sequences from the corresponding 3D structures was performed by structure-based alignment utilizing the 3D-coffee alignment tool [24]. The superpositioning and structural analysis was performed by TURBO FRODO program [20] and the ConSurf program was used for the identification of functional regions by surface-mapping using phylogenetic data [25].

2.5. Molecular dynamics simulations

Molecular dynamics calculations were performed as isothermal–isobaric ensemble under physiological conditions at temperatures of 298, 308, 318 and 328 K. All molecular dynamics simulations were run with the GROMACS 3.2 software package [26] using the GROMOS-96 (43a1) force field [27]. The temperature and pressure were controlled using the Berendsen method [28] with coupling time constants of 0.1 and 3.0 ps for temperature and pressure, respectively. The LINCS algorithm [29] was used to constrain protein covalent bonds involving hydrogen atoms, and the SETTLE algorithm [30] was used to constrain water molecules. The "leap-frog" algorithm [31] was used to integrate the equations of motion with a time step of 2.0 fs over a total time of 5.0 ns. Initial velocities were obtained from a Maxwell distribution at 298 K, and long-range interactions were treated using the particle-mesh Ewald sum (PME) method [32] with a cutoff of 1.5 nm. The long-range electrostatic contributions were updated every 20 fs, and the van der Waals interactions were calculated with a cutoff of 1.5 nm. The edges of the cubic simulation boxes were initially fixed at 8.5 nm, and contained about 19000 simple-point charge (SPC) water molecules [33] (concentration of ~53.0 mol L^{-1}). The Cl^- and Na^+ counter-ions were inserted in the most electrostatically favorable positions in order to locally neutralize the system. All simulations were equilibrated for 100 ps restraining the positions of the protein atoms. The atomic trajectories were analyzed by monitoring the peptide and residue root mean square deviation (RMSDs) of atomic positions relative to the crystal structure.

3. Results and discussion

3.1. Crystal structure

Crystals of rXynA were obtained as previously described [15], and belong to the orthorhombic space group $P2_12_12$ with cell parameters $a = 50.90$, $b = 70.37$ and $c = 42.04$ Å. The Matthews coefficient ($V_m = 1.68$ Å^3 Da^{-1}) indicates the presence of one molecule per asymmetric unit with a corresponding solvent content of 26.15%. Table 1 presents the full refinement statistics of the final model, which shows that rigid-body model refinement using data in the resolution range of 20.0–2.5 Å resulted in a correlation coefficient of 65.4% and a R_{factor} of 36.4%. Structure refinement converged to a crystallographic residual of 16.2% for all data between 42.03 and 1.75 Å (without sigma or intensity cutoff, $R_{free} = 20.9\%$ for 5% of the data). The refined structural model of the rXynA contains 185 amino acid residues, 1 tartrate molecule, and 112 solvent water molecules per asymmetric unit. Stereochemical analysis of the final model indicates that the main-chain dihedral angles for all residues are located in the permitted regions of the Ramachandran diagram, and that the RMSD from ideal values are within permitted ranges. Residual electron density was observed at the surface of the molecule, and was attributed to a single tartrate molecule which is hydrogen bonded by Thr106, Gln135, Ser136, and two solvent water molecules, and forms additional hydrogen bonds with the Ser74 in a symmetry equivalent protein molecule.

Fig. 1A shows that the rXynA has the canonical β-sandwich 'right-hand' fold of family G/11 xylanases, in which the individual β-strands thread back and forth between the two packed β-sheets to form the finger and palm domains. Resi-

Table 1
Data collection and refinement statistics

Data collection	
Temperature (K)	100
Wavelength used (Å)	1.427
Detector	MARCCD
Space group	P2(1)2(1)2
Unit cell parameters (Å)	$a = 50.90$, $b = 70.37$ and $c = 42.04$
Resolution range (Å)	42.03–1.70
No. of observed reflections	21487
Data completeness (%)	83.5 (81.3)
No. of unique reflections	14449
I/sigma(I)	7.16 (2.5)
[a]R_{merge} (%)	9.2 (26.9)
V_M (Å^3 Da^{-1})	1.68
Solvent content (%)	26.15
Molecules per asymmetric unit	1
Molecular replacement	
Correlation coefficients (%)	
Rotation	33.7
Translation	52.3
Rigid body refinement	65.4
Rigid body refinement R-factor (%)	36.4
Refinement	
R_{factor} (%)	16.2
R_{free} (%)	20.9
RMSD bond distances (Å)	0.01
RMSD bond angles (°)	1.42
Average B_{factor} (Å^2)	23.1

Values in parentheses are for the high-resolution bin.
[a]$R_{merge} = \Sigma|I(h)_I - \{I(h)\}|/\Sigma\{I(h)\}$, where I_h is the observed intensity of the ith measurement of reflection h and $\{I(h)\}$ is the mean intensity of reflection h calculated after scaling.

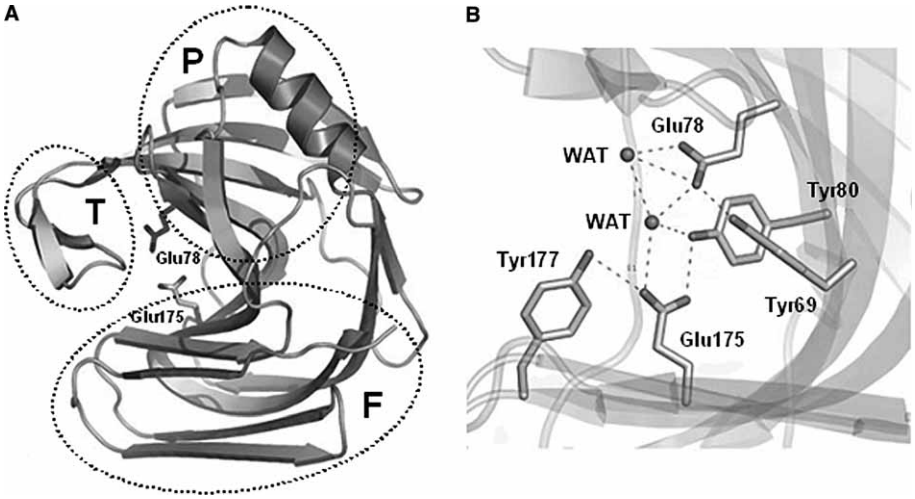

Fig. 1. The three-dimensional structure of the rXynA. (A) Ribbon representation including the catalytic residues Glu78 and Glu 172 located at the base of the cleft formed by the palm (P) and fingers (F) domains. Access to the active site cleft is determined by the position of the thumb (T) domain. (B) Detail of the active site region showing the network of hydrogen bonds formed by Tyr69, Glu78, Tyr80, Glu175, Tyr177 and the positionally conserved solvent water (WAT) molecules.

dues lining the cleft formed between these two domains contribute to the substrate binding and active sites of the protein. An extended loop between the B7 and B8 strands forms the so-called thumb domain, and a loop between the B6 and B9 strands forms a cord between the two β-sheet domains (Fig. 1A) [34]. The active site is defined by a network of hydrogen bonded residues including Glu78 and Glu175, two structurally conserved water molecules, and the neighboring Tyr69 and Tyr80 residues that are involved in substrate binding (Fig. 1B). A two-step acid–base mechanism for xylan hydrolysis has been proposed in which proton transfer occurs to and from an oxygen atom in an equatorial position at the anomeric center [35]. All the positions of the catalytic residues involved in this mechanism are fully conserved in the rXynA crystal structure.

3.2. Thermostability of the rXynA

Previous studies have shown that the profile of the far ultraviolet circular dichroism spectra shows a minimum at 216 nm [14], which is typical for β-sheet rich proteins and is in accord with the secondary structure content observed in the crystal structure. Fig. 2 presents the thermal denaturation curve of the rXynA as monitored by the loss of secondary structure measured at 216 nm, which reveals that the transition from the native to the denatured enzyme starts at a temperature of 328 K. Previous results have demonstrated that the rXynA has an optimum temperature for catalysis of 55 °C (328 K) [14], which corresponds exactly to the maximum temperature at which the rXynA maintains a native secondary structure. At temperatures above this value both the catalytic activity and β-sheet secondary structure are lost. With the aim of understanding the structural basis of the thermostability of this protein, a series of molecular dynamics simulations were performed at four temperatures between 298 and 328 K.

3.3. Molecular dynamics

The atomic trajectories of rXynA were analyzed by monitoring the RMSD of protein atom positions and the mean RMSD

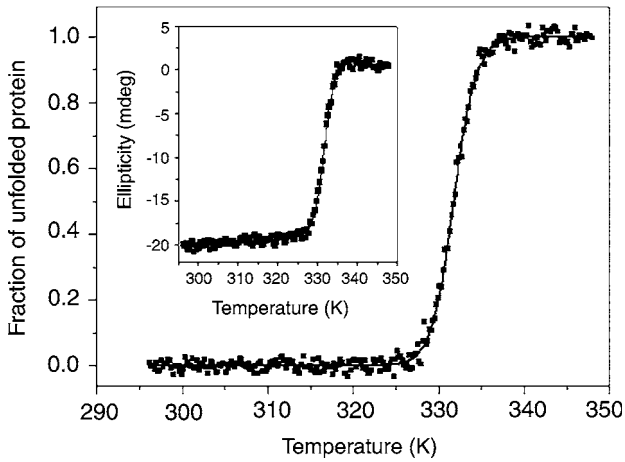

Fig. 2. Thermal denaturation of the rXynA as monitored by the change in circular dichroism in the ultraviolet region between 200 and 250 nm. The fraction of unfolded protein as a function of temperature (main panel). The inset presents the raw ellipticity data at 216 nm measured during the experiment (for clarity only half the total number of data points are presented). In both the main panel and insert, the solid lines represent the curves obtained after data fitting (see Section 2), which yielded a melting temperature (T_m) of 331.8 K.

per residue during a time period of 5 ns during the molecular dynamics calculations in the isothermal–isobaric ensemble under physiological conditions at 298, 308, 318 and 328 K. Fig. 3 shows the RMSD of rXynA at different temperatures, from which mean RMSD values of 0.130 ± 0.016 nm (at 298 K), 0.148 ± 0.015 nm (308 K), 0.143 ± 0.014 nm (318 K) and 0.175 ± 0.030 nm (328 K) were calculated. These results demonstrate that the protein conformations are highly stable at all temperatures used in the simulations, an overview confirmed by the mean RMSD values per residue at the different temperatures (Fig. 4). Mean RMSD values of most positions in the palm domain (residues 41–50, 68–81, 93–110, 126–132 and 145–168), on which are located several active site and aromatic substrate-binding residues, demonstrate low deviations at all temperatures. The majority of positions in the finger do-

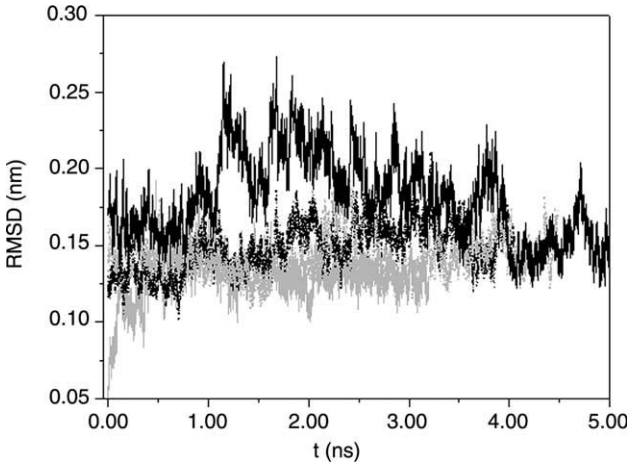

Fig. 3. RMSD of atomic positions in the molecular dynamics simulations of the rXynA at temperatures of 298 K (solid grey lines), 308 K (dotted black lines), 318 K (dotted grey lines) and 328 K (solid black lines). The positions of the protein atoms in the crystallographic structure were used as the reference for the RMSD calculations.

main (residues 1–40, 52–67, 83–87 and 169–185) also show reduced RMSD values, which suggests that the protein has a generally high stability even at 328 K. In contrast, many regions in the vicinity of glycine residues (including positions 10–15, 20–22, 26–28, 100–104, 118–124 and 135–140) show a higher mean RMSD per residue at all temperatures, which reflects the elevated mobility of the protein segments containing these residues.

The comparison of the rXynA amino acid sequence with four other G/11 xylanases (Fig. 5) reveals that many tyrosine (Tyr53, Tyr69, Tyr79, Tyr80, Tyr107, Tyr130 and Tyr169) and tryptophan residues (Trp9, Trp71 and Trp155) are highly conserved. These residues not only play a key role in substrate binding, but also contribute to the hydrophobic interactions that confer rigidity and compactness to the palm domain and active-site pocket. Other hydrophobic residues (Val37, Val82, Pro90, Ile120 and Phe125) are also conserved, and are likely to be important in the stability of the secondary and tertiary structures. Fig. 5 further demonstrates that the majority of glycine residues are also highly conserved, and occupy positions throughout the thumb and finger domains and in the cord/connecting loops of the two packed β-sheets. The flexibility of these glycine residues is generally elevated at all temperatures (see Fig. 4), although the regions around Gly12-Gly14, Gly23, Gly28 and Gly62 show no clear pattern of temperature dependent conformation change. In contrast, the region around Gly122 on the β-turn in the thumb domain presents a clear trend in which an increase in temperature results in significantly increased conformation change.

The thumb domain is highly conserved throughout the family G/11 xylanases, and comparison of crystal structures has suggested that the thumb loop is the most flexible region of the molecule [36]. This is supported by molecular dynamics simulations, and has led to the suggestion that the elevated flexibility of the thumb loop is important to allow substrate access to the active site residues [37]. The distance variations in the molecular dynamics simulations between these two domains are shown in Fig. 6, which reveals that the distance between the palm domain and thumb loop is around of 1.30 nm at temperatures below the catalytic temperature optimum. However, at the optimum catalytic temperature of 328 K, the distance between the palm and thumb domains increases to 1.65 nm, and the substrate-binding cleft adopts an open conformation. These distances are significantly greater than those observed in previous molecular dynamics simulation studies [37], and we speculate that the optimum temperature of catalytic activity is the consequence of the exposure of the active site cleft by temperature dependent conformation change in the thumb domain.

These results are in accord with previous NMR studies which demonstrate that the conformation changes of the xylanase A from *Bacillus circulans* on binding a substrate analogue are confined to the substrate binding region and are relatively slight, the exception being the significant conformation changes observed in the thumb domain [38]. Both the NMR study and the molecular dynamics simulation reported here

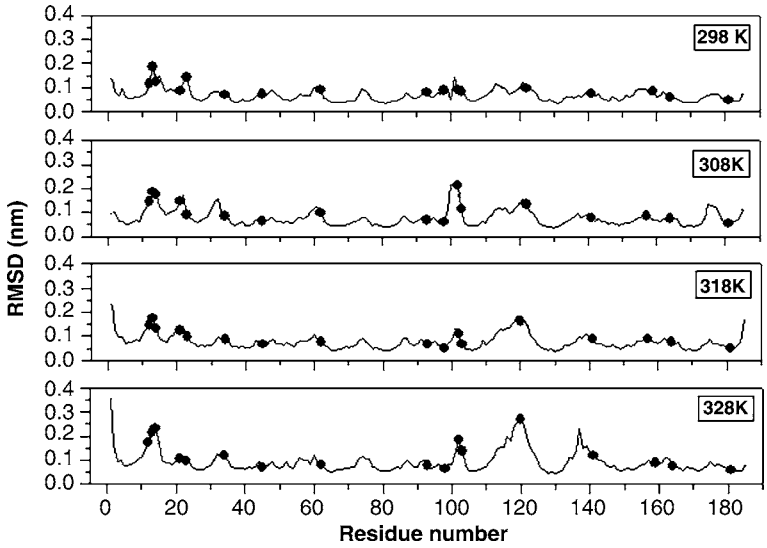

Fig. 4. RMSD per residue. The results of four separate simulations are presented, at temperatures between 298 and 328 K (as indicated on the figure). Conserved glycine residues at positions 12, 13, 14, 21, 23, 34, 45, 62, 93, 98, 104,105, 122, 159, 164 and 181 are indicated by the solid circles.

Fig. 5. Multiple amino acid sequence alignment of the rXynA (PDB code 1XXN) with other family G/11 xylanases. The sequences and corresponding PDB codes are; endoxylanase 11A from *Chaetomium thermophilum*, (1H1A, [39]), xylanase from *Paecilomyces varioti bainier* (1PVX, [40]), endo-1,4-β-xylanase from *Thermomyces lanuginosus*, (1YNA, [36]), and endoxylanase from *Nonomuraea flexuosa* (1M4W, [39]). The adopted numbering scheme starts at −10 so as to place the N-terminal alanine residue of rXynA at position 1. Glycine residues are shown with a grey background.

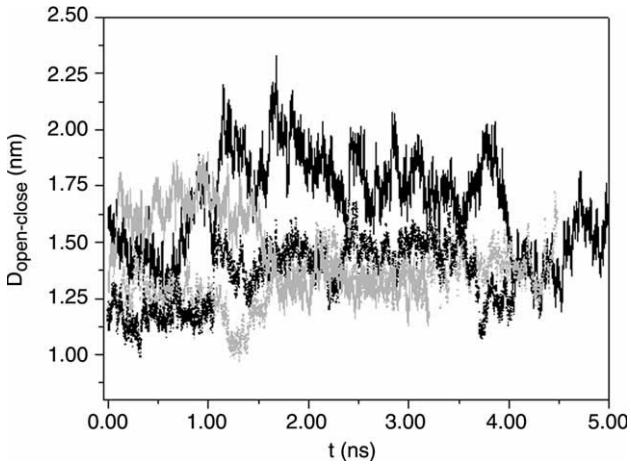

Fig. 6. Variation in the distance between the thumb and palm domains during the molecular dynamics simulations of the rXynA at temperatures of 298 K (solid grey lines), 308 K (dotted black lines), 318 K (dotted grey lines) and 328 K (solid black lines).

indicate that the palm and finger domains are essentially rigid structures, and the enhanced flexibility necessary for catalysis lies in those segments in the immediate vicinity of glycine residues. This conclusion focuses attention on the temperature dependence of the conformation change in the thumb domain, which is identified as a key event in determining the optimum catalytic temperature of the enzyme. This work suggests that site-directed mutagenesis studies with the aim of decreasing the flexibility in this region may offer an alternative strategy for rational design of thermostable xylanases.

Acknowledgements: This work was funded by FAPESP doctorate fellowships 01/08012-0 (R.R.), 03/13082-3 (M.T.M.), 03/01457-2 (DSV), FAPESP SMOLBnet project 01/7537-2, CNPq and the Pro-Reitoria de Pesquisa-USP (PRP-USP).

References

[1] Coutinho, P.M. and Henrissat, B. (1999). Available from: <http://afmb.cnrs-mrs.fr/CAZY/>.
[2] Henrissat, B. and Davies, G. (1997) Structural and sequence-based classification of glycoside hydrolases. Curr. Opin. Struct. Biol. 7, 637–644.
[3] Henrissat, B. and Davies, G.J. (2000) Glycoside hydrolases and glycosyltransferases. Families, modules, and implications for genomics. Plant Physiol. 124, 1515–1519.
[4] Lee, Y.E., Lowe, S.E., Henrissat, B. and Zeikus, J.G. (1993) Characterization of the active site and thermostability regions of endoxylanase from *Thermoanaerobacterium saccharolyticum* B6A-RI. J. Bacteriol. 175, 5890–5898.
[5] Fontes, C.M., Hazlewood, G.P., Morag, E., Hall, J., Hirst, B.H. and Gilbert, H.J. (1995) Evidence for a general role for non-catalytic thermostabilizing domains in xylanases from thermophilic bacteria. Biochem. J. 307 (Pt 1), 151–158.
[6] Eriksson, A.E., Baase, W.A., Zhang, X.J., Heinz, D.W., Blaber, M., Baldwin, E.P. and Matthews, B.W. (1992) Response of a protein structure to cavity-creating mutations and its relation to the hydrophobic effect. Science 255, 178–183.
[7] Georis, J., de Lemos Esteves, F., Lamotte-Brasseur, J., Bougnet, V., Devreese, B., Giannotta, F., Granier, B. and Frere, J.M. (2000) An additional aromatic interaction improves the thermostability and thermophilicity of a mesophilic family 11 xylanase: structural basis and molecular study. Protein Sci. 9, 466–475.
[8] Plesniak, L.A., Connelly, G.P., Wakarchuk, W.W. and McIntosh, L.P. (1996) Characterization of a buried neutral histidine residue in *Bacillus circulans* xylanase: NMR assignments, pH titration, and hydrogen exchange. Protein Sci. 5, 2319–2328.

[9] Torronen, A. and Rouvinen, J. (1997) Structural and functional properties of low molecular weight endo-1,4-beta-xylanases. J. Biotechnol. 57, 137–149.
[10] Turunen, O., Vuorio, M., Fenel, F. and Leisola, M. (2002) Engineering of multiple arginines into the Ser/Thr surface of *Trichoderma reesei* endo-1,4-beta-xylanase II increases the thermotolerance and shifts the pH optimum towards alkaline pH. Protein Eng. 15, 141–145.
[11] Wakarchuk, W.W., Sung, W.L., Campbell, R.L., Cunningham, A., Watson, D.C. and Yaguchi, M. (1994) Thermostabilization of the *Bacillus circulans* xylanase by the introduction of disulfide bonds. Protein Eng. 7, 1379–1386.
[12] Andrews, S.R., Taylor, E.J., Pell, G., Vincent, F., Ducros, V.M., Davies, G.J., Lakey, J.H. and Gilbert, H.J. (2004) The use of forced protein evolution to investigate and improve stability of family 10 xylanases. The production of Ca^{2+}-independent stable xylanases. J. Biol. Chem. 279, 54369–54379.
[13] Gupta, M.N. (1991) Thermostabilization of proteins. Biotechnol. Appl. Biochem. 14, 1–11.
[14] Ruller, R., Rosa, J.C., Faca, V.M., Greene, L.J. and Ward, R.J. (2005). Efficient constitutive expression of *Bacillus subtilis* Xylanase A in *Escherichia coli* DH5alpha under the control of the Bacillus BsXA promotor. Biotechnol. Appl. Biochem., in press.
[15] Murakami, M.T., Ruller, R., Ward, R.J. and Arni, R.K. (2005) Crystallization and preliminary X-ray crystallographic studies of the mesophilic xylanase A from *Bacillus subtilis* 1A1. Acta Cryst. F61, 219–220.
[16] Otwinowski, Z. and Minor, W. (1997) Processing of X-ray diffraction data collected in oscillation mode. Meth. Enzymol. 276, 307–326.
[17] Navaza, J. (1994) AMoRe: an automated package for molecular replacement. Acta Crystallogr. A50, 157–163.
[18] Wakarchuk, W.W., Campbell, R.L., Sung, W.L., Davoodi, J. and Yaguchi, M. (1994) Mutational and crystallographic analyses of the active site residues of the Bacillus circulans xylanase. Protein Sci. 3, 467–475.
[19] Murshudov, G.N., Vagin, A.A. and Dodson, E.J. (1997) Refinement of macromolecular structures by the maximum-likelihood method. Acta Crystallog., 240–255.
[20] Jones, T.A. (1985) Interactive computer graphics: FRODO. Methods Enzymol. 115.
[21] Laskowski, R.A., MacArthur, M.W., Moss, D.S. and Thorton, J.M. (1993) PROCHECK: a program to check the stereochemical quality of protein structure. J. Appl. Crystallogr. 26.
[22] Sa, J.M., Chioato, L., Ferreira, T.L., De Oliveira, A.H., Ruller, R., Rosa, J.C., Greene, L.J. and Ward, R.J. (2004) Topology of the substrate-binding site of a Lys49-phospholipase A2 influences Ca^{2+}-independent membrane-damaging activity. Biochem. J. 382, 191–198.
[23] Yadav, S. and Ahmad, F. (2000) A new method for the determination of stability parameters of proteins from their heat-induced denaturation curves. Anal. Biochem. 283, 207–213.
[24] Poirot, O., Suhre, K., Abergel, C., O'Toole, E. and Notredame, C. (2004) 3DCoffee@igs: a web server for combining sequences and structures into a multiple sequence alignment. Nucleic Acids Res. 32, W37–W40.
[25] Glaser, F., Pupko, T., Paz, I., Bell, R.E., Bechor-Shental, D., Martz, E. and Ben-Tal, N. (2003) ConSurf: identification of functional regions in proteins by surface-mapping of phylogenetic information. Bioinformatics 19, 163–164.
[26] Lindahl, E., Hess, B. and van der Spoel, D. (2001) GROMACS 3.0: A package for molecular simulation and trajectory analysis. J. Mol. Mod. 7, 306–317.
[27] van Gunsteren, W.F., Billeter, S.R., Eising, A.A., Hünenberger, P.H., Krüger, P., Mark, A.E., Scott, W.R.P. and Tironi, I.G. (1996) Biomolecular Simulation: The GROMOS96 Manual and User Guide, Biomos, Groningen.
[28] Berendsen, H.J.C., Postma, J.P.M., DiNola, A. and Haak, J.R. (1984) Molecular dynamics with coupling to an external bath. J. Chem. Phys. 81, 3684–3690.
[29] Hess, B., Becker, H., Berendsen, H.J. and Fraaije, J.G.E.M. (1997) Lincs: a linear constraint solver for molecular simulations. J. Comp. Chem. 18, 1463–1472.
[30] Miyamoto, S. and Kollman, P.A. (1992) SETTLE: An analytical version of the SHAKE and RATTLE algorithm for rigid water models. J. Comp. Chem. 13, 952–962.
[31] Hockney, R.W. and Goel, S.P. (1974) Quiet high-resolution computer models of a plasma. J. Comp. Phys. 14, 148–158.
[32] Darden, T., York, D. and Pedersen, L. (1993) Particle mesh Ewald. An $N\log(N)$ method for Ewald sumsin large systems. J. Chem. Phys. 98, 10089–10092.
[33] Berendsen, H.J.C., Postma, J.P.M., van Gunsteren, W.F. and Hermans, J. (1981) Interactions models for water in relation to protein hydration, in: Intermolecular Forces (Pullman, B., Ed.), Reidel Publishing Company, Dordrecht.
[34] Torronen, A., Harkki, A. and Rouvinen, J. (1994) Three-dimensional structure of endo-1,4-beta-xylanase II from Trichoderma reesei: two conformational states in the active site. Embo J. 13, 2493–2501.
[35] Sinnot, M.L. (1990) Catalytic mechanisms of enzymic glycosyl transfer. Chem. Rev. 90, 1171–1202.
[36] Gruber, K., Klintschar, G., Hayn, M., Schlacher, A., Steiner, W. and Kratky, C. (1998) Thermophilic xylanase from *Thermomyces lanuginosus*: high-resolution X-ray structure and modeling studies. Biochemistry 37, 13475–13485.
[37] Muilu, J., Torronen, A., Perakyla, M. and Rouvinen, J. (1998) Functional conformational changes of endo-1,4-xylanase II from *Trichoderma reesei*: a molecular dynamics study. Proteins 31, 434–444.
[38] Connelly, G.P., Withers, S.G. and McIntosh, L.P. (2000) Analysis of the dynamic properties of *Bacillus circulans* xylanase upon formation of a covalent glycosyl-enzyme intermediate. Protein Sci. 9, 512–524.
[39] Hakulinen, N., Turunen, O., Janis, J., Leisola, M. and Rouvinen, J. (2003) Three-dimensional structures of thermophilic beta-1,4-xylanases from *Chaetomium thermophilum* and *Nonomuraea flexuosa*. Comparison of twelve xylanases in relation to their thermal stability. Eur. J. Biochem. 270, 1399–1412.
[40] Eswaramoorthy, S., Vithayathil, P.J. and Viswamitra, M.A. (1994) Crystallization and preliminary X-ray crystallographic studies of thermostable xylanase crystals isolated from *Paecilomyces varioti*. J. Mol. Biol. 243, 806–808.

3) Significância Bio-Funcional dos Resultados

Nesse trabalho, uma gama de técnicas foi aplicada na abordagem de distintos processos biológicos como sistema hemostático, danificação de membranas biológicas e termoestabilidade de proteínas.

A partir de estudos com proteínas que interferem na integridade de membranas biológicas, desvendou-se o mecanismo de ação da família de enzimas esfingomielinases D, resultado o qual pode servir como base para o desenvolvimento de um tratamento eficaz para acidentes aracnídeos do gênero *Loxosceles*, que ainda não existe. Na mesma área de disrupção de membranas biológicas, descobriu-se uma potente molécula anti-dermonecrótica a partir de estudos estruturais e fisiológicos, a qual potencialmente serviria como tratamento complementar/alternativo para acidentes ofídicos botrópicos, que tem uma ocorrência superior a 30 000 casos/ano somente no Brasil.

Na área de manutenção e regeneração do sistema hemostático, diversas proteínas que interferem em diferentes níveis, desde a coagulação até a fibrinólise, foram caracterizadas. Um novo sítio de reconhecimento de substratos macromoleculares do FXa foi estruturalmente delineado e representa um novo caminho para desenvolvimento racional de drogas anti-trombóticas. Um mecanismo alternativo de ativação de proteína C realizada pela protac®, que independe de trombomodulina um co-fator essencial na ativação fisiológica, foi elucidado e os estudos estruturais indicaram um possível fator duplo de cargas e carboidratos no reconhecimento, interação e ativação. A rápida ação de protac® vem sendo usada para diversos testes clínicos *in vivo* para quantificação de proteína S e C e testes funcionais de ambas.

Por último, os estudos com xilanases meso- e termofilicas, que servem como ótimo modelos de estudos dos determinantes estruturais da termoestabilidade, demonstraram um papel essencial da flexibilidade das xilanases na sua funcionalidade a altas temperaturas, ao contrário que se pensava, quanto maior a rigidez da molécula maior sua resistência ao stress termodinâmico e mecânico. No momento, métodos de evolução molecular *in vitro* combinados com métodos cristalográficos e dinâmica molecular estão sendo usadas para delinear as bases moleculares da termoestabilidade das xilanases família G/11.

4) Referências Bibliográficas

Bithell, T.C. (1998) Hematologia Clínica, first ed., pp. 615-654, Malone, N. York.

Colman, R.W., Marder, V.J., Salzman, E.W., Hirsh, J. (1994) Haemostasis and Thrombosis: Basic Principles and Clinical Practice, third ed., pp.3-16, Lippincott Company Philadelphia.

Dauter, Z., Dauter, M., Rajashankar, K.R. (2000) *Acta Crystallogr D Biol Crystallogr.* **56**, 232-237.

Gempeler-Messina, P. M., Volz, K., Bu¨hler, B., and Muller, C. (2001) *Haemostasis* **31**, 266–272.

Halkier, T. (1991) Mechanisms in Blood Coagulation, Fibrinolysis and the Complement System, first ed., pp. 129-160, Cambridge University Press, N. York.

Kisiel., W., Kondo, S., Smith, K. J., McMullen, B. A., and Smith, L. F. (1987) *J. Biol. Chem.* **262**, 12607–12613.

Lee, S., Lynch, K.R. (2005) *Biochem J.* **391**, 317-323.

Mann, K.G. (1999) *Thrombosis and Haemostasis* **82**, 165-174.

Marsh, N., and Williams, V. (2005) *Toxicon* **45**, 1171–1181.

Neurath, H. (1984) *Science* **224**,350-356.

Stanssens, P., Bergum, P.W., Gansemans, Y., Jespers, L., Laroche, Y., Huang, S., Maki, S., Messens, J., Lauwereys, M., Cappello, M., Hotez, P. J., Lasters, I., Vlasuk, G.P. (1996) *Proc. Natl. Acad. Sci. USA* **93**, 2149-2154.

Tu, A. T. (1991) Handbook of Natural Toxins, first ed., pp. 827–830, Marcel Dekker, New York.

Vargaftig, B.B., Prado-Franceschi, J., Chignard, M., Lefort, J., Marlas, G. (1980) *Eur. J. Pharmacol.* **68**, 451–464.

Yamazaki, Y., Matsunaga, Y., Nakano, Y., Morita, T. (2005) *J. Biol. Chem.* **280**, 29989-29992.

Zhang, Y., Wisner, A., Maroun, R. C., Choumet, V., Xiong, Y., and Bon, C. (1997) *J. Biol. Chem.* **272**, 20531–20537.

5) Adendos

a. Experiência

- Biologia estrutural
- ***Cristalografia de macromoléculas (especialidade)***
- Modelagem e docking molecular
- Simulação de dinâmica molecular
- SAXS

- Bioquímica & Biologia Molecular
- Expressão e purificação de proteínas
- Caracterização funcional e bioquímica de proteínas
- Técnicas espectroscópicas (UV-vísivel, CD,...)

b. Cursos de aprimoramento

Automatização da cristalização de proteínas. University of Hamburg / EMBL (Hamburgo, Alemanha). Sob orientação do Prof. Dr. Christian Betzel.

Faseamento de proteínas. IFSC/USP. Sob orientação do Prof. Dr. Igor Polikarpov e Prof. Dr. Ronaldo A. Nagem.

Expressão e purificação de proteínas. FMRP/USP. Sob orientação do Prof. Dr. Roy E. Larson.

Purificação e caracterização de toxinas. Instituto Butantan. Sob orientação da Dra. Ana Marisa Chudzinski-Tavassi.

Sequenciamento químico de proteínas. FMRP/USP. Sob orientação do Prof. Dr. Lewis Greene.

Expressão gênica e clonagem. FMRP/USP. Sob orientação do Prof. Dr. Vanderlei Rodrigues.

Enovelamento de proteínas por calorimetria e técnicas espectroscópicas. Curso de Verão do LNLS. Sob orientação do Prof. Dr. Carlos H. I. Ramos.

Purificação e cristalização de macromoléculas. IBILCE/UNESP. Sob orientação do Prof. Dr. Raghuvir Krishnaswamy Arni.

c. Doutorado sanduíche – EMBL/DESY – Alemanha

O doutorado-sanduíche foi realizado na Universidade de Hamburgo, nos trabalhos com expressão e purificação de proteínas, e no *European Molecular Biology Laboratory / Deutsches Elektronen-Synchrotron* (EMBL-DESY), nos experimentos de cristalização, coleta de dados e refinamento, sob orientação do Prof. Dr. Christian Betzel. Os experimentos de difração de raios X foram realizadas no HASYLAB (Hamburger Synchrotronstrahlungslabor) que é um complexo voltado para estudos em ciências da vida do síncrotron DESY.

No grupo do Prof. Christian Betzel tive a oportunidade de trabalhar com a última tecnologia na cristalização de macromoléculas, o qual dispunha de um laboratório unicamente voltado para cristalização contendo um robô de cristalização, robô de preparação de solução, espalhamento dinâmico de luz *in situ* e robô de caracterização de cristais, que automatiza completamente o trabalho de cristalização.

Um equipamento construído pelo grupo do Prof. Betzel, Spectro-Imager 501, completamente automatiza a análise de experimentos de cristalização e aquisição de imagens que permite analisar milhares de condições de cristalização. Esse sistema combina espalhamento dinâmico de luz *in situ* e análise de cristais com luz branca e ultravioleta que permite identificar e diferenciar cristais de sais com cristais de proteínas (figura 2). Antes desse equipamento, o método mais confiável de testar se um cristal era ou não de proteína, era a difração propriamente dita, que despendia muito tempo para otimização de condições muitas vezes duvidosas.

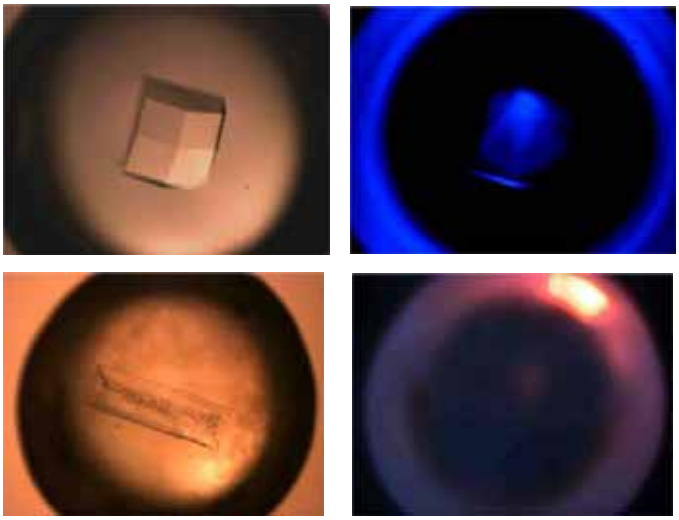

Figura 10: Cristal de proteína irradiado com luz branca (esquerda, acima) e luz ultravioleta a 280 nm (direita, acima). Cristal de sal irradiado com luz branca (esquerda abaixo) e luz ultravioleta (direita, abaixo).

d. Premiações

Vencedor do X Prêmio Jovem Talento em Ciências da Vida promovido pela GE HealthCare e SBBq ocorrido na XXXV Reunião Anual da SBBq (2006), Águas de Lindóia, SP.

O trabalho sobre esfingomielinases D foi selecionado **Six Top Choices** no congresso anual de 2005 da *American Crystallographic Association* com *Scolarship Award.*

e. Seminários & Palestras

Palestra intitulada "Structural Aspects of Toxins: Blood Coagulation and Membrane Disruption" no Departamento de Bioquímica e Microbiologia da Faculdade de Química / Universidade de Hamburgo na Alemanha 2006.

Palestra intitulado "Multi-functionality of Toxins" na XXXV Reunião Anual da SBBQ 2006.

Seminário intitulado "Estrutura-Função de proteínas" no Departamento de Física no IBILCE/UNESP 2005.

Seminário intitulado "Faseamento de proteínas por quick cryo-soaking" no Departamento de Física 2005.

f. Manuscritos Científicos Completos

Rios-Steiner, J.L, **Murakami, M.T.,** Tulinsky A., Arni, R.K., Active site and Exosite Inhibition of Factor X: Structure of Des-Gla Factor Xa Inhibited by the Potent Nematode Anticoagulant Protein NAP5 from *Ancylostoma caninum*. J. Mol. Biol. (Submetido).

Murakami, M.T., Steiner, J.R., Weaver, S.E., Tulinsky, A., Geiger, J.H., Arni, R.K., Intermolecular Interactions and Characterization of the Novel Factor Xa Exosite Involved in Macromolecular Recognition and Inhibition: Crystal Structure of Human Gla-Domainless Factor Xa complexed with the Anticoagulant Protein NAPc2 from the Hematophagous Nematode *Ancylostoma caninum*. J. Mol. Biol. 2006 (In press).

Murakami, M.T., Viçoti, M.M., Abrego, J.R.B., Lourenzoni, M.R., Cintra, A.C.O., Arruda, E.Z., Tomaz, M.A., Melo, P.A., Arni, R.K., Interfacial surface charge and free accessibility to the putative active site are essential requirements for the activity of Lys49 phospholipase A_2 homologues. Toxicon 2006 (In press).

Murakami, M.T., Fernandes-Pedrosa, M.F., de Andrade, S.A., Gabdoulkhakov, A., Betzel, C., Tambourgi, D.V., Arni, R.K., Structural insights into the catalytic mechanism of sphingomyelinases D and evolutionary relationship to glycerophosphodiester phosphodiesterases. Biochem Biophys Res Commun. 2006 342, 323-9.

De Andrade, S.A., **Murakami, M.T.,** Cavalcante, D.P., Arni, R.K., Tambourgi, D.V., Kinetic and mechanistic characterization of the Sphingomyelinases D from Loxosceles intermedia spider venom. Toxicon 2006 47, 380-6.

Murakami, M.T., Gabdoulkhakov, A., Genov, N., Cintra, A.C., Betzel, C., Arni, R.K., Insights into metal ion binding in phospholipases A2: ultra high-resolution crystal structures of an acidic phospholipase A2 in the Ca2+ free and bound states. Biochimie 2006 88, 543-9.

Murakami, M.T., Melo, C.C., Angulo, Y., Lomonte, B., Arni, R.K., Structure of myotoxin II, a catalytically inactive Lys49 phospholipase A2 homologue from Atropoides nummifer venom. Acta Crystallograph Sect F Struct Biol Cryst Commun. 2006 62, 423-6.

Murakami, M.T., Ruller, R., Ward, R.J., Arni, R.K., Crystallization and preliminary X-ray crystallographic studies of the mesophilic xylanase A from Bacillus subtilis 1A1. Acta Crystallograph Sect F Struct Biol Cryst Commun. 2005 61, 219-20.

Murakami, M.T., Arni, R.K., Vieira, D.S., Degreve, L., Ruller, R., Ward, R.J., Correlation of temperature induced conformation change with optimum catalytic activity in the recombinant G/11 xylanase A from Bacillus subtilis strain 168 (1A1). FEBS Lett. 2005 579, 6505-10.

Murakami, M.T., Arni, R.K., Thrombomodulin-independent activation of protein C and specificity of hemostatically active snake venom serine proteinases: crystal structures of native and inhibited Agkistrodon contortrix contortrix protein C activator. J Biol Chem. 2005 280, 39309-15.

Murakami, M.T., Arni, R.K., Crystallization and preliminary X-ray crystallographic studies of Protac, a commercial protein C activator isolated from

Agkistrodon contortrix contortrix venom. Biochim Biophys Acta. 2005 1752, 202-4.

Murakami, M.T., Arruda, E.Z., Melo, P.A., Martinez, A.B., Calil-Elias, S., Tomaz, M.A., Lomonte, B., Gutierrez, J.M., Arni, R.K., Inhibition of myotoxic activity of Bothrops asper myotoxin II by the anti-trypanosomal drug suramin. J Mol Biol. 2005 350, 416-26.

Murakami, M.T., Fernandes-Pedrosa, M.F., Tambourgi, D.V., Arni, R.K., Structural basis for metal ion coordination and the catalytic mechanism of sphingomyelinases D. J Biol Chem. 2005 280, 13658-64.

Murakami, M.T., Gava, L.M., Zela, S.P., Arruda, E.Z., Melo, P.A., Gutierrez, J.M., Arni, R.K., Crystallization and preliminary X-ray diffraction analysis of suramin, a highly charged polysulfonated napthylurea, complexed with a myotoxic PLA2 from Bothrops asper venom. Biochim Biophys Acta. 2004 1703, 83-5.

Murakami, M.T., Michelan-Duarte, S., Cintra, A.C., Arni, R.K., Crystallization and high-resolution X-ray diffraction data collection of an Asp49 PLA2 from Bothrops jararacussu venom both in the presence and absence of Ca2+ ions. Biochim Biophys Acta. 2004 1703, 79-81.

Magro, A.J., **Murakami, M.T.,** Marcussi, S., Soares, A.M., Arni, R.K., Fontes, M.R., Crystal structure of an acidic platelet aggregation inhibitor and hypotensive phospholipase A2 in the monomeric and dimeric states: insights into its oligomeric state. Biochem Biophys Res Commun. 2004 323, 24-31.

Zela, S.P., Fernandes-Pedrosa, M.F., **Murakami, M.T.,** de Andrade, S.A., Arni, R.K., Tambourgi, D.V., Crystallization and preliminary crystallographic analysis of SMase I, a sphingomyelinase from Loxosceles laeta spider venom. Acta Crystallogr D Biol Crystallogr. 2004 60, 1112-4.

Murakami, M.T., Arni, R.K., A structure based model for liposome disruption and the role of catalytic activity in myotoxic phospholipase A2s.Toxicon 2003 42, 903-13.

Ketelhut, D.F., de Mello, M.H., Veronese, E.L., Esmeraldino, L.E., **Murakami, M.T.,** Arni R.K., Giglio, J.R., Cintra, A.C., Sampaio, S.V., Isolation, characterization and biological activity of acidic phospholipase A2 isoforms from Bothrops jararacussu snake venom. Biochimie 2003 85,983-91.

Murakami, M.T., Zela, S.P., Gava, L.M., Michelan-Duarte, S., Cintra, A.C., Arni, R.K., Crystal structure of the platelet activator convulxin, a disulfide-linked

alpha4beta4 cyclic tetramer from the venom of Crotalus durissus terrificus. Biochem Biophys Res Commun. 2003 310, 478-82.

Murakami, M.T., Watanabe, L., Gava, L.M., Zela, S.P., Cintra, A.C., Arni, R.K., Initial structural analysis of an alpha4beta4 C-type lectin from the venom of Crotalus durissus terrificus. Acta Crystallogr D Biol Crystallogr. 2003 59, 1813-5.

Bortoleto, R.K., **Murakami, M.T.,** Watanabe, L., Soares, A.M., Arni, R.K., Purification, characterization and crystallization of Jararacussin-I, a fibrinogen-clotting enzyme isolated from the venom of Bothrops jararacussu. Toxicon 2002 40, 1307-12.

g. Trabalhos Completos em Congressos

Murakami, M.T., Arni, R.K. (2006) Structural basis for the activation of the anticoagulant pathway by the protein C activator isolated from Agkistrodon contortrix contortrix venom, XXXV Reunião Annual da SBBq, Águas de Lindóia, SP, Brasil.

Murakami, M.T., Fernandes-Pedrosa, M.F., de Andrade, S.A., Gabdoulkhakov, A., Betzel, C., Tambourgi, D.V., Arni, R.K. (2006) Structural insights into the catalytic mechanism of sphingomyelinases D and evolutionary relationship to glycerophosphodiester phosphodiesterases, XXXV Reunião Annual da SBBq, Águas de Lindóia, SP, Brasil.

Lourenzoni, M.R., **Murakami, M.T.,** Degreve, L., Arni, R.K. (2006) The dimeric structures of the Lys49 phospholipases A2, a comparative study by molecular dynamics, XXXV Reunião Annual da SBBq, Águas de Lindóia, SP, Brasil.

Murakami, M.T., Arni, R.K. (2006) Alternative activation of the protein C pathway by the protein C activator isolated from Agkistrodon contortrix contortrix venom, XXXVII Latin-American School of Physics, São José do Rio Preto, SP, Brasil.

Viçoti, M.M., **Murakami, M.T.,** Arni, R.K., Abrego, J.R.B., Structural studies in solution of Crotoxin by small angle X-ray scattering, XXXVII Latin-American School of Physics, São José do Rio Preto, SP, Brasil.

Ruller, R., Ferreira, T.L., **Murakami, M.T.,** Arni, R.K., Ward, R.J. (2005) Directed evolution of thermoestability in the xilanases A from Bacillus subtilis, XXXIV Reunião Annual da SBBq, Águas de Lindóia, SP, Brasil.

Murakami, M.T., Fernandes-Pedrosa, M.F., Tambourgi, D.V., Arni, R.K. (2005) Molecular basis for activity of Smases D from snake venoms, XXXIV Reunião Annual da SBBq, Águas de Lindóia, SP, Brasil.

Murakami, M.T., Cintra, A.C.O., Arni, R.K. (2005). Degree of protonation of a D49 phospholipase A2 from ultra high-resolution diffraction data, XXXIV Reunião Annual da SBBq, Águas de Lindóia, SP, Brasil.

Murakami, M.T., Ruller, R., Ward, R.J., Arni, R.K. (2004) Crystal structure and thermostability of the family 11 xylanase from *Bacillus subtilis*, LAPS, Angra dos Reis, RJ, Brasil.

Murakami, M.T., Zela, S.P., Arni, R.K. (2004) Specificity and structural analysis of convulxin, Symposium of the Pan American Section of the International Society on Toxinology, Angra dos Reis, RJ, Brasil.

Murakami, M.T., Gava, L.M., Melo, P.A., Gutiérrez, J.M., Arruda, E.Z., Arni, R.K. (2004) Binding site of suramin in K49 PLA2s, Symposium of the Pan American Section of the International Society on Toxinology, Angra dos Reis, RJ, Brasil.

Zela, S.P., **Murakami, M.T.,** Michelan, S., Gava, L.M., Arni, R.K. (2004) High-yield purification of serine proteases from snake venoms, Symposium of the Pan American Section of the IST, Angra dos Reis, RJ, Brasil.

Viçoti, M.M., Zela, S.P., **Murakami, M.T.,** Arni, R.K. (2004) Characterization of the pH and temperature stability of convulxin using dynamic light scattering, Symposium of the Pan American Section of the International Society on Toxinology, Angra dos Reis, RJ, Brasil.

Murakami, M.T., Zela, S.P., Watanabe, L., Gava, L.M., Michelan-Duarte, S., Cintra, A.C.O., Arni, R.K. (2004) Convulxin, a C-type lectin, exists as a cyclic ab tetramer: Crystal structure and analysis at 2.4Å, XXXIII Reunião Anual da SBBq, Caxambu, MG, Brasil.

Murakami, M.T., Michelan-Duarte, S., Brandt, F.H.C., Gava, L.M., Zela, S.P., Cintra, A.C.O., Arni, R.K. (2004) Atomic resolution crystal structure of two acidic PLA2s, siiispiiia and siiispiiib, from *Bothrops jararacussu* venom, XXXIII Reunião Anual da SBBq, Caxambu, MG, Brasil.

Gava, L.M., **Murakami, M.T.,** Zela, S.P., Laure, C.J., Arni, R.K. (2004) Structural studies of giroxin, a serine protease from the venom of *Crotalus durissus terrificus*, XXXIII Reunião Anual da SBBq, Caxambu, MG, Brasil.

Gaspar, R.T., **Murakami, M.T.**, Arni, R.K. (2004) Structure and stability jof the dimeric form of K49 PLA2s, XXXIII Reunião Anual da SBBq, MG, Brasil

Zela, S.P., **Murakami, M.T.,** Gava, L.M., Arni, R.K., Pedrosa, M.F., Andrade, S., Tambourgi, D.V. (2004) Dynamic light scattering and preliminary structural analysis of Smase I, a sphingomyelinase isolated from the venom of *Loxosceles laeta*, XXXIII Reunião Anual da SBBq, Caxambu, MG, Brasil.

Cabral, C., Gava, L.M., Gaspar, R.T., **Murakami, M.T.,** Angulo, Y., Lomonte, B., Arni, R.K. (2004) pH dependence of the quaternary structure of K49 phospholipases: Crystal structure of Anum II from *Bothrops nummifer* venom and structural compariso]ns, XXXIII Reunião Anual da SBBq, Caxambu, MG, Brasil.